MULTIDISCIPLINARY CENTER FOR EARTHQUAKE ENGINEERING RESEARCH
A National Center of Excellence in Advanced Technology Applications

ISSN 1520-295X

Cyclic Testing of Braces Laterally Restrained by Steel Studs to Enhance Performance During Earthquakes

by

Oguz C. Celik, Jeffrey W. Berman and Michel Bruneau
University at Buffalo, State University of New York
Department of Civil, Structural and Environmental Engineering
Ketter Hall
Buffalo, NY 14260

Technical Report MCEER-04-0003

March 16, 2004

This research was conducted at the University at Buffalo, State University of New York and was supported primarily by the Earthquake Engineering Research Centers Program of the National Science Foundation under award number EEC-9701471.

NOTICE

MULTIDISCIPLINARY CENTER FOR EARTHQUAKE ENGINEERING RESEARCH
A National Center of Excellence in Advanced Technology Applications

Cyclic Testing of Braces Laterally Restrained by Steel Studs to Enhance Performance During Earthquakes

by

Oguz C. Celik[1], Jeffrey W. Berman[2] and Michel Bruneau[3]

Publication Date: March 16, 2004
Submittal Date: August 5, 2003

Technical Report MCEER-04-0003

NSF Master Contract Number EEC-9701471

1 Visiting Professor, Department of Civil, Structural and Environmental Engineering, University at Buffalo, State University of New York; Associate Professor, Division of Theory of Structures, Faculty of Architecture, Istanbul Technical University
2 Graduate Student, Department of Civil, Structural and Environmental Engineering, University at Buffalo, State University of New York
3 Professor, Department of Civil, Structural and Environmental Engineering, University at Buffalo, State University of New York

MULTIDISCIPLINARY CENTER FOR EARTHQUAKE ENGINEERING RESEARCH
University at Buffalo, State University of New York
Red Jacket Quadrangle, Buffalo, NY 14261

Preface

The Multidisciplinary Center for Earthquake Engineering Research (MCEER) is a national center of excellence in advanced technology applications that is dedicated to the reduction of earthquake losses nationwide. Headquartered at the University at Buffalo, State University of New York, the Center was originally established by the National Science Foundation in 1986, as the National Center for Earthquake Engineering Research (NCEER).

Comprising a consortium of researchers from numerous disciplines and institutions throughout the United States, the Center's mission is to reduce earthquake losses through research and the application of advanced technologies that improve engineering, pre-earthquake planning and post-earthquake recovery strategies. Toward this end, the Center coordinates a nationwide program of multidisciplinary team research, education and outreach activities.

MCEER's research is conducted under the sponsorship of two major federal agencies: the National Science Foundation (NSF) and the Federal Highway Administration (FHWA), and the State of New York. Significant support is derived from the Federal Emergency Management Agency (FEMA), other state governments, academic institutions, foreign governments and private industry.

MCEER's NSF-sponsored research objectives are twofold: to increase resilience by developing seismic evaluation and rehabilitation strategies for the post-disaster facilities and systems (hospitals, electrical and water lifelines, and bridges and highways) that society expects to be operational following an earthquake; and to further enhance resilience by developing improved emergency management capabilities to ensure an effective response and recovery following the earthquake (see the figure below).

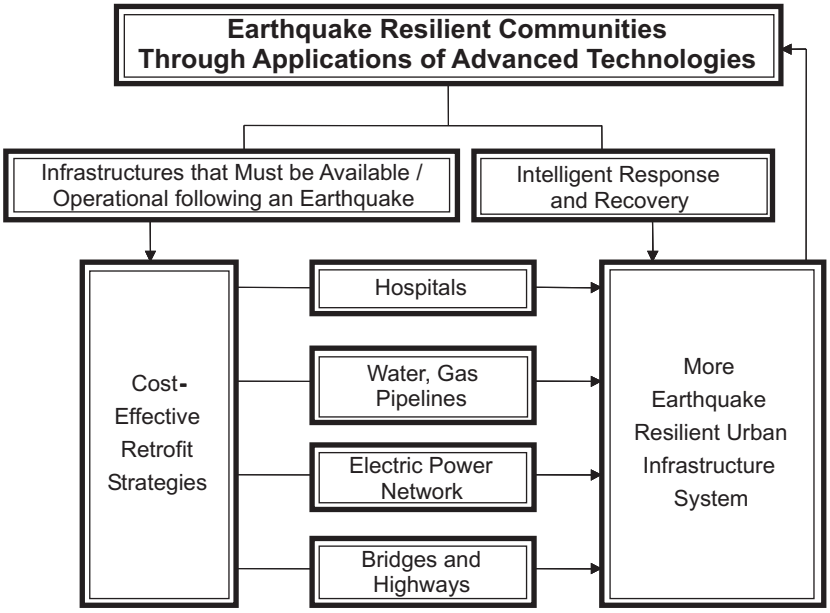

A cross-program activity focuses on the establishment of an effective experimental and analytical network to facilitate the exchange of information between researchers located in various institutions across the country. These are complemented by, and integrated with, other MCEER activities in education, outreach, technology transfer, and industry partnerships.

This report describes an experimental investigation into the seismic behavior and efficiency of using braced steel infills for steel framed buildings. Cold formed steel studs (CFSS), typically used in nonstructural partition walls, were studied to determine if they could be used to laterally restrain braces against buckling and thus enhance their seismic performance. Four specimens were designed and cyclically tested: single square tube braces with and without vertical CFSS and rectangular solid bar X braces with and without CFSS members. The effects of KL/r ratio, bracing configuration and cross-sectional type of braces were studied, as well as behavior characteristics of the specimens with an emphasis on hysteretic energy dissipation. As a result, the CFSS members showed promise for use in new buildings or as a retrofitting technique in buildings that lack strength, lateral stiffness and ductility.

ABSTRACT

Braces of steel frames are subjected to large axial displacements in tension and compression under severe earthquake excitations. Hysteretic behavior of brace members is complex, especially in the inelastic range. Previous studies have revealed that substantial amounts of cumulative energy can be dissipated in steel braces in the post buckling range when those members are subjected to reversed cyclic displacements. Many studies and codes suggest that stocky braces be used in seismically active regions. In fact, following that thinking, buckling restrained brace technologies have been developed and implemented in the seismic design and retrofit of buildings.

This report investigates the effects of KL/r ratio, bracing configuration, and cross sectional type of braces on the hysteretic characteristics of concentrically braced frames with and without cold formed steel studs (CFSS) infills designed to laterally restrain braces and delay their buckling. Four specimens were designed and cyclically tested. Specimens have either single diagonal tube or solid bar braces with and without CFSS and U brackets, providing out-of-plane and in-plane buckling restraint. Behavioral characteristics of the specimens are quantified with an emphasis on hysteretic energy dissipation.

Experimental results show that, at the same ductility levels, the cumulative energy dissipation of braced frames can be significantly increased when CFSS members are used to laterally restrain the braces against buckling. However, when tubular cross sections are used for braces, local buckling led to a reduced fracture life compared to the case without CFSS members. On the other hand, CFSS members appear to be relatively more effective when solid bar braces having large slenderness (tension-only braces) are used, since the difference between dissipated energies with and without studs is substantial.

ACKNOWLEDGEMENTS

This research was supported in whole by the Earthquake Engineering Research Centers Program of the National Science Foundation (NSF) under Award Number EEC-9701471 to the Multidisciplinary Center for Earthquake Engineering Research (MCEER).

The first author thanks the Istanbul Technical University (ITU) President Office and ITU Faculty of Architecture for their partial support during his stay in Buffalo, under Grant to Support Long Term Research Activities Abroad For Young Researchers.

All tests were conducted in the Structural Engineering and Earthquake Simulation Laboratory (SEESL) at SUNY at Buffalo. The invaluable assistance of the laboratory staff Duane Kozlowski, Scot Weinreber, Dick Cizdziel, and Mark Pitman is greatly acknowledged.

However, any opinions, findings, conclusions, and recommendations presented in this report are those of the authors and do not necessarily reflect the views of the sponsors and the people.

TABLE OF CONTENTS

TABLE OF CONTENTS (continued)

TABLE OF CONTENTS (continued)

LIST OF ILLUSTRATIONS

LIST OF ILLUSTRATIONS (continued)

LIST OF ILLUSTRATIONS (continued)

LIST OF ILLUSTRATIONS (continued)

LIST OF ILLUSTRATIONS (continued)

LIST OF ILLUSTRATIONS (continued)

LIST OF ILLUSTRATIONS (continued)

LIST OF ILLUSTRATIONS (continued)

LIST OF ILLUSTRATIONS (continued)

LIST OF ILLUSTRATIONS (continued)

LIST OF ILLUSTRATIONS (continued)

LIST OF TABLES

NOTATIONS

a,b	axial hinge parameters for braces per FEMA or parameters used to fit the experimental data in Bounding Surface Model (BSM)
A_g	gross area of brace
b_f	outside width of tube section
c	residual strength ratio of brace per FEMA
d	distance from current force to bound line in BSM or section depth
d_{in}	value of d at initiation of each load reversal in BSM
D	diameter of circular tube
E, E_s	modulus of elasticity
E_H	hysteretic energy dissipation
E_{HN}	normalized hysteretic energy dissipation
F_{cr}	critical stress in compression
F_y	yield stress
h	height of boundary frame or hardening shape parameter in BSM
h_w	outside height of tube section
K	effective length factor
L	specimen width or laterally unbraced length of brace
L_D	clear length of brace
n_j	number of cycles to be performed in load step j
n_o	number of cycles with a peak displacement less than δ_y or δ_b
P	brace axial force
P_n	flexural buckling strength of brace
r	minimum radius of gyration
R	seismic force modification factor
R_b	slope of bounding lines in BSM
R_{ki}	initial stiffness in BSM
R_{kii}	initial stiffness prior to any displacement reaching the yield displacement in BSM
R_{kp}	plastic tangent stiffness in BSM
R_{kt}	tangent stiffness at the current displacement in BSM

t	tube thickness
T_n	nominal tensile strength of brace
V_y	yield (or buckling) base shear strength
δ	brace axial displacement
δ_b	specimen top horizontal displacement at brace buckling
δ_{max}	maximum displacement reached during the next cycle of loading in BSM
δ_y	specimen top horizontal displacement at brace yielding or initial yield displacement of boundary frame in BSM
Δ	increment in peak displacement
Δ_C	axial shortening in axial hinge model
Δ_f	theoretical fracture life of brace
$\Delta_{f,exp}$	experimental fracture life of brace
ΔF	incremental base shear in BSM
Δ_T	axial elongation in axial hinge model
$\Delta\delta$	incremental displacement in BSM
ε_y	axial yield strain
ϕ_c	resistance factor for compression
ϕ_t	resistance factor for tension
λ, λ_c	brace slenderness parameter
μ	displacement ductility ratio

ABBREVIATIONS

AISC	American Institute of Steel Construction
ASTM	American Society for Testing and Materials
ATC	Applied Technology Council
BIB	Buckling Inhibited Braces
BRB	Buckling Restrained Braces
BSM	The Bounding Surface Model
CBSF	Concentrically Braced Steel Frames
CFSS	Cold Formed Steel Studs
CP	Collapse Prevention
CSA	Canadian Standards Association
EBF	Eccentrically braced Frames
FEMA	Federal Emergency Management Agency
IO	Immediate Occupancy
LD	Limited Ductility
LRFD	Load and Resistance Factor Design
LS	Life Safety
MCEER	Multidisciplinary Center for Earthquake Engineering Research
MD	Moderately Ductile
OCBF	Ordinary Concentrically Braces Frames
SCBF	Special Concentrically Braces Frames
SEESL	Structural Engineering and Earthquake Simulation Laboratory
SMRF	Special Moment Resisting Frames

SECTION 1
INTRODUCTION

1.1 Motivation

Concentrically braced steel frames are commonly used to resist earthquakes by providing lateral stiffness, strength, and ductility. However, upon cyclic loading, progressive loss of compression strength and energy dissipation in compression results in less than ideal hysteretic loops. To improve the hysteretic characteristics of braces, cold formed steel studs (CFSS) of the type often used in non-structural partition walls could be used to laterally restrain braces against buckling and enhance their seismic performance. This would require special design of CFSS members, to resist elastically the out-of-plane forces developing at the onset of brace buckling.

To investigate the validity of such a solution (i.e. whether CFSS wall units could be used to achieve the above objective, how effective they are, and if they improve the hysteretic behavior as anticipated or not), four specimens have been designed and cyclically tested in the Structural Engineering and Earthquake Simulation Laboratory (SEESL) at SUNY at Buffalo. Single square tube braces with and without vertical CFSS, and solid rectangular solid bar X braces with and without CFSS members, were tested under quasi-static displacement histories.

This research report presents development of this test program, the data obtained during reversed cyclic testing of the four tested frames and analysis of these data. To the knowledge of the authors, CFSS members have not been used for this purpose before. Displacement-controlled cyclic testing of these specimens enabled to compare their strength, stiffness, maximum displacement ductility, and cumulative hysteretic energy dissipation capacities. For tubular sections, experimental and theoretical fracture lives are also compared.

1.2 Scope

This research investigates the seismic behavior and efficiency of a proposed braced steel infill for steel framed buildings. The infill types considered in this study could be implemented in new buildings or as a retrofitting technique in seismically vulnerable

buildings lacking of strength, lateral stiffness, and ductility. Based on this, the scope of this research is to provide:

- A brief review of hysteretic models for seismic analysis of braced frames
- Documentation of the experimental system, material types used and loading protocol imposed on the specimens
- Preliminary analysis results for the specimens using 2D nonlinear static pushover analysis to predict their monotonic behavior
- Presentation of the data obtained from cyclic testing
- Comparison of hysteretic energy dissipation capacities of each specimen
- Interpretation of the obtained data and discussion of several factors on the observed structural behavior

1.3 Outline

In Section 2, a brief review of available theoretical and experimental research on the hysteretic behavior of steel brace elements and braced steel frames is given.

In Section 3, the experimental program, testing set-up, data acquisition systems, instrumentation, and material properties are described.

In Section 4, the experiments are presented. Observations are made on the overall behavior of the specimens, the extent of damage at some specific story drifts, and collapse mechanisms.

In Section 5, test results are analyzed. Hysteretic loops representing the cyclic behavior are given. The strength, stiffness, and cyclic energy dissipation of the specimens are quantified. System and member strengths, brace energy dissipation, and strains in braces at specific story drift values are interpreted using available test data.

In Section 6, general conclusions from this research and recommendations for future work on this subject are given.

SECTION 2
LITERATURE REVIEW

2.1 General

Many steel buildings rely on different kinds of bracing systems to ensure ductile response and control story drifts under severe earthquakes. A fundamental understanding of the hysteretic behavior of brace members is important and relevant to the work presented in this report. Many theoretical and experimental studies have investigated the complex, inelastic cyclic behavior of steel braces. This work is summarized in Section 2.3 including some recent studies on unbonded braces presented in Section 2.4. Examples of how some key parts of this knowledge have been codified are illustrated in Section 2.5. Since the hysteretic behavior of concentrically braced steel frames (CBSF), as a system, highly depends on the inelastic cyclic behavior of individual steel braces, much of the previous studies focused on the behavior of a single brace element rather than on overall system behavior.

2.2 Basic Behavior of Steel Braces

During severe earthquakes, steel braces in framed buildings are subjected to cyclic axial forces which may cause braces to alternatively buckle and stretch in the inelastic range. Theoretical and experimental studies have demonstrated that steel braces can dissipate seismic energy during an earthquake if some special ductile detailing is provided.

Hysteretic loops for brace elements are more complex than for steel flexural members. Hysteretic loops of an axially loaded brace are usually unsymmetrical with observed deterioration in the buckling strength at each subsequent cycle. The introduction of increasing residual out-of-straightness upon repeated cycling, and hysteretic degradation of the tangent modulus (the Baushinger effect) is partly responsible for this deterioration of buckling strength with cycling. The impact of this post buckling brace behavior must be accounted for in the design of boundary frames and for brace end connections.

Generic idealized hysteretic behavior of steel braces having different slenderness categories is schematically illustrated in Figure 2-1. Here, P and δ denote axial force and corresponding axial displacement respectively. In a short brace that does not exhibit buckling (assuming local buckling is prevented), tension and compression response can theoretically be equal to

each other, providing a more stable behavior when compared to longer braces (Figure 2-1a). Unbonded braces are a type of buckling-restrained braces that can exhibit a behavior similar to that of short braces, as described in Section 2.4.

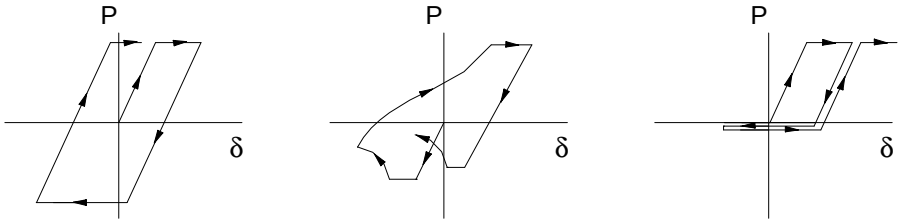

(a) Short Brace (b) Intermediate Brace (c) Long Brace

FIGURE 2-1 Simplified Representation of Brace Hysteretic Behavior for Short, Intermediate and Long Slenderness (Adapted from Nakashima and Wakabayashi,1992)

At the other extreme, long slender braces can yield in tension, but have no compression strength (Figure 2-1c). Behavior of intermediate braces is somewhat between that of short and long braces (Figure 2-1b). This behavior is more complex and was the subject of most researches summarized in Section 2.3.

While many parameters can affect brace behavior (e.g. modulus of elasticity, strength ratio between brace and gusset plate, connection flexural stiffness, etc.), the inelastic hysteretic behavior of restrained axial member is most influenced by the member "effective slenderness ratio" and width-to-thickness ratio of parts of the brace cross-section.

2.3 Previous Research on Hysteretic Behavior of Braces

This subsection first reviews past experimental and theoretical studies on the hysteretic response of concentrically braced steel frames.

Zayas et al. (1980a) subjected six circular tube brace members to severe cyclic inelastic loading. The specimens were 1/6 scale models of braces of the type used for offshore platforms. Different end fixity conditions such as pinned and fixed were examined. Impact of sectional properties on cyclic behavior was also investigated using different diameter-to-wall thickness (D/t) ratios (33 vs. 48). Axial load-displacement hysteretic loops, axial load versus midspan lateral deflection hysteretic loops, brace deflected shapes, brace energy dissipation

and inelastic axial strains, curvatures and rotation in plastic regions were plotted. Emphasis was on deterioration of buckling load with inelastic cycling and comparison with code-based buckling formulas in effect at that time. It was concluded that cyclic inelastic loading caused a reduction of the buckling load. The effect of annealed and unannealed material properties of structural tubes on the behavior was discussed. Since local buckling was a major contributor to early collapse in thin walled specimens, use of lower D/t ratios was suggested to delay local buckling failures under repeated cyclic loads. The responses of fixed-ended brace exhibited less pinched hysteretic loops, slower deterioration of capacity, delayed onset of local buckling and more energy dissipation compared to those of the pinned-end braces. This difference essentially came from the reduced buckling length of the members.

Zayas et al. (1980b) experimentally investigated the behavior of two 1/6 scale steel offshore towers subjected to large cyclic inelastic loadings applied in a quasi-static manner, simulating damaging earthquake excitations. In this study, braces with lower KL/r and D/t ratios performed better, exhibited fuller hysteretic loops, deteriorated less and were more resistant to local buckling. Buckling braces contributed notably to the energy dissipation of the tested frames. The efficiency of energy dissipation decreased rapidly after local buckling. It was also shown that a properly designed, detailed and constructed tubular braced frame could demonstrate full hysteretic loops and substantial energy dissipation capacity under reversed cyclic inelastic displacements. An energy dissipation efficiency criterion was formulated for comparison with equivalent elastic-perfectly plastic systems. The tested frames retained energy dissipation efficiencies above 50%.

Black et al. (1980) studied the inelastic hysteretic behavior of axially loaded wide flanges, structural tees, double angles, double channels as well as thick and thin-walled square and round tubes. Two types of boundary condition, fixed and hinged, were considered. They experimentally observed that the points of inflection on deflected curves remain relatively fixed as plastic hinges developed during inelastic buckling, and consequently that effective slenderness ratios remained valid in the inelastic range. This slenderness ratio was deemed to have a most important impact on hysteretic behavior. Hysteretic envelopes were also presented to compare the specimens with different loading histories. All hysteretic curves were normalized to the axial yield force and corresponding axial displacement. In agreement

with previous work, significant reduction in buckling strength was observed to occur during inelastic cyclic loading.

Jain et al. (1980) generated experimental and analytical data on the inelastic cyclic behavior of tube and angle braces. Deterioration of the buckling strength upon cyclic loading was pointed out. The impact of connection details on low-cycle fatigue life was underlined. Annealing was found to increase the fatigue life of the member prior to collapse.

Ikeda et al. (1984) developed a refined phenomenological hysteretic model for simulating inelastic cyclic buckling behavior of steel braces. This consisted of straight line segments defined by simple rules to capture buckling strength deterioration, plastic growth (which can be defined as plastic lengthening after each inelastic cycle), and a few other brace behaviors. Since phenomenological brace hysteretic models are defined in terms of control input parameters, the study proposed a systematic method for selecting input parameters based on available experimental results. Furthermore, a series of simple quasi-static analyses were conducted to evaluate the new model and its limits. Note that phenomenological models are generally based on simplified hysteretic rules that only mimic the observed axial load-displacement behavior of braces, and are empirical in nature.

Ikeda and Mahin (1984) presented a physical hysteretic model for cyclic inelastic behavior of steel braces. They broke-down the physical hysteretic behavior of braces into a number of "zones", as illustrated in Figure 2-2.

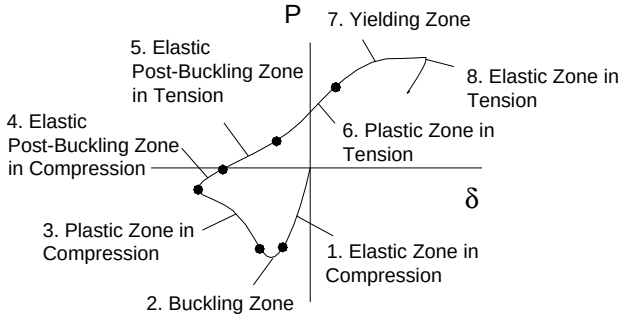

FIGURE 2-2 Physical Meaning of a Brace Hysteretic Loop (Adapted from Ikeda and Mahin, 1984)

Each zone was used to explain a specific axial force- displacement behavior, with corresponding axial force-plastic hinge moment curves, and axial force-plastic hinge rotation curves. The refined model simulates the cyclic inelastic buckling behavior of braces more precisely than corresponding phenomenological models, but still neglects local buckling effects, the gradual spread of plastification along the length of the brace, and only partially account for the Baushinger effect by modeling the progressive degradation of the tangent modulus during cycles. Sensitivity analyses on the behavior of braced frames using the proposed model were included in the study, on the basis of which the use of stocky braces was recommended over slender braces.

Khatib et al. (1988) investigated the inelastic cyclic behavior of chevron-braced frames, and as a result of parametric studies, formulated design recommendations. They also demonstrated the sensitivity of the inelastic response of chevron-braced frames to the characteristics of ground excitations, and their tendency to form soft stories which may translate into excessive local ductility demands. Depending on brace slenderness and beam stiffness, numerical analyses results showed that considerable force redistributions might occur in chevron-braced frames and affect their overall seismic performance. Furthermore, it was shown that chevron-braced frames have distinctive hysteretic loops compared to other types of braced frames.

Jain et al. (1993) analytically examined the impact of a dual system consisting of a moment resisting frame acting in parallel with a concentrically braced steel frame subjected to both monotonically increasing loads and seismic loading. The relative strengths and stiffnesses of the frames comprising the dual systems were varied. Ductility demands on members, overall building deflections and story drifts were examined under the action of ten earthquake records. It was concluded that improved performance, such as reduced ductility demands and more uniform distribution of yield throughout the structure, could be achieved.

Tremblay et al. (1996) re-evaluated seismic aspects of structural steel design in light of the lessons learned from the 1995 Hyogo-ken Nanbu earthquake. Past and current seismic design provisions for steel structures in Japan were presented and compared with the Canadian requirements at that time. Fracture of bracing members or their connections was observed in many concentrically braced frames.

Tremblay and Filiatrault (1996) experimentally investigated the issue of impact loading in inelastic tension-only concentrically braced steel frames subjected to earthquakes by conducting shake table tests of half scale two-story models. The hysteretic loops obtained from the shake table test results revealed a small increase in tensile forces developed in the braces attributable to an increase of the yield strength under high strain rates. A dynamic amplification factor of 1.15 for the yield strength of tension-only braces was proposed for code applications.

Remennikov and Walpole (1997) investigated the seismic behavior of low-rise steel braced buildings using an empirical analytical hysteretic brace model developed and calibrated using experimental data. Inelastic dynamic analyses were carried out on several bracing configurations to understand the effect of brace slenderness and redistribution of forces in the post buckling range. Based on analytical results, they proposed that the structural ductility factor (μ) for concentrically braced frames not be greater than 3. They emphasized the need for capacity design in order not to underestimate the internal forces in building elements under severe earthquakes.

Tremblay (2000) performed an analytical study to evaluate the influence of the brace slenderness ratio on the seismic performance of concentrically braced steel frames. Nonlinear time history dynamic analyses were carried out on typical building structures. The brace slenderness (λ) was varied from 0.35 to 2.65 for tension-compression brace design and from 0.85 to infinity for tension-only brace design, where the brace slenderness λ is defined as:

$$\lambda = \frac{KL}{r}\sqrt{\frac{F_y}{\pi^2 E}} \qquad (2\text{-}1)$$

where

r = Minimum radius of gyration

F_y = The yield stress

E = Modulus of elasticity of the material

K = Effective length factor

L = Brace length

Results indicated that the inelastic demand in the tension-compression bracing systems decreased with increasing brace slenderness, whereas, for tension-only bracing systems, the inelastic demand generally increased with increasing the brace slenderness. For both bracing systems, it was also found that higher inelastic demand was generally associated with a concentration of inelastic damage over the height of the structures. An upper slenderness limit of λ=2.65 (which corresponds to KL/r of 200 for a 345 MPa (50 ksi) grade steel) was proposed for tension-compression bracing systems. The use of tension-only design of braces was deemed acceptable provided that the slenderness ratio is kept below the same limit. For both systems, limitations on building heights were suggested to prevent the formation of soft-story mechanisms.

Tremblay (2002) surveyed past experimental studies on the inelastic response of diagonal steel bracing members subjected to cyclic inelastic loading. Parameters affecting the overall response of concentrically braced steel frames such as maximum brace compressive strength at first buckling, force in the compression braces upon yielding of the tension braces, maximum brace tensile strength, minimum post-buckling strength of braces at compression ductility levels of 2.0, 3.0, 5.0, lateral brace deformations and fracture of rectangular hollow sections were quantified. The impact of steel yield strength and different loading histories on the shape of brace hysteresis curves was also discussed. Lee and Bruneau (2002) also surveyed past experimental results to quantify the progressive compressive strength degradation of braces, and their contribution to hysteretic energy dissipation. These two studies point to (and quantify) the rapid degradation of these quantities upon inelastic cyclic loading.

2.4 Studies on Buckling-Restrained Braces (BRB)

Since the design philosophy of the specimens in this study, to some extent, could reflect similar design concepts followed in other buckling-restrained brace technologies (mostly developed and used in Japan and in the USA), some recent studies on unbonded braces are reviewed here.

Clark et al. (2000) analytically and experimentally investigated the behavior of steel unbonded braces for energy dissipation. The results of nonlinear time history dynamic analyses showed that frames with unbonded braces could be designed to have lower interstory drift and base shear than the special moment resisting frames (SMRF). Large-scale tests of unbonded braces were carried out to demonstrate their stable hysteretic behavior. For this purpose, three braces were subjected to a wide range of tests. These braces exhibited substantial and stable energy dissipation capacity up to large displacements producing 2% strain in the braces. The core steel in these braces provided stable energy dissipation by yielding under reversed axial loading, while the surrounding concrete-filled tube prevented buckling.

Iwata et al. (2000) experimentally investigated four different types of commercially available buckling-restrained braces. Hysteretic and fracture characteristics as well as cumulative energy dissipation of these braces were discussed. All specimens were found to have sufficiently stable hysteretic curves without significant strength and stiffness deteriorations up to 1% strain in the braces. However, under higher strains, the four specimens exhibited different performances due to their buckling-restrained methods. Generally speaking, the steel braces wrapped in an unbonding material and placed in a tube filled with mortar dissipated more cumulative energy than the others.

Huang et al. (2000) conducted static and dynamic cyclic tests for moment resisting frames with and without unbonded braces as supplemental hysteretic dampers. Hysteretic curves, cumulative energy dissipations, and interstory drift ratios were presented. These unbonded braces were observed to absorb the majority of the input energy from the simulated earthquake loadings. Contribution of the unbonded braces to the lateral stiffness of frames was high. The boundary frame members remained elastic even at large interstory drifts.

Chen et al. (2001) presented the hysteretic behavior of buckling-inhibited braces (BIB) made of low yield strength steel. Four large-scale specimens were tested to collapse. The use of BIB prevented early buckling and fracture that usually occur in conventional braces, and developed full strength, significant ductility, and energy dissipation. These braces were used in a 0.4-scale three-story frame, and this frame was tested on a shake table using the El Centro ground acceleration records. In terms of the maximum interstory drifts, the specimens

achieved without failure performance levels of full operational (0.2% drift) up to 0.2g, operational (0.5% drift) up to 0.36g, and life safe (1.5% drift) up to 0.93g. These performance levels are based on the Vision 2000 *Committee of Structural Engineers Association of California* (1995).

Ko et al. (2002) described an application where buckling-restrained yielding braces were used in the construction of a medical facility. Nonlinear pushover analyses were carried out to demonstrate the performance advantages of these braces over an alternative EBF system. Tests on two identical large-scale specimens were also performed. Both braces exhibited predictable stable hysteretic behavior.

Black et al. (2002) conducted tests on five buckling-restrained unbonded braces. Results from this test program indicated that unbonded braces could deliver ductile, stable and repeatable hysteretic behavior. The plastic deformation capacity of the braces exceeded the specified requirements both in terms of ultimate deformation and in terms of cumulative plastic strain. A hysteretic model was proposed to approximate the dynamic response of structures with unbonded braces. Additional parametric studies also indicated that simple bilinear models could satisfactorily represent the brace nonlinear behavior.

2.5 Review of Current Codes

Significant research on the behavior of steel braces was conducted in the 1970s and 1980s. Many code provisions, details and limitations until the early 1990s were based on these studies. Since the hysteretic loops for concentrically braced frames (CBF) were less ideal with observed pinching due to a progressive strength degradation upon repeated buckling of the compression brace (especially in tension-only braced frames), CBF were assigned response modification factors (R) on the order of 75% of what were assumed for moment frames in the USA. This contributed to the wide-spread use of moment frames in areas of high seismicity. However, from 1992 to date, the design requirements for CBF in the AISC Seismic Provisions have evolved. In the 1997 edition, a new category CBF was introduced as special concentrically braced frames (SCBF) on the basis that CBF could exhibit ductile and stable hysteretic behavior with adequate energy dissipation during cyclic inelastic buckling if ductile detailing was provided. Higher R values were assigned for SCBF (20%

higher than for ordinary CBF). Some relaxation on the maximum brace slenderness ratio permitted for SCBFs were also introduced. However, emphasis on promoting stocky braces over slender braces still remains despite the fact that the fracture life of stocky braces is known to be generally less than for slender braces.

Existing building codes impose several limitations in the design and detailing of steel braces to ensure a satisfactory ductile behavior. The earthquake resistant design requirements for concentrically braced steel frames relevant to this study are reviewed below for three codes, namely, AISC *Seismic Provisions for Structural Steel Buildings* (AISC, 2002), CAN/CSA-S16-2001 (2001) *Limit States Design of Steel Structures*, and FEMA 356 (2000) *Prestandard and Commentary for the Seismic Rehabilitation of Buildings*. Emphasis is given on frames with tension-compression tube braces, and on frames with tension-only braces, which are of interest in this research.

2.5.1 AISC Seismic Provisions (2002)

The AISC Seismic Provisions (AISC, 2002) categorizes the braced frames into two groups: Special concentrically braced frames (SCBF) and ordinary concentrically braced frames (OCBF). In SCBF, the slenderness of bracing members, KL/r, is limited to $5.87\sqrt{E_s/F_y}$ (which corresponds to KL/r of 141 for a 345 MPa (50 ksi) grade steel). Rectangular hollow structural sections must have a flat width-to-wall thickness ratio b/t or h/t no greater than $0.64\sqrt{E_s/F_y}$ (which corresponds to h/t of 15.4 for a 345 MPa (50 ksi) grade steel), where $b=b_f - 3t$ and $h=h_w - 3t$, and where b_f, h_w, and t, are the outside width, outside height, and thickness of the tube cross section. This formula is valid unless the walls are stiffened.

2.5.2 CAN/CSA-S16-2001 (2001)

The Canadian Standard on *Limit States Design of Steel Structures* CAN/CSA-S16-01 (2001) provides requirements for the seismic design of bracing members in concentrically braced steel frames and their connections. Concentrically braced steel frames are categorized in two groups: Moderately Ductile Concentrically Braced Frames (Type MD) and Limited Ductility Concentrically Braced Frames (Type LD).

Moderately Ductile Concentrically Braced Frames includes tension-compression bracing systems, chevron braced systems, tension-only bracing systems, and other bracing systems for which stable inelastic response could be demonstrated. Tension-compression concentric bracing systems are limited to eight stories. Tension-only bracing systems cannot exceed four stories, and are only permitted if all columns are fully continuous over the entire building height and have constant cross-section. For diagonal bracing members of any kind, upper limit for the slenderness ratio, KL/r, is 200.

In velocity-or acceleration related- seismic zones 2 or higher, width to thickness ratios are limited to $330/\sqrt{F_y}$ (which corresponds to h/t of 17.8 for a 345 MPa (50 ksi) grade steel) for rectangular and square HSS when $KL/r \leq 100$, and to $10000/F_y$ (which corresponds to d/t of 29 for a 345 MPa (50 ksi) grade steel) for circular HSS. When KL/r = 200, the b/t ratios for HSS members are limited to $420/\sqrt{F_y}$ (which corresponds to b/t of 22.6 for a 345 MPa (50 ksi) grade steel). When $100 \leq KL/r \leq 200$, linear interpolation can be used. In other zones, the b/t ratios of HSS members cannot exceed $420/\sqrt{F_y}$. In the above formulas, the specified minimum yield strength, F_y, should be in MPa.

Limited Ductility Concentrically Braced Frames can dissipate limited amounts of energy through yielding of bracing members. Tension-compression concentric braced frames are limited to twelve stories. Tension-only systems cannot exceed eight stories, and must have all columns continuous and constant cross-section over a minimum of two stories. In single and two-story structures, the slenderness ratio of diagonal bracing members cannot exceed 200 for compression members and 300 for tension members. There are no width-thickness limits for tension-only braces. In velocity- and acceleration-related seismic zones of 2 and lower, the b/t ratios for braces are limited to $525/\sqrt{F_y}$ (which corresponds to b/t of 28.3 for a 345 MPa (50 ksi) grade steel). The requirements regarding ductile rotational behavior of brace members or connections given for the Type MD Concentrically Braced Frames, are waived in velocity-and acceleration-related seismic zones of 3 and lower if the brace slenderness ratio is greater than 100.

2.5.3 FEMA 356 (2000)

FEMA 356 (2000) *Prestandard and Commentary for the Seismic Rehabilitation of Buildings*, defines steel braced frames as those frames that develop seismic resistance primarily through axial forces in their components. For the purpose of assessing acceptable seismic performance, nonlinear push-over analysis of braced frames are recommended, considering the nonlinear yielding and buckling load-deformation behavior of braces. In lieu of relationships derived from experiment or analysis, the nonlinear load-deformation behavior of braces is modeled as depicted in Figure 2-3. The shape of the nonlinear force-displacement curve is representative of ductile behavior, and defined by the five points A to E shown in Figure 2-3. The parameters a, b, and c are used to characterize the model.

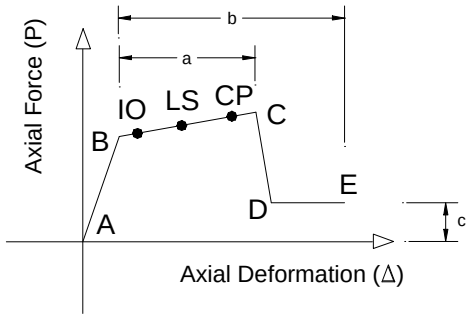

FIGURE 2-3 Axial Force-Axial Deformation Relation and Acceptance Criteria for Braces in Nonlinear Static Procedure, FEMA 356 (2000)

Stable inelastic behavior is developed from B to C, a plateau of length "a". The total plastic deformation length "b" includes a strain hardening range and a strength-degraded range. Significant strength degradation occurs from C to D, with a sustainable strength from D to E, accounting for the ability to support gravity loads. The residual sustainable strength from D to E, is "c", expressed in terms of a percentage of the brace axial yield strength which depends on cross sectional shape, direction of loading, and width-to-thickness ratios in hollow sections. Along segment B to C various seismic performance levels are defined as a function of member deformations (and indirectly, damage). Target performance levels IO, LS, and CP indicate typically immediate occupancy, life safety, and collapse prevention.

For rectangular cold-formed tubular braces in compression, when $d/t \leq 90/\sqrt{F_y}$ (which corresponds to d/t of 12.7 for a 345 MPa (50 ksi) grade steel), a,b, and c are specified as $0.5\Delta_c$, $7\Delta_c$, and 0.4 of the buckling strength respectively. Performance levels IO, LS, and CP

are met if member deformations are limited to $0.25\Delta_c$, $4\Delta_c$, and $6\Delta_c$ respectively, where Δ_c is the axial deformation at expected buckling load. When $d/t \geq 190/\sqrt{F_y}$ (which corresponds to d/t of 26.9 for a 345 MPa (50 ksi) grade steel), a,b, and c are specified as $0.5\Delta_c$, $3\Delta_c$, and 0.2 of the buckling strength respectively. Performance level limits for IO, LS, and CP are set at $0.25\Delta_c$, $1\Delta_c$, and $2\Delta_c$ respectively. Linear interpolation can be used between those d/t limit values. In the above formulas, the specified minimum yield strength, F_y, should be in ksi.

For braces in tension, a,b, and c are specified as $11\Delta_T$, $14\Delta_T$, and 0.8 of the yield strength respectively, where Δ_T is the axial deformation at expected tensile yielding load. Performance level limits for IO, LS, and CP are set at $0.25\Delta_T$, $7\Delta_T$, and $9\Delta_T$ respectively.

The static nonlinear procedure for steel braced frames proposed by FEMA 356 has been incorporated into SAP2000 (CSI, 1998), and will be used in the estimation of load-displacement diagrams to collapse for the specimens considered in this study.

SECTION 3
EXPERIMENTAL SETUP

3.1 General

This section provides specific details on the experimental setup, design considerations for the specimens, and instrumentation. Two boundary frames previously designed and constructed by Berman (2002) were used, but modified to accommodate different beam-to-column connections as well as steel stud and gusset connections, as described later. Additional design checks were carried out to make sure the boundary frame and its connections were safe for the contemplated applications. For one of the two boundary frames, to avoid premature low-cycle fatigue failures in the beam-to-column connections, these connections were replaced prior to testing. All the dimensions in beams and columns as well as connection angles were also kept constant from specimen to specimen to allow a more uniform comparison of the strength, stiffness and seismic energy dissipation capacity of several proposed retrofit designs.

Four specimens were designed and constructed using concentric braces. Both square tubular and solid rectangular sections were used as brace members. Two of the specimens had closely spaced vertical cold-formed steel studs introduced to reduce the buckling length of the braces, approaching to some degree (but not perfectly) the philosophy of buckling-restrained braced frames. Information on the infill types used in this research is given in Section 3.2. All specimens were designed in accordance with the AISC Seismic Provisions (AISC, 2002), AISC LRFD Specifications (AISC, 1999), and AISI (1996) codes as appropriate.

A tall reaction frame located in the University at Buffalo's Structural Engineering and Earthquake Simulation Laboratory (SEESL) was used to provide support for the lateral load applied to the specimens (Figures 3-1, 3-2, 3-3, 3-4). This frame is rated to resist lateral loads of up to 1112 kN (250 kips) at a height of 2.4 m (8 ft.) or lower.

3.2 Specimen Design

The boundary frame dimensions were selected to be representative of bay dimensions for frames located into a test-bed structure called the "MCEER Demonstration Hospital" (Yang

and Whittaker, 2002). The boundary frame with an aspect ratio (L/h) of 2.0 is taken from that hospital's structural system where L and h are the bay width and the height of the specimen respectively, but actual scale of the boundary frame is 1/2 of the prototype due to limitations of the testing apparatus.

Four specimens were considered in this study, namely:

- Specimen F1: Concentrically braced frame with single tube brace and vertical cold-formed steel studs (CFSS) spaced at 457.2 mm (18 in.) center-to-center
- Specimen F2: Concentrically braced frame with single tube brace and without vertical cold-formed steel studs
- Specimen F3: Concentrically braced frame with solid rectangular X braces and vertical cold-formed steel studs (CFSS) spaced at 457.2 mm (18 in.) center-to-center
- Specimen F4: Concentrically braced frame with solid rectangular X braces and without vertical cold-formed steel studs

Test set-up and specimens are shown in Figures 3-1 to 3-4 respectively. The above choice of specimens made it possible to compare the seismic energy dissipation behavior of frames with either slender or stocky brace members, the latter achieved by presence of the studs providing intermediate lateral supports and thus reducing the effective slenderness of the braces. The vertical CFSS were installed on both sides of the braces and connected to them. The connectors were detailed such as to reduce the length of the brace to prevent displacements both in the in-plane and out-of-plane directions. The intended result was a more stable, less pinched hysteretic loops with less stiffness and strength degradation under reversed cyclic loading. In essence, the objective was to use common nonstructural elements (such as steel stud walls), slightly modified, to help enhance the seismic behavior of a common concentric braced frame to near that of an idealized buckling prevented (or axially yielding) brace with hysteretic behavior schematically illustrated in Figure 3-5.

Note that in some cases, the above selected infill systems with CFSS on both sides of bracing members may result in an overall infill thickness (CFSS + brace) in excess of the flange width of the columns (depending on the story height and the brace type used). From the

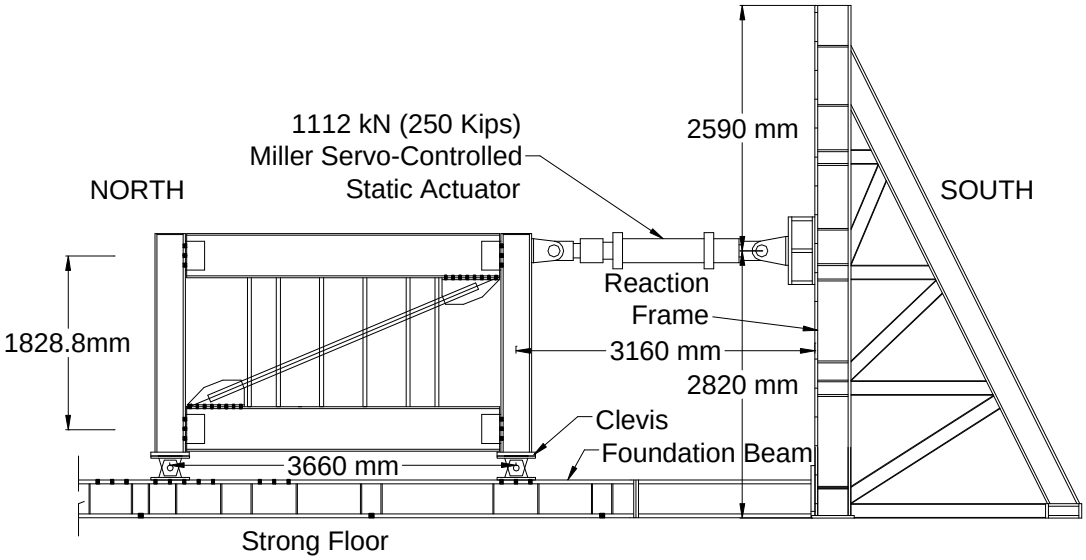

FIGURE 3-1 Test Set-Up for Specimen F1

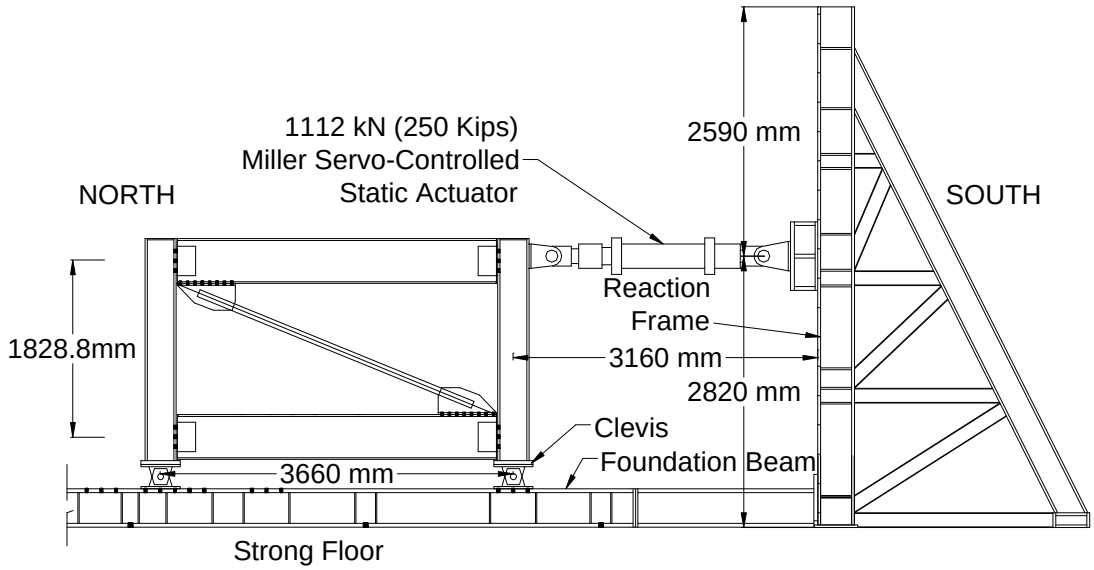

FIGURE 3-2 Test Set-Up for Specimen F2

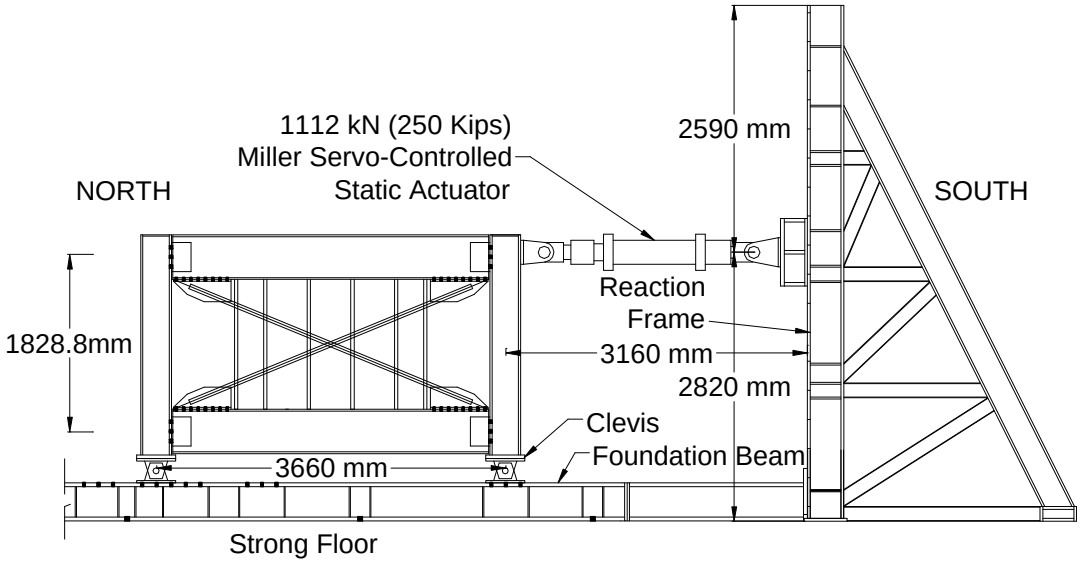

FIGURE 3-3 Test Set-Up for Specimen F3

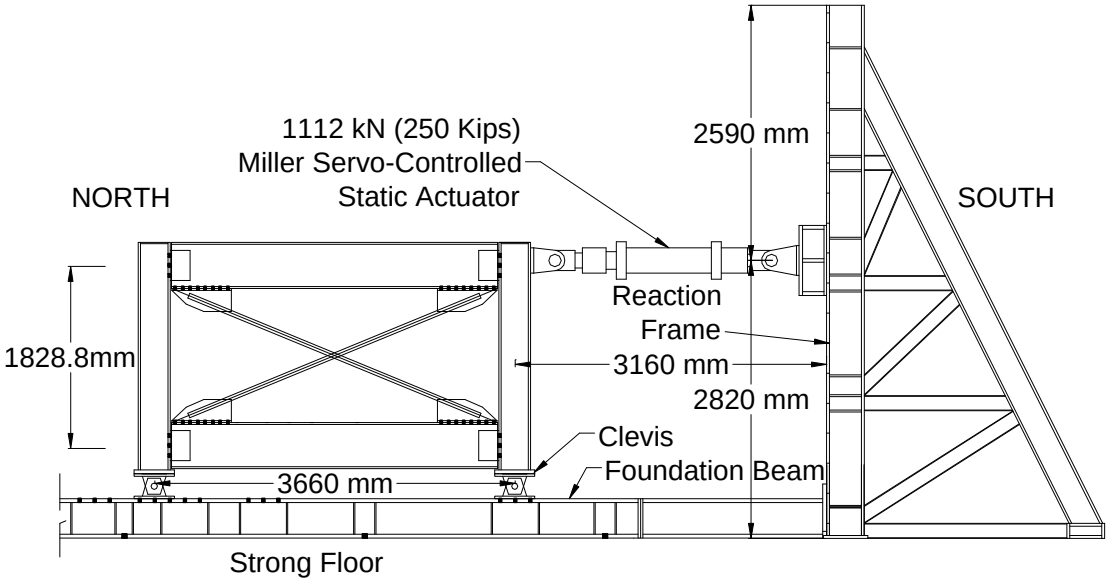

FIGURE 3-4 Test Set-Up for Specimen F4

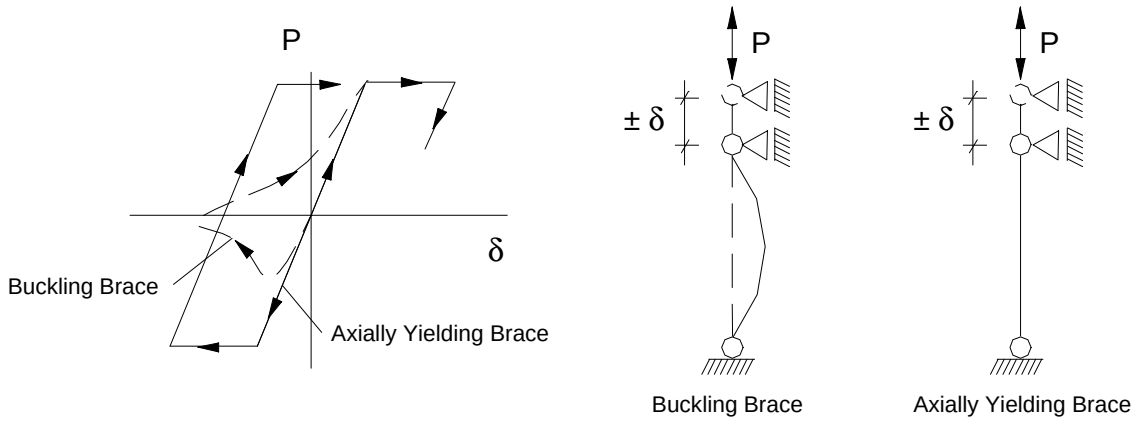

FIGURE 3-5 Specimen Design Concept: Hysteretic Behavior of Buckling and Axially Yielding Braces

architectural point of view, although this choice would lead to a small percent loss in the floor area, with appropriate architectural detailing, one could take the advantage of these walls to provide effective sound (in an interior wall) or thermal insulation (in an exterior wall) using double layer insulation material which could be inserted into each CFSS layers. Additionally, fire resistance for the infill and the boundary frame could also be provided when high density gypsum boards are selected as wall panels.

It was decided not to connect the X-braces at their mid-spans in Specimens F3 and F4, to ensure that all the brace segments (in Specimen F3) between studs would have sensibly the same buckling strength. Also, since the reference specimen for comparison was Specimen F3, the same detail was used in Specimen F4.

Finally, tubes and solid bars were used to investigate the impact of local buckling on hysteretic behavior. Since the fracture life of tube braces may be reduced significantly due to local buckling effects, one could question the usefulness of preventing global buckling of tubular braces. Specimens F1 and F2 allow to compare the fracture life of tube brace systems having low and high effective slenderness ratios.

3.3 Materials

ASTM A572 Gr.50 steel was used for the boundary frame and its beam-to-column and column-to-base plate connections. Coupon tests were not done for the boundary frame

members as the beams and columns were designed to remain elastic. However, cyclic tests were performed on the bare frames to characterize their hysteretic behavior as described later.

Dietrich CFSS products were used in this project. These studs are manufactured from corrosion resistant galvanized steel having a yield point of 50 ksi for 16 to 10 gages, and 33 ksi for all other gages. A 12 gage stud with 33 ksi yield point was used in this research. The minimum permitted tolerance on steel thickness per AISI (1996) is 95% of the specified thickness, and shapes are usually manufactured to match this lower permitted value. Properties for the light gage studs used here were taken from the Dietrich Product Data (2001).

Gas metal arc welding was selected for all welded connections. Miller S-22P12 24 V constant speed wire feeder and AWS A5.18: ER70S-6, ASME SFA 5.18 MIG (metal inert gas) continuous welding wires with 1.14mm diameter were used during the welding of the braces to the gusset plates. All welds were visually inspected, and no defects were found.

The solid bar braces, gussets and angle connectors for the studs were also ASTM A572 Gr.50. U brackets used as in-plane buckling restrainers, were ASTM A36 grade steel. The tube material was ASTM A500 Gr.B with minimum yield stress of 317 MPa (46 ksi). Bolts used for connections of the specimens are listed in Table 3.1, where actual clamping thickness refers to the thickness of the parts being connected by the bolts.

TABLE 3-1 Bolts Used

Steel Grade	Diameter (mm)	Actual Clamping Thickness (mm)	Quantity	Used to Connect
A490	25.4	39.1	96	Gussets-to-Boundary Frame
A307	12.7	12.1	96	Studs-to-Angle Connectors
A307	12.7	29.1	96	Angle Connectors-to-Beam
A307	12.7	81.4	24	U Brackets-to-Stud (F1)
A307	12.7	56.0	48	U Brackets-to-Stud (F3)

3.4 Details of Specimens

Boundary frame design details can be found in Berman (2002). Higher safety factors were used during the design of the boundary frames as it was designed to remain elastic under the maximum actuator force in a steel plate shear wall application in which demands on the

beams and columns were much larger. Member and connection design and detailing were carried out in accordance with the provisions of AISC (2002).

Double web-angle beam-to-column connections were welded to the beam web using typical 8mm fillet welds all around the angle legs. The upper and lower welds on the beams were terminated at 25mm from the face of the other leg to provide improved resistance to low-cycle fatigue. Connection to the column flanges used six 31.75mm (1¼") diameter A490 bolts designed to resist the maximum actuator load. Boundary frame details, such as beam-to-column, column-to-base plate, and column base plate-to-clevis, are shown in Figures 3-6 to 3-8. Typical all around 5mm fillet welds were used in the column-to-base plate connection. Six 38.1mm (1½") diameter A490 bolts were used to connect the 25.4mm (1in.) thick column base plates to the clevises. All the bolts used in beam-to-column and column base plate-to-clevis were designed as slip-critical bolts.

Braces were designed to be the largest possible that could be tested without exceeding the maximum force capacity of 1112kN (250Kips) of the largest actuator available in the laboratory, with a safety factor of 1.50, and taking strain hardening effects into account. As a result, single tube brace of 76.2mm by 76.2mm (3in.x3in.) with t=7.94mm (5/16in.) wall thickness, and solid X braces having a cross section of 25.4mm by 50.8mm (1in.x2in.), were selected. Square tube and solid rectangular bar brace details are given in Figure 3-9. Tube braces had 431.8mm long and 12.7mm wide slots at each end for welded connection to gussets.

Detailed geometric dimensions of Specimens F1 to F4 are illustrated in Figures 3-10 to 3-13 respectively. Note that all boundary frames and their member connections are identical for each specimen. Furthermore, tube brace-to-gusset and gusset-to-beam connections for Specimens F1 and F2, and solid bar brace-to-gusset and gusset-to-beam connection details for Specimens F3 and F4 are given in Figures 3-14 and 3-15 respectively.

All cold-formed steel studs used in Specimen F1 and Specimen F3 were 5½" CSJ 12 gage by Dietrich (2001). Their sectional dimensions were determined to resist the forces generated by the braces at the onset of buckling in the out-of-plane direction. These lateral forces were estimated to equal 5% percent of the compressive strength of the brace, by analogy to the

stiffness and strength lateral bracing design requirements suggested in Salmon and Johnson (1996) for discrete braces.

Connections for thin-walled members were done using A307 Grade, 12.7mm diameter bolts supplied by Johnson Fastener Corp., a local supplier. Cold-formed stud-to-beam connection details for Specimens F1 and F3 are shown in Figures 3-16 and 3-17 respectively.

Details regarding custom made U brackets used as in-plane buckling restrainers, are given in Figures 3-18 and 3-19. These U brackets restrainers were used to prevent introducing holes in the small braces, which could have triggered net section failures during severe axial displacements. Essentially two types of U brackets were designed for each specimen with CFSS. The distinctive feature of the connection detail around the brace and CFSS intersection region is that there is no mechanical connection to the braces. CFSS members are connected to each other via their inner flanges using a long, 12.7mm diameter bolt passing through the holes on the brackets. U brackets and CFSS members were to be in perfect contact with the brace surfaces to provide a direct load transfer. Small spacers having the same section of the bar brace were used in Specimen F3 to fill the gap in the connection.

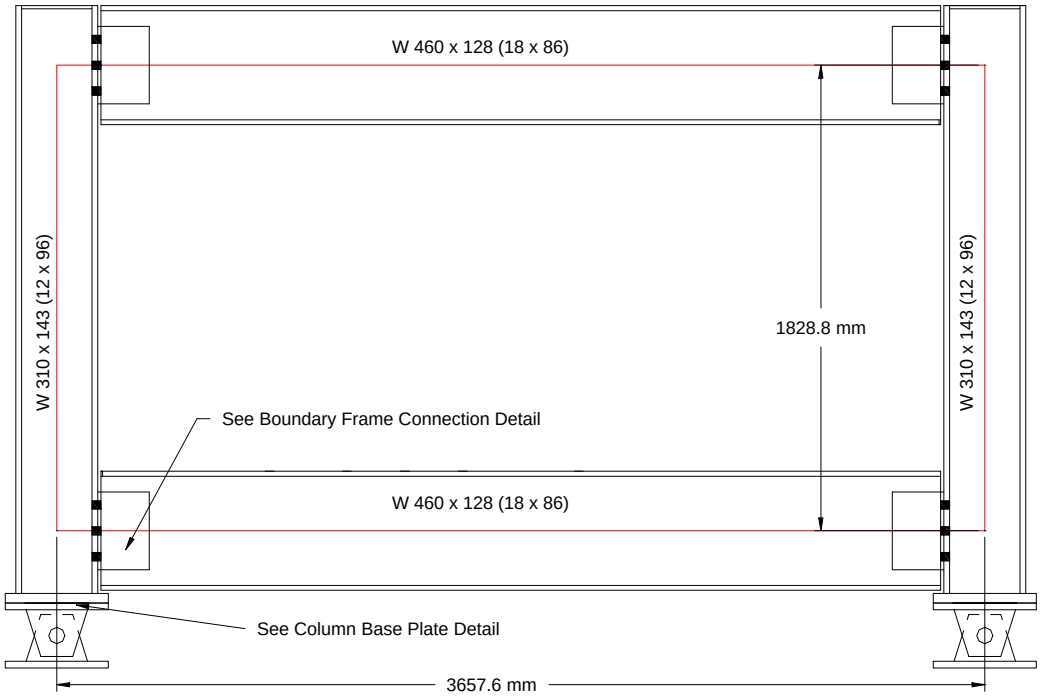

FIGURE 3-6 Boundary Frame General View

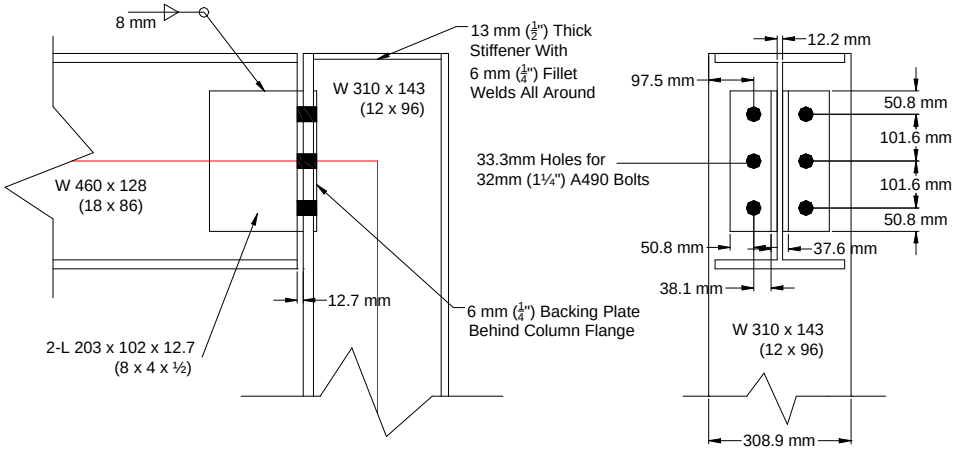

FIGURE 3-7 Double Web-Angle Beam-to-Column Connection Detail

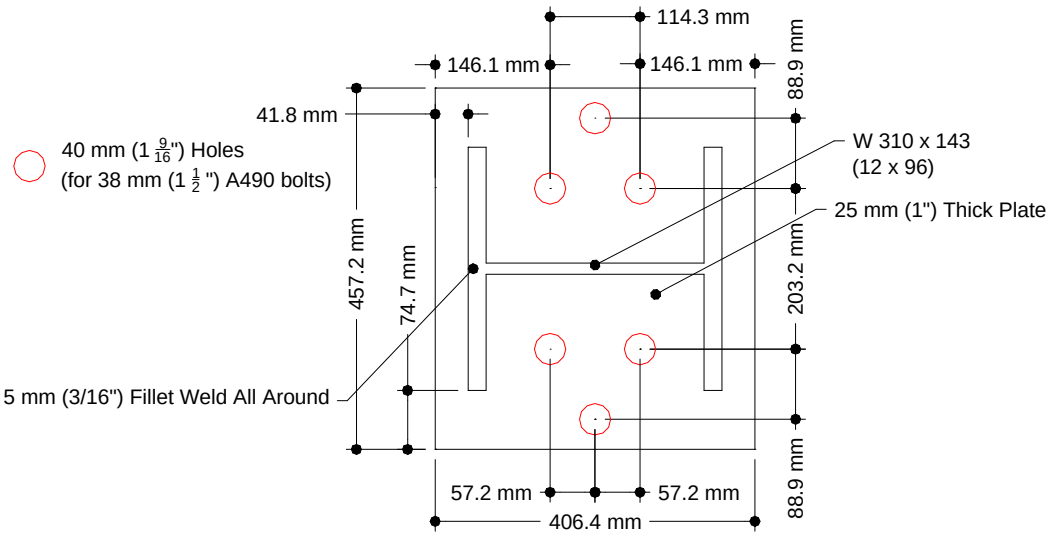

FIGURE 3-8 Column Base Plate Detail

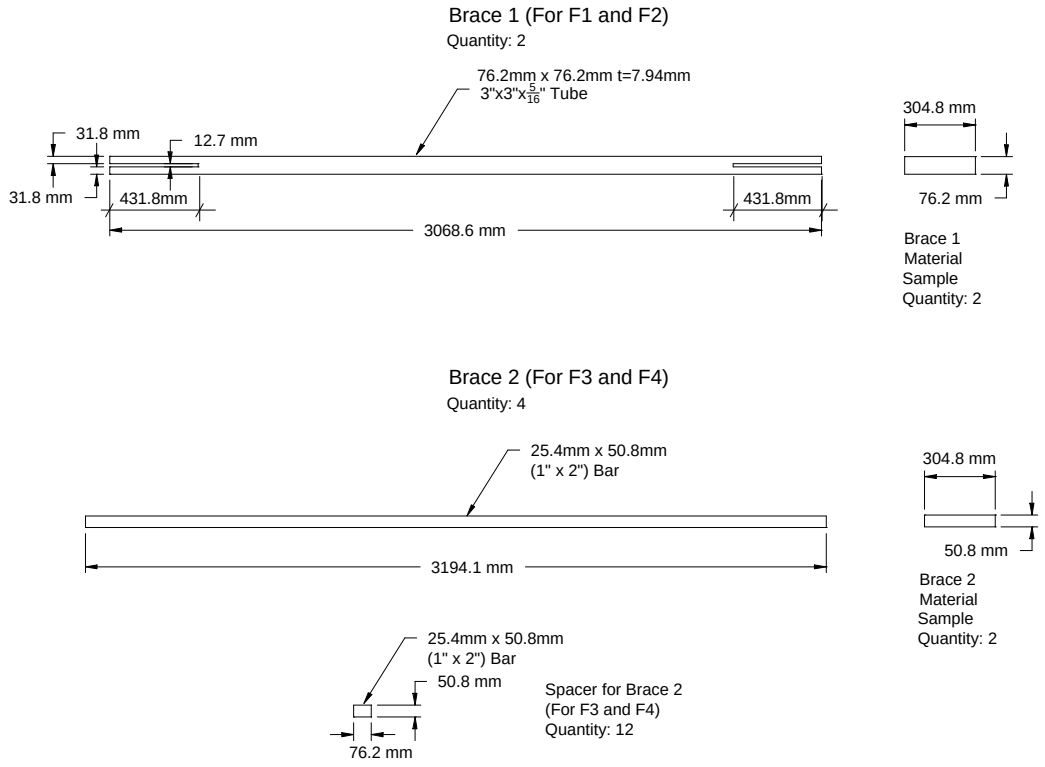

FIGURE 3-9 Details of Steel Brace Members for the Specimens

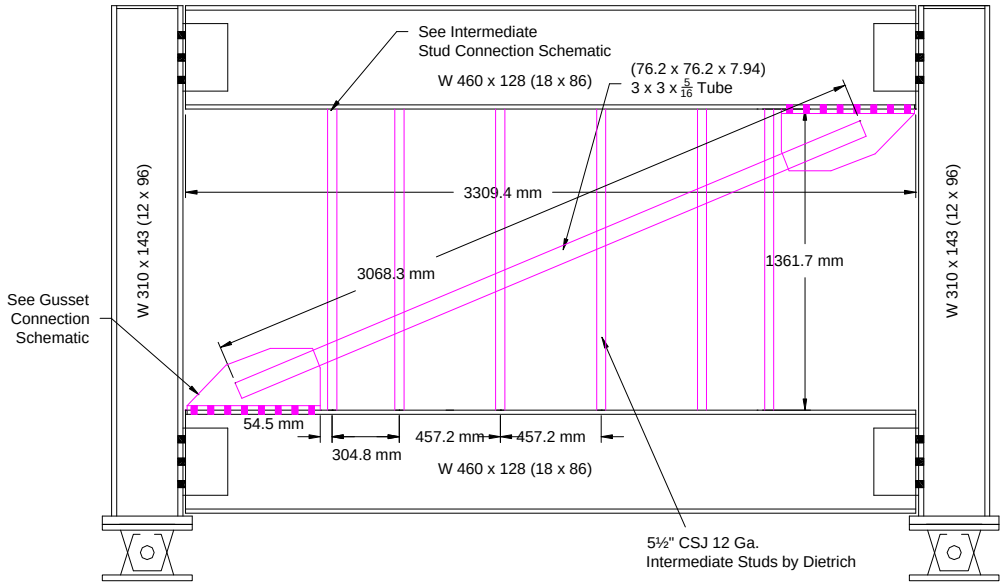

FIGURE 3-10 Schematic of Specimen F1

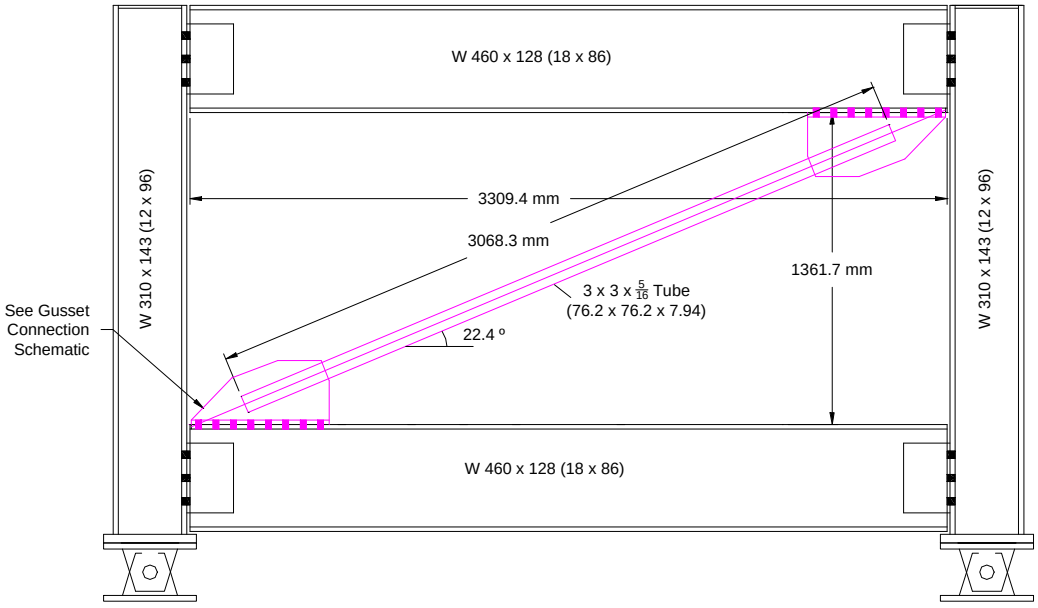

FIGURE 3-11 Schematic of Specimen F2

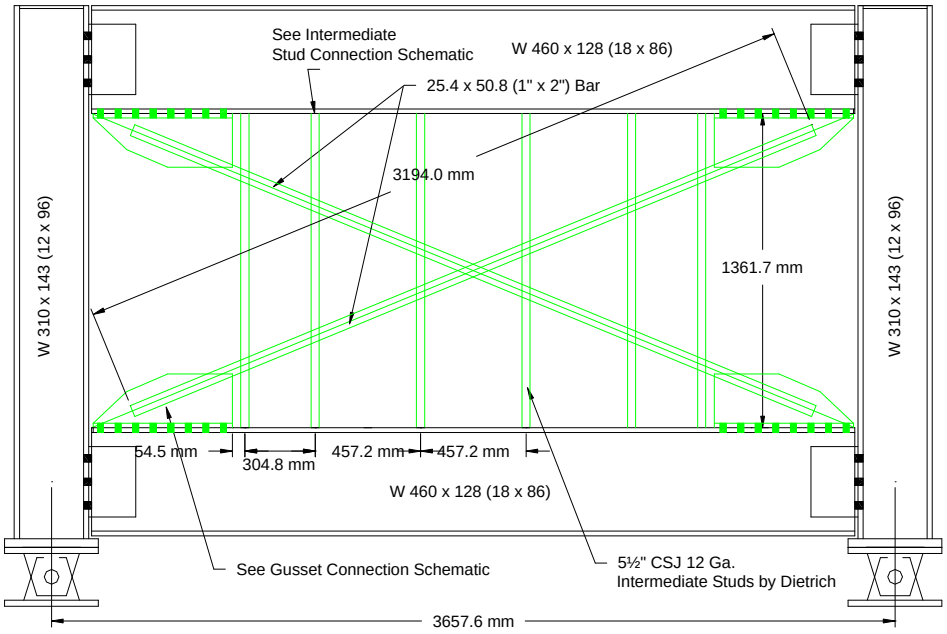

FIGURE 3-12 Schematic of Specimen F3

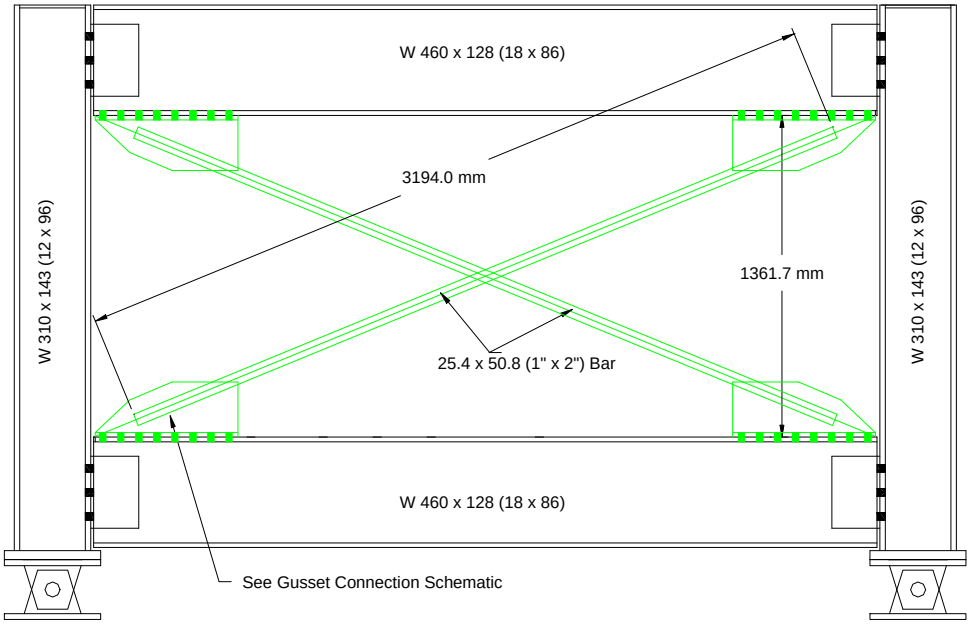

FIGURE 3-13 Schematic of Specimen F4

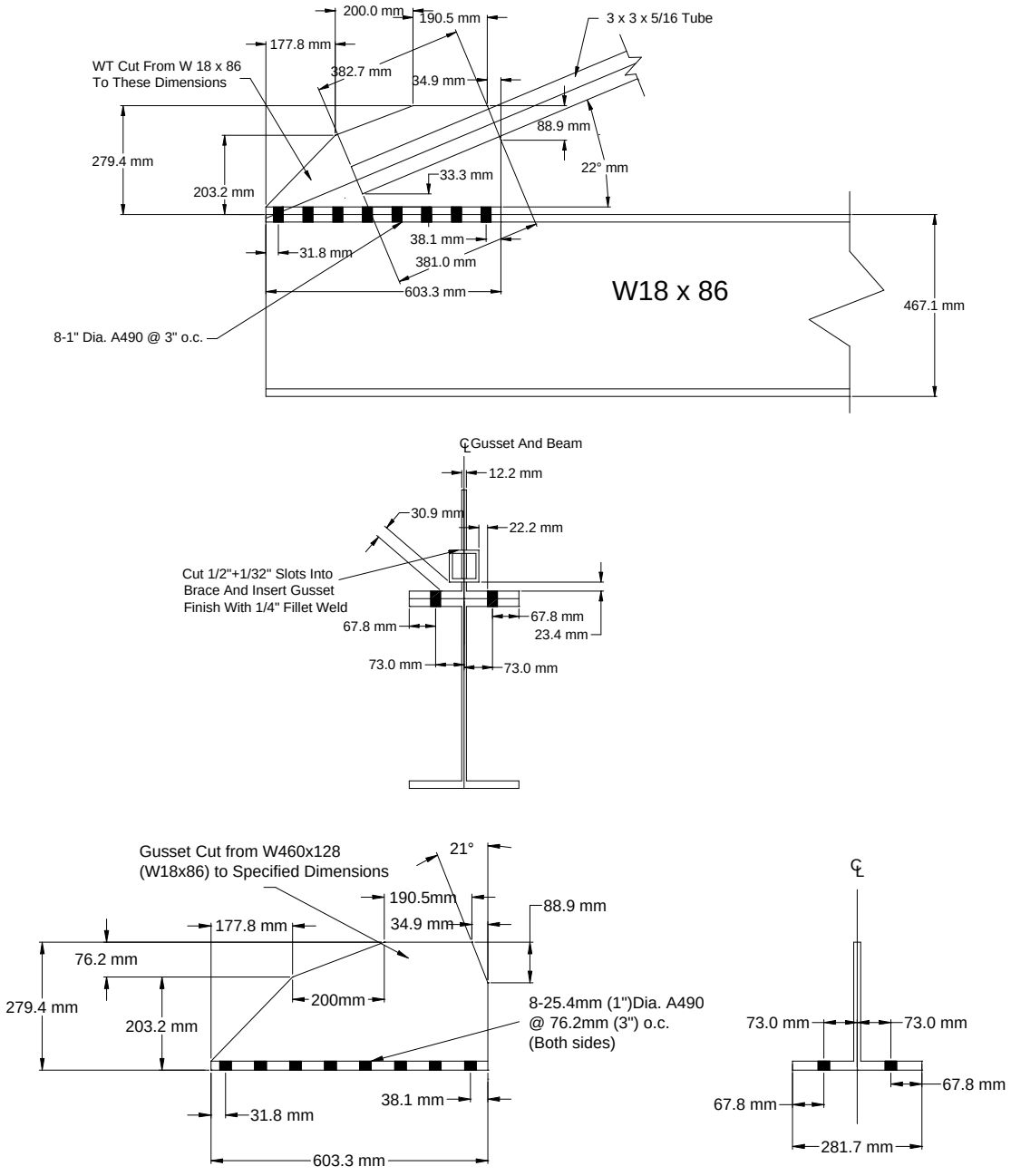

Gusset 1 (For F1 and F2)
Quantity: 4

FIGURE 3-14 Tube Brace-to-Gusset and Gusset-to-Beam Connection Details for Specimens F1 and F2

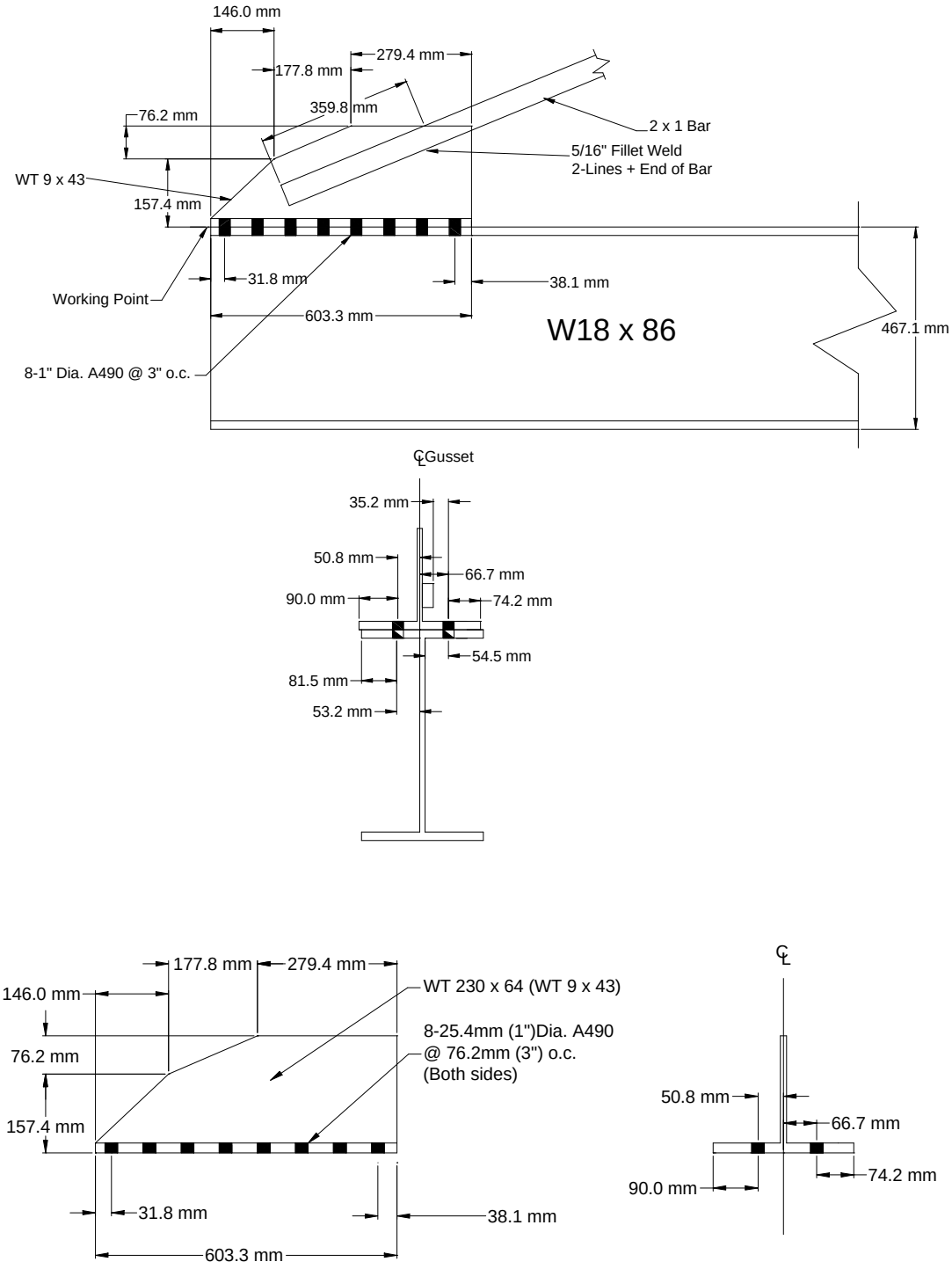

Gusset 2 (For F3 and F4)
Quantity: 8

FIGURE 3-15 Bar Brace-to-Gusset and Gusset-to-Beam Connection Details for Specimens F3 and F4

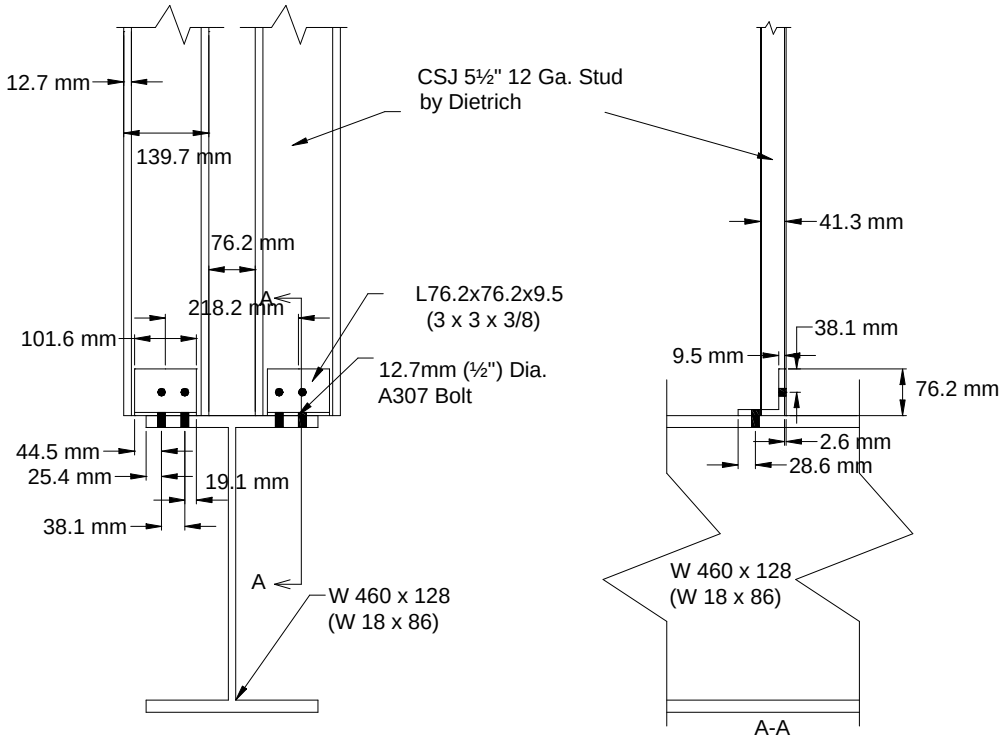

FIGURE 3-16 Cold-Formed Steel Stud-to-Beam Connection Details for Specimen F1

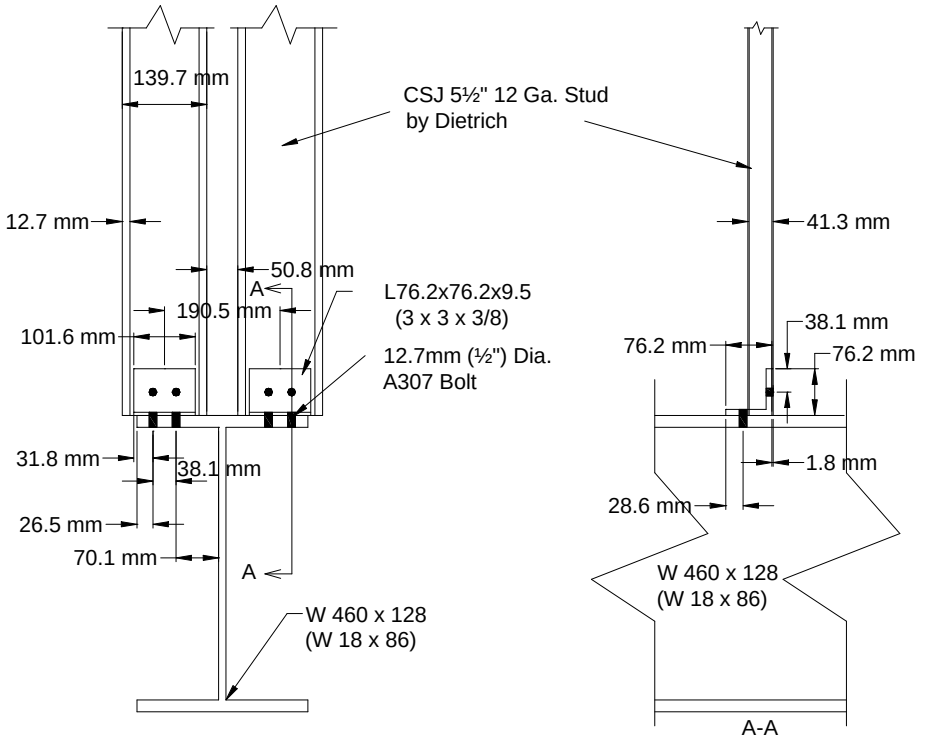

FIGURE 3-17 Cold-Formed Steel Stud-to-Beam Connection Details for Specimens F3

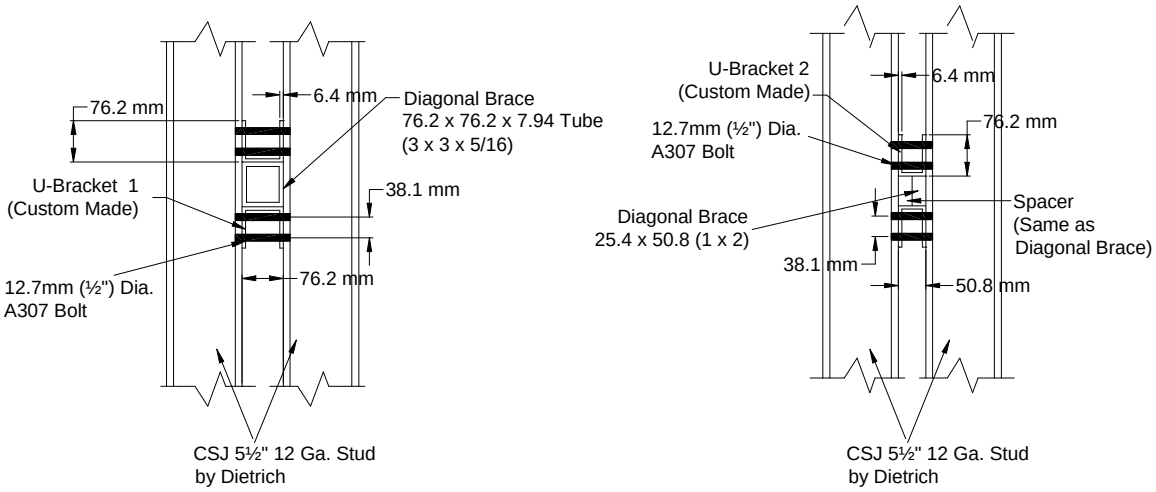

FIGURE 3-18 U-Brackets-to-Cold Formed Steel Stud Bolted Connection Details for Specimens F1 and F3

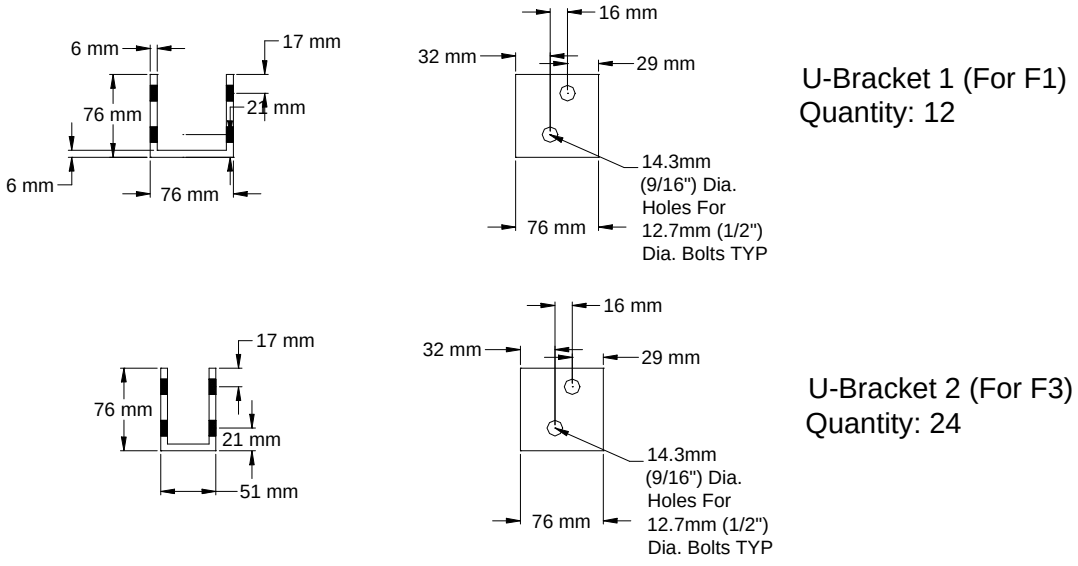

FIGURE 3-19 U-Brackets for Brace-to-Cold Formed Steel Stud Connection

3.5 Coupon Tests

ASTM Standard coupon tests (ASTM, 2002) were carried out to determine the brace material yield stress and strains. Four coupons from the tubes and two from the solid bar braces (Figure 3-20a) were prepared and tested in the Axial-Torsion MTS Machine (Figure 3-20b) in the University at Buffalo's Structural Engineering and Earthquake Simulation Laboratory (SEESL). Strain gauges were used to obtain strains in the coupons.

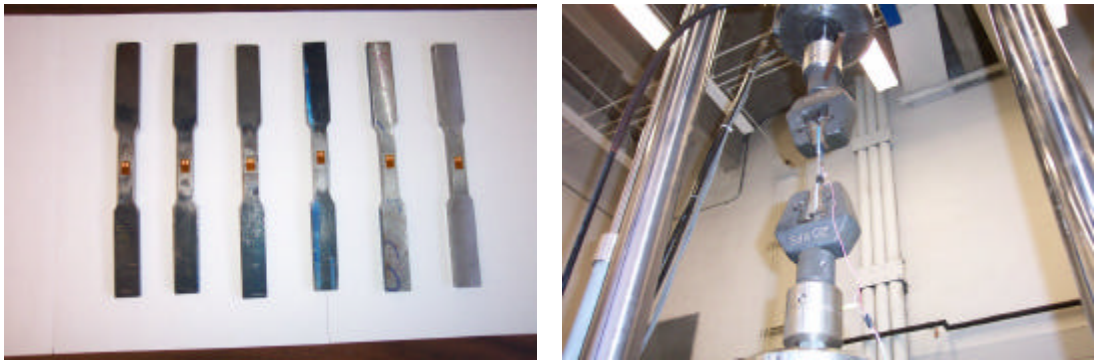

(a) **(b)**

FIGURE 3-20 Coupon Tests: (a) Coupons from the Brace Members (b) MTS Axial-Torsion Testing Machine

Results are presented in Table 3.2. The yield strength of the tube brace coupons is calculated using a 0.2% strain offset, since this steel exhibited no definite yield plateau. The solid bar coupons had an elastic-plastic behavior.

TABLE 3-2 Coupon Test Results

Coupon	Thickness (mm)	Width (mm)	Area (mm^2)	F_y (MPa)	ε_y (mm/mm)	Total Elongation (%)
Bar-1	9.5	12.7	120.7	384	0.00191	10.2
Bar-2	9.6	12.7	121.9	370	0.00193	8.6
Tube-1	7.4	12.7	94.0	380	0.00386	NA
Tube-2	7.4	12.7	94.0	395	0.00463	8.6
Tube-3	7.2	12.7	91.4	381	0.00404	7.8
Tube-4	7.3	12.7	92.7	383	0.00408	9.4

Stress-strain diagrams of the coupons are depicted in Figure 3-21. Note that Coupon Tube 1 did not fracture due to grip slippage, threfore no reliable data were available for elongation.

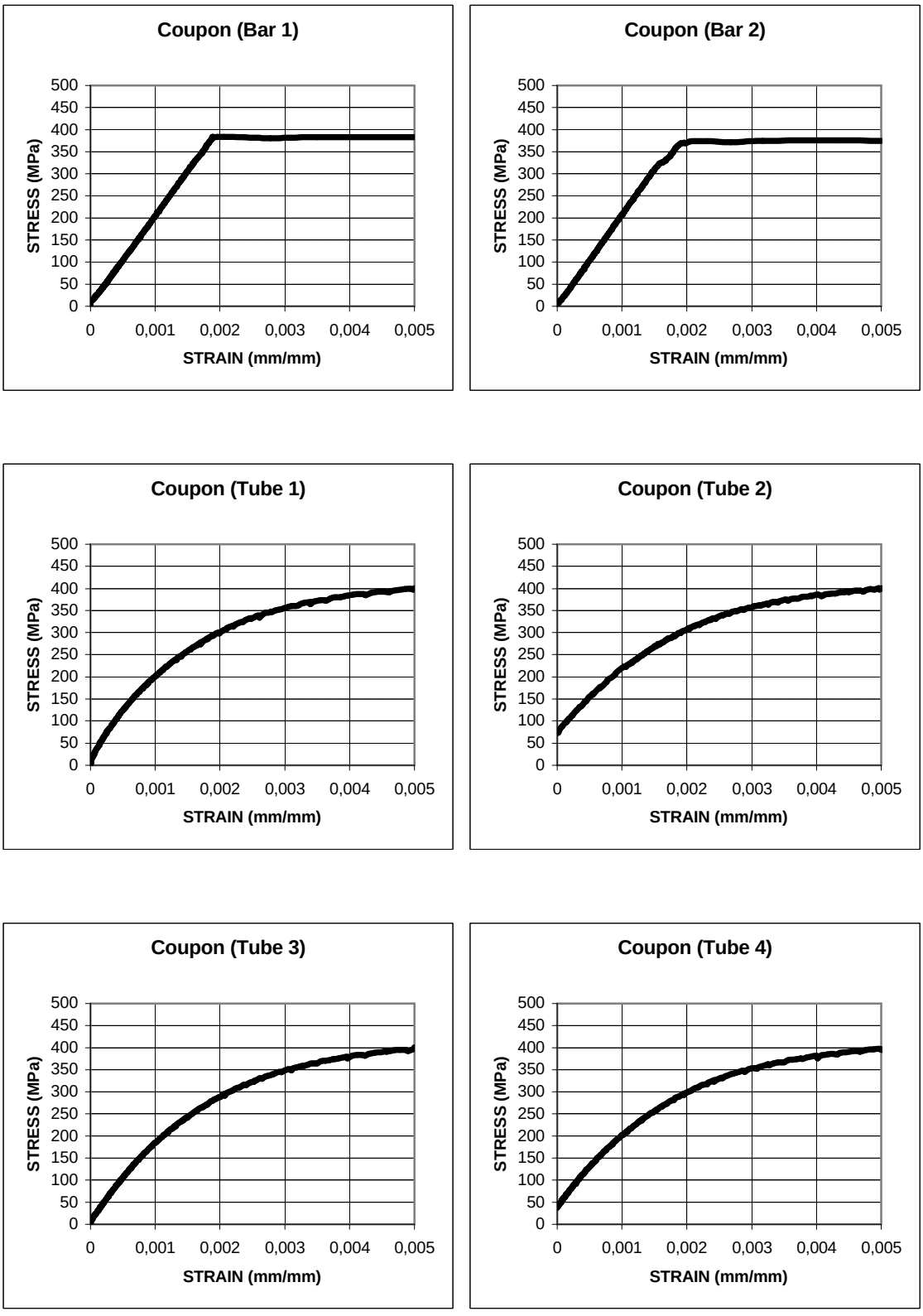

FIGURE 3-21 Stress-Strain Diagrams for Brace Coupons-Data Truncated at 0.005 (mm/mm) Strain Level

This material data were used in static pushover analyses of the specimens conducted using SAP2000 (CSI, 1998) to predict the load-displacement curves of the specimens. No coupon tests were performed on the cold-formed steel studs, boundary frame elements, and connections, since no failure was expected in those elements.

3.6 Specimen Construction

3.6.1 General

Construction sequence is reported in this section. In general, bolts in the beam-to-column connections, column base plate-to-clevis, clevis-to-foundation beam, and gusset-to-beam connections, were tightened using a HYTORC Blitz 4-A hydraulic torque wrench to their specified tension following the "turn-of-the-nut" method described in the AISC LRFD manual (AISC, 2001). Nuts of the bolts used in stud-to-angle, angle-to-beam, and stud-to-stud connections were in snug-tight condition. To achieve full contact on every surface between the braces and the vertical studs as well as between the U brackets and the braces, holes for the bolts on the stud flanges were marked in-place prior to drilling.

3.6.2 Specimen F1

First, holes for gussets and angle connectors were drilled on the beam flanges. The boundary frame was then assembled by torquing the bolts in the beam-to-column connections. Gussets and angle connectors were installed, and their bolts were tightened. Tube brace was placed, adjusted to its specified angle, and welded to the gussets. Cold-formed steel studs were temporarily placed, and the holes for bolts were marked in-place. This procedure was followed for every stud. The studs were then removed after marking. The holes were drilled, and the studs were re-installed in the frame. All bolts were mounted in loose condition first, and after final adjustments using a digital level, all bolts were tightened to be snug-tight.

Prior to testing, final check of in-plane and out-of-plane plumbness of the studs was done. Specimen F1 was then mounted on the clevises located on the steel foundation beam. Six 38.1mm diameter A490 bolts were used to connect each column base plate to the corresponding clevis, and then to attach the clevis to the foundation beam. The Miller servo-controlled static rated actuator with a load capacity of 1112 kN (250 kip) and an available stroke of 203.2mm (8") was mounted to the reaction frame using six 25.4mm diameter high

strength threaded rods. Four similar rods were used to connect the actuator to the test specimen. The actuator was equipped with swivels at each end and end plates with threaded holes to accept the rods. Figure 3-22a to 3-22c show general and close-up views from Specimen F1 prior to testing. Inside view of the infill system between CFSS, angle connectors for studs, stud-to-tube brace connection (U bracket as in-plane buckling restrainer), stud-to-upper beam connection, stud-to-lower beam connection, brace-to-stud connection (in-plane and out-of-plane buckling restrainers), general infill view, tube brace-to-lower beam connection, tube brace-to-upper beam connection, all around fillet welding for brace-to-gusset slotted connection, gusset-to-lower beam bolted connection, connection detail around gusset, and boundary frame-to-foundation beam bolted connection details are indicated Figures 3-22d to 3-22 p respectively.

3.6.3 Specimen F2

Preparation of Specimen F2 was relatively easier than the first specimen. After testing of Specimen F1, cold-formed steel studs and the tube brace were removed. A new, identical tube was then installed in the frame, adjusted to its specified angle, and welded to the gussets. This time the other two gussets were used to weld the tube. In other words, the orientation of the tube brace of Specimen F2 was in the opposite direction of the tube used in Specimen F1. Figures 3-23a and 3-23b show welding process, and a general view after completion of the specimen assembly.

3.6.4 Specimen F3

A new boundary frame having new beam-to-column connections was used for the testing of Specimens F3 and F4. Similarly, holes for gussets and angle connectors were drilled on the beam flanges. The boundary frame was then assembled by torquing the bolts in the beam-to-column connections. New gussets and angle connectors were installed, and their bolts were tightened. Solid bar X brace was placed, adjusted to its specified angle, and welded to the gussets. Cold-formed steel studs were temporarily placed, and the holes for bolts were marked in-place. The studs were then removed after marking. The holes were drilled, and the studs were re-installed in the frame. All bolts were mounted in loose condition first, and after final adjustments, all bolts were tightened to be snug-tight.

Prior to testing, final check of in-plane and out-of-plane plumbness of the studs was done. Specimen F3 was then mounted on the clevises located on the steel foundation beam in the same way as was done for Specimen F1. Installation of solid bar braces, assembly of vertical studs, general view of Specimen F3, new double angle beam-to-column connections, brace-to-stud connection (in-plane and out-of-plane buckling restrainers), closer view to buckling restrainers and spacers, cross over detail for solid bar braces, inside view of infill between studs, closer view to middle region, brace-to-gusset welded and gusset-to-lower beam bolted connections, and angle connectors for vertical studs are illustrated in Figures 3-24a to 3-24q respectively.

3.6.5 Specimen F4

After testing of Specimen F3, cold-formed steel studs and the solid bar braces were removed. New gussets were installed in the frame. Identical solid bar braces were then placed in the frame, adjusted to its specified angle, and welded to the gussets. Placing new gussets, welding of the braces to the gussets, cross over detail of braces, brace-to-gusset welded and gusset-to-upper beam bolted connections, same connection viewed from the other side, and Specimen F4 after construction and in-place in test frame are given in Figures 3-25a to 3-23f.

(a)

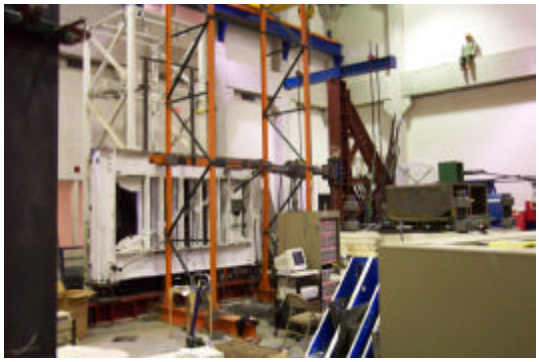

(b)

(c)

(d)

(e)

(f)

FIGURE 3-22 Construction Details for Specimen F1: (a) General View; (b) Experimental Set-Up; (c) Closer View of Boundary Frame; (d) Inside View of Infill Between Studs; (e) Angle Connectors for Studs; (f) Stud-to-Tube Brace Connection (U Bracket In-plane Buckling Restrainer)

(g)

(h)

(i)

(j)

(k)

(l)

FIGURE 3-22 Construction Details for Specimen F1 (continued): (g) Stud-to-Upper Beam Connection; (h) Stud-to-Lower Beam Connection; (i) Brace-to-Stud Connection (In-plane and Out-of-Plane Buckling Restrainers); (j) General Infill View; (k) Tube Brace-to-Lower Beam Connection; (l) Tube Brace-to-Upper Beam Connection

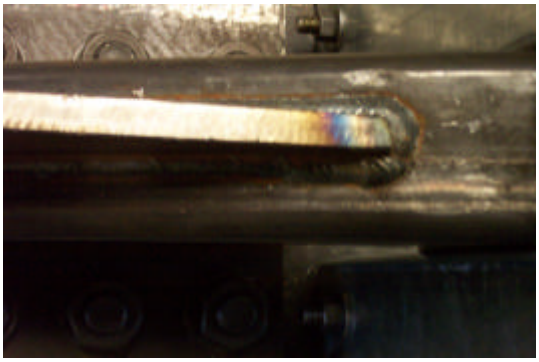

(m)

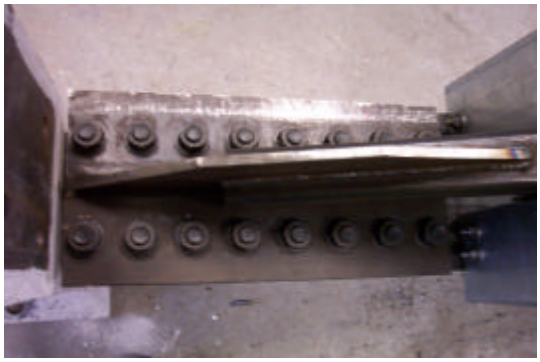

(n)

(o)

(p)

FIGURE 3-22 Construction Details for Specimen F1 (continued): (m) All Around Fillet Welds for Brace-to-Gusset Slotted Connection; (n) Gusset-to-Lower Beam Bolted Connection; (o) Connection Detail Around Gusset; (p) Boundary Frame-to-Foundation Beam Bolted Connection

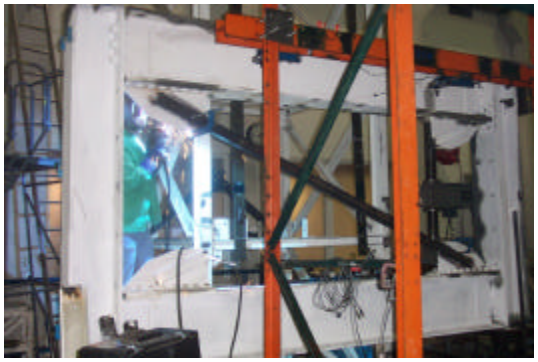

(a)

(b)

FIGURE 3-23 Construction Details for Specimen F2:
(a) Tube Welding; (b) General View

(a)

(b)

(c)

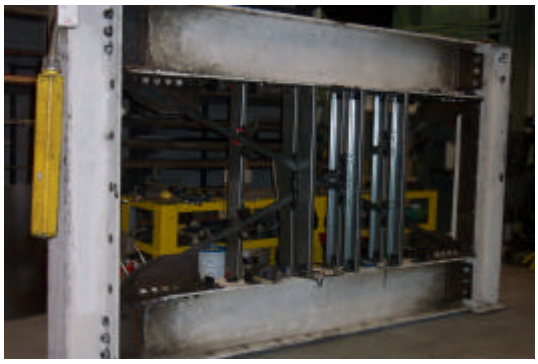

(d)

(e)

(f)

(g)

FIGURE 3-24 Construction Details for Specimen F3: (a) Welded Solid Bars; (b,c,d,e,f) Assembly of Vertical Studs; (g) Specimen F3 After Construction

(h) **(i)** **(j)**

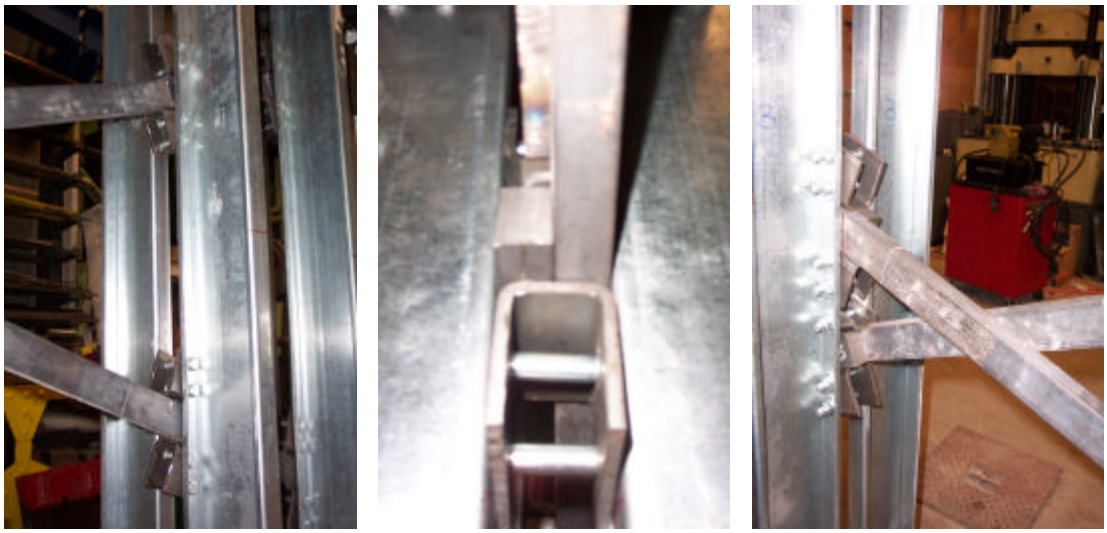

(k) **(l)** **(m)**

FIGURE 3-24 Construction Details for Specimen F3 (continued): (h) Specimen F3 After Construction; (i,j) Beam-to-Column Double Angle Bolted Connection; (k) Brace-to-Stud Connection (In-plane and Out-of-Plane Buckling Restrainers); (l) Closer View to Buckling Restrainers and Spacer; (m) Cross Over Detail for Solid Bar Braces (No Connection at the Intersection)

(n)

(o)

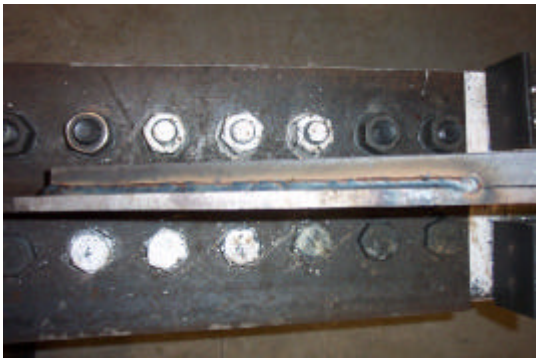

(p)

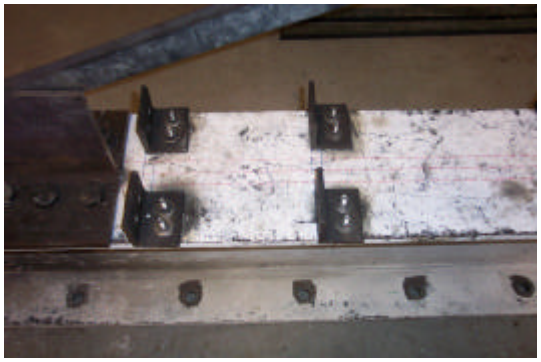

(q)

FIGURE 3-24 Construction Details for Specimen F3 (continued): (n) Inside View of Infill Between Studs; (o) Closer View to Middle Region (p) Brace-to-Gusset Welded and Gusset-to-Lower Beam Bolted Connections; (q) Angle Connectors for Vertical Studs

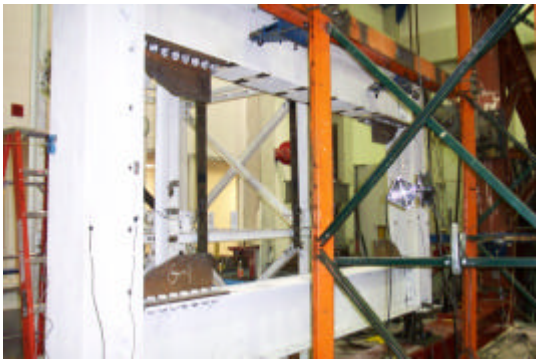

(a)

(b)

(c)

(d)

(e)

(f)

FIGURE 3-25 Construction Details for Specimen F4: (a) New Gussets; (b) Solid Brace Welding; (c) Cross Over Detail for Solid Bar Braces (No Connection at the Intersection); (d) Brace-to-Gusset Welded and Gusset-to-Upper Beam Bolted Connections; (e) Same, Viewed from Other Side; (f) Specimen F4 After Construction and In-place in Test Frame

3.7 Instrumentation

3.7.1 Strain Gauges

Instrumentation layout for Specimens F1 to F4 is shown in Figures 3-26 to 3-29 respectively. Vishay Measurements Group, CEA-06-125UW-120 type (120 ohm resistance) strain gauges were used to instrument all four specimens, and installed per manufacturer's recommendations. In total, 40, 28, 52 and 40 strain gauges were installed on Specimens F1, F2, F3, and F4 respectively. A few gauges were used at the mid-point of each column and beam of the boundary frames to monitor the internal forces and verify that they remained elastic, as designed. These gauges were re-used for each subsequent test.

Each tube and solid bar brace was instrumented by twelve strain gauges. Three points were selected along each brace and four strain gauges were used at each selected point, i.e. one on each face of the member at the midpoint of each side. No strain gauges were attached on the web angles of the beam-to-column connections, column base plates, or gussets and stud end connections, since these were designed to remain elastic at the maximum applied load. In Specimens F2 and F4, strain gauges were mounted on the braces at $L_D/4$, $5L_D/8$ and $7L_D/8$ measured from the lower gusset-brace intersection point, where L_D is the clear diagonal length of a brace measured as the distance between the lower and upper brace-to-gusset connection points. In the specimens with concentric braces and cold formed steel studs (F1, F3), a slightly different layout for the strain gauges was selected to clear the obstruction created by the vertical studs. Strain gauges were installed between the second and third, third and forth, forth and fifth studs (counting from the north). These gauges were placed at a horizontal distance of 114.3mm (1/4 of the intermediate stud spacing) from the stud vertical centerline. The strain gauges were configured as quarter bridges.

Cold formed steel studs were instrumented only on one section flange at the midheight of the stud length. The east and west sides of the studs (outward sides) were selected for the strain gauge application by assuming a symmetric stress and strain distribution over the stud cross section. Since the studs were all galvanized steel, it was necessary first to remove the galvanized layer over a small area of the stud flange to provide an appropriate surface for strain gauge application.

3.7.2 Temposonics

The magnetostrictive transducers (Temposonics) layout was identical for all specimens. T1W was used for displacement control during testing, and T1E served as a backup. TP1 and TP2 were used to measure brace longitudinal displacements, and TP3 was installed at 45° from the horizontal to indirectly measure frame sway, again as backup data. To further quantify sway of the frame as a function of height, T2 and T3 were mounted to measure drift of the north column outer flange at the levels of midheight of the column, and at the level of the bottom beam centerline. T4 was used to monitor movement of the north clevis (if any) with respect to the foundation beam.

3.7.3 Potentiometers

Six diplacement potentiometers (DP) were used to measure the vertical and horizontal displacement of the foundation beam under the south clevis, and for measuring the opening and closing of the web-angle connections. The latter was achieved by placing a DP horizontally on top of the beam flange at each beam-to-column connection. The DP layout was the same for all four specimens.

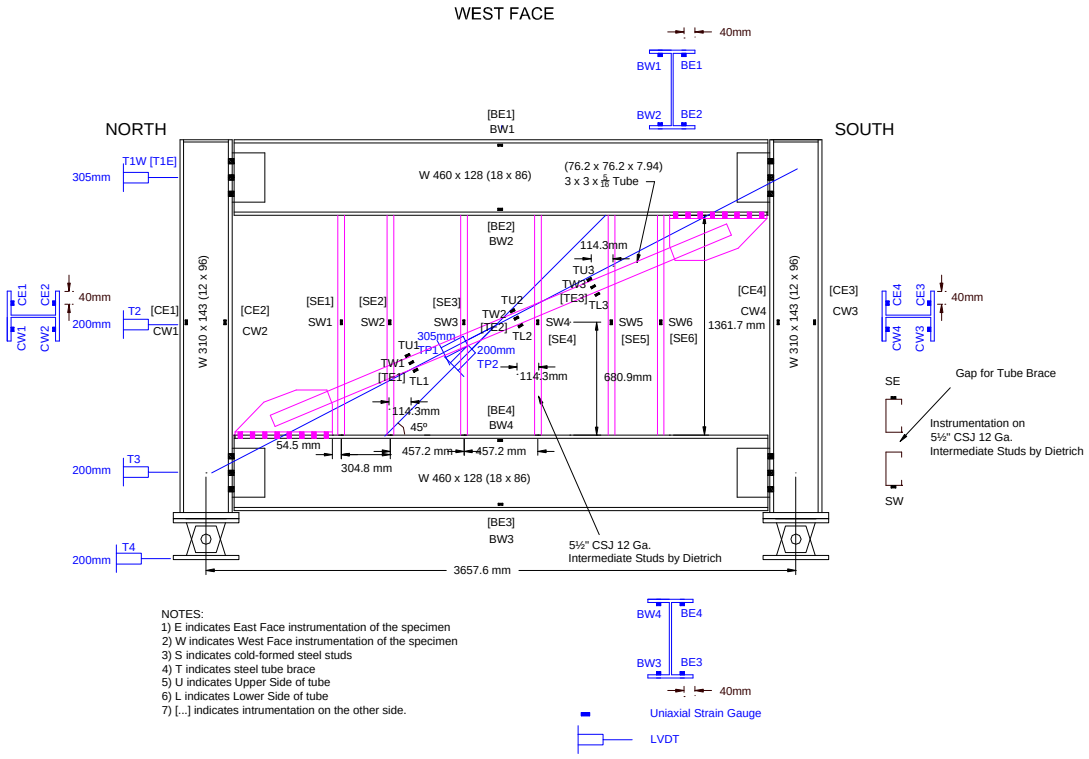

(a)

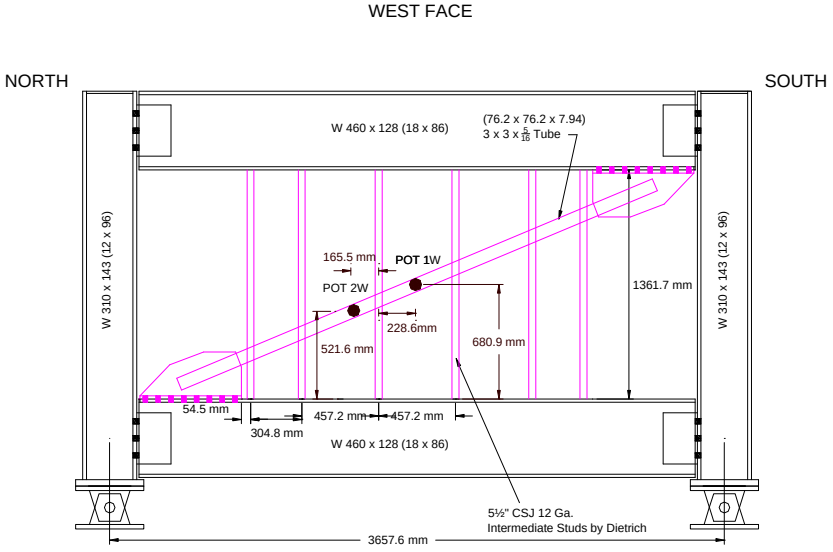

(b)

FIGURE 3-26 Instrumentation for Specimen F1: (a) In-Plane Displacement Measurement (Temposonics) and Strain Gauges; (b) Out-of-Plane Displacement Measurement (Potentiometers)

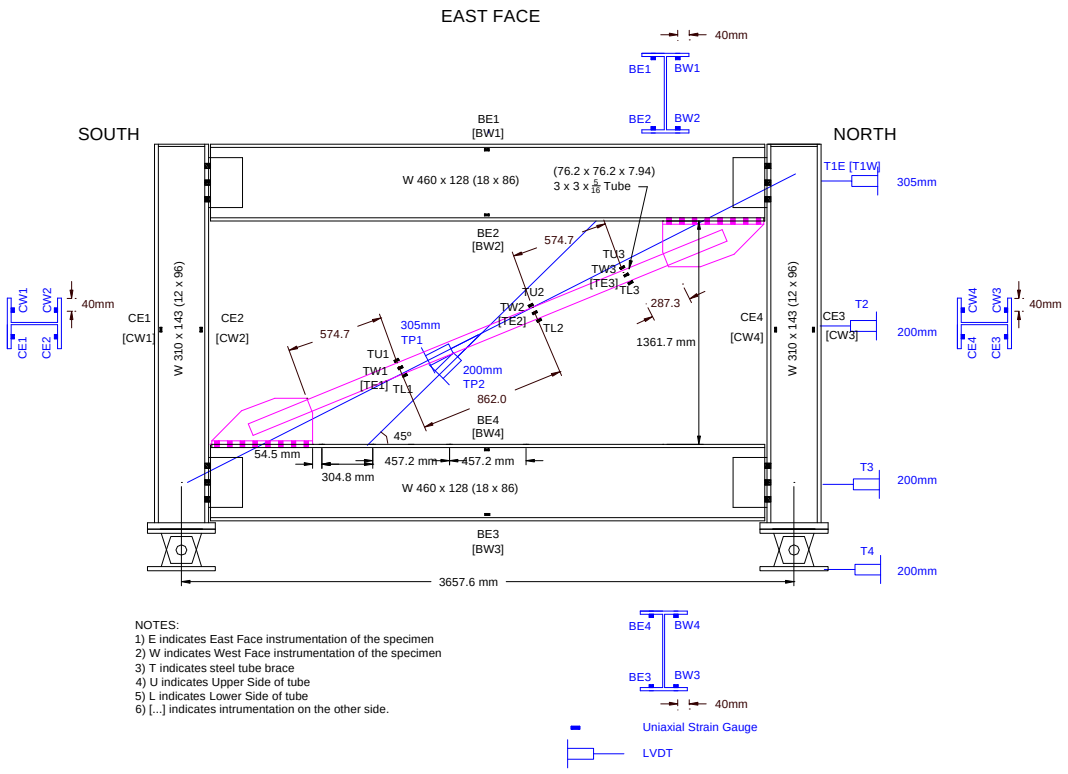

(a)

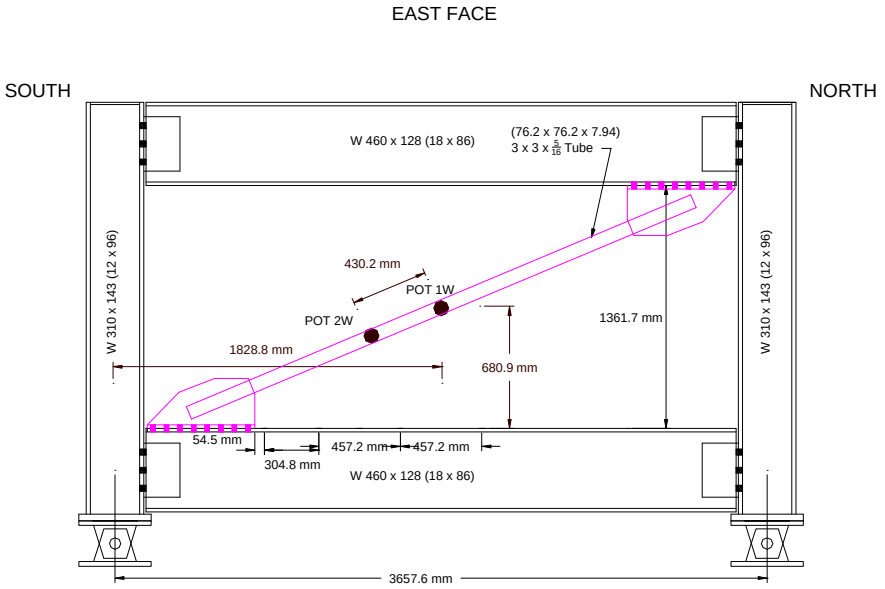

(b)

FIGURE 3-27 Instrumentation for Specimen F2: (a) In-Plane Displacement Measurement (Temposonics) and Strain Gauges; (b) Out-of-Plane Displacement Measurement (Potentiometers)

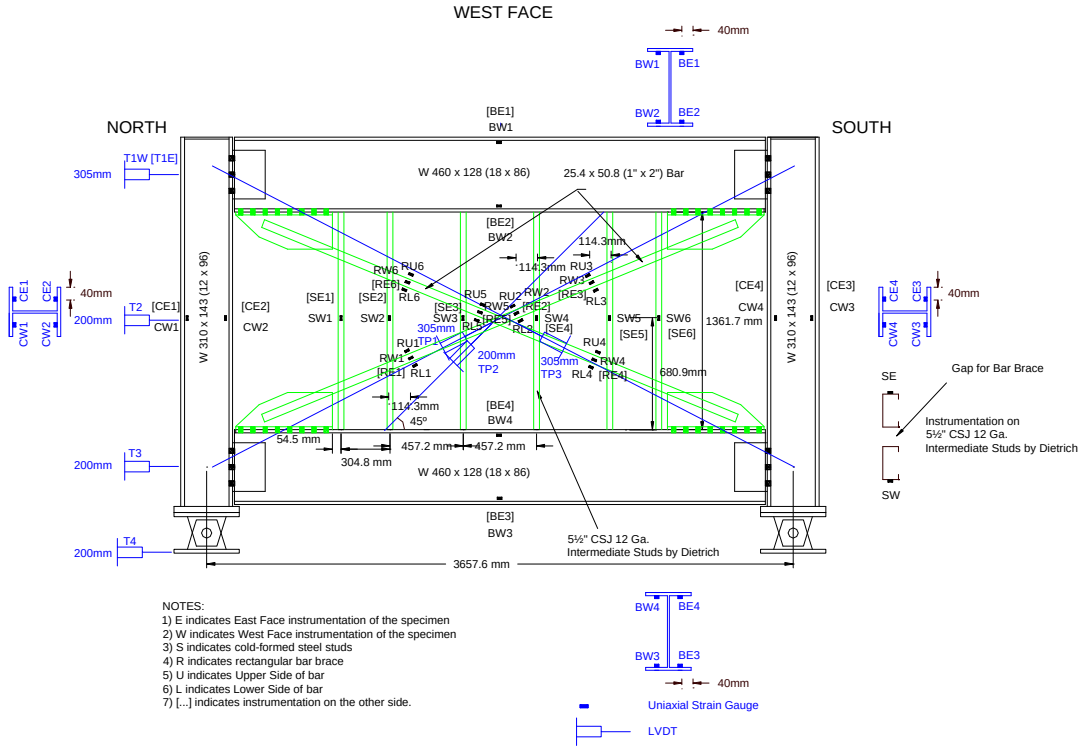

(a)

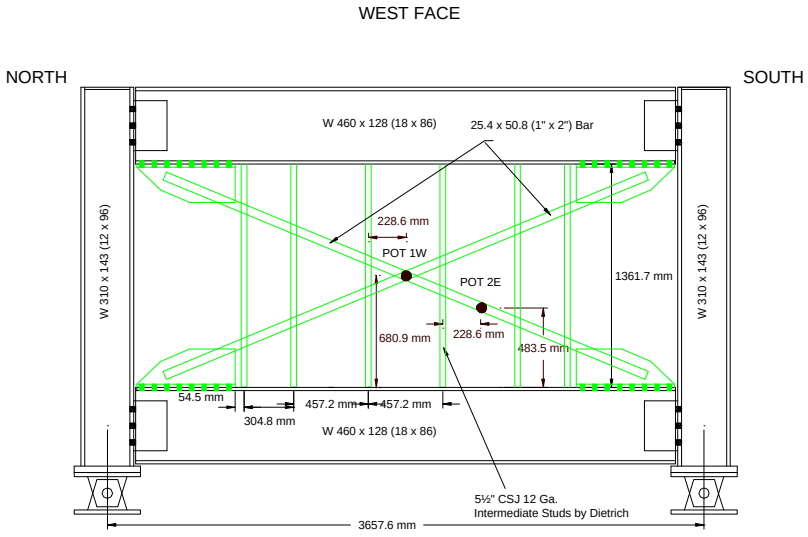

(b)

FIGURE 3-28 Instrumentation for Specimen F3: (a) In-Plane Displacement Measurement (Temposonics) and Strain Gauges; (b) Out-of-Plane Displacement Measurement (Potentiometers)

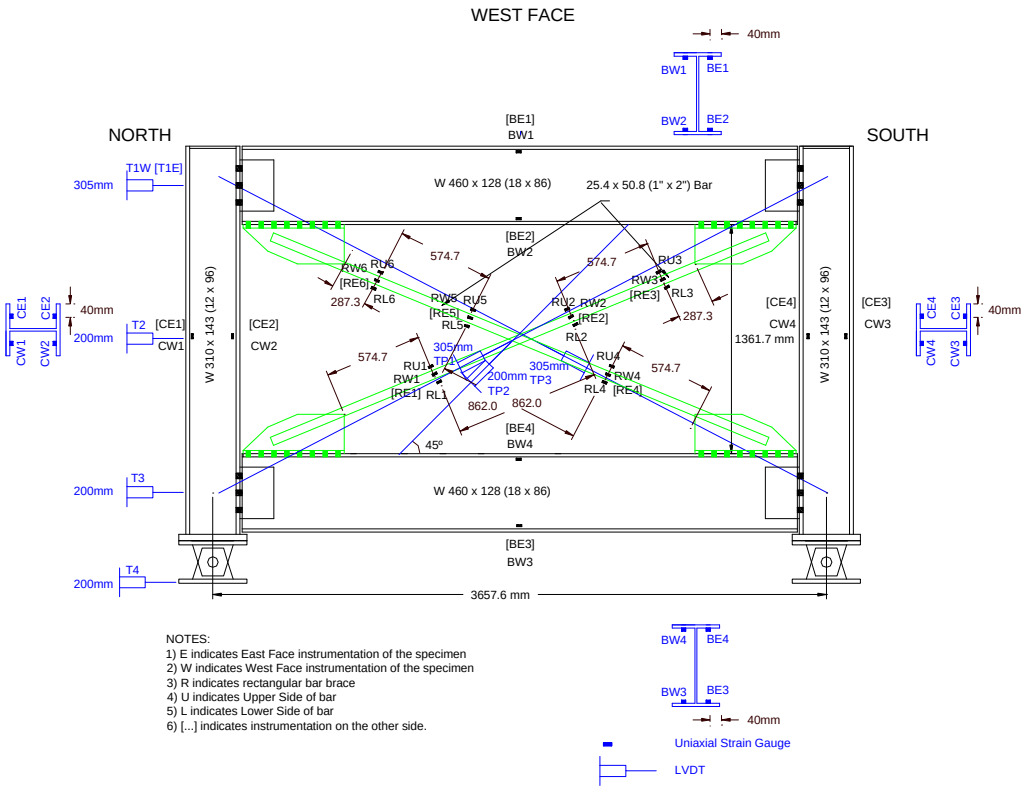

(a)

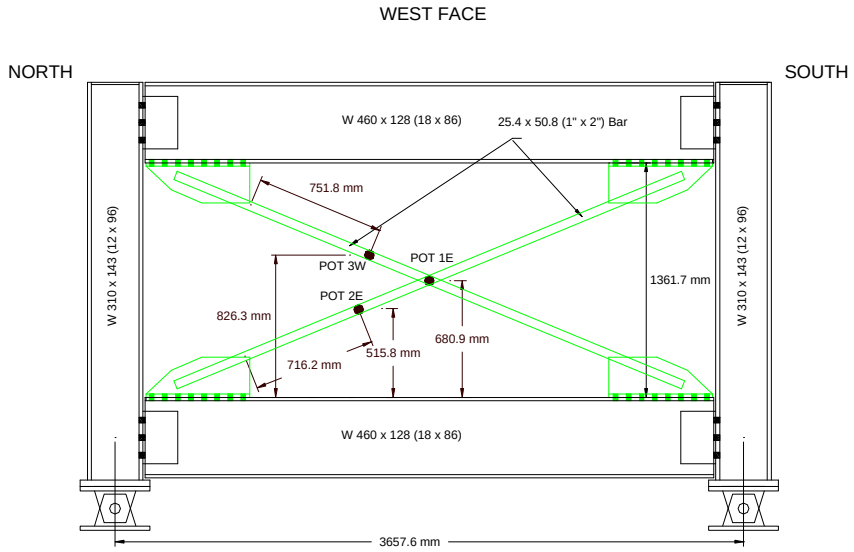

(b)

FIGURE 3-29 Instrumentation for Specimen F4: (a) In-Plane Displacement Measurement (Temposonics) and Strain Gauges; (b) Out-of-Plane Displacement Measurement (Potentiometers)

3.8 Data Acquisition System

Measurement Group 2310 strain gauge conditioning amplifiers were used for conditioning, amplification and filtering of strain gauges. The conditioners were also used for filters on displacement and force channels. Filtering was set at 10 Hz and in a 4-pole Butterworth configuration. An Optim Electronics MEGADAC 5414AC was used for data acquisition. The MEGADAC 5415AC has 16-bit resolution and a maximum sampling rate of 250 KHz (for these experiments, a sampling rate of 3 Hz was used). The input cards used were all AD885SH-1; they are simultaneous sample and hold with differential inputs. The cards were set up with a gain of 1 (all gain was done with the 2310's) and the filtering was bypassed. A general view from the data acquisition system is given below in Figure 3-30.

FIGURE 3-30 Data Acquisition System

3.9 Lateral Bracing

Lateral bracing was provided at the top beam of the specimens. This was provided by roller supports cantilevering from two tower frames erected on the east and west side of the specimen (Figure 3-31). The rollers were aligned to act (if necessary) at the upper third level of the web of top beam. A gap of approximately 3mm was left between the beam web and each roller so that the roller would only be engaged if out-of- plane deflections closed that gap. The frames supporting the rollers on each side of the specimen were secured to the

strong floor using high strength threaded rods. A laser level was used to monitor the out-of-plane movement of the specimens during testing. The east and west towers were also connected to each other at their tops using a couple of 12.7mm diameter steel tension rods.

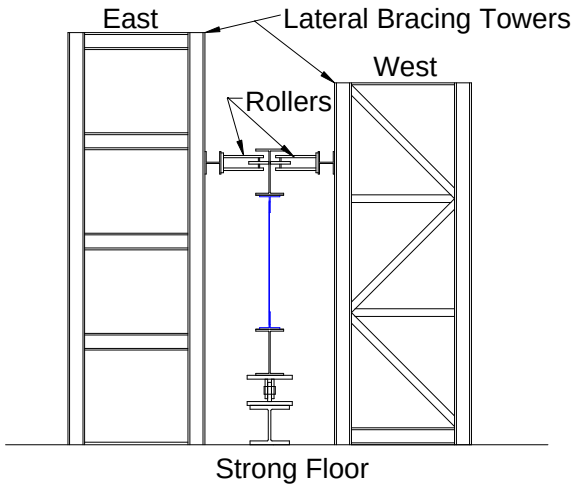

FIGURE 3-31 Lateral Bracing for the Specimens

SECTION 4
EXPERIMENTAL RESULTS

4.1 General

This section presents the loading protocol used in testing, the principles followed in the numerical estimation of specimen yield loads and corresponding displacements, and the experimental observations including cyclic inelastic displacement histories of the four tested specimens. Test results are plotted in the form of hysteretic loops to provide information on cyclic energy dissipation capacities, deterioration of brace buckling loads under cyclic displacements, and the extent of plastification in the braces along brace length.

4.2 Loading Protocol

Each specimen was subjected to quasi-static testing in accordance with the ATC-24 (1992) *Guidelines for Cyclic Seismic Testing of Components of Steel Structures* testing protocol. The displacement history recommended in ATC-24 testing program consists of stepwise increasing displacement cycles (multiple step test) as illustrated in Figure 4-1.

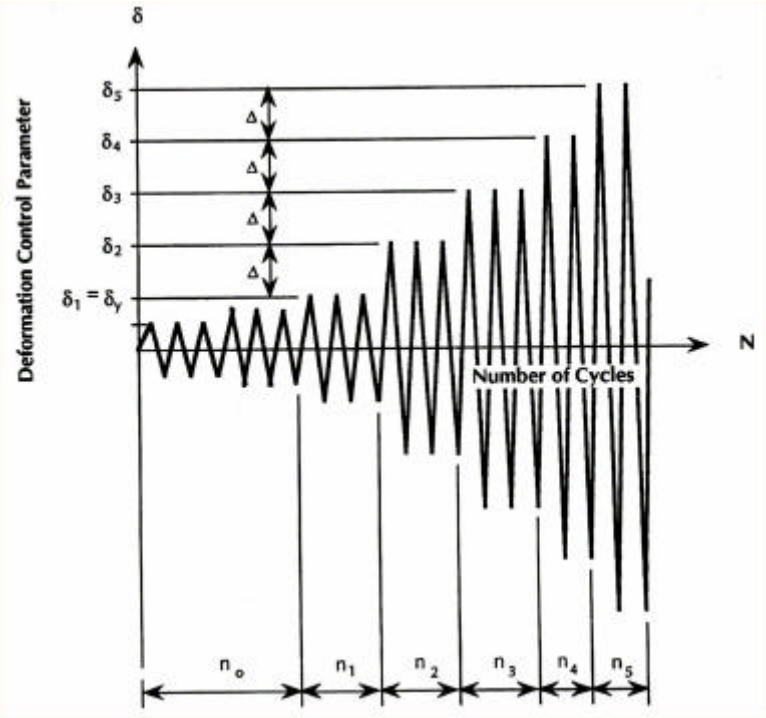

FIGURE 4-1 ATC-24 Displacement History for Cyclic Testing

In this loading protocol, the cycles are symmetric in peak displacements. On that figure, δ_j is the peak displacement at loading step j. Similarly, n_j and Δ are the number of cycles to be performed in load step j, and the increment in peak displacement between two consecutive steps respectively. The number of cycles n_o with a peak displacement less than δ_y, the yield displacement, is typically 6. The number of cycles with peak displacement equal to δ_y, as well as the number of cycles n_2 and n_3 with peak displacements $\delta_2=\delta_y+\Delta$ and $\delta_3=\delta_y+2\Delta$, is set equal to 3, while the number of cycles n_4 to n_m with peak displacements $\delta_4=\delta_y+3\Delta$ to $\delta_m=\delta_y+(m-1)\Delta$ is recommended to be taken as 2.

Since the top horizontal displacement of the specimens is directly related to the brace axial displacement, this horizontal value was taken as the displacement control parameter for all tests. As the study of cyclic inelastic buckling behavior of the brace elements was the objective of this study, special care was taken during the tests to identify the point of buckling initiation for the braces. In Specimen F1 in which the tension yield and buckling strengths of the brace were close to each other, the load was first applied to have tension in the brace, and in the above procedure, the experimentally obtained δ_y (specimen top horizontal displacement at brace tension yielding) was taken as the test control parameter. To facilitate comparison between the results obtained for Specimens F1 and F2 in subsequent sections, the same cyclic displacement history that was applied to Specimen F1 (i.e. absolute displacement values) was applied to Specimen F2. On the contrary, in Specimen F3 in which tension yield and buckling strengths of restrained X braces were different from each other, with buckling occurring first, in the above procedure, the experimentally obtained δ_b (specimen top horizontal displacement at the onset of brace buckling) was taken as the test control parameter. Again, to facilitate comparisons between Specimens F3 and F4, the same cyclic displacement history that was applied to Specimen F3 was applied to Specimen F4.

The yield displacement for each specimen was theoretically estimated via pushover analysis in SAP2000. Elastic cycles (i.e. 1/3 and 2/3 of yield) were essentially based on these estimates; however, for the inelastic cycles that were applied as per the above protocol, experimentally obtained yield displacement was used throughout the testing. However, in some cases, as described later, some adjustments were necessary for the displacement cycles in the elastic range, and values recorded did not exactly match those 1/3 and 2/3 values.

Nonetheless, at least three-cycles were applied prior to the specimen yield displacement in all cases.

Theoretical yield and buckling values of specimen's forces and displacements were used to initially control the tests. The experimentally obtained values were determined at the onset of visible nonlinearity in the force-displacement curve, or by the point from which the actuator force tended to drop abruptly (during buckling). Elastic cycles were performed in a force-controlled mode. Once the yield (or buckling) displacement had been identified experimentally, the subsequent cycles in the inelastic range were carried out using displacement control. The rate of loading was controlled manually and as continuously as possible. However, in the inelastic loading steps, testing was stopped periodically as appropriate to inspect the specimen and take photographs.

4.3 Estimation of Specimen Pushover Curves

To estimate the lateral loads and the corresponding lateral displacements of the specimens at brace tension yielding and brace buckling, and also to follow the overall specimen behavior beyond these points, static pushover analyses were carried out prior to testing. Specimen pushover curves for braces alone were superimposed with those for the bare frame to construct the full system behavior. More details are given in Appendix A.

4.4 Experimental Observations

This section summarizes the experimental observations made during each cyclic test. All specimen tests were recorded using a digital camcorder and a computer camera. The small camera was attached on top of one of the lower gussets providing a view along the brace. The behavior of each specimen, both in the elastic and inelastic ranges, is reported below. Note that, as a convention for the following discussion, in case of tube brace, positive (+) forces denote the loading case that generates tension in brace, while the negative (-) ones denote the loading case that generates compression in brace. In case of X braces, positive (+) forces denote loading towards the south, generating tension in the bar welded to the west faces of the gussets and compression in the other, while the negative (-) ones denote loading towards the north, generating tension in the actuator side upper brace (the bar welded to the east faces of the gussets) and compression in the other.

4.4.1 Specimen F1

Specimen F1 was first subjected to a lateral load producing tension in the brace (note that the same convention was adopted for Specimen F2). Horizontal force-displacement hysteretic behavior obtained for Specimen F1 is given in Figure 4-2. The magnitude of the cyclic displacement history for Specimen 1 is summarized in Table 4-1.

Specimen F1 exhibited practically linear elastic behavior under the first three cycles at 3.8mm, 0.16% drift, as well as during the three elastic cycles at 2/3 of the yield displacement (7.6mm, 0.32% drift). The experimental initial stiffness was slightly lower than the computed one at these steps (i.e. the specimen was more flexible than predicted). Some initial noises were heard, possibly generated by the end and intermediate stud connections, but there was no evidence of damage. The lateral force values were almost the same in either loading direction indicating a symmetric elastic response.

Specimen F1 reached its experimental yield displacement in tension at 11.4mm ($+1\delta_y$), 0.48% drift, and 636.1 kN base shear force. These specific values were determined on the basis of occurrence of a significant nonlinearity on the hysteretic curves, and at the same time by checking the strain gauge recordings at critical sections in the tube brace. At the end of Cycle 9, the specimen had exhibited some minor stable hysteretic loops, but no damage was observed in the secondary elements. During Cycles 9 through 12, whitewash flaking occurred in the regions where yielding has developed.

Some strength degradation was observed in the hysteretic curves during the second excursion at $\pm 2\delta_y$ (22.8mm, 0.96% drift). The specimen was inspected after this, but no evidence of visible damage was found. Tension yielding in the tube propagated along the brace length as recorded by strain gauges. Maximum base shear reached during this step was 827.4 kN (brace in tension).

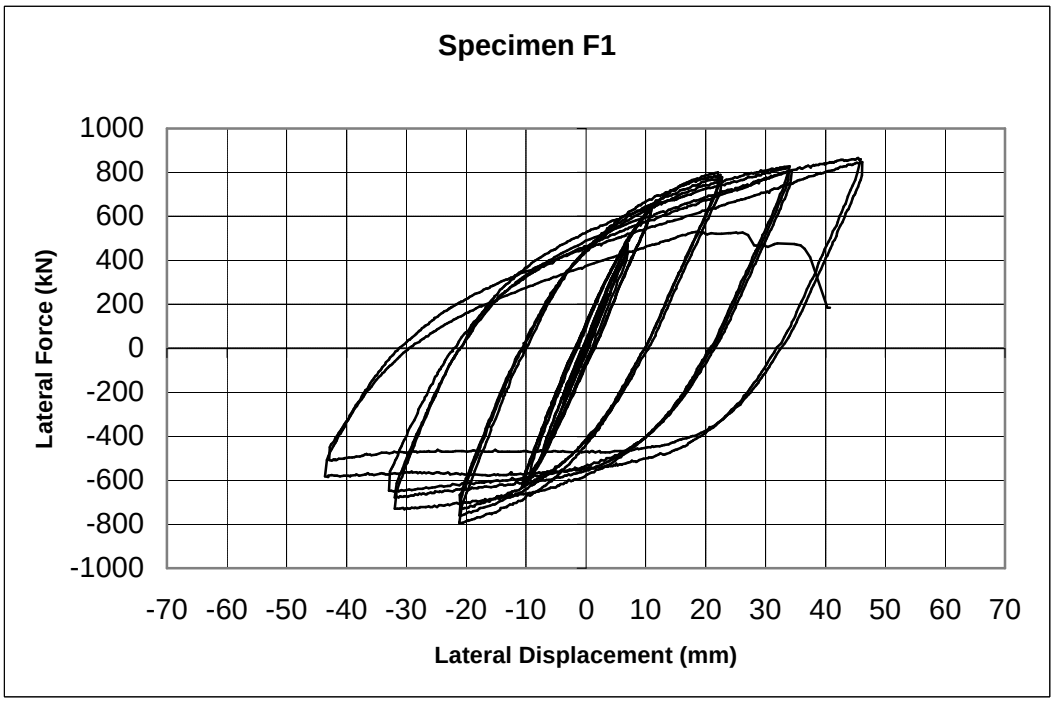

FIGURE 4-2 Hysteresis for Specimen F1

TABLE 4-1 Cyclic Displacement History of Specimen F1

Displacement Step	Number of Cycles	Cumulative No. of Cycles	Displacement (Δ/δ_y)	Displacement (mm)	Drift (%)
1	3	3	0.33	3.8	0.16
2	3	6	0.67	7.6	0.32
3	3	9	1	11.4	0.48
4	3	12	2	22.8	0.96
5	3	15	3	34.2	1.44
6	2.5	17.5	4	45.6	1.92

As a next step, the specimen was then subjected to $\pm 3\delta_y$ (34.2mm, 1.44% drift). During the second half cycle loading (with the brace in compression), the middle segment of the brace (between the third and the fourth studs counting from the north) buckled in the out-of-plane direction from the west to the east. The lateral force reached at this point was 734.0 kN. The boundary frame and its connections were inspected, and no traces of inelastic behavior were found. At a time very close to the end of the second excursion at $\pm 3\delta_y$, during Cycle 14, an unexpected failure in the actuator's connection system occurred in the laboratory, and testing was stopped. It was resumed fifteen days later, starting from the last excursion at $+3\delta_y$ (first half of Cycle 14). The previously buckled middle brace segment experienced further severe lateral displacement during this cycle. The direction of buckling for the tube brace remained unchanged. As the number of inelastic cycles increased, local inelastic deformations in the CFSS elements in the brace-to-stud connection areas (flange and a part of web next to the brace) progressed. This suggested possible loss of local bearing capacity of the thin-walled studs. A visible separation between the brace and the middle-row studs developed. This resulted in a deterioration of the buckling capacity of the brace in subsequent cycles. Local buckling in the tube brace also initiated at this displacement level. Residual deformations both in the brace and in the studs were more pronounced at the end of Cycle 15. A general view from the west side of the specimen, out-of-plane buckling mode of brace segments, local buckling in the middle brace segment, yielding areas with whitewash flaking, and separation between the brace and the studs are shown in Figures 4-3a to 4-3f respectively.

During the two cycles at $\pm 4\delta_y$ (45.6mm, 1.92% drift), damage further increased compared to the $\pm 3\delta_y$ cycles. During Cycle 16, deterioration of the buckling load capacity was significant. The third, fourth, and fifth vertical studs (counting from the north) exhibited severe lateral torsional buckling behavior. Residual kinks developed at mid-height of these studs. The extent of local buckling in the middle tube brace segment progressed rapidly, and the out-of-plane displacements along other brace segments (i.e. between other studs) became more visible. A general view from the west side of the specimen, out-of-plane buckling mode of brace segments, development of local buckling in the middle brace segment, yielding along the brace length, separation between the brace and the studs, and general views from the east side are illustrated in Figures 4-4a to 4-4h respectively.

During the second application of $\pm 4\delta_y$ (45.6mm, 1.92% drift) at Cycle 17, all previously observed types of damages became more severe. During the third cycle at $+4\delta_y$ (Cycle 18), with the brace in tension, fracture initiated at the tube mid-length, starting from the corners of the cross-section into the webs. West side of the tube fractured first, then it propagated towards the east. Figures 4-5a to 4-5d show the propagation of fracture in the local buckling area, respectively. Fracture propagated over the entire brace cross-section as displacement increased, and a maximum lateral force of only 511.5 kN was reached before total fracture. During this last half cycle, the progress of fracture in the tube brace is depicted in Figures 4-6a to 4-6f.

While damage at that point was significant in the middle studs, they were nonetheless effective in restraining the tube brace from buckling during the elastic cycles, and some of the early inelastic cycles, in minimizing the deterioration of the buckling strength during the inelastic cycles, and in reducing the out-of-plane displacements of the tube brace. Pictures taken from the specimen just after the test, at zero force and displacement, and at various stages after some or all of the studs had been removed are also included in Figures 4-7a to 4-7m.

U brackets connections survived the whole range of loading without any loss of strength. No bolt or weld failure in any zone of the specimen was observed during the testing.

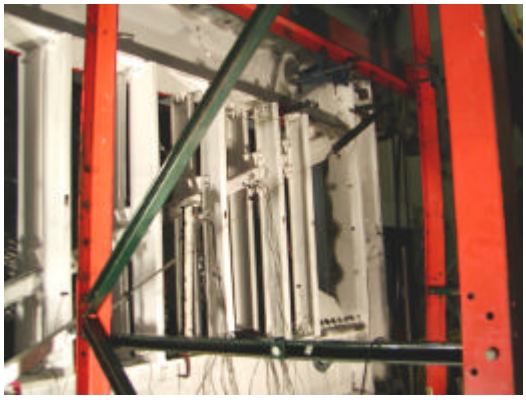

(a)

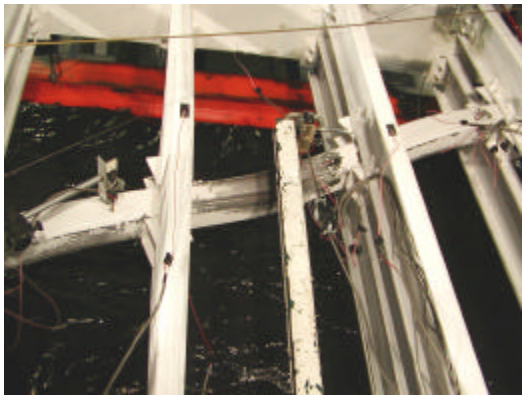

(b)

(c)

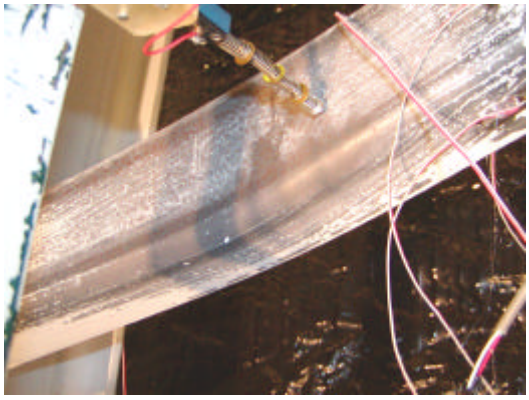

(d)

(e)

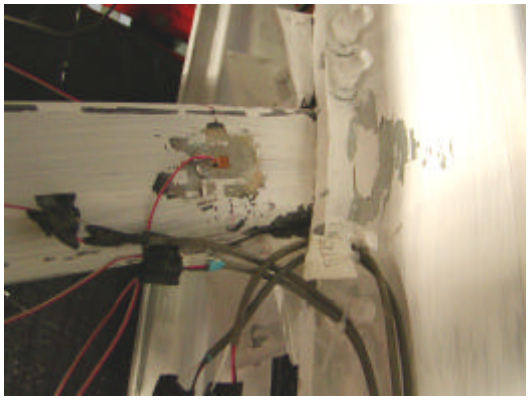

(f)

FIGURE 4-3 Damage Level in Specimen F1 (Cycle 15, - 3d_y): (a) General View; (b,c) Out-of-Plane Buckling Mode of Brace Segments; (d) Development of Local Buckling in Middle Brace Segment; (e) Spread of Plastification Along Whole Brace Segments; (f) Separation between Brace and Studs and Bearing Failure of Studs

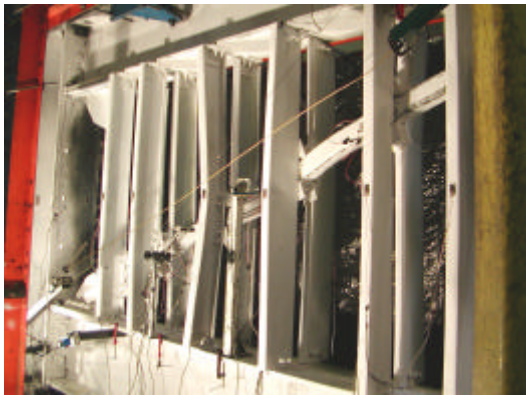

(a)

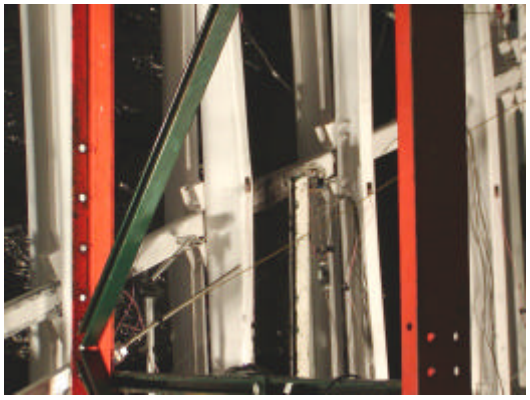

(b)

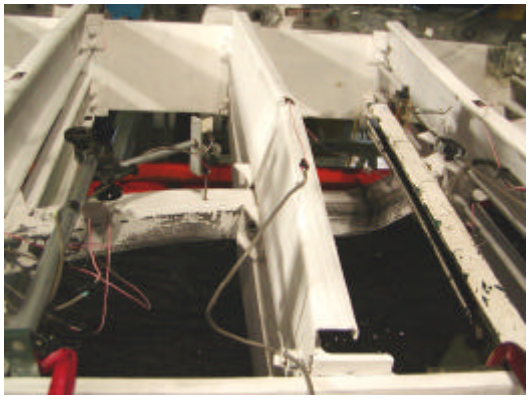

(c)

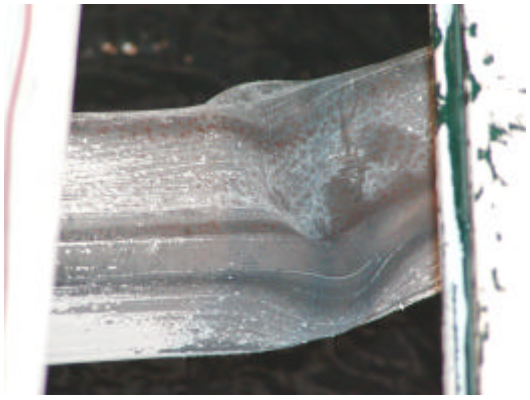

(d)

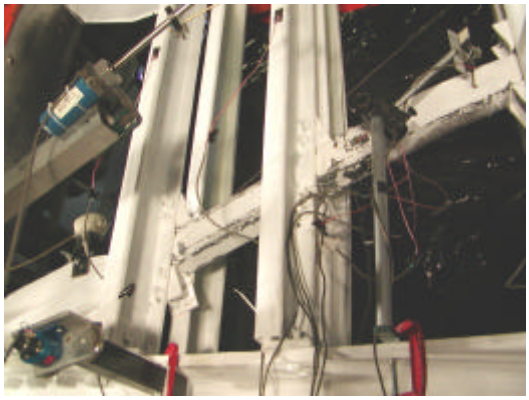

(e)

(f)

FIGURE 4-4 Damage Level in Specimen F1 (Cycle 16, - 4d_y): (a) General View; (b,c) Out-of-Plane Buckling Mode of Brace Segments; (d) Development of Local Buckling in Middle Brace Segment; (e) Spread of Plastification Along Whole Brace Segments; (f) Separation between Brace and Studs and Bearing Failure of Studs

(g) **(h)**

FIGURE 4-4 Damage Level in Specimen F1 (Cycle 16, - 4d_y) (continued): (g,h) Specimen East Views

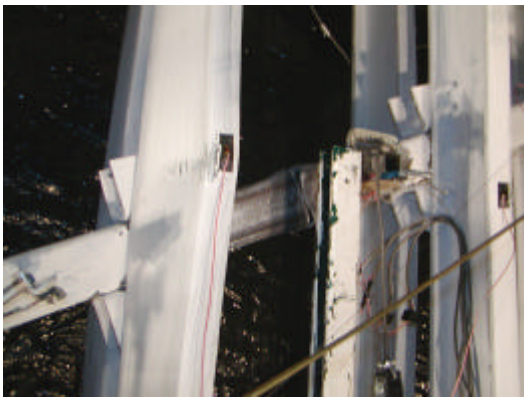

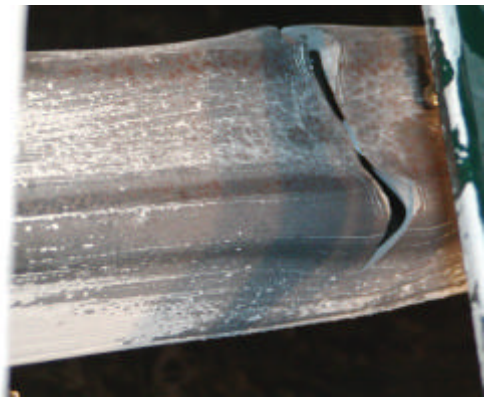

(a) **(b)**

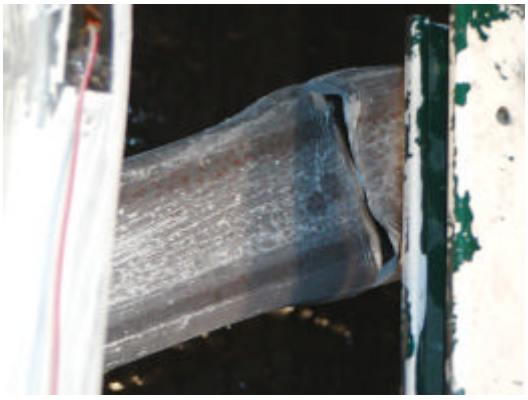

(c) **(d)**

FIGURE 4-5 Damage Level in Specimen F1 (Cycle 18, + 4d_y): (a,b,c) Fracture of Tube Brace Middle Section (West); (d) Separation between Brace and Studs and Bearing Failure of Studs

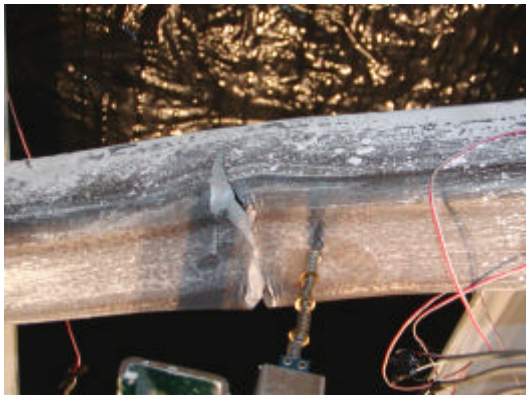

(a)

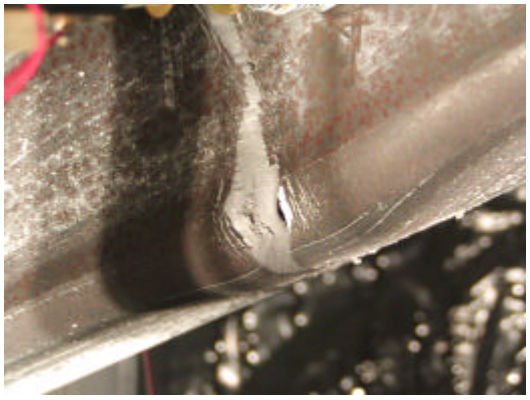

(b)

(c)

(d)

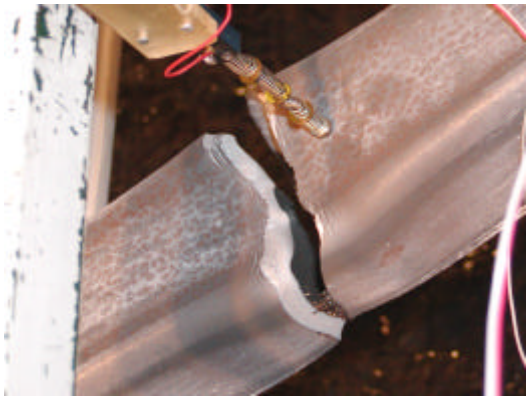

(e)

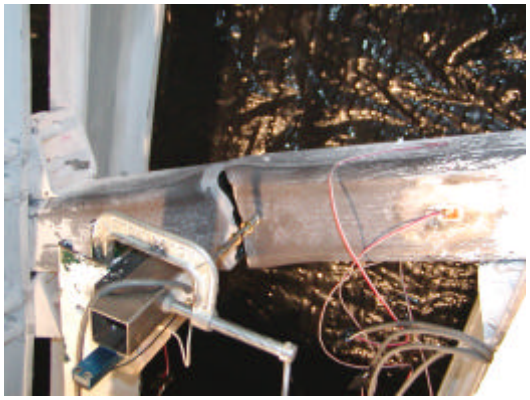

(f)

FIGURE 4-6 Damage Level in Specimen F1 (Cycle 18, + 4d_y): (a,b,c,d) Propagation of Fracture Along Tube Brace Cross-Section; (e,f) Total Fracture Failure of Tube Brace

(a)

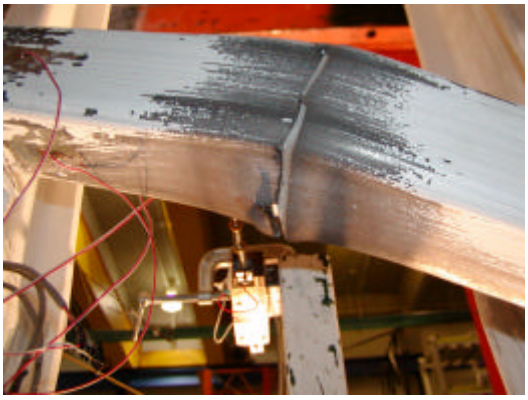

(b)

(c)

(d)

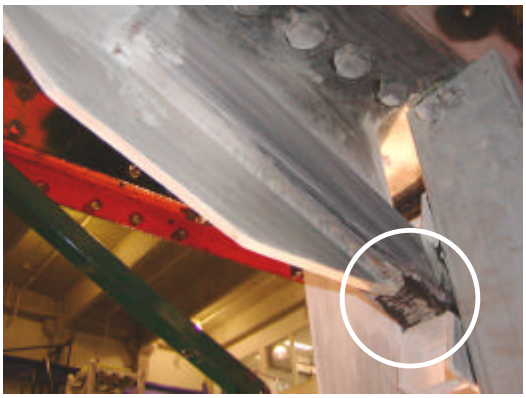

(e)

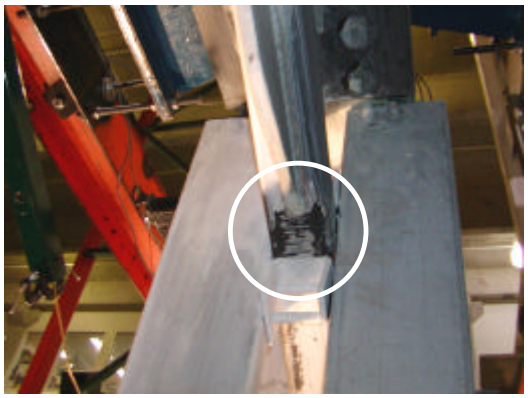

(f)

FIGURE 4-7 Post-Testing Images at Zero Displacement: (a) General View from the West (circles show yielded or buckled regions); (b) Fractured Section; (c) Brace-to-Stud Connection; (d) Yielding in Side Brace Segment; (e,f) Yielding in Brace at Brace-to-Gusset Connection

(g)

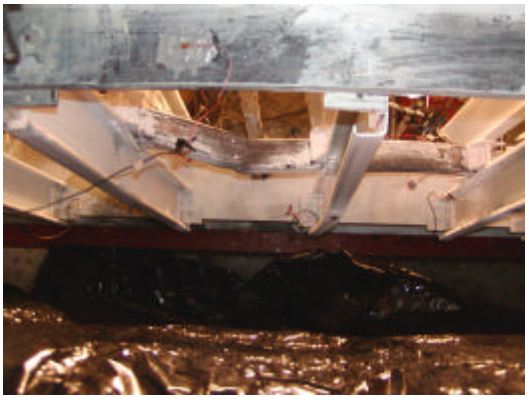

(h)

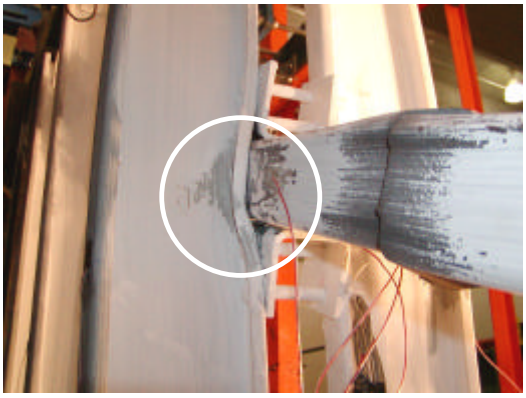

(i)

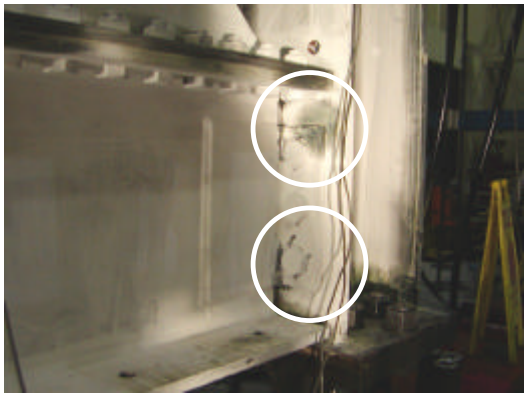

(j)

(k)

(l)

(m)

FIGURE 4-7 Post-Testing Images at Zero Displacement (continued): (g) Inside View Along Brace; (h) Top View; (i) Closer View to Brace-to-Stud Connection; (j) Beam-to-Column Lower Connection (South); (k) Specimen after Cutting Studs; (l) Brace View from South; (m) Middle Stud Bearing Failure Detail (After Removing Brace)

4.4.2 Specimen F2

Specimen F2 was subjected to the same displacement history than Specimen F1 to facilitate comparison of the relative hysteretic energy dissipation capacity of the two specimens. However, as stated later, additional cycles were performed for Specimen F2 beyond the maximum displacements reached for Specimen F1, until failure, to allow determination of the fracture life of the tube brace. Experimentally obtained horizontal force-displacement hysteresis for Specimen F2 is given in Figure 4-8. The magnitude of the cyclic displacement history for Specimen F2 is summarized in Table 4-2.

Specimen F2 exhibited a linear behavior during the first three elastic cycles at 1/3 of the yield displacement (3.8mm, 0.16% drift). These cycles produced sufficiently close tension and compression axial forces in the brace. During the cycles at 2/3 of the yield displacement (7.6mm, 0.32% drift), it was found that a significant amount of out-of-plane movement in the test set-up had developed under higher actuator forces. Testing was stopped, the test setup was scrutinized closely prior to the application of $\pm 1\delta_y$, and additional measures for preventing this movement were taken by improving the lateral bracing system to the tested frame. General view of the specimen and some instrumentation are illustrated in Figures 4-9a to 4-9d.

Testing was continued starting from $+1\delta_y$ (11.4mm, 0.48% drift), with the tube in tension. When the base shear force reached 511.5 kN, and the story displacement was $-0.89\delta_y$ (10.2mm, 0.43% drift), the brace buckled in the out-of-plane direction. Buckling initiated with a slight, yet visible, out-of-plane movement of the tube brace towards the west. Whitewash flaking occurred in the regions where yielding developed. The residual buckled shape of the brace was very visible at the end of the last cycle at $\pm 1\delta_y$ (Cycle 9). Some degree of nonlinearity in the hysteretic curves was observed both in tension and compression. Strain gauge recordings also exhibited higher strains beyond the specified yield strain.

No damage in the vicinity of the boundary frame and brace connections was detected, but on the south lower gusset, whitewash flaked following a yield line on the gusset web. This gusset was bent in the out-of-plane direction towards the east about the axis of the yield line.

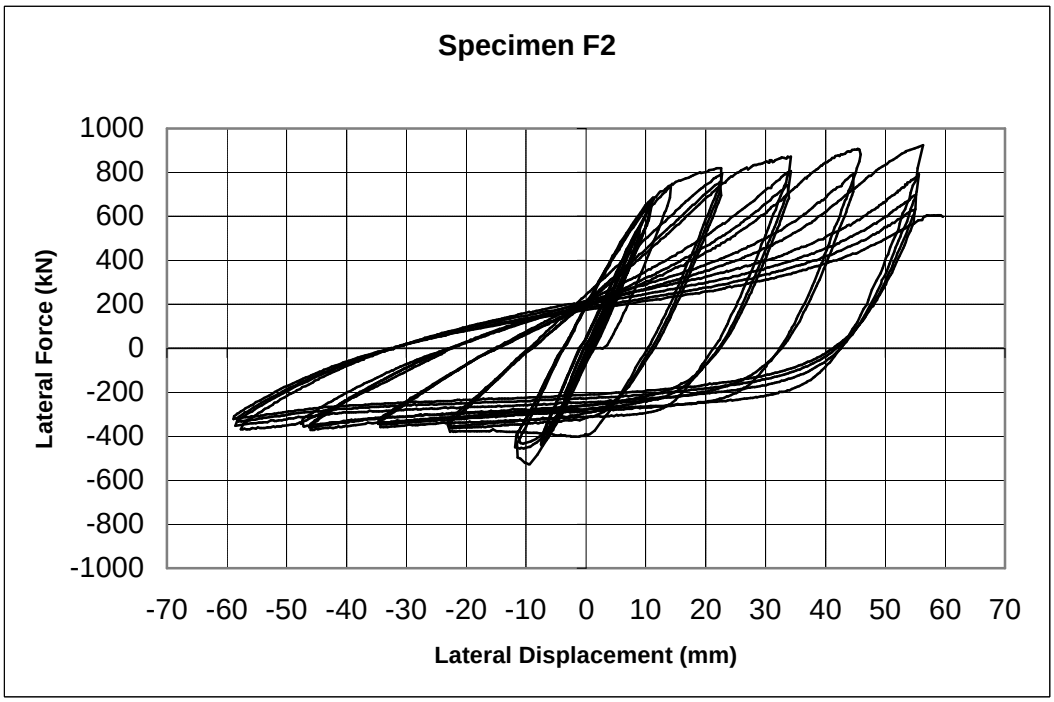

FIGURE 4-8 Hysteresis for Specimen F2

TABLE 4-2 Cyclic Displacement History of Specimen F2

Displacement Step	Number of Cycles	Cumulative No. of Cycles	Displacement (Δ/δ_y)	Displacement (mm)	Drift (%)
1	3	3	0.33	3.8	0.16
2	3	6	0.67	7.6	0.32
3	3	9	1	11.4	0.48
4	3	12	2	22.8	0.96
5	3	15	3	34.2	1.44
6	2	17	4	45.6	1.92
7	4	21	5	57.0	2.40
8	0.5	21.5	6	68.4	2.88

The west and the east views of out-of-plane buckling of the brace, yielding of the brace around the north upper gusset, progress of out-of-plane displacement by cycling, and buckling mode at Cycle 9 are given in Figures 4-10a to 4-10f respectively.

During the first three cycles at $\pm 2\delta_y$ (22.8mm, 0.96% drift), the out-of-plane displacement was beyond the capacity of the potentiometers used in the middle region of the brace, and they were therefore removed. A maximum base shear force of 822.9 kN was reached. Yielding at the north top brace-to-gusset connection progressed with whitewash flaking. At this step, an increase in the yielding at the south lower gusset was observed. Again, out-of-plane residual displacement of the tube brace relatively increased at the end of the 12^{th} Cycle. Due to cyclic buckling of the brace, pinching in the hysteretic curves occurred. Some photographs showing the general views from both frame sides, yielding at upper brace-to-gusset connection (west and east views), yielding at south lower gusset, and a top view at Cycle 12, are presented in Figures 4-11a to 4-11f.

Yielding at around mid-length of the brace due to alternating buckling and tension yielding along the brace length progressed at the three cycles of $\pm 3\delta_y$ (34.2mm, 1.44% drift). Strength degradation (brace in tension) was recorded at the end of this step. No trace of local buckling was observed. Note that back and forth bending behavior of the lower south gusset became more severe with increasing cycles at this loading step. Specimen views from both sides, yielding at upper brace-to-gusset connection, plastification of brace middle region at buckling, and yielding at south lower gusset are shown in Figures 4-12a to 4-12f.

The specimen was then subjected to two cycles of $\pm 4\delta_y$ (45.6mm, 1.92% drift). The degree of yielding both in the north upper and the lower south gusset regions increased. The maximum base shear was 903.0 kN. Some noises, probably from bolt slippage, were heard. Out-of-plane displacement reached a magnitude equal to a couple of brace cross sectional dimensions. At the end of 17^{th} Cycle, there was no sign of fracture or any other local failure in the specimen. Note that the tube brace in Specimen F1 had fractured at this displacement level. Similarly, specimen views from both sides, yielding at upper brace-to-gusset connection, plastification of brace middle region at buckling, and yielding at south lower gusset are shown in Figures 4-13a to 4-13f.

Since the replication of the cyclic displacement history of Specimen F1 was complete, more cycles at larger displacements were required to determine the fracture life of the brace. As such, two additional cycles of $\pm 5\delta_y$ (57.0mm, 2.40% drift) were performed. During the compression cycle of the first excursion, snapping noises seemed to come from the specimen. Testing was stopped after a big bang was heard. The specimen was then inspected. It was found that at the end of Cycle 19, local buckling of the tube middle section had initiated, and severe yielding and fracture along the yield lines at the south upper beam-to-column angle connections had occurred. Development of damage level at similar locations in the specimen is presented in Figures 4-14a to 4-14f. After this loading step, it was decided to continue testing at the same displacement level, since there had not been any significant drop in the load level. Two additional cycles at $\pm 5\delta_y$ were thus applied. Local buckling became more visible and some traces of fracture lines were observed at the tube mid-length cross-section. The north upper brace-to-gusset connection exhibited some signs of fracture along the tube section. At the end of this cycle, the specimen was still capable of sustaining displacement cycles with no significant strength deterioration. A general view of the specimen and a closer view from the brace are depicted in Figures 4-15a and 4-15b for this additional loading step.

Then, it was decided to increase the displacement level to $\pm 6\delta_y$ (68.4mm, 2.88% drift). During the first half cycle of the first cycle (Cycle 22), a visible separation between the tube section and the fillet weld occurred. This resulted in a total fracture at the tube cross-section starting from the bottom tube wall and gradually developing to the side and finally ending on the upper walls. Testing was terminated at this level. Photographs indicating the propagation of fracture at the brace-to-gusset connection point are illustrated in Figures 4-16a to 4-16d.

The occurrence of net section failure without development of the full connection capacity was not anticipated for this specimen. However, the overall behavior of specimen F2 was still stable and the fracture life of the tube was longer than that of the tube brace used in Specimen F1.

Pictures taken from the specimen just after the test, at zero load and displacement, are also included in Figure 4-18a to 4-18f.

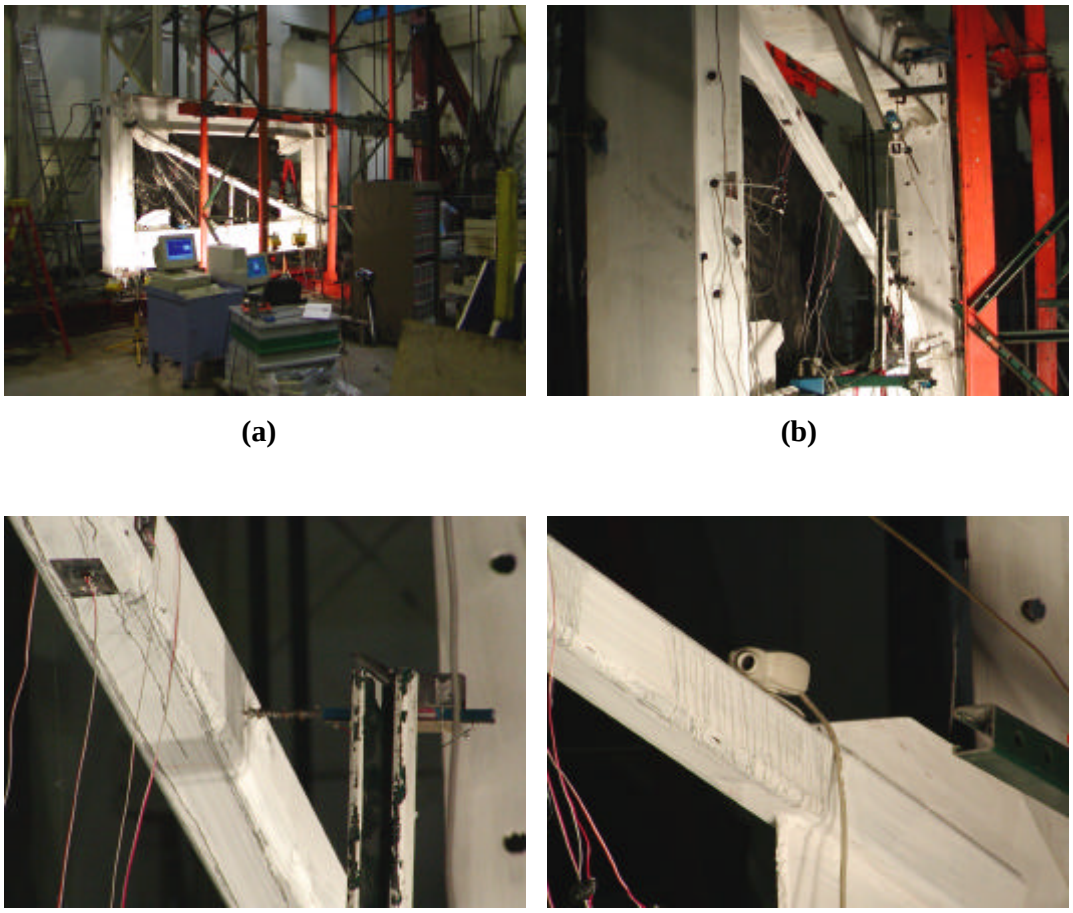

(a) **(b)**

(c) **(d)**

FIGURE 4-9 Specimen F2 Prior to Testing: (a,b) General Views; (c) Measurement of Out-of-Plane Displacements; (d) Computer Camera Installment

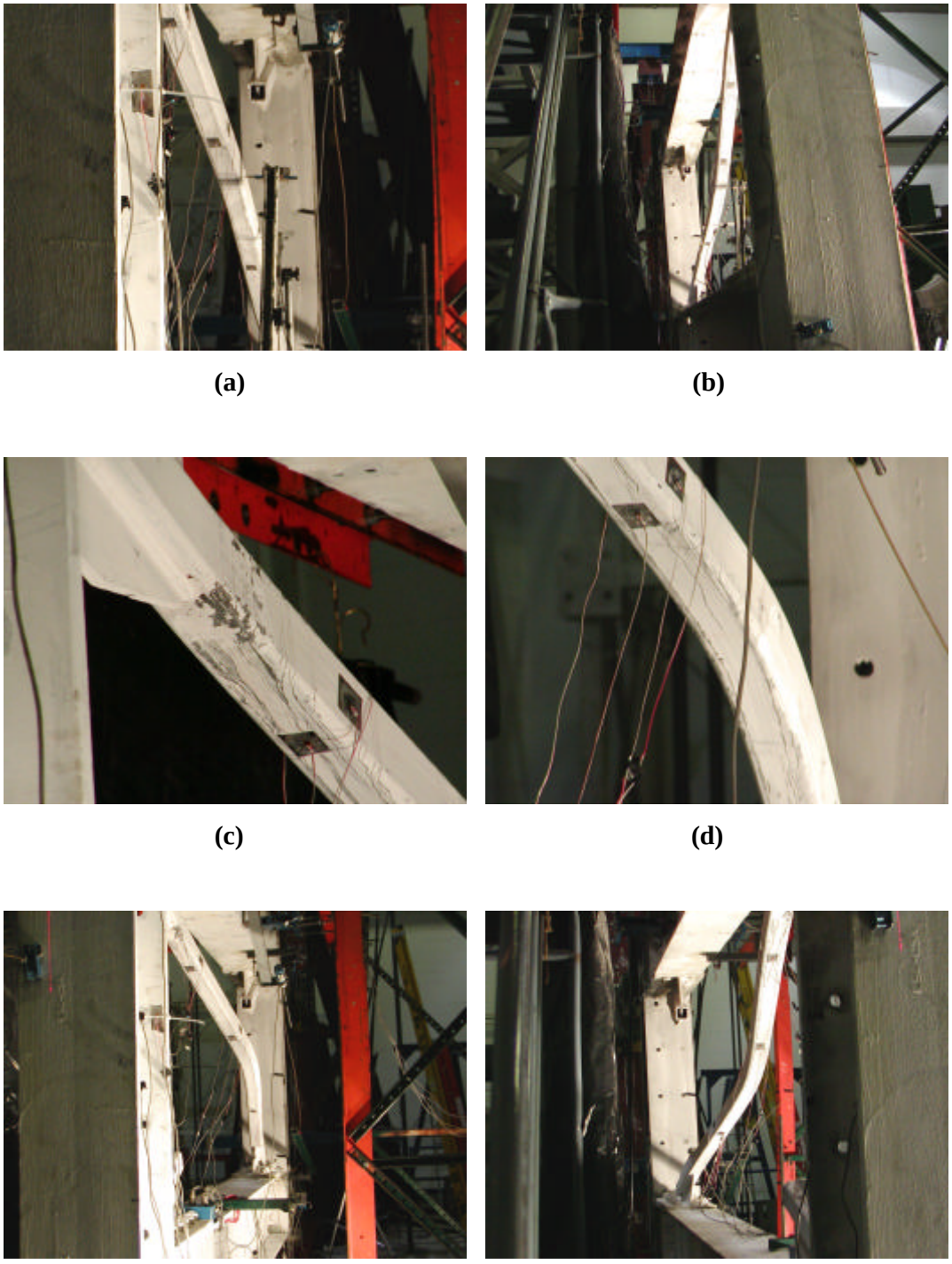

(a) **(b)**

(c) **(d)**

(e) **(f)**

FIGURE 4-10 Behavior of Specimen F2: (a) Out-of-Plane Brace Buckling (Cycle 7, -0.89d_y); (b) Out-of-Plane Brace Buckling (Cycle 8, -1d_y); (c) Brace Yielding around the North Upper Gusset at (Cycle 9, -1d_y); (d) Progress of Out-of-Plane Displacement; (e,f) Buckling Mode at (Cycle 9, -1d_y)

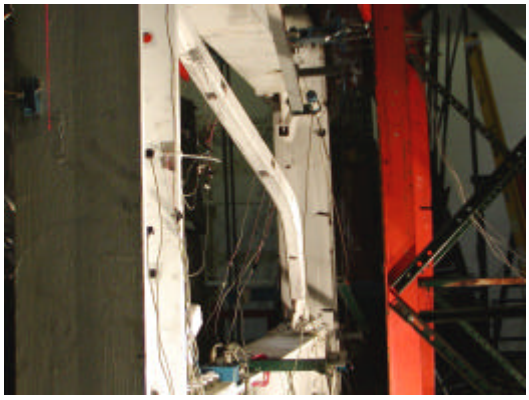

(a)

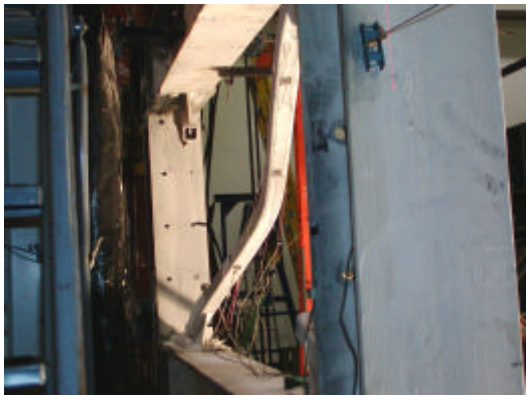

(b)

(c)

(d)

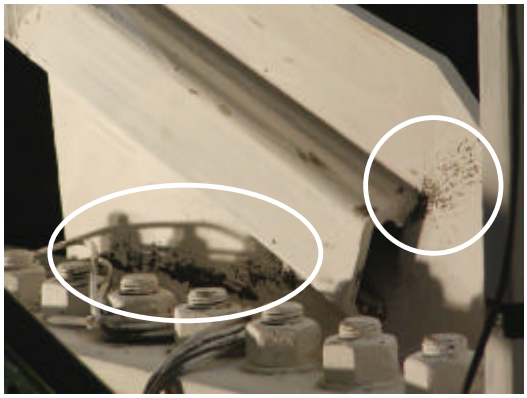

(e)

(f)

FIGURE 4-11 Damage Level in Specimen F2 at ±2d_y: (a,b) General Views (Cycle 10, -2d_y); (c) Yielding at North Upper Brace-to-Gusset Connection (West View) (Cycle 11, -2d_y); (d) North Upper Brace-to-Gusset Connection (East View); (e) Yielding at South Lower Gusset (Cycle 11, -2d_y); (f) Buckling Mode (Top View) (Cycle 12, -2d_y)

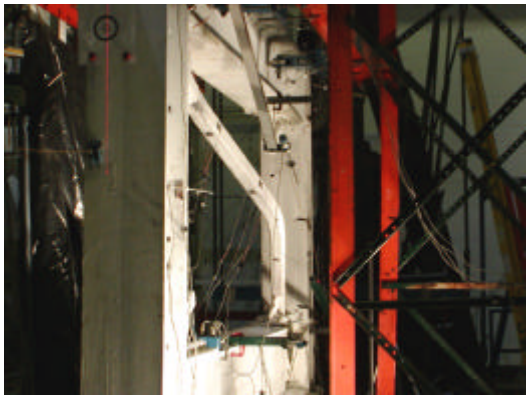

(a)

(b)

(c)

(d)

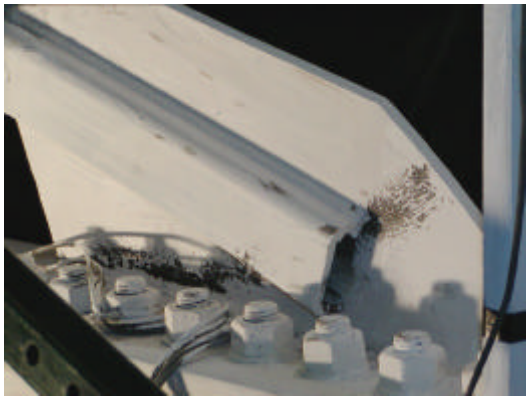

(e)

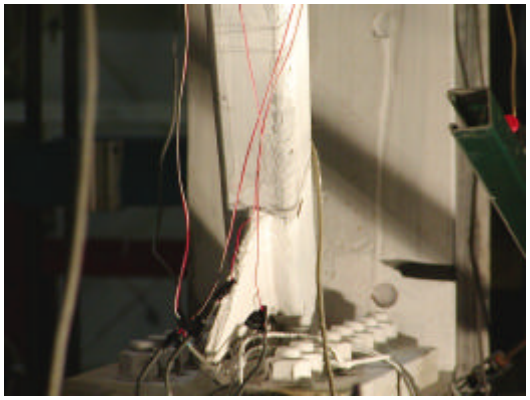

(f)

FIGURE 4-12 Damage Level in Specimen F2 at ±3d_y: (a,b) General Views (Cycle 13, -3d_y); (c) Yielding at North Upper Brace-to-Gusset Connection (West View) (Cycle 13, -3d_y); (d) Development of Out-of-Plane Displacement; (e,f) Yielding at South Lower Gusset (Cycle 13, -3d_y)

(a)

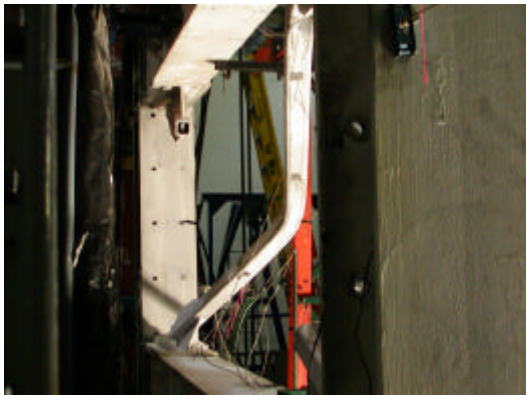

(b)

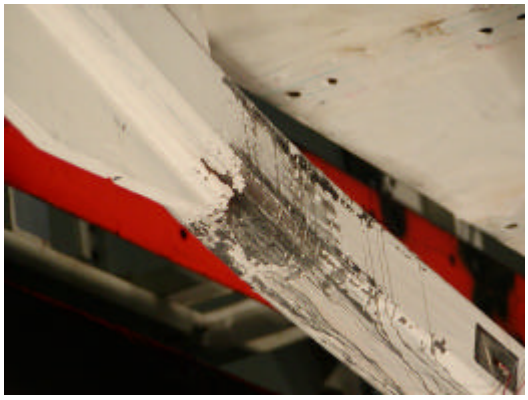

(c)

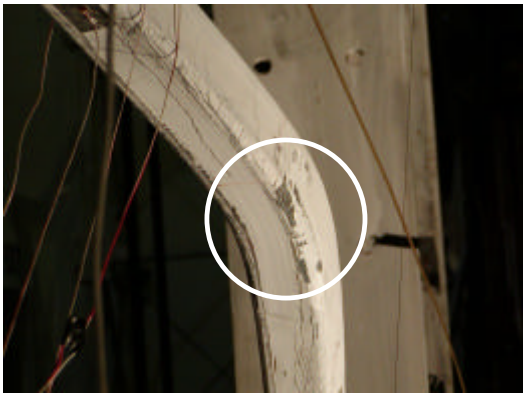

(d)

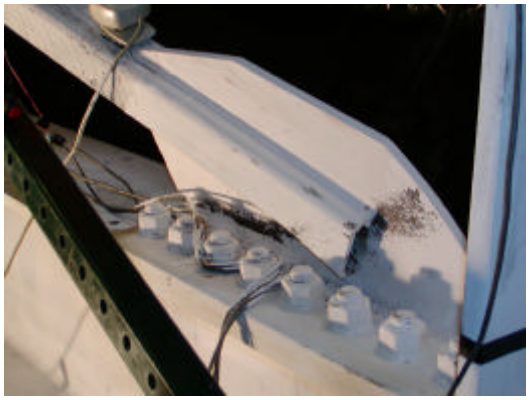

(e)

(f)

FIGURE 4-13 Damage Level in Specimen F2 at ±4d_y: (a,b) General Views (Cycle 16, -4d_y); (c) Yielding at North Upper Brace-to-Gusset Connection (West View) (Cycle 16, -4d_y); (d) Development of Out-of-Plane Displacement; (e,f) Severe Out-of-Plane Bending of South Lower Gusset (Cycle 16, -4d_y)

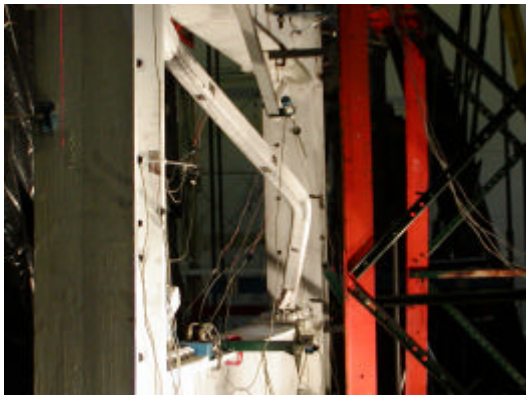

(a)

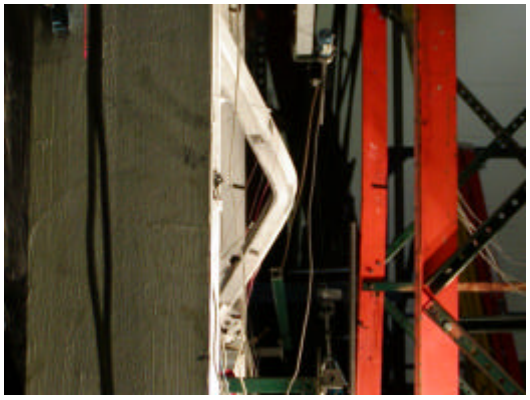

(b)

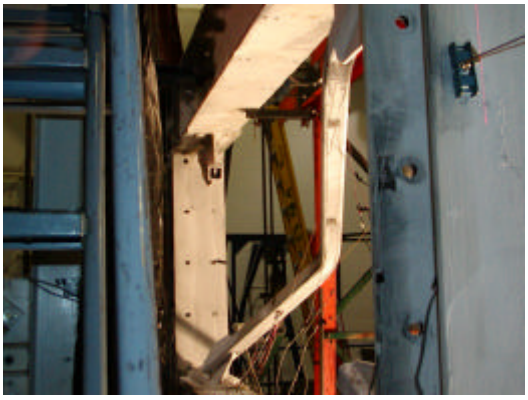

(c)

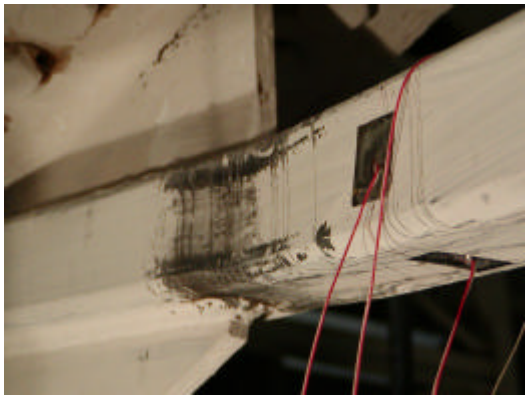

(d)

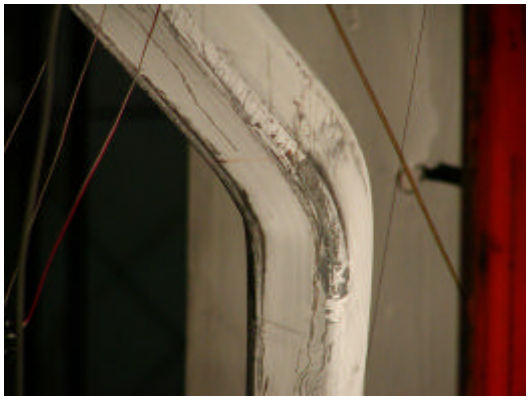

(e)

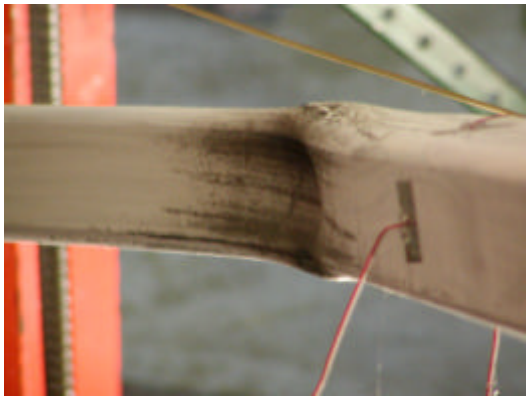

(f)

FIGURE 4-14 Damage Level in Specimen F2 at ±5d_y: (a,b,c) General Views (Cycle 18, -5d_y); (d) Yielding at North Upper Brace-to-Gusset Connection (West View) (Cycle 18, -5d_y); (e) Development of Out-of-Plane Displacement (Cycle 19, -5d_y); (f) Local Buckling at Mid-Length (Cycle 19, -5d_y)

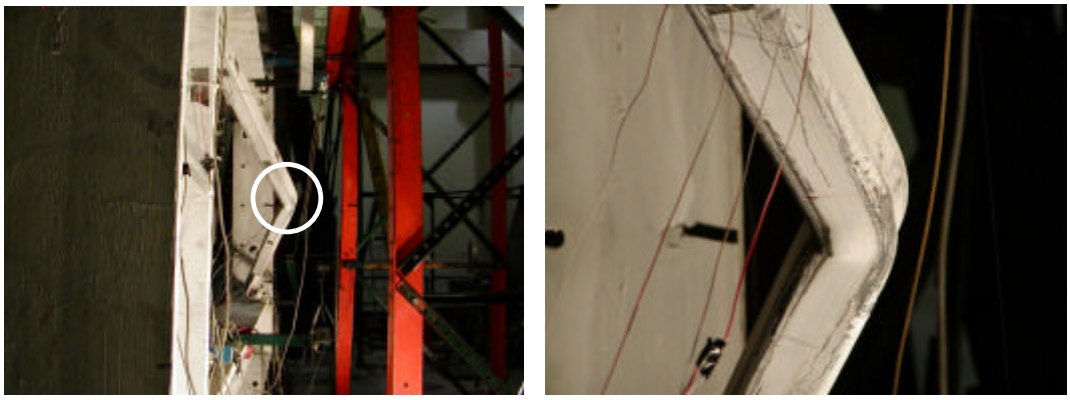

(a) **(b)**

FIGURE 4-15 Damage Level in Specimen F2 at ±5d_y: (a) General View (Cycle 21, -5d_y); (b) Closer Look at Brace Middle Region (Cycle 21, -5d_y)

(a) **(b)**

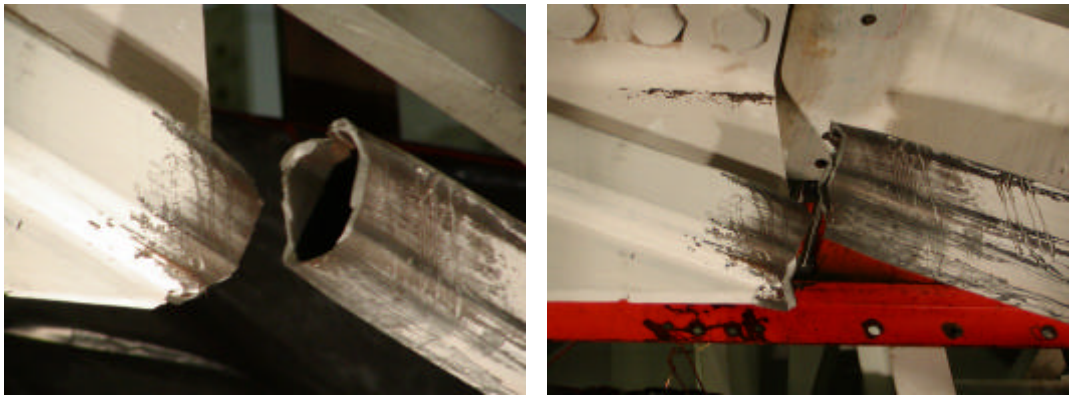

(c) **(d)**

FIGURE 4-16 Damage Level in Specimen F2 at ±6d_y: (a,b) Initiation of Fracture (Cycle 22, +6d_y); (c,d) Total Fracture of the Tube (Cycle 22, +6d_y)

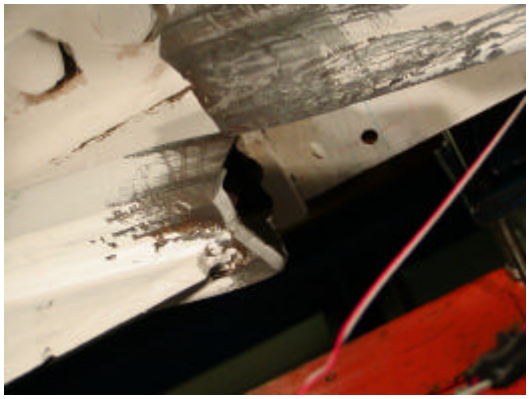

(a)

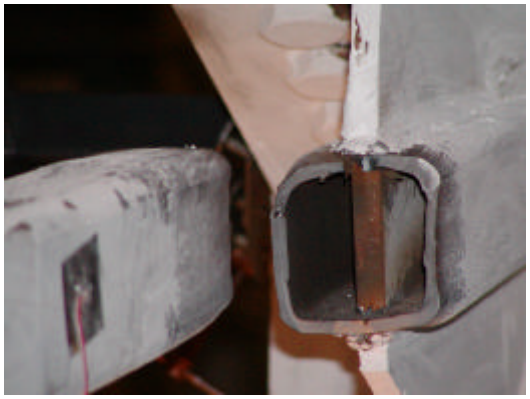

(b)

(c)

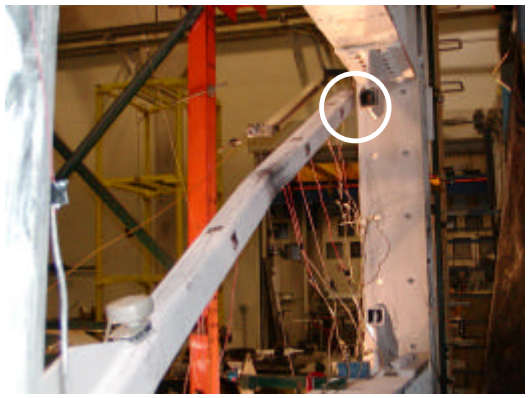

(d)

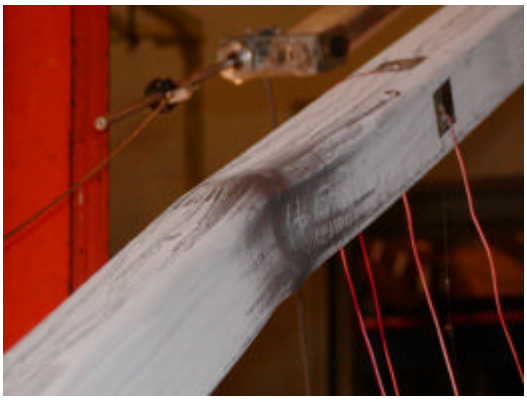

(e)

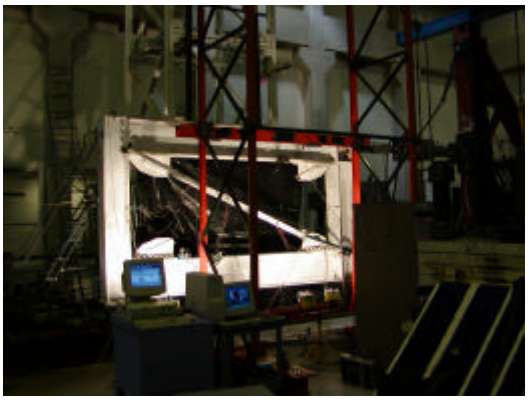

(f)

FIGURE 4-17 Specimen F2 at Zero Load and Zero Displacement: (a,b,c) Closer Views from Fractured Section; (d,e) Residual Brace Displacement; (f) General View from the West After Testing

4.4.3 Specimen F3

Specimen F3 was first loaded towards the south, producing tension in the west-side brace and compression in the east-side brace (as stated before, the same convention was adopted for Specimen F4). Experimentally obtained horizontal force versus top displacement hysteresis for Specimen F3 is given in Figure 4-18. The magnitude of the cyclic displacement history for Specimen 3 is also summarized in Table 4-3. Prior to testing, some pictures from Specimen F3, are illustrated in Figures 4-19a to 4-19f.

During the three cycles at 2.4mm, 0.11% drift and the three cycles at the second displacement level (5.1mm, 0.23% drift), the specimen's behavior was elastic and cyclic symmetric. Following the three elastic cycles at 9.1mm, 0.41% drift, the upper brace segment between the forth and the fifth studs (counting from the north), suddenly buckled towards the east with an audible noise at 11.9mm, 0.54% drift. Buckling caused an abrupt decrease in the actuator load, and an increase in the displacement. This experimental displacement level was then identified to be the experimental buckling point ($1\delta_b$) for Specimen F3. The actuator force was 898.5kN. Typically, whitewash flaking occurred in the buckled segment and in the lower north gusset connection region.

During the subsequent cycles at $\pm 1\delta_b$, parts of the braces among the studs exhibited a wavy buckled shape. Both bars yielded in compression and tension, and a residual middle displacement was visible in the buckled segment. At the end of Cycle 12, the fifth stud on the west side exhibited bearing failure due to cyclic brace buckling at the contact point. Specimen general view from the west side at brace buckling, a closer view from the buckled segment, separation of braces at cross over region, yielded regions on the braces, and bearing failure of studs are illustrated in Figures 4-20a to 4-20f.

During the three cycles at $\pm 2\delta_b$ (23.8mm, 1.08% drift), the magnitude of the buckled waves grew. There were visible residual out-of-plane displacements at zero force at the end of excursions. Both tension and compression yielding progressed over the braces. Some signs of disconnection in the CFSS and brace regions were observed.

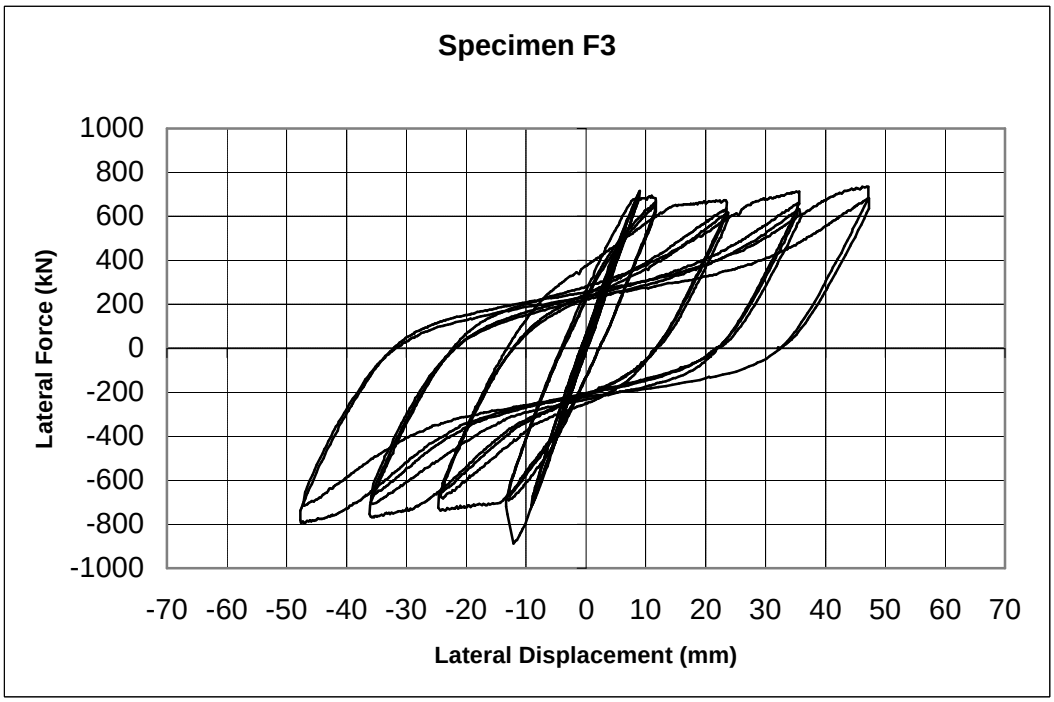

FIGURE 4-18 Hysteresis of Specimen F3

TABLE 4-3 Cyclic Displacement History of Specimen F3

Displacement Step	Number of Cycles	Cumulative No. of Cycles	Displacement (Δ/δ_y)	Displacement (mm)	Drift (%)
1	3	3	0.20	2.4	0.11
2	3	6	0.43	5.1	0.23
3	3	9	0.76	9.1	0.41
4	3	12	1	11.9	0.54
5	3	15	2	23.8	1.08
6	3	18	3	35.7	1.62
7	2	20	4	47.6	2.16

After further inspection, the fourth stud on the west side was found to have reached it's bearing capacity with a local failure. During Cycle 15, audible sounds arose, and the specimen was closely investigated, however, no defect was found. Maximum base shear was 716.2 kN. Closer views as the buckled shapes and yielded parts in the infill middle region, separation of the braces in the cross over region, yielding of the brace around stud-to-brace connection, disconnection in stud-to-brace connection, and the development of bearing failure in stud flanges are given in Figures 4-21a to 4-21f respectively.

The specimen was then subjected to three cycles at $\pm 3\delta_b$ (35.7mm, 1.62% drift). Since the out-of-plane displacements exceeded the capacity of the potentiometers used in the middle of the brace, they were removed. Classical buckling shapes of the braces became more visible. Every brace segment had out-of-plane residual displacements under subsequent excursions. Disconnection between the middle studs and the braces was more visible. Stretching in the tension braces produced some sounds, indicating that the infill system was undergoing significant inelastic distortions. In the middle region of the specimen where the braces meet, since they had buckled in the same direction (towards the west), they remained in contact Maximum base shear was 760.6 kN. A specimen general view from the west side, an example of yielded brace segment, separation of braces in the middle region, compression yielding of upper brace and tension yielding of lower brace, brace yielding near lower gusset, and the bearing failure of stud are shown in Figures 4-22a to 4-22f respectively.

Two cycles of $\pm 4\delta_b$ (47.6mm, 2.16% drift) were performed as final excursions. The magnitude of the buckling waves increased, disconnection in the brace-to-CFSS connection regions grew, and the sounds due to distortion of the infill were more audible. However, no sign of fracture in any specific location in the specimen was observed. All gussets behaved elastically in this case, and did not deflect in the out-of-plane direction. No defects were observed in the brace-to-gusset welded connections. The maximum base shear at this step was 787.3 kN. Some images taken from the previously damaged locations are presented in Figures 4-23a to 4-23f.

The specimen was inspected after the testing especially in the yielding and buckling areas. The behavior of boundary frame and its connections was satisfactory. The overall hysteretic

behavior of specimen F3 was stable. Note that fracture had initiated in Specimen F1 approximately at this displacement level because of substantial cyclic local buckling. In Specimen F2, local buckling had developed without fracture.

Some pictures taken from the specimen just after the test, at zero load and displacement level, are given in Figure 4-24a to 4-24f. Residual buckles and yielded regions show the substantial inelastic behavior of this infill system. Also, post testing images from the brace member, stud bolted connections, U brackets, and stud bearing failure region are illustrated in Figures 4-25a to 4-25f.

The reason for stopping the test at $\pm 4\delta_b$ for Specimen F3 was to not damage the boundary frame beam-to-column connections, since the same boundary frame had to be used for testing Specimen F4.

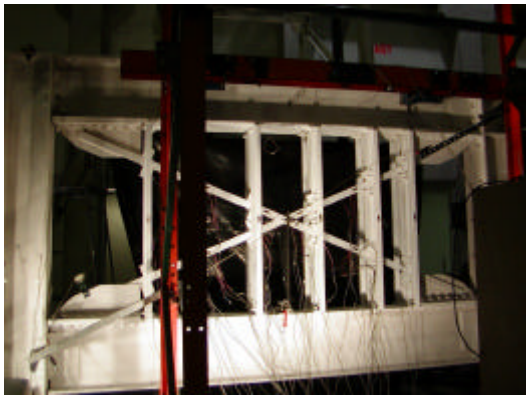

(a)

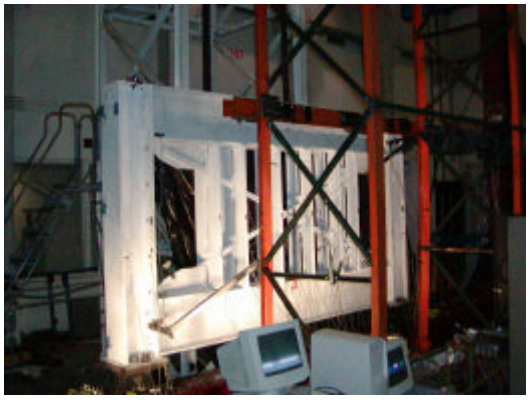

(b)

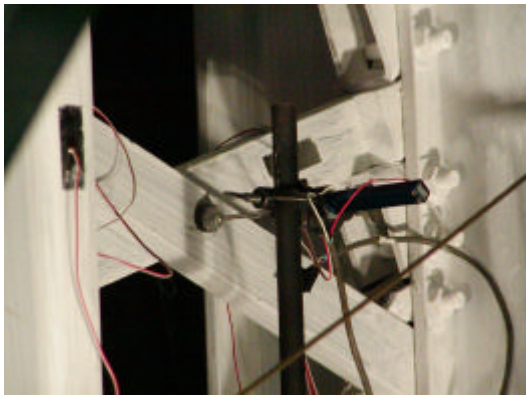

(c)

(d)

(e)

(f)

FIGURE 4-19 Specimen F3 Prior to Testing: (a,b) General Views; (c) Measurement of Out-of-Plane Displacements (Potentiometers); (d) Computer Camera on the Lower South Gusset; (e) Stud-to-Brace Connection Region (In-Plane and Out-of-Plane Buckling Restrainers); (f) Beam-to-Column Bolted, Brace-to-Gusset Welded, and Gusset-to-Lower Beam Bolted Connections

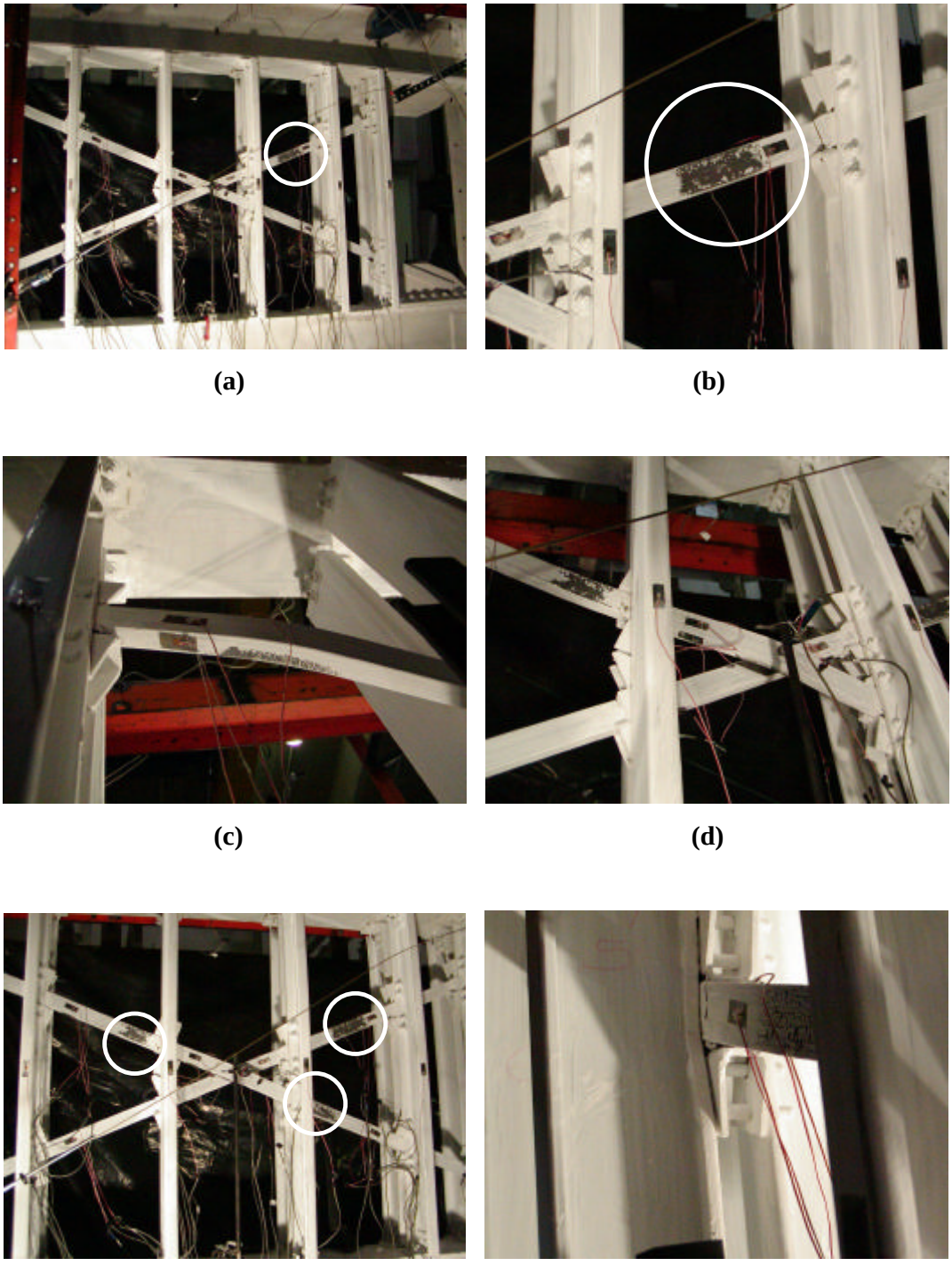

FIGURE 4-20 Behavior of Specimen F3: (a) General View at Brace Buckling (Cycle 10, 1d_y); (b,c) Same, Closer Views; (d) Separation of Braces at Cross Over Region; (e) Yielded Regions Along Braces; (f) Initiation of Bearing Failure in Studs (Cycle 12, 1d_y)

(a)

(b)

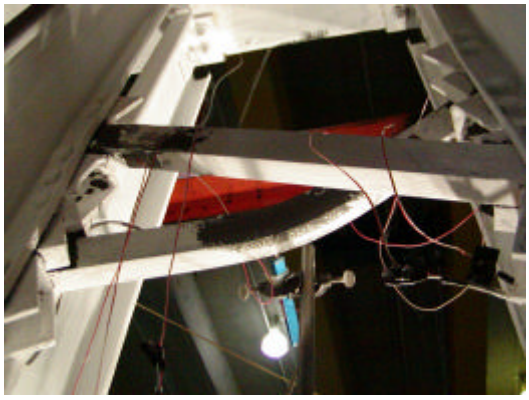

(c)

(d)

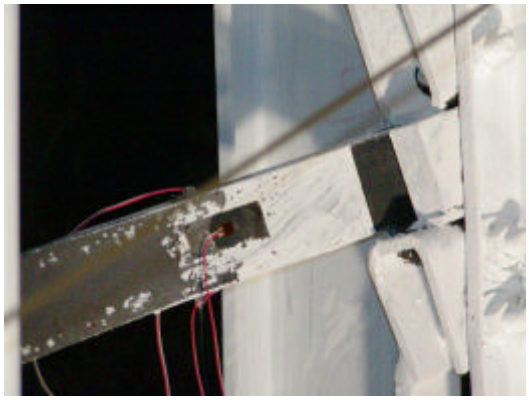

(e)

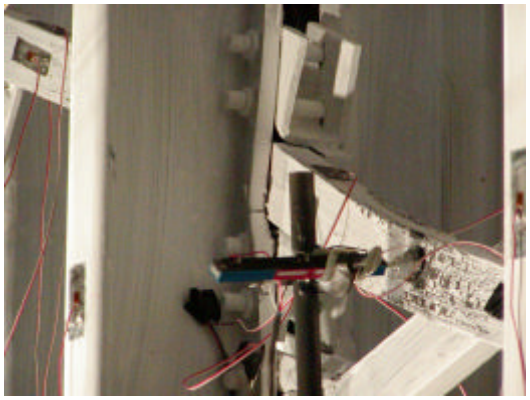

(f)

FIGURE 4-21 Behavior of Specimen F3: (a,b) Buckled Shapes and Yielded Regions (Cycle 13, -2d_y); (c) Separation of Braces in Cross Over Region; (d) Yielding of Brace Around Stud-to-Brace Connection; (e) Disconnection in Stud-to-Brace Connection; (f) Bearing Failure in Studs (Cycle 15, -2d_y)

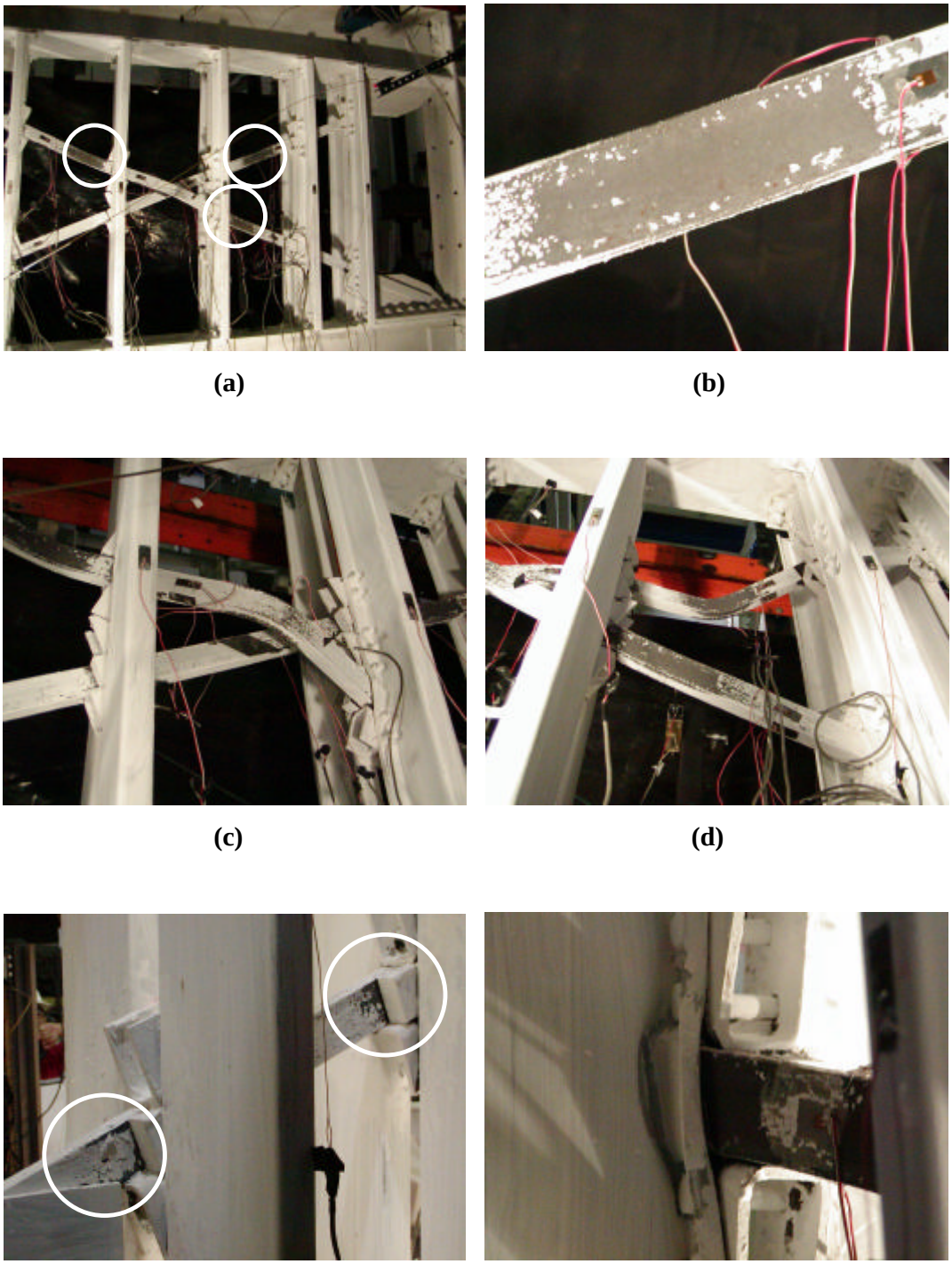

FIGURE 4-22 Behavior of Specimen F3: (a) General View (Cycle 16, -3d_y); (b) Brace Yielding, Same (Cycle 16, 3d_y); (c) Separation of Braces at Cross Over Region (Cycle 16, -3d_y); (d) Yielding in Tension and Compression Braces (Cycle 17, 3d_y); (f) Yielding of Brace Near Gusset (Cycle 18, 3d_y); (f) Bearing Failure in Studs (Cycle 18, -3d_y)

(a)

(b)

(c)

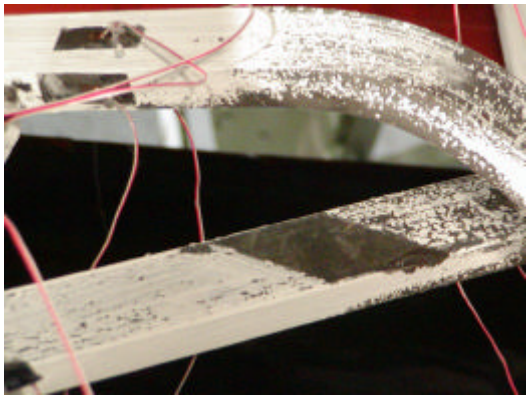

(d)

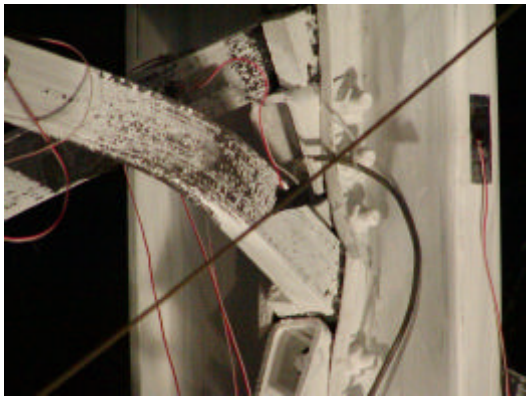

(e)

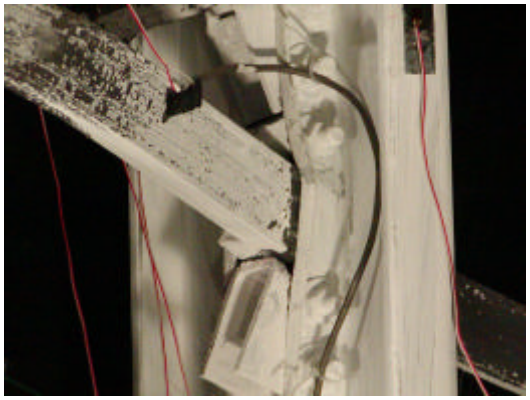

(f)

FIGURE 4-23 Behavior of Specimen F3: (a,b,c) Classical Buckling Shapes and Yielding Regions (Cycle 19, $\pm 4d_y$); (d) Separation of Braces in Cross Over Region; (e,f) Yielding of Braces and Bearing Failure in Studs (Cycle 20, $-4d_y$)

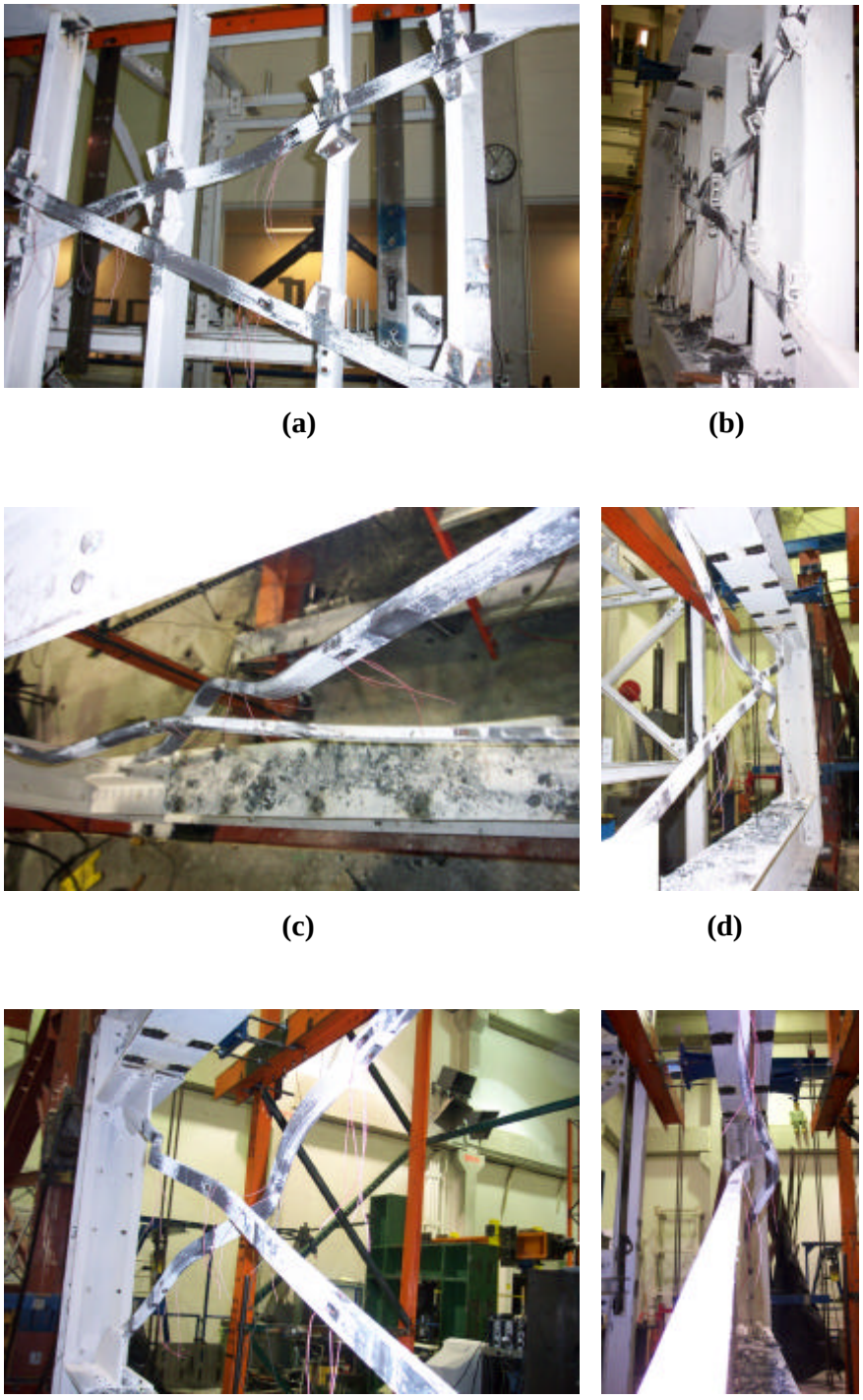

(a) **(b)**

(c) **(d)**

(e) **(f)**

FIGURE 4-24 Post Testing Views from Specimen F3 at Zero Load and Displacement: (a,b) General Views After Cutting Out West Side Studs; (c) General View from Top; (d,e) General Views After Cutting Out East Side Studs; (f) Residual Out-of-Plane Displacements of Braces

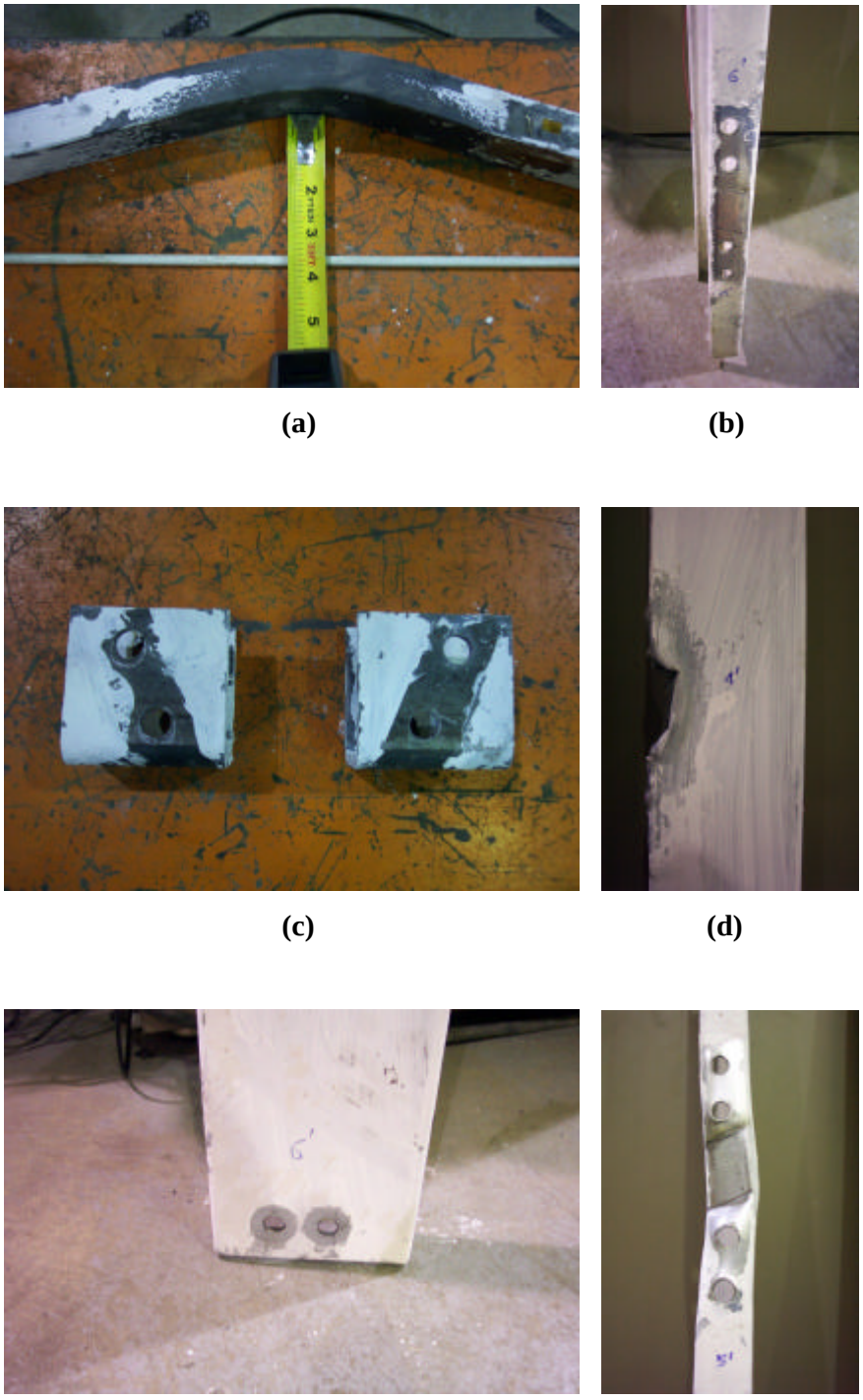

(a) **(b)**

(c) **(d)**

(e) **(f)**

FIGURE 4-25 Post Testing Images from Specimen F3 Members: (a) Residual Deformation of Brace; (b) Undamaged Edge Stud; (c) Undamaged U Brackets; (d) Close View from Damaged Stud Region; (e) Undamaged Stud End Connection; (f) Stud Middle Region Bearing Damage-Undeformed Bolt Holes

4.4.4 Specimen F4

Specimen F4 was subjected to the same displacement history than Specimen F3 to allow to compare the respective hysteretic energy dissipation. Experimentally obtained horizontal force versus displacement hysteresis for Specimen F4 is shown in Figure 4-26. The magnitude of the cyclic displacement history for Specimen F4 is summarized in Table 4-4. Pre-testing pictures taken from this specimen are illustrated in Figures 4-27a and 4-27b.

Specimen F4 exhibited a linear behavior during the first three elastic cycles (2.4mm, 0.11% drift). The base shear was 182.4 kN. During the next cycle at (5.1mm, 0.23% drift), the east side brace buckled at (3.0mm, 0.14% drift) in the out-of-plane direction (towards the west). The base shear was 213.5 kN. In the subsequent cycles at the same displacement, there was no residual displacement, because the buckling was in the elastic range. The last three elastic cycles for Specimen F3 were then performed at 9.1mm, 0.41% drift. Strain gauge recordings indicated yielding in the braces at this step. The maximum base shear was 502.6 kN. Residual buckled shapes at zero force due to brace buckling in both braces occurred. Separation between the braces at the cross-over point reached 12.7mm. Behavior of the specimen during these elastic cycles is illustrated in Figures 4-28a to 4-28d.

Specimen F4 was then subjected to $\pm 1\delta_b$ (11.9mm, 0.54% drift). Whitewash flaked in the tension braces' end connections. Maximum base shear was 516.0 kN. Large out-of-plane displacements were substantial, exceeding half of the column flange width in magnitude. Yielding progressed along both braces, mostly concentrating at the brace end and in the brace middle length regions. At the end of Cycle 15, residual out-of-plane buckled deformations at mid-length of brace reached 90mm at zero force. Specimen general views when the west brace in tension and compression, separation of braces in the middle region, yielding of west side brace upper north end, yielding of west side brace lower south end, and the yielding of brace middle part and residual displacement at the end of Cycle 12 are given in Figures 4-29a to 4-29f respectively.

During the cycles at $\pm 2\delta_b$ (23.8mm, 1.08% drift), strain gauge recordings indicated that attained strains were beyond the yield limit over the entire braces. Infill distortions produced some sounds, however, no sign of damage to any part in the specimen was observed.

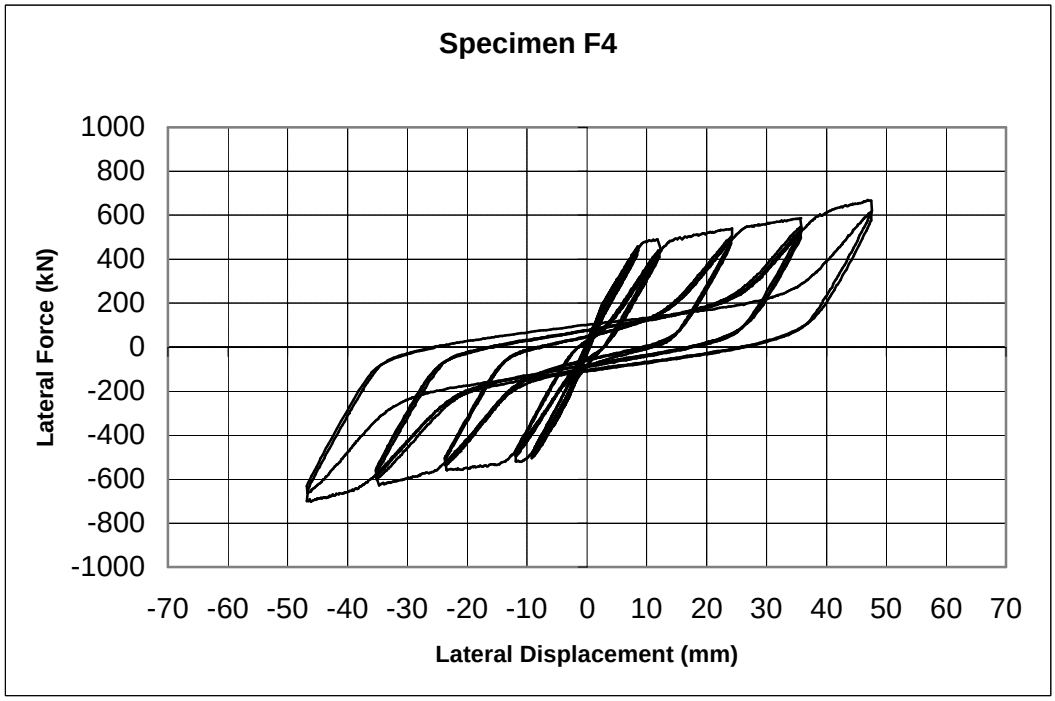

FIGURE 4-26 Hysteresis of Specimen F4

TABLE 4-4 Cyclic Displacement History of Specimen F4

Displacement Step	Number of Cycles	Cumulative No. of Cycles	Displacement (Δ/δ_y)	Displacement (mm)	Drift (%)
1	3	3	0.20	2.4	0.11
2	3	6	0.43	5.1	0.23
3	3	9	0.76	9.1	0.41
4	3	12	1	11.9	0.54
5	3	15	2	23.8	1.08
6	3	18	3	35.7	1.62
7	2	20	4	47.6	2.16

At the end of the second excursion at zero force, out-of-plane brace residual displacement was 203mm. Boundary frame connections were also inspected, and no defect was found. A maximum base shear of 547.1 kN was attained during Cycle 13. Base shear forces dropped slightly at the subsequent cycles at this displacement level. Specimen general views when the west brace in tension and compression, out-of-plane displacement of the west brace, brace yielding around the middle region, progresses of yielding of west side brace lower south end and west side brace upper north end are presented in Figures 4-30a to 4-30f respectively.

The specimen was then subjected to three cycles at $\pm 3\delta_b$ (35.7mm, 1.62% drift). Residual out-of-plane displacements of the brace increased substantially, and reached 267mm at the end of Cycle 16. Noise appeared to come from around the gusset regions. Spread of yielding in the braces in tension and compression resulted in pinching on the hysteretic curves. Maximum base shear was 622.8 kN during Cycle 16. Some images from previously damaged areas are given in Figures 4-31a to 4-31f.

Two final cycles at $\pm 4\delta_b$ (47.6mm, 2.16% drift) were performed. No sign of fracture in any part of the braces and in their connections was observed. Some noises were heard possibly due to bolt slippage. Also, at this displacement level, inelastic behavior of the bottom beam-to-column double angle connections became visible. Maximum base shear was 662.8 kN. Testing was terminated at the end of Cycle 20, since the beam-to-column connections of the boundary frame exhibited inelastic behavior by yielding of web angles and had to be "protected" from failure because the bare frame had to be tested thereafter. Then, the specimen was recentered to zero displacement and zero force. At this position, residual out-of-plane separation between the braces was 346mm. General views when the west brace in tension and compression, maximum out-of-plane displacements of the east and the west braces, yielding of west side brace upper north end, and yielding of west side brace lower south end are given in Figures 4-32a to 4-32f respectively.

As before, the specimen was inspected after testing, especially in the damaged areas. The behavior of boundary frame was satisfactory up to $\pm 3\delta_b$. However, after this point, as stated above, beam-to-column connections behaved inelastically. Specimen F4 exhibited no fracture in any member. Post testing images taken from the specimen at zero load and displacement level are given in Figure 4-33a to 4-33f.

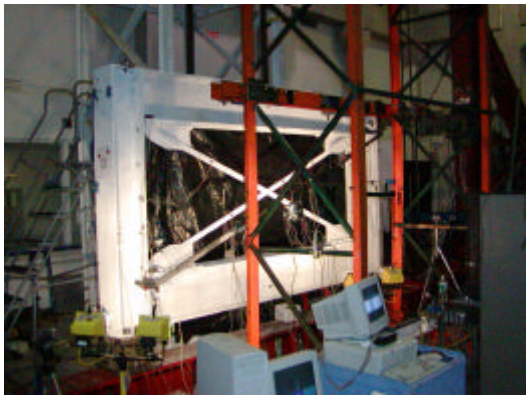

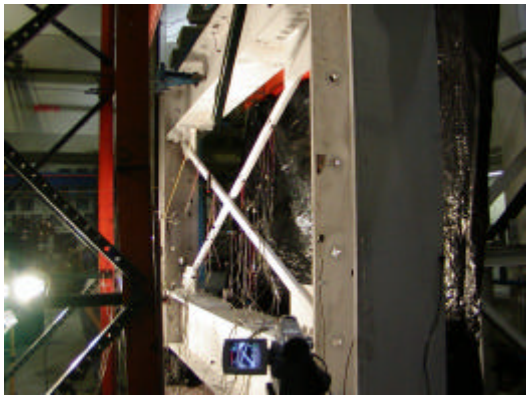

(a) **(b)**

FIGURE 4-27 Specimen F4 Prior to Testing: (a,b) General Views

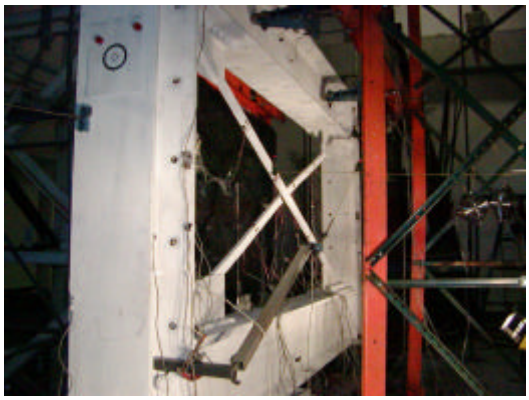

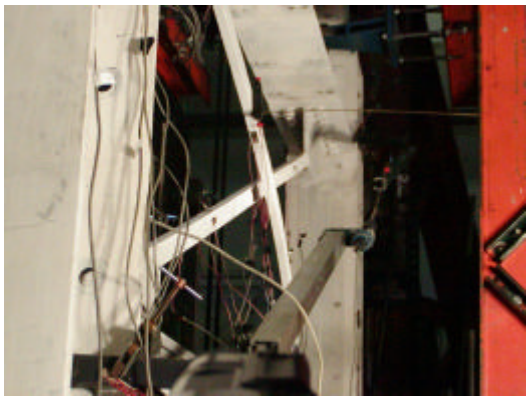

(a) **(b)**

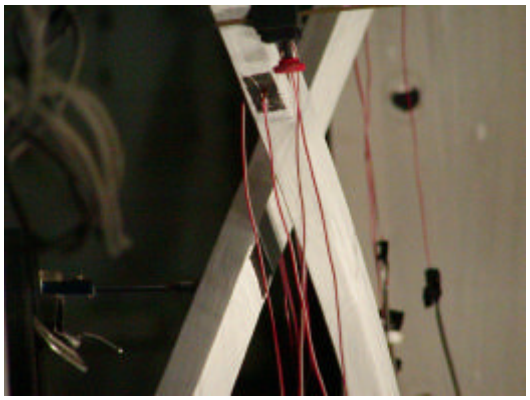

(c) **(d)**

FIGURE 4-28 Behavior of Specimen F4: (a,b) General Views from the West and the East at Brace Buckling (Cycle 4, 0.25d_y); (c,d) Separation of Braces in Cross Over Region (Cycle 9, 0.76d_y)

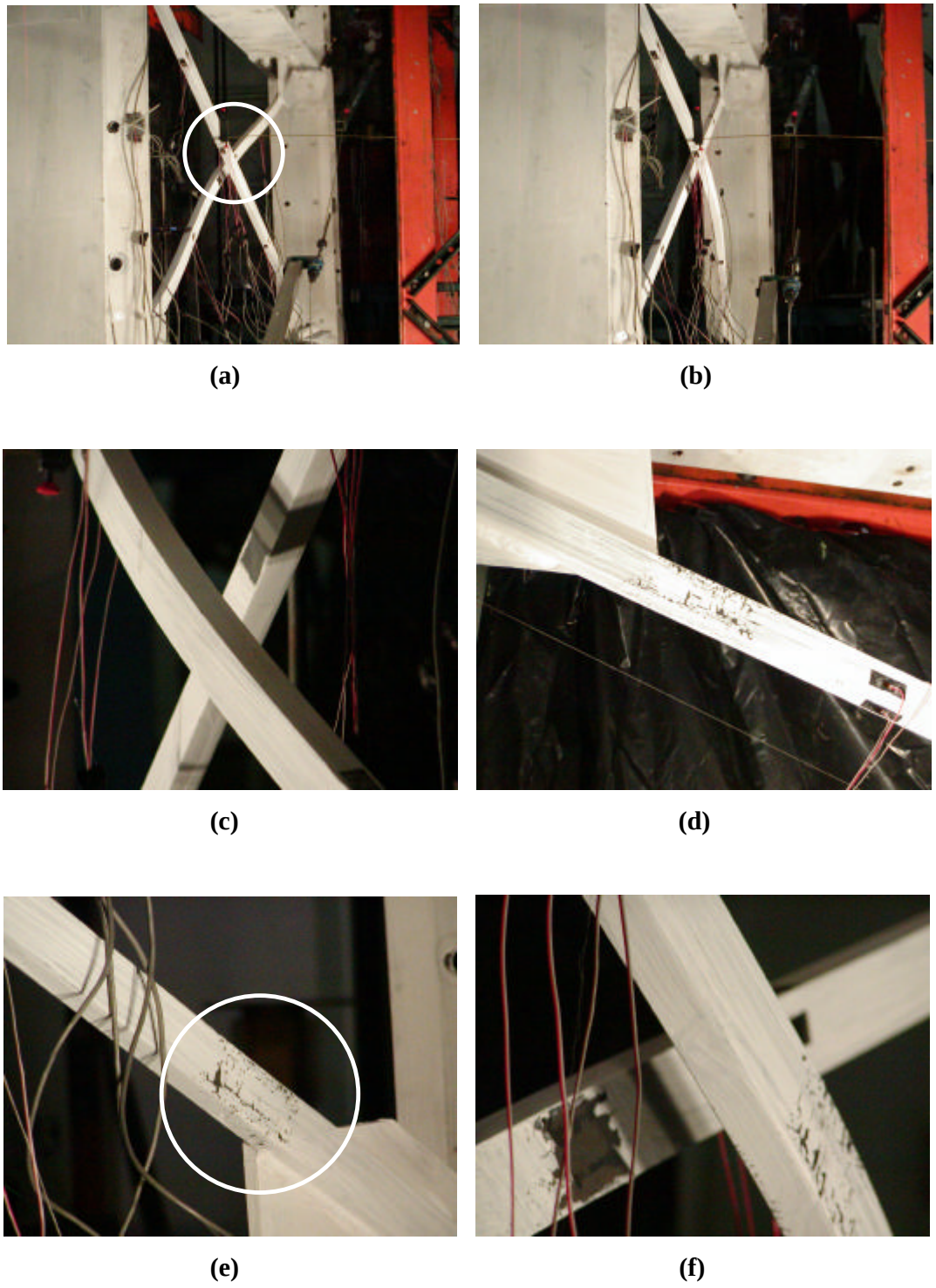

FIGURE 4-29 Behavior of Specimen F3: (a) General View at (Cycle 10, 1d_y); (b) General View at (Cycle 11, -1d_y); (c) Separation of Braces in Cross Over Region; (d) Yielding of West Side Brace Upper North End; (e) Yielding of West Side Brace Lower South End; (f) Yielding of Brace Middle Part and Residual Displacement (End of Cycle 12)

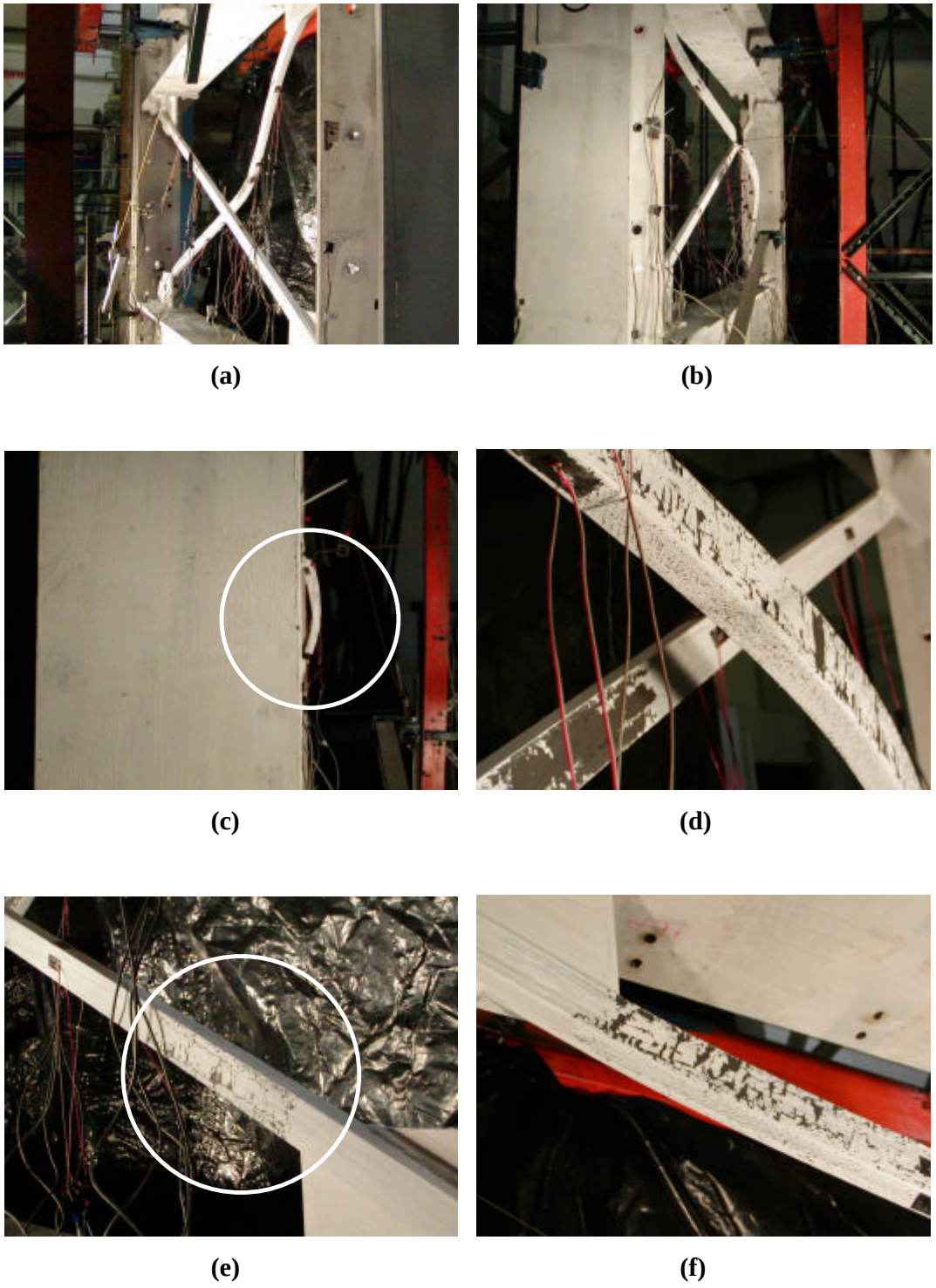

FIGURE 4-30 Damage Level in Specimen F4 at ±2d_y: (a) General View (Cycle 13, 2d_y); (b) General View (Cycle 13, -2d_y); (c) Out-of-Plane Displacement of West Brace (Cycle 14, -2d_y); (d) Same, Closer View; (e) Yielding of West Brace South Lower End; (f) Yielding of West Brace North Upper End (Cycle 15, 2d_y)

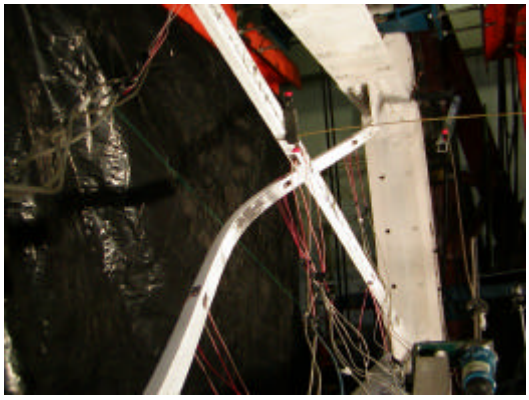

(a)

(b)

(c)

(d)

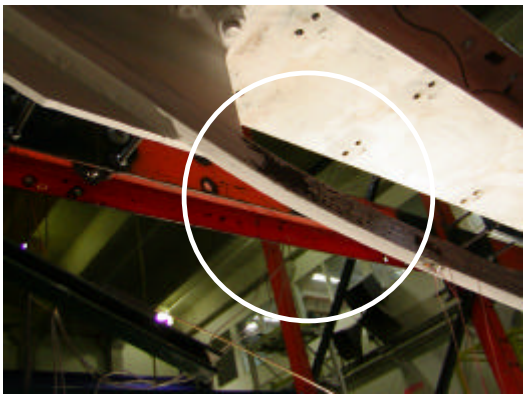

(e)

(f)

FIGURE 4-31 Damage Level in Specimen F4 at ±3d_y: (a) General View (Cycle 18, 3d_y); (b) General View (Cycle 18, -3d_y); (c) Yielding of West Brace North Upper End; (d) Yielding of West Brace South Lower End; (e) Yielding of East Brace South Upper End; (f) Same, West View

(a)

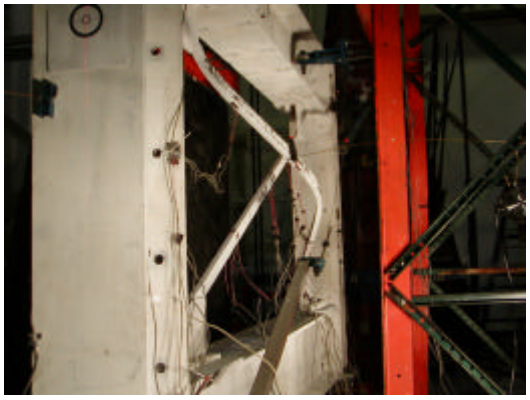

(b)

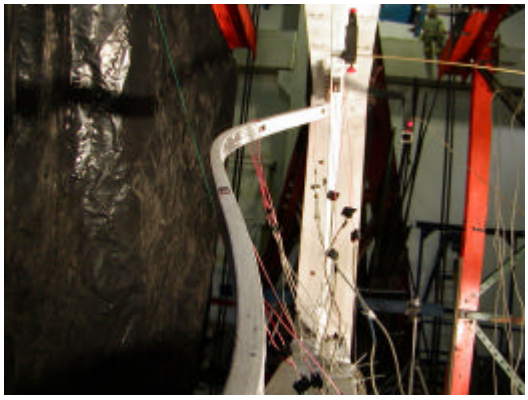

(c)

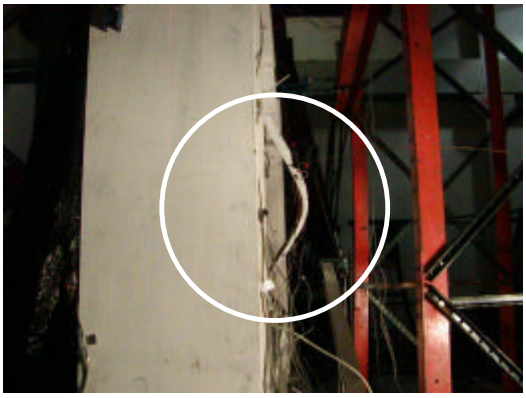

(d)

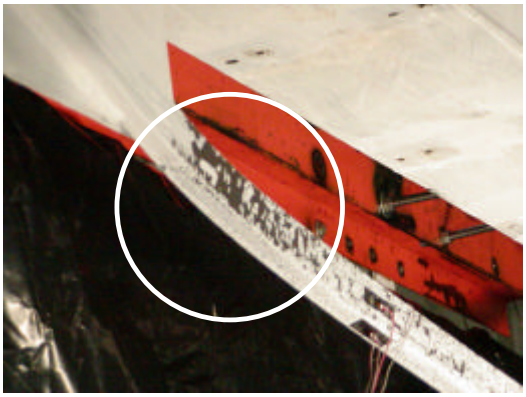

(e)

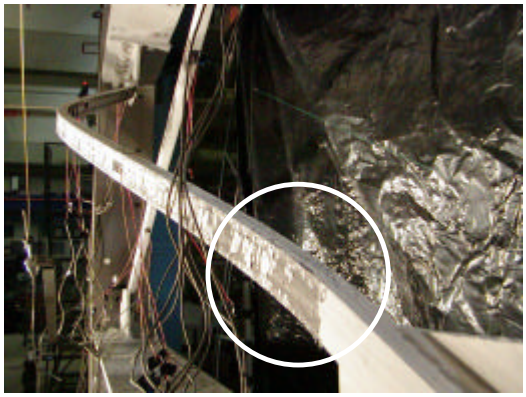

(f)

FIGURE 4-32 Damage Level in Specimen F4 at ±4d_y: (a) General View (Cycle 19, 4d_y); (b) General View (Cycle 19, -4d_y); (c) Out-of-Plane Displacement of East Brace (Cycle 20, 4d_y); (d) Out-of-Plane Displacement of West Brace (Cycle 20, -4d_y); (e) Yielding of West Brace North Upper End; (f) Yielding of West Brace South Lower End

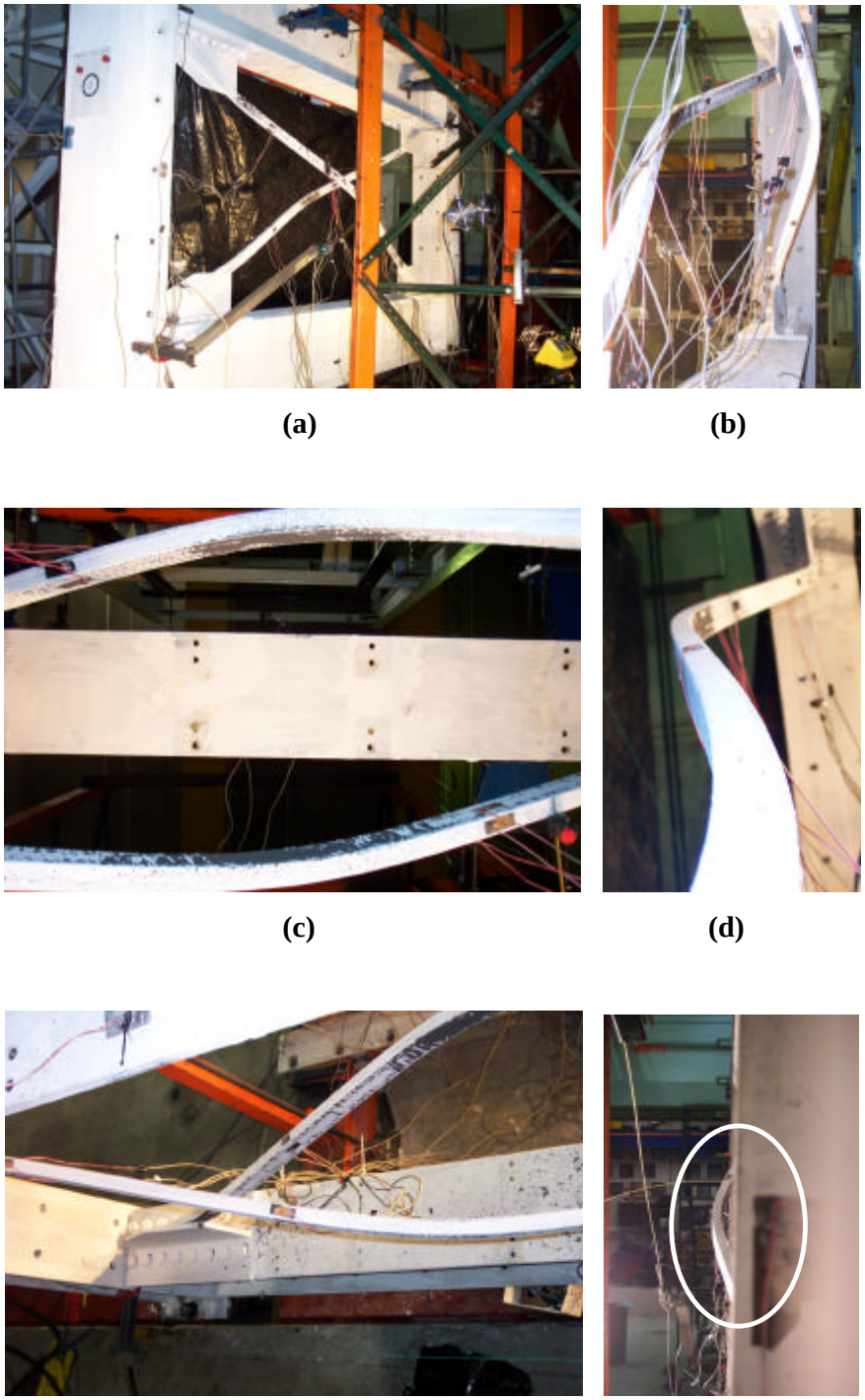

(a) **(b)**

(c) **(d)**

(e) **(f)**

FIGURE 4-33 Post Testing Images from Specimen F4 at Zero Force and Displacement: (a) General View of Specimen F4; (b) General View of East Side from the South; (c) Middle Region View from Bottom to Top; (d) Closer View Along Brace Axis; (e) Top View; (f) Residual Out-of-Plane Displacement of West Side Brace

4.4.5 Cyclic Testing of Bare Frames

To quantify the potential effect of the semi-rigid frame connections on the overall braced frame behavior, the boundary frames without infill were subjected to a series of displacement cycles. Since the first bare frame had been tested prior to this study, experimental data for Bare Frame 1 were already available. Testing for the second bare frame was performed after the last specimen test (Specimen F4), and therefore this bare frame was subjected to cycles of progressively increasing displacements until fractures developed in their beam-to-column double angle connections. Shown in Table 4-5 is the cyclic displacement history imposed on Bare Frame 2. Three-cycles were only applied at 12.7mm, 0.69% drift, which is close to the yield drifts of the specimens tested. Two-cycles at other drift levels were found sufficient for this bare frame testing. Data captured from bare frame tests are illustrated in Figures 4-34a and 4-34c. Both bare frames' hysteretic behaviors were also modeled using the bounding surface model presented in Appendix B and the results are shown in Figures 4-34b and 4-34d. Further information on the parameters used in this model is discussed in Appendix B.

TABLE 4-5 Cyclic Displacement History of Bare Frame 2

Displacement Step	Number of Cycles	Cumulative No. of Cycles	Displacement (mm)	Drift (%)
1	2	2	3.2	0.17
2	2	4	6.4	0.34
3	3	7	12.7	0.69
4	2	9	19.1	1.04
5	2	11	25.4	1.39
6	2	13	31.8	1.74
7	2	15	38.1	2.08
8	2	17	44.5	2.43
9	2	19	50.8	2.78
10	2	21	57.2	3.13
11	2	23	63.5	3.47

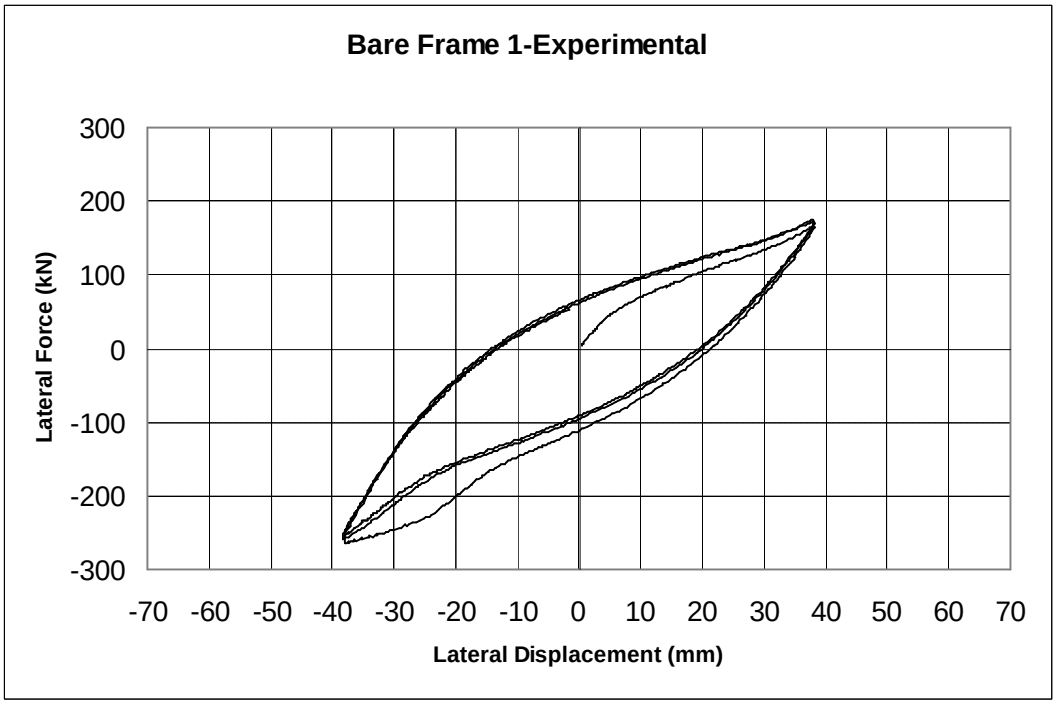

(a)

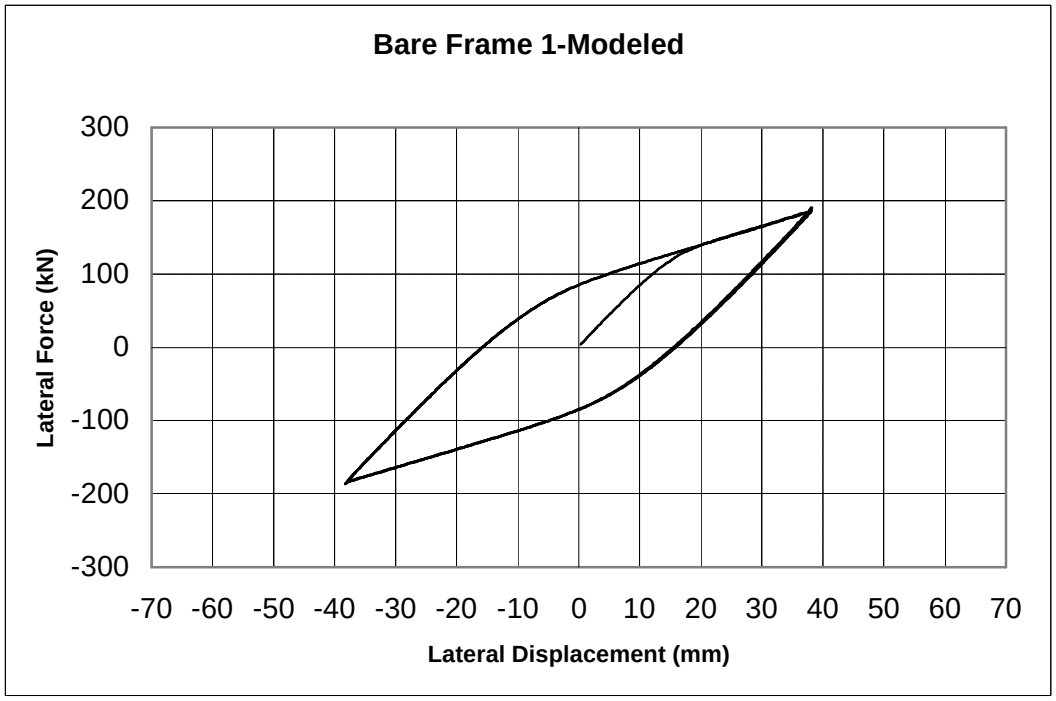

(b)

FIGURE 4-34 Hysteresis Curves for Bare Frames:
(a) Bare Frame 1 (Experimental); (b) Bare Frame 1 (Modeled)

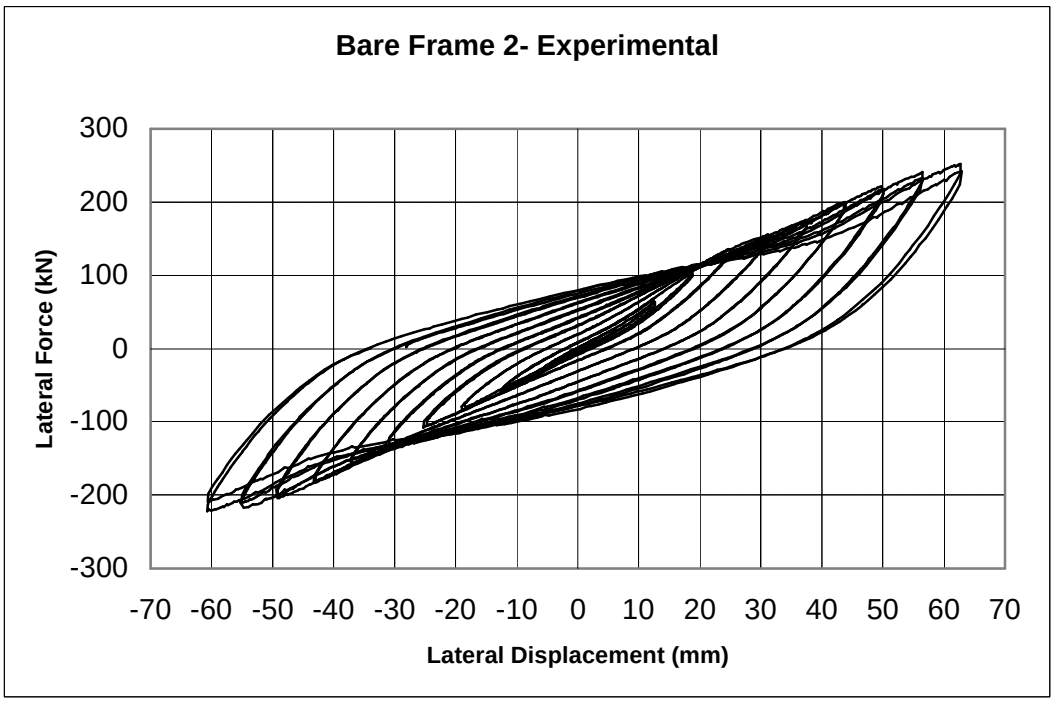

(c)

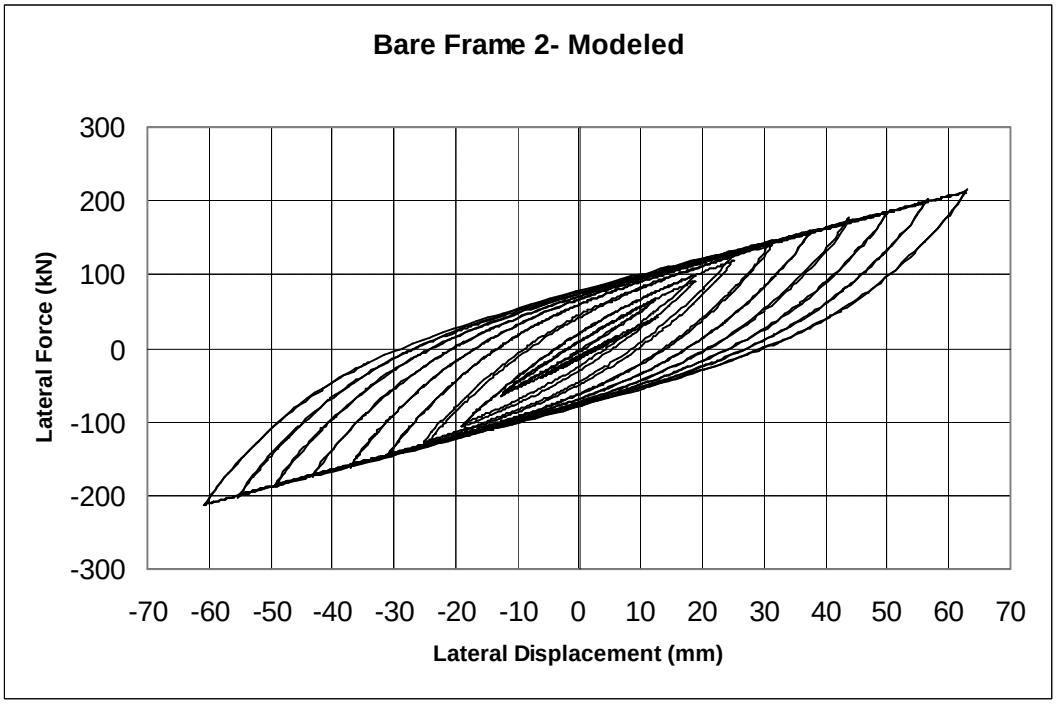

(d)

FIGURE 4-34 Hysteresis Curves for Bare Frames (continued): (c) Bare Frame 2 (Experimental); (d) Bare Frame 2 (Modeled)

SECTION 5
DISCUSSION OF RESULTS

5.1 General

This section discusses reversed cyclic test results of steel frames infilled with four different concentric bracing systems, which were presented in the previous sections. Overall behavior of each specimen at various drift levels is evaluated in terms of base shear versus drift hysteretic curves. Percent drift is computed as the difference between the horizontal displacements at the middle of the top and bottom beams of the specimen divided by the distance between these points (1828.8 mm) and multiplied by 100. To quantify the effect of the boundary frames on behavior, similar hysteretic curves were generated for infill-only cases using the numerical results of the Bounding Surface Method given in Appendix B. For each case, cumulative energy dissipations for the total frame, infill, and the boundary frame (modeled) are computed and plotted against cumulative number of cycles. Fracture lives of tube braces in Specimens F1 and F2 are calculated using the Lee and Goel (1987) and Tremblay et al. (2003) models. Variation of brace out-of-plane displacement with base shear is illustrated. Cold formed steel studs (CFSS) strains at various frame drift levels are plotted to better understand their performances. Additionally, behavioral properties of the specimens, such as initial stiffness, strength at first brace yielding or buckling, total and infill cumulative energy dissipations, maximum displacement ductility reached, and the ratio of experimental to predicted effective length factors for the braces are tabulated. These experimental values are then used to discuss the effectiveness of each infill system. Strain gauge data captured during the testing are plotted and given in Appendices C, D, E, and F.

5.2 Specimen F1

5.2.1 Base Shear-Drift Hystereses

Experimental base shear force versus drift hysteresis curves for Specimen F1 and Bare Frame 1 (modeled as per the procedure described in Appendix B) are shown in Figure 5-1. Results for the case of infill only (i.e. after subtracting the contribution of the bare frame) are illustrated in Figure 5.2. Up to 0.96% drift ($2\delta_y$), the specimen did not show significant deterioration in strength and stiffness, in other words, the behavior was almost cyclic symmetric with comparable axial yielding in tension and compression.

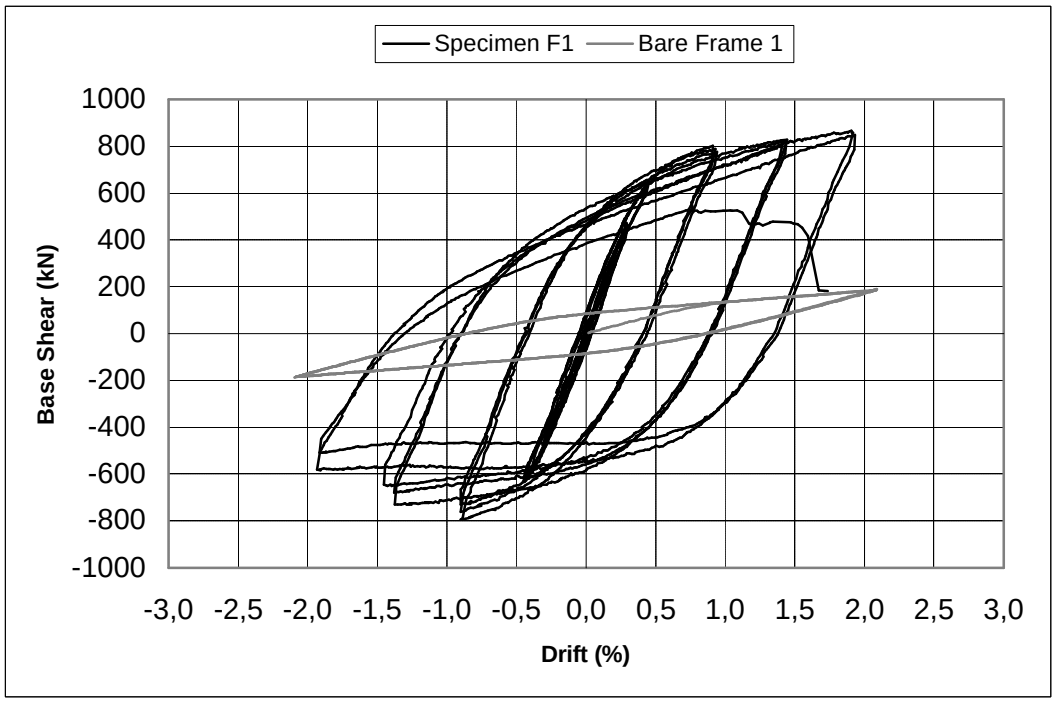

FIGURE 5-1 Specimen F1 and Modeled Bare Frame 1 Hystereses

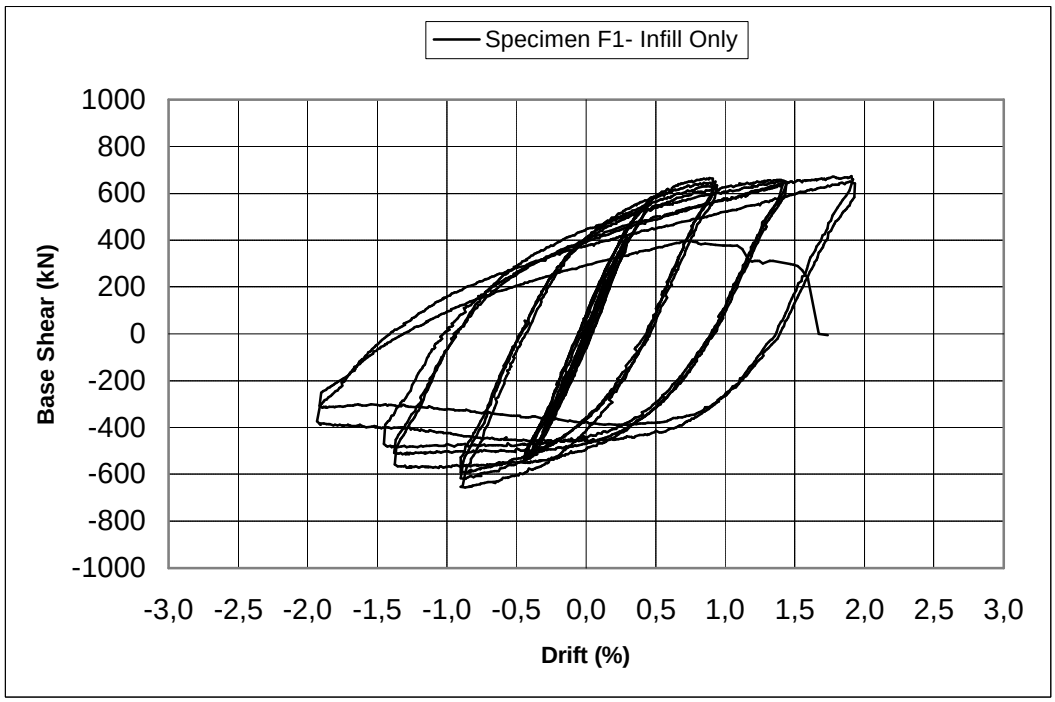

FIGURE 5-2 Specimen F1 Hysteresis (Infill Only)

Beyond this drift level, the shape of the hysteresis curves for Specimen F1 gradually becomes one-sided upon repeated inelastic buckling of the tubular brace member. However, the difference between the buckling and tension strengths in each cycle is still significantly less than would be expected in absence of lateral bracing by the studs.

At 1.44% drift ($3\delta_y$), a decrease in buckling strength is observed due to the development of local buckling in the tube. On the tension side, as expected from the coupon tests, strength increases at each displacement cycle until fracture starts to develop. The ratio of the maximum achieved strength (brace in tension) to the yield base shear is 1.32. Deterioration of the brace post buckling resistance at various drift levels is relatively slow. During the first excursions of compression cycles at 0.96%, 1.44%, and 1.92% drifts, the ratio of the compression strength at that cycle to the peak compression strength reached during the test dropped to 1.00, 0.93, and 0.74. Ratios at the same drift levels for the infill only case are 1.00, 0.87, and 0.60. Strain gauge data (in Appendix C) show that 2% strain was reached in the brace at 1.92% drift. A displacement ductility ratio (μ) of 4 was achieved when the tension and compression strengths of the specimen were, respectively, 100% and 67% of the maximum values obtained experimentally. As seen from Table 5.1, the contribution of the infill to the initial stiffness is 88%.

TABLE 5-1 Behavioral Characteristics of Tested Specimens

Specimen	Total Initial Stiffness (kN/mm)	Initial Stiffness-Infill (kN/mm)	Yield or Buckling Base Shear (kN)	Yield or Buckling Disp. (kN)	Max. Drift (%)	μ	$\frac{K_{exp}}{K_{theoretical}}$	Total Energy (kN.m)	Infill Energy (kN.m)
F1	88.8	78.2	636.1	11.4	1.92	4	1.08	274	227
F2	61.4	51.0	511.5	10.2	2.88	6*	1.81***	310	192
F3	136.0	125.7	898.5	11.9	2.16	4	0.97	205	169
F4	106.6	96.3	182.4	3.0	2.16	4**	1.25	95	37

* Reached displacement ductility based on the yield displacement of Specimen F1.
** Reached displacement ductility based on the buckling displacement of Specimen F3.
*** This large difference comes from the increase in the brace clear length due to inelastic gusset behavior as discussed in Section 5.3.1

Furthermore, the elastic experimental effective length factor (K) was calculated to be 1.08, compared to a theoretical value of 1.00 (taking L as the diagonal distance between stud centers). This value has been obtained using the measured tube strain gauge data for Specimen F1 given in Appendix C, in Figure C-3. This was done by using axial strains below the yield level to calculate the bending moment diagram on the brace; the maximum of the distances between two successive inflection points on the deflected shape (points of zero moment on the bending moment diagram) was taken as the effective length of the brace.

Figure 5-3 shows the theoretical pushover curves envelope proposed by FEMA 368 (2001) (including the bare frame contribution) superposed on top of the hysteretic curves. Calculation details to obtain the pushover curves are given in Appendix A. The initial stiffness and the base shear at brace buckling are respectively approximately 35% and 5% over-predicted by FEMA 368. On the tension side, the maximum achieved base shear is about 16% over-predicted. These differences may be attributed to FEMA 368 modeling assumptions. Fuller hysteretic loops indicate that the contribution of the brace in compression to the total energy dissipation is substantial, and greater than predicted by FEMA 368.

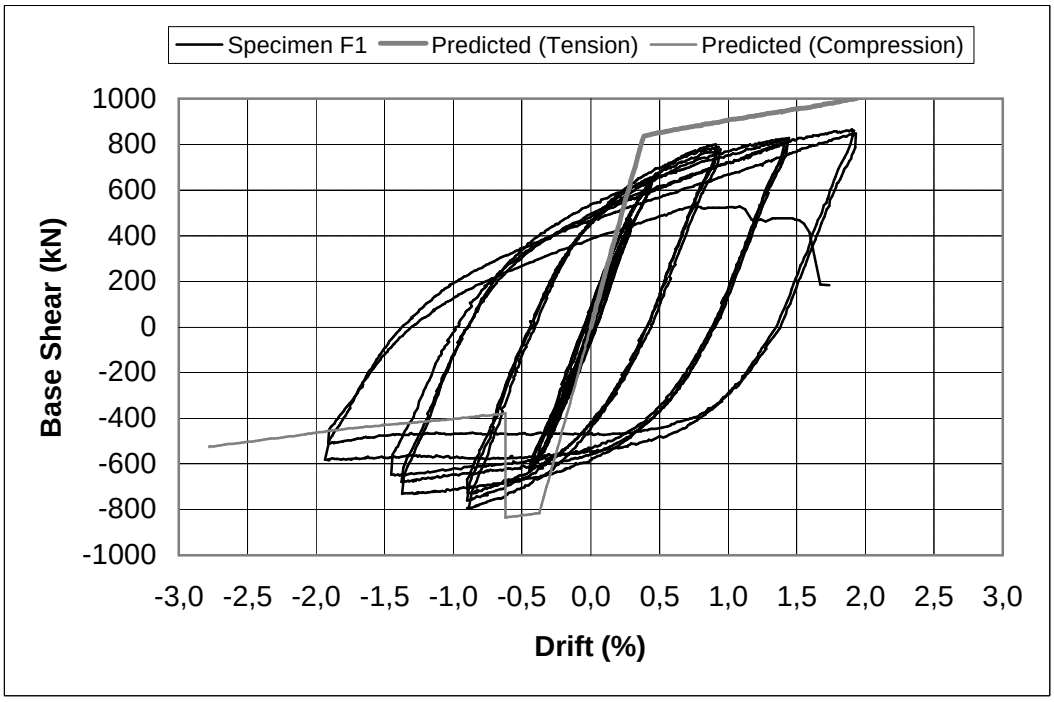

FIGURE 5-3 Experimental Hysteresis and Predicted Pushover Curves for Specimen F1

5.2.2 Fracture Life of Tube Brace

Experimental fracture life ($\Delta_{f,exp}$) of the tube brace is obtained from the hysteretic curves following the procedure proposed by Lee and Goel (1987). The steps of this procedure are:

- Hysteresis curves normalized by yield strength and the corresponding yield displacement are first constructed.
- The tension branch of the hysteresis is divided into two regions, Δ_1 and Δ_2, defined at 1/3 of the yield strength. Δ_1 is the tension deformation from the load reversal point to 1/3 of the yield strength point displacement, while Δ_2 is from 1/3 yield strength point to the unloading point.
- Experimental fracture life is then calculated using

$$\Delta_{f,exp} = \sum \left(0.1\Delta_1 + \Delta_2\right) \tag{5-1}$$

An experimental value of $\Delta_{f,exp}$=32.9 was found for this specimen. Theoretical fracture lives (Δ_f) introduced in Lee and Goel (1987) and Tremblay et al. (2003) methods were also calculated using the following formulas:

Lee and Goel Model

$$\Delta_f = C_s \frac{(46/F_y)^{1.2}}{[(b-2t)/t]^{1.6}} \left(\frac{4b/d+1}{5}\right) \tag{5-2}$$

where

C_s= 1560 (a numerical constant)

F_y= yield stress (ksi)

b= gross width of section

d= gross depth of section

t= thickness of section

Tremblay et al. Method

$$\Delta_f = C_s \frac{(317/F_y)^{1.2}}{[(b-2t)/t]^{0.5}} \left(\frac{4b/d+1}{5}\right)^{0.8} \times (70)^2 \qquad \text{for} \quad KL/r < 70 \qquad (5\text{-}3a)$$

$$\Delta_f = C_s \frac{(317/F_y)^{1.2}}{[(b-2t)/t]^{0.5}} \left(\frac{4b/d+1}{5}\right)^{0.8} \times (KL/r)^2 \qquad \text{for} \quad KL/r \geq 70 \qquad (5\text{-}3b)$$

where C_s determined experimentally by Tremblay et al. is 0.0257 (a numerical constant). Note that in Eq. (5-3a) and (5-3b), F_y should be in MPa.

Numerical values of Δ_f=48.2 and 36.1 were obtained for the Lee and Goel and the Tremblay et al. methods respectively. The ratios of the experimental to theoretical values for these two models are 0.68 and 0.91. For this specimen, the Tremblay et al. method agrees reasonably well with the experimental one, since the recommended empirical formula covers width-to-thickness ratio, KL/r, and the yield strength. The Lee and Goel model does not consider brace slenderness in its fracture life formulation.

5.2.3 Hysteretic Energy Dissipation

For any cycle, the area under the experimentally obtained hysteretic curve gives the dissipated energy through inelastic behavior. Since the cumulative energy dissipation is a useful measure of seismic efficiency of a structural system, these values were calculated, and the variation of cumulative energy dissipation with cumulative number of cycles are plotted in Figure 5-4 for the total frame, infill-only, and the boundary frame contributions. As expected, no significant energy was dissipated during the elastic cycles, and as the brace yields in tension and buckles in compression, the cumulative energy increases rapidly. Figure 5-4 and Table 5.1 show that 83% of the total energy was dissipated by the infill versus 17% for the boundary frame. Strain gauges located on the boundary frame beams and columns remained within the elastic limits throughout the test, as per the design intent. However, inelastic behavior of the beam-to-column double angle connections was observed at large drift ratios, which explain the appreciable contribution of the bare frame to the cumulative energy dissipation at larger drifts seen in Figure 5-4.

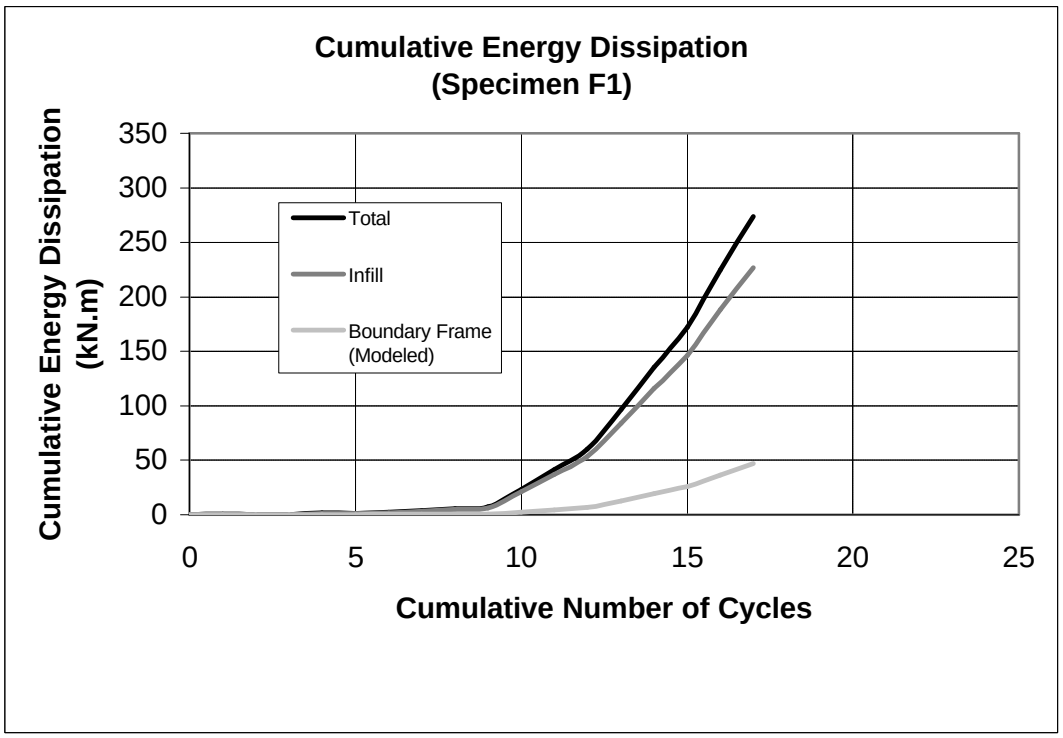

FIGURE 5-4 Cumulative Energy Dissipation by Component for Specimen F1

5.2.4 Base Shear versus Out-of-Plane Displacement Hystereses

In order to evaluate the effectiveness of CFSS members in reducing brace slenderness, base shear versus out-of-plane displacement hystereses are given in Figure 5-5. The location and the labels of the displacement potentiometers are given in Section 3, in Figure 3-26b. Note that data were truncated as the potentiometer 10mm maximum range was exceeded. Figure 5.5 shows that residual out-of-plane deformations usually develop during the inelastic cycles. The increase in the residual out-of-plane deformations at a cycle as compared to a previous cycle is lesser for Specimen F1 than the braces in Specimens F2, F3, and F4, as will be shown later. Reduction of the brace buckling strength is partly due to increases in these cumulative residual out-of-plane deformations.

Out-of-plane displacement demand is constrained by the presence of CFSS, and this is discussed later by comparison to Specimen F2 in Section 5.3.4. However, this produced high out-of-plane forces transmitted to CFSS members, and the intermediate CFSS members suffered damage during the testing. A comparison of the impact of stud and brace configurations in Specimen F3 is also made in Section 5.4.5.

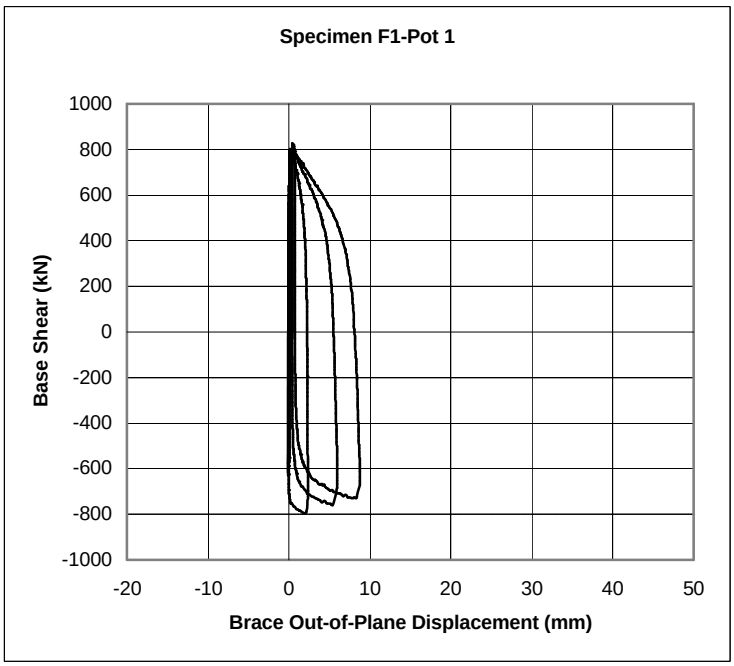

(a)

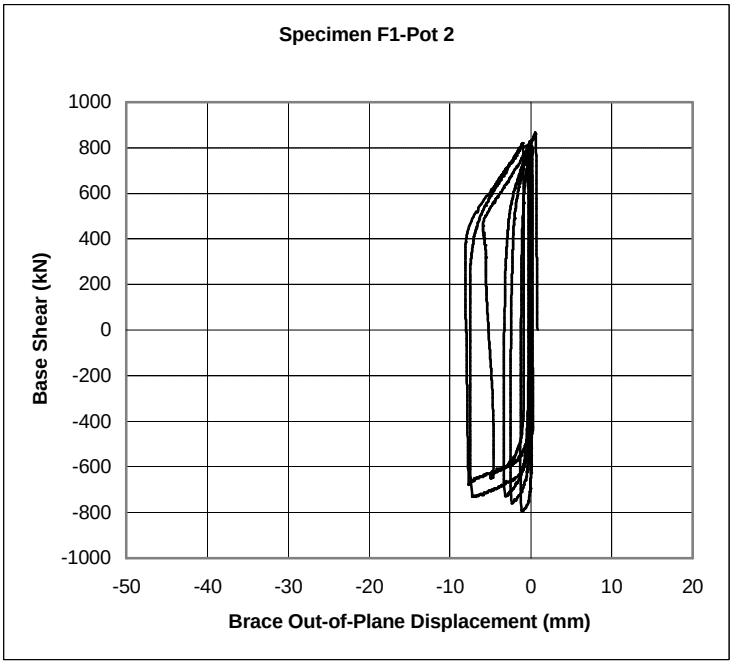

(b)

FIGURE 5-5 Base Shear-Out of Plane Displacement Hystereses for Specimen F1: (a) Pot 1W (West Side Brace Middle Pot-Cycles 1-13); (b) Pot 2W (West Side Brace Intermediate Pot-Cycles 1-16)

5.2.5 Performance of CFSS Members

Specimen F1 exhibited ductile, stable, and unpinched hysteretic behavior mainly provided by the existence of the CFSS members. These members and U brackets prevented out-of-plane and in-plane brace buckling at the early stages of cyclic loading. After several cycles at displacement levels greater than the yield displacement, bearing failure of the intermediate studs led to loss of contact between the buckling restrainers and the brace, which resulted in reduced base shear strength and system stiffness. Figures 5-6 and 5-7 show the west and east sides stud maximum axial strains at various drift levels. Although, up to approximately 1.5% drift, the studs performed well with no significant inelastic behavior, after this drift level, some of the intermediate studs behaved beyond the elastic limits.

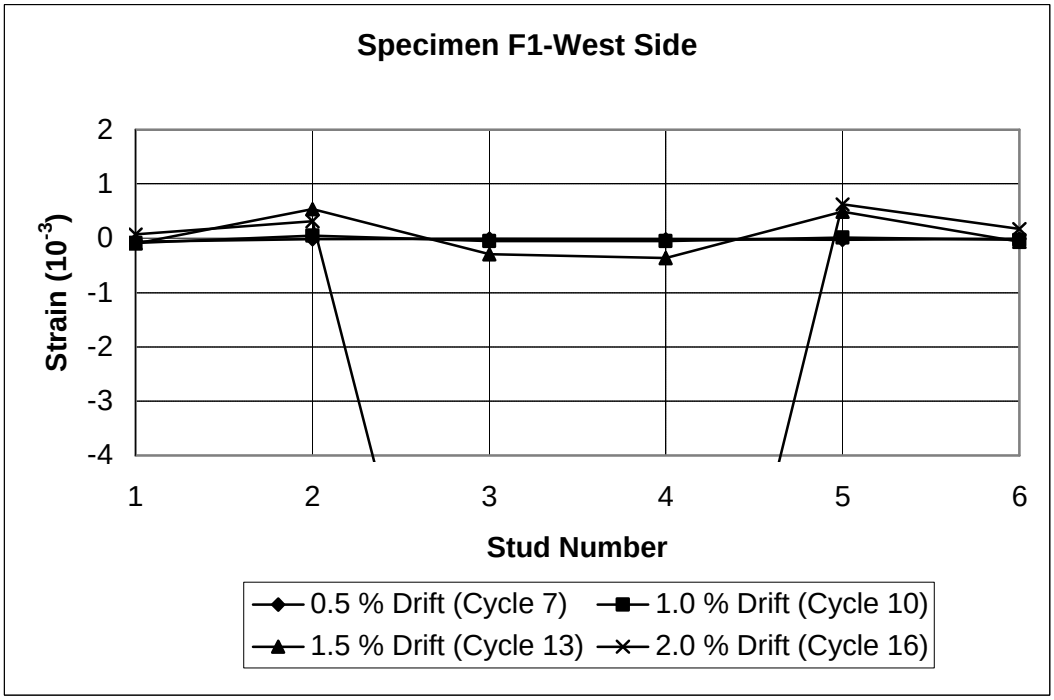

FIGURE 5-6 West Side Stud Strains at Various Drift Levels

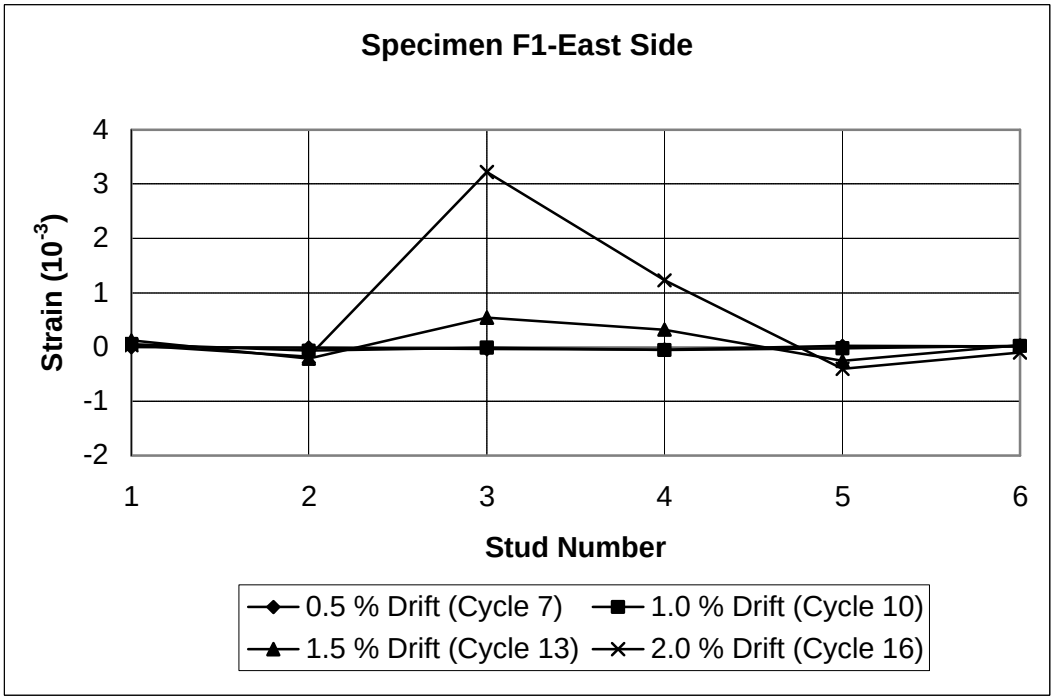

FIGURE 5-7 East Side Stud Strains at Various Drift Levels

5.3 Specimen F2

5.3.1 Base Shear-Drift Hystereses

The base shear force versus drift hysteresis for Specimen F2 is shown in Figure 5-8 superimposed with the hysteresis of Bare Frame 1 (modeled as per the procedure described in Appendix B). Results for the case of infill only (i.e. after subtracting the contribution of the bare frame) are illustrated in Figure 5.9. Specimen F2 exhibited ductile and stable cyclic behavior up to 2.40% drift, although some pinching is obvious in the hystereses. Up to 0.48% drift, the hystreresis curves are cyclic symmetric, however, in the aftermath of brace buckling, they become one-sided due to the deterioration in buckling strength. On the tension side, strength increases until fracture develops. The ratio of the maximum tension strength to the yield strength is 1.26.

During the first excursions of compression cycles at 0.48%, 0.96%, 1.44%, 1.92%, and 2.40% drifts, the ratio of the compression strength at that cycle to the peak compression strength reached during the test dropped to 1.00, 0.76, 0.58, 0.46, and 0.44. For infill-only case, ratios at the same drifts are 1.00, 0.82, 0.53, 0.47, and 0.46. Note that the largest relative deterioration in buckling strength occurs at the two preceding cycles just after the buckling cycle. During the following cycles, there is no significant change in this ratio since it begins to stabilize. Residual buckling strengths of 0.59 (total frame) and 0.16 (infill) were obtained at the last compression cycles prior to fracture versus a proposed constant value of 0.40 given in FEMA 368 (2001). Strain gauge data (in Appendix D) show that 1.5% strain was reached in the tubular brace at 2.50% drift. Specimen F2 exhibited a displacement ductility ratio (μ) of 6, when the tension and compression strengths were 65% and 46% of the maximum achieved peak strengths.

Table 5.1 shows that the contribution of the brace to the initial stiffness is 83%. The experimental elastic K factor was found to be 0.90 compared to a theoretical value of 0.5 (taking L as the clear brace length between gussets). This value has been obtained using the measured tube strain gauge data for Specimen F2 given in Appendix D, in Figure D1, and following the same procedure to obtain the moment diagram as was done for Specimen F1 before.

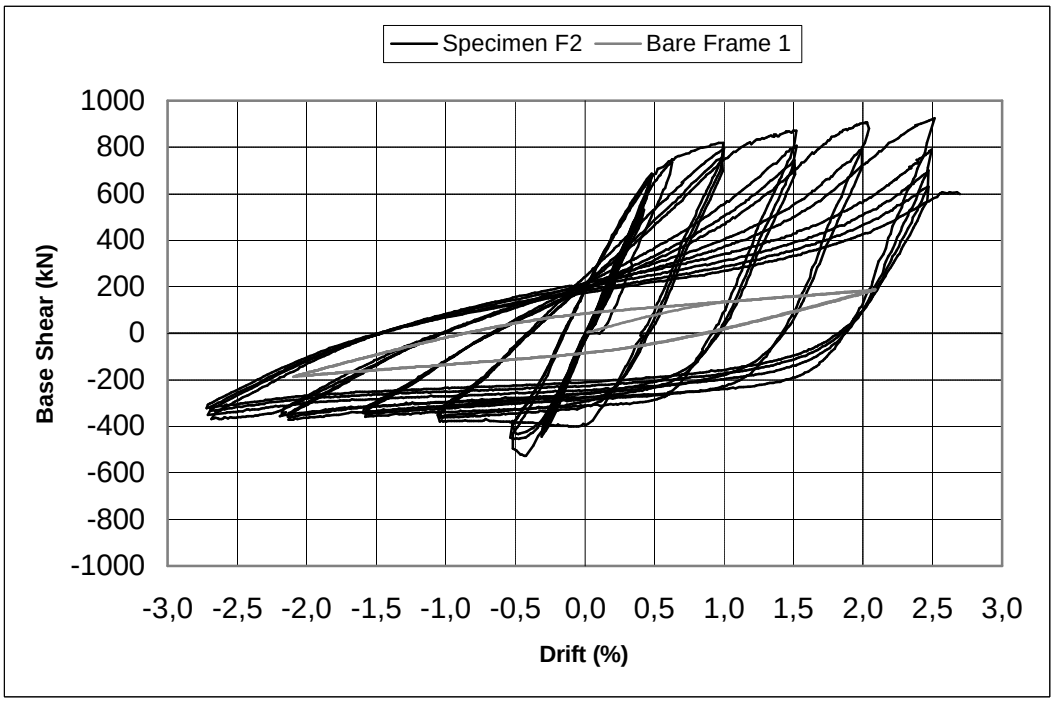

FIGURE 5-8 Specimen F2 and Modeled Bare Frame 1 Hystereses

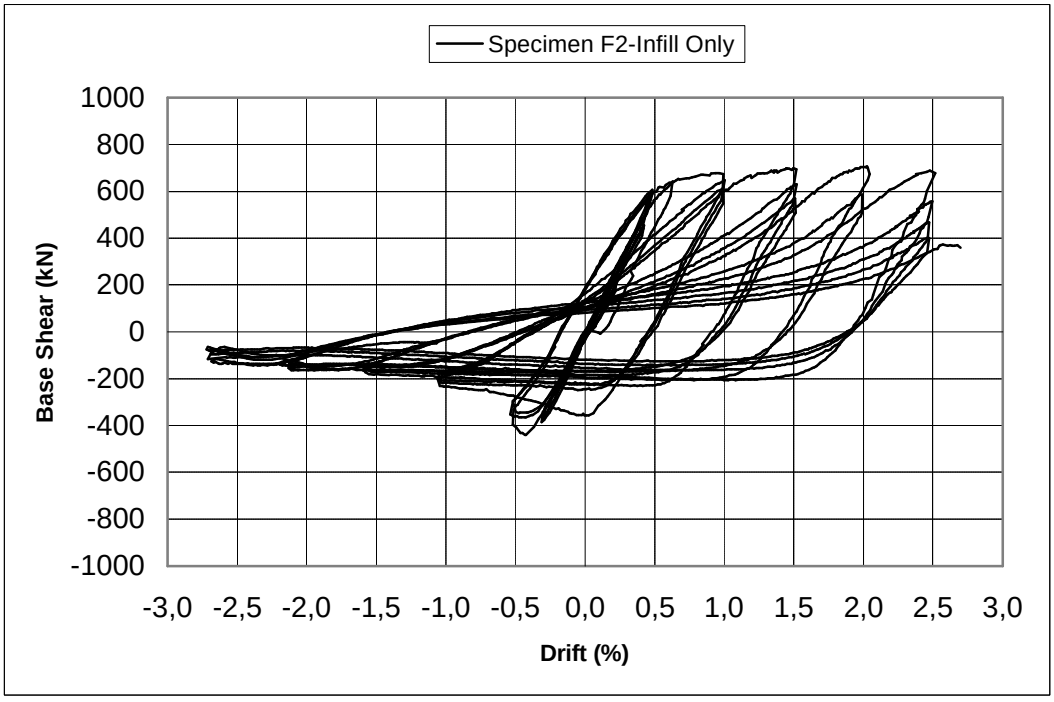

FIGURE 5-9 Specimen F2 Hysteresis (Infill Only)

This difference in the experimental and predicted K factors is due to the inelastic behavior of the lower south gusset plate (as illustrated in Section 4), which in turn resulted in a longer effective length. This gusset was bent back and forth in the out-of-plane direction during the early stages of testing, resulting in a longer brace length and ultimately a lower buckling strength. However, using this experimental clear brace length (clear length of the brace plus the diagonal distance up to the yield line in the gusset) gives an experimental elastic K factor to be 0.78.

Shown in Figure 5-10 are the theoretical pushover curves envelope (including the bare frame contribution) superposed on top of the hysteretic curves. Calculation details in obtaining the pushover curves are given in Appendix A. The initial stiffness and the negative base shear at brace buckling are approximately 93% and 41% over-predicted respectively. The reason for this was explained above. Moreover, since the bare frame was subjected to many cycles of displacements in Specimen F1 testing, the contribution of the bare frame to the initial stiffness was small due to the inelastic behavior of its beam-to-column connections. On the tension side, the maximum achieved base shear is about 11% over-predicted.

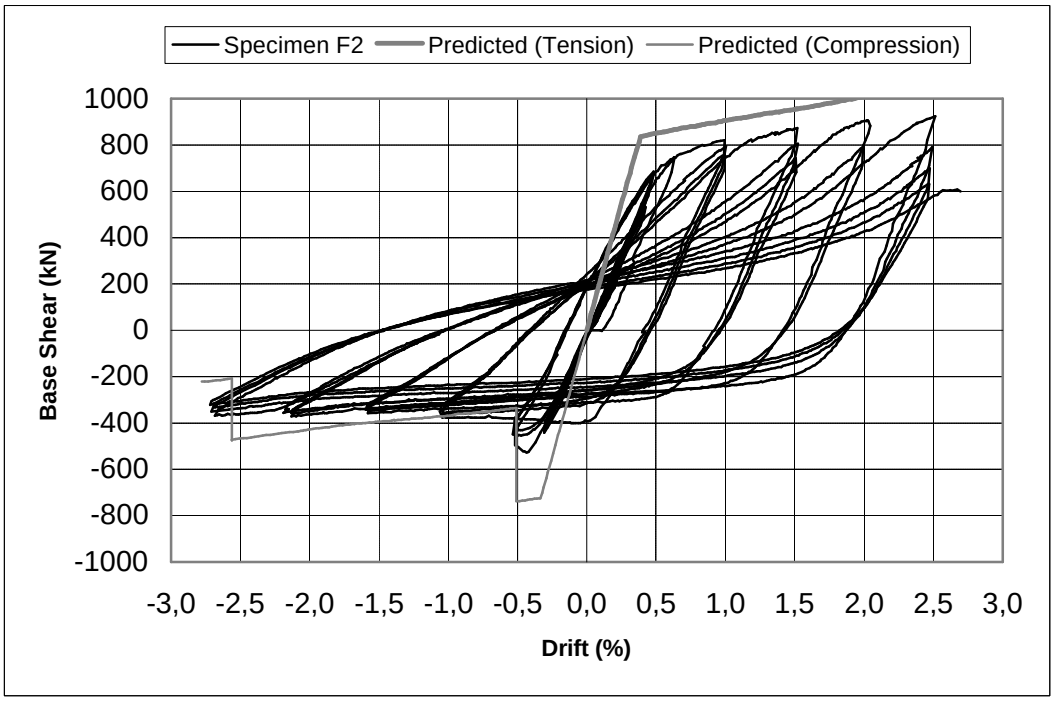

FIGURE 5-10 Experimental Hysteresis and Predicted Pushover Curves for Specimen F2

5.3.2 Fracture Life of Tube Brace

Experimental and theoretical fracture lives of the tube brace are obtained using the obtained hysteretic curves and the methods described in Section 5.2.2. An experimental value of $\Delta_{f,exp}$=64.7 was calculated for this specimen. Note that the cycles at $3\delta_y$ (1.44% drift) and above contributed to the fracture life most (83% of the total). Theoretical fracture lives Δ_f=48.2 and 43.9 are obtained using the Lee and Goel and the Tremblay et al. methods respectively (using the experimental KL/r value of 77.3). The ratios of the experimental to theoretical values for these two models are 1.34 and 1.47. Both methods underestimates the fracture life of the tube brace, and the Lee and Goel model gives closer results in this case.

5.3.3 Hysteretic Energy Dissipation

The variation of cumulative energy dissipation against cumulative number of cycles is plotted in Figure 5-11 for the total frame, infill-only, and the boundary frame contributions. Appreciable energy was dissipated after the elastic cycles, and increased in the following cycles. Also of interest in Table 5.1 is the total energy dissipation is substantial. 62% of the total energy was dissipated by the infill versus 38% for the boundary frame. Strain gauges mounted on the boundary frame beams and columns remained within the elastic limits, as expected. However, Figure 5-11 shows that contribution of the bare frame to cumulative energy dissipation at larger drifts is appreciable due to inelastic behavior of the beam-to-column connections (also some web angles fractured).

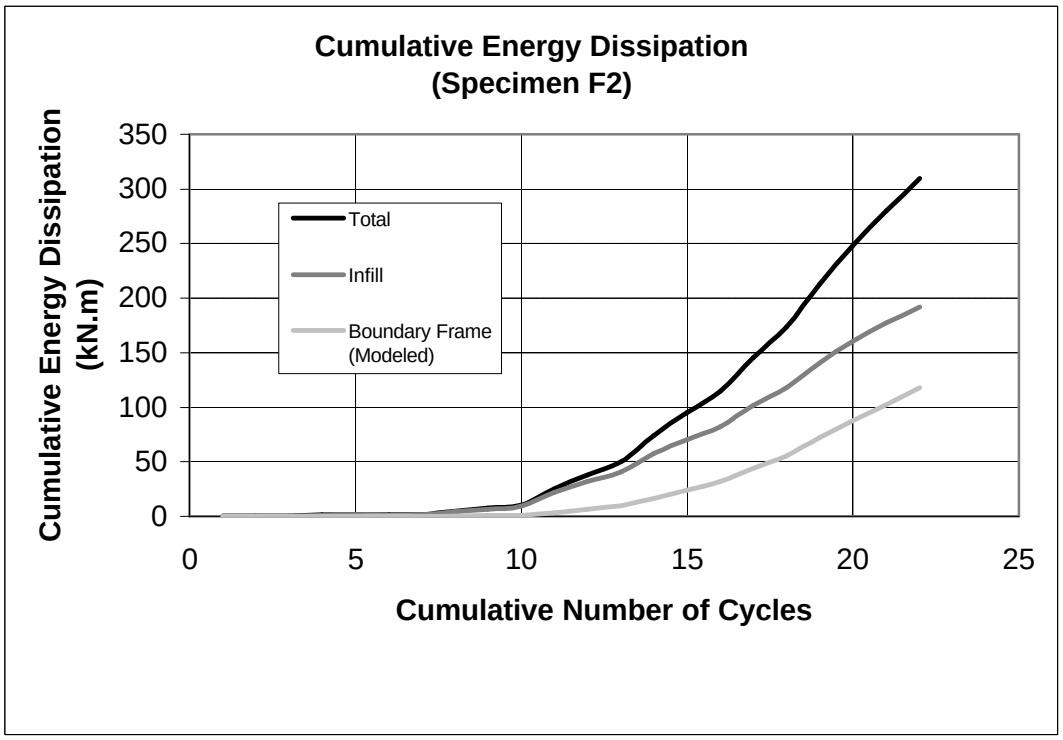

FIGURE 5-11 Cumulative Energy Dissipation by Component for Specimen F2

5.3.4 Base Shear versus Out-of-Plane Displacement Hystereses

Base shear versus out-of-plane displacement hystereses are given in Figure 5-12. The location and the labels of the displacement potentiometers are given in Section 3, in Figure 3-27b. Note that data were truncated as the potentiometer capacities were exceeded. It is evident from Figure 5-12 that residual out-of-plane deformations develop upon cyclic buckling and increase substantially with cycling. These cumulative out-of-plane deformations reduced the buckling strength at inelastic compression cycles. Out-of-plane displacement demand is large in this case due to the inexistence of CFSS, and the brace underwent large displacements prior to fracture as illustrated in Section 4. At the same displacement level, while out-of-plane deformations were negligible and remained in the elastic ranges for Specimen F1, these deformations became more pronounced, with large residual displacements during cycling in Specimen F2.

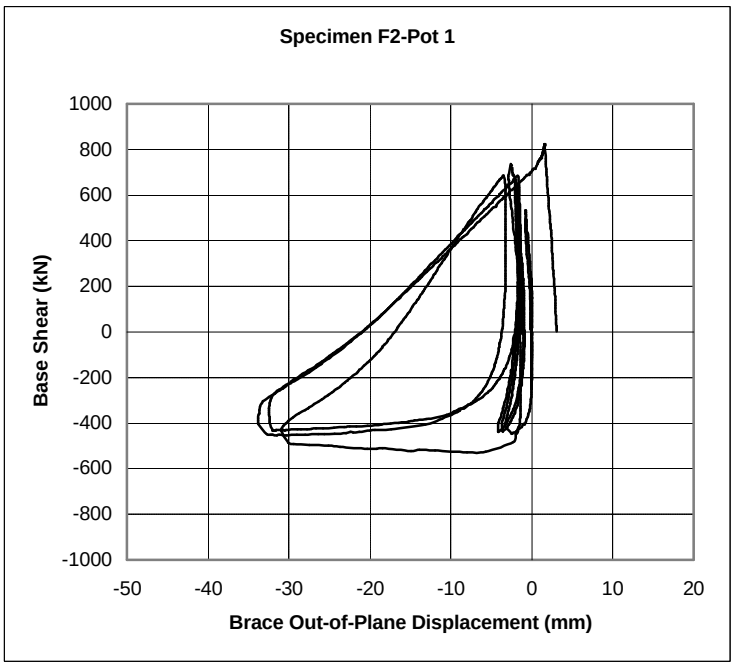

(a)

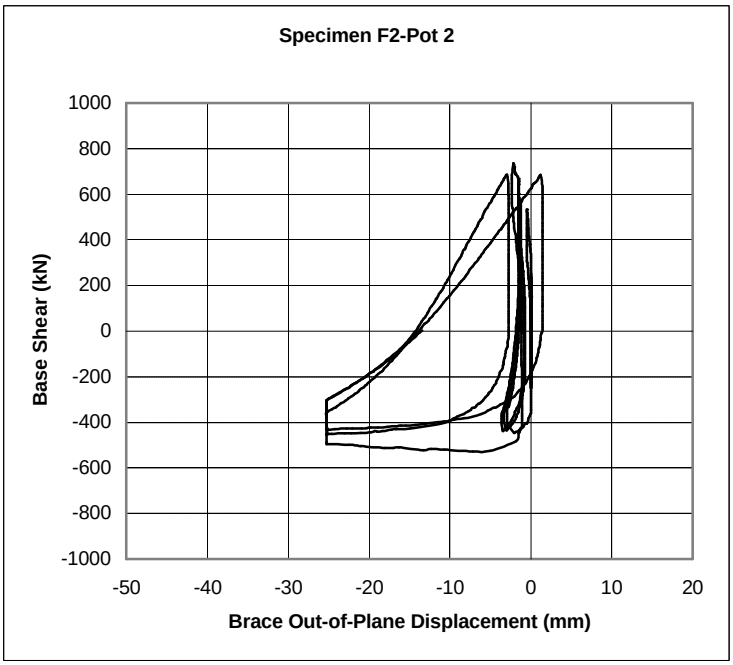

(b)

FIGURE 5-12 Base Shear-Out of Plane Displacement Hystereses for Specimen F2: (a) Pot 1W (West Side Brace Middle Pot-Cycles 1-10); (b) Pot 2W (West Side Brace Intermediate Pot-Cycles 1-9)

5.4 Specimen F3

5.4.1 Base Shear-Drift Hystereses

Experimental base shear force versus drift hysteresis curves for Specimen F3 and Bare Frame 2 (modeled as per the method introduced in Appendix B) are shown in Figure 5-13. The loops after subtracting the contribution of the bare frame are illustrated in Figure 5.14. Up to approximately 0.50% drift, the specimen did not show deterioration in strength and stiffness. At the onset of buckling of the east side brace segment between the fourth and the fifth studs (counting from the north), the base shear dropped abruptly. The peak base shear force during test was reached prior to this buckling. After buckling, the hysteresis for Specimen F3 stabilizes and fuller curves on both tension and compression sides develop. Negative and positive base shear forces reached differ slightly from each other, which is attributable to the symmetric X brace configuration of the specimen. For negative and positive base shears, absolute ratios of the maximum negative and positive base shears at final cycles to the peak base shear at brace buckling are 0.89 and 0.83 respectively. Base shear forces gradually increased during the first cycle of each displacement increment, and seems to somewhat decrease slightly during the second and third cycles thereafter.

The overall behavior of Specimen F3 was ductile and stable up to 2.16% drift, although pinching in the hysteretic loops is apparent. During the second and third cycles at each imposed drift level, the hysteresis curves tend to meet at the peak point (peak oriented hysteretic curve) of the previously obtained hysteresis.

Variation in the negative base shear (in the direction of the initially buckled brace in compression) illustrates the deterioration of brace post buckling resistance at various drift levels. However, since one of the brace always in tension and the bare frame strain hardens, the total base shear can actually increase at large displacements. In fact, during the first excursions of compression cycles, the ratio of the negative base shear (total specimen) at that cycle to the negative peak base shear at 0.54%, 1.08%, 1.62%, and 2.16% drifts dropped to 1.00, 0.83, 0.85, and 0.89. For the infill-only case, same ratios are 1.00, 0.75, 0.73, and 0.73.

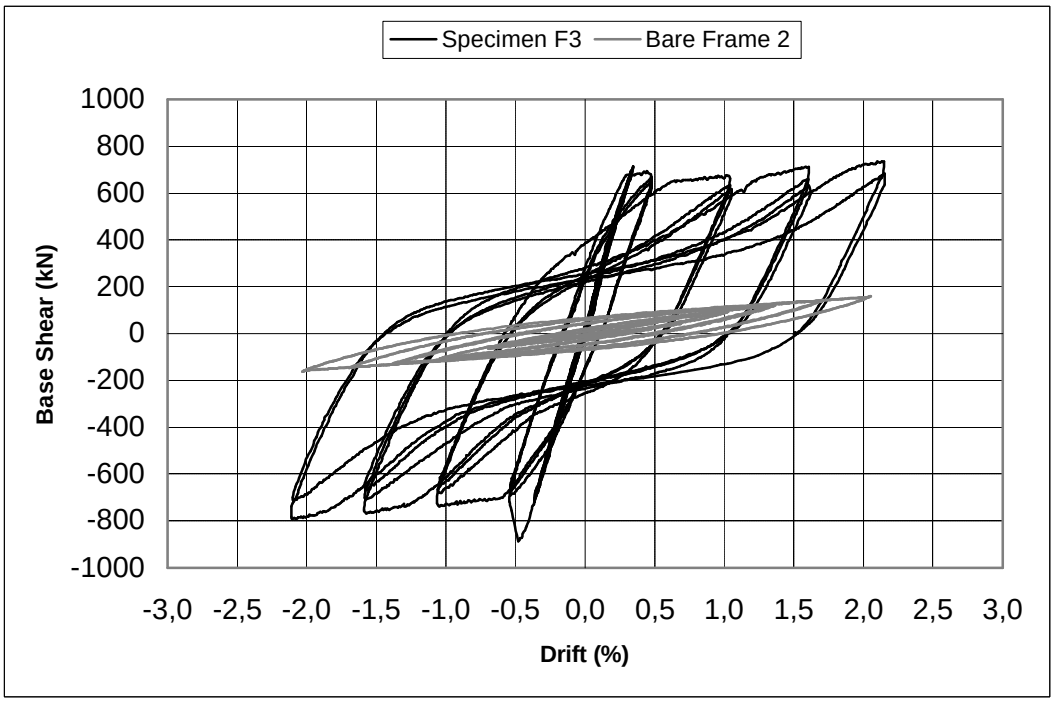

FIGURE 5-13 Specimen F3 and Modeled Bare Frame 2 Hystereses

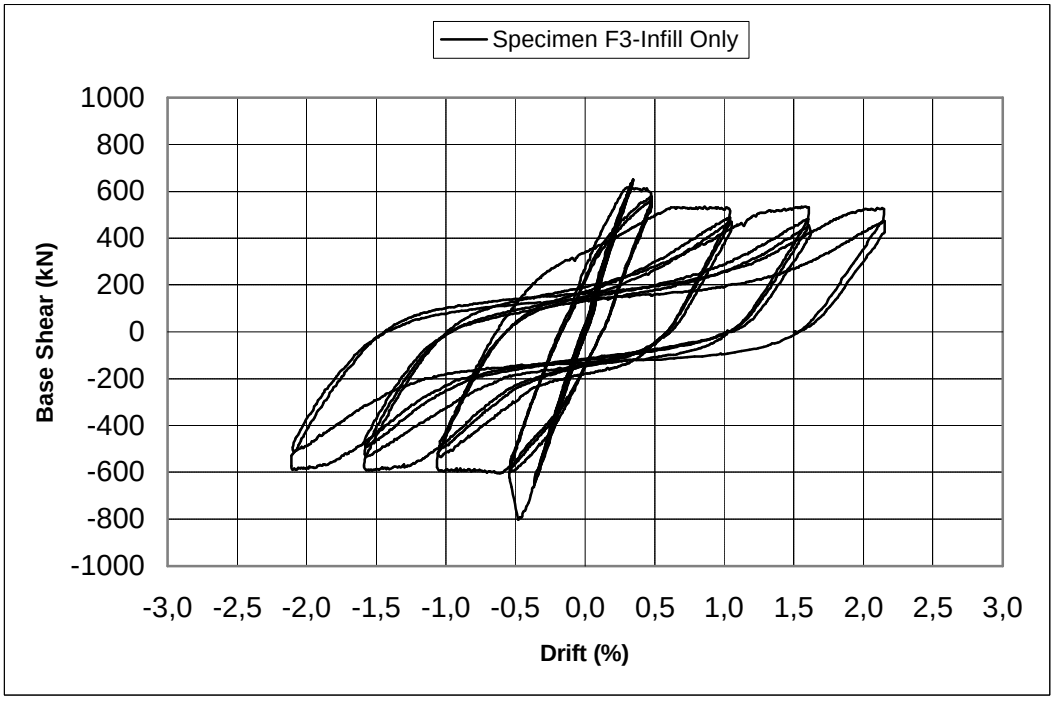

FIGURE 5-14 Specimen F3 Hysteresis (Infill Only)

Similarly, for the positive side, same ratio (with the positive peak shear) at same drifts reached 1.00, 0.94, 0.99, and 1.03, and for the negative side, 1.00, 0.82, 0.82, and 0.81 were obtained. Strain gauge data (in Appendix E) show that the bar braces exhibited stable energy dissipation up to 2.16% drift, producing about 3% maximum strain (including axial and bending effects) in the mid-length of the east side brace. In other parts of the braces, maximum 1.5% axial strains were reached (average axial strain was 1.02%), which indicates that the bar braces underwent significant plastic deformations. A displacement ductility ratio (μ) of 4 was achieved without any significant strength and stiffness degradation with the exception of initial buckling values. Table 5.1 indicates the substantial increase in stiffness for this specimen. The contribution of the infill to the initial stiffness is 92%. Furthermore, an experimental elastic effective length factor (K) of 0.97 was obtained for a length L taken as the diagonal distance between the stud centers. The strain gauge data for Specimen F3 given in Appendix E in Figure E-3 were used to calculate this elastic experimental K factor.

Figure 5.15 demonstrates the predicted pushover curves as per FEMA 368 (following the procedure given in Appendix A) superimposed on the hysteretic curves of Specimen F3.

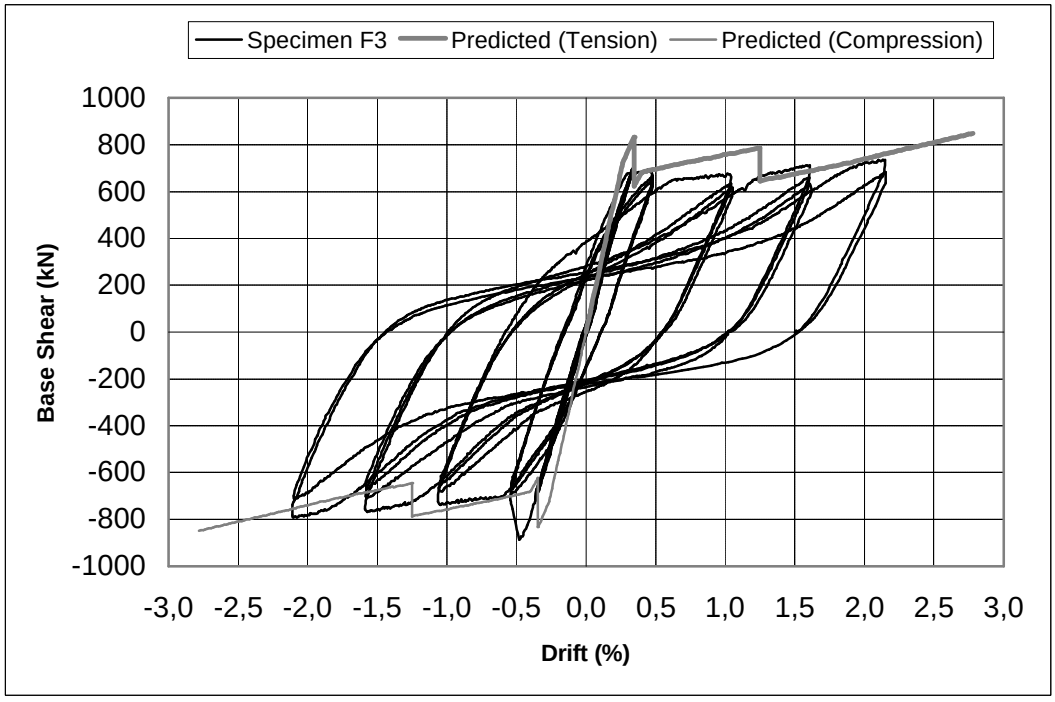

FIGURE 5-15 Experimental Hysteresis and Predicted Pushover Curves for Specimen F3

The initial stiffness and the negative base shear at brace buckling are approximately 11% over-estimated and 6% under-estimated respectively. Pushover analysis curves match reasonably well with the experimental results. This could be attributed to the fact that the material properties of solid bar brace members are more bilinear and therefore better modeled by the selected bilinear material model (with strain hardening), which was incorporated into the analysis.

5.4.2 Hysteretic Energy Dissipation

Figure 5-16 illustrates the variation of cumulative energy dissipation with cumulative number of cycles for the total frame, infill-only, and the boundary frame contributions. As expected, no significant energy was dissipated during the elastic cycles, and starting from the brace buckling cycle, the cumulative energy increases rapidly. Figure 5-16 and Table 5.1 reveal that 82% of the total energy was dissipated by the infill versus 18% for the boundary frame. Again, strain gauges mounted on the boundary frame beams and columns remained within the elastic limits throughout the test, as per the design intent. However, inelastic behavior (web angle yielding) of the beam-to-column double angle connections was observed at larger drift ratios.

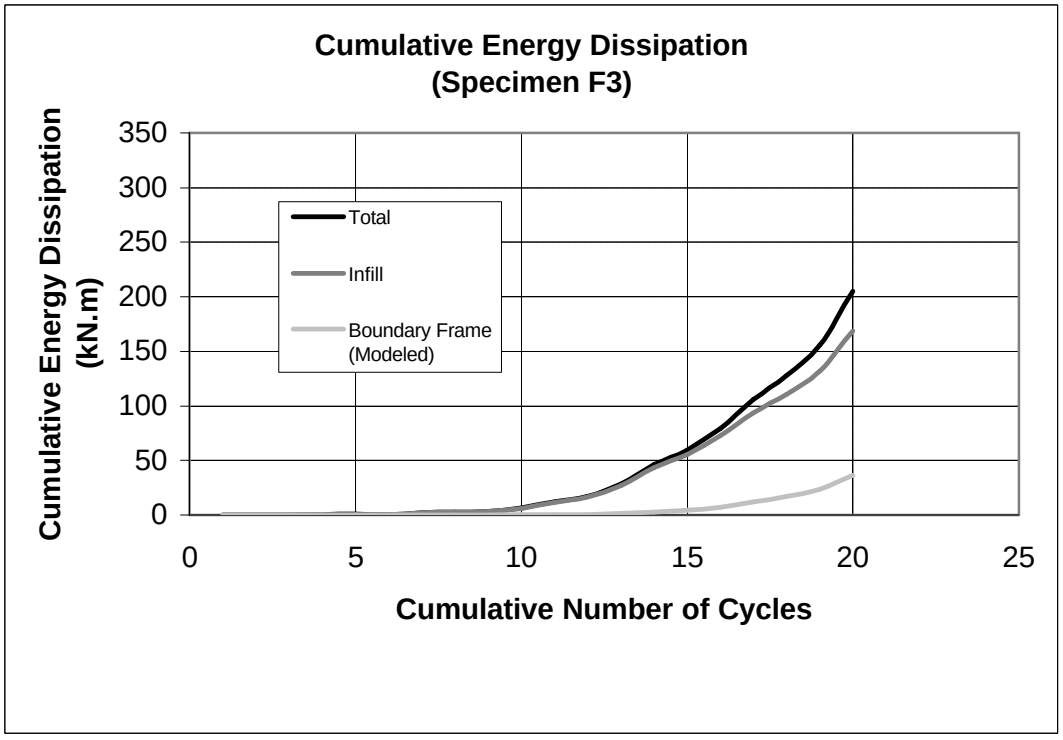

FIGURE 5-16 Cumulative Energy Dissipation by Component for Specimen F3

5.4.3 Base Shear versus Out-of-Plane Displacement Hystereses

To evaluate the effectiveness of CFSS members in reducing brace slenderness, base shear versus out-of-plane displacement hystereses are given in Figure 5-17. The location and the labels of the displacement potentiometers are given in Section 3, in Figure 3-28b. Note that the data for Pot 1W illustrated in Figure 5-17a, were truncated as the potentiometer capacity was exceeded. Figure 5-17b gives the out-of-plane displacements spanning all cycles for Pot 2E, since the maximum displacement range was not exceeded. These curves seem to be relatively full as compared to those of Specimen F4, as given later in Section 5.5.3. However, apparent residual out-of-plane deformations upon unloading still exist. During the inelastic cycles, the development of cumulative residual out-of-plane deformations resulted in a decrease in the brace buckling strength.

Out-of-plane displacement demand is constrained by the presence of CFSS, and this is discussed later by comparison to Specimen F4 in Section 5.5.3. However, this produced higher out-of-plane forces locally transmitted to CFSS members, and the intermediate CFSS members were slightly damaged during the testing.

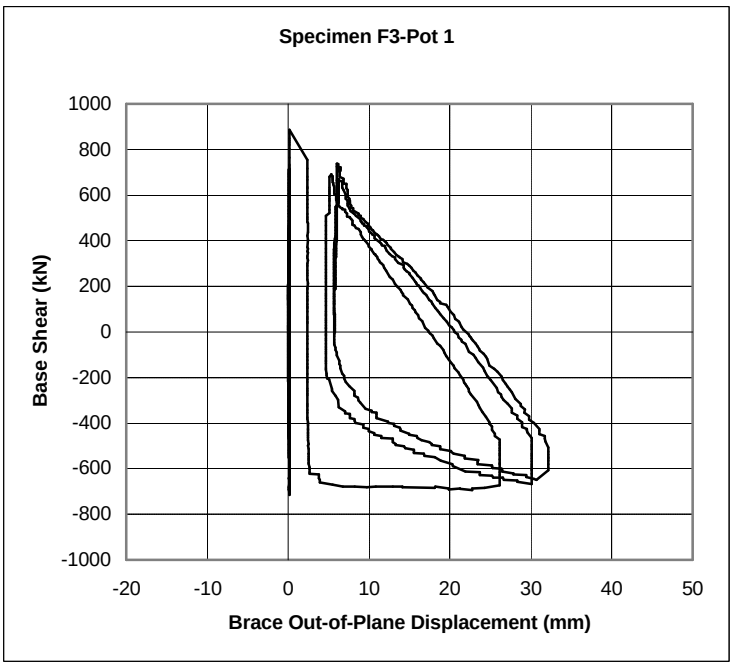

(a)

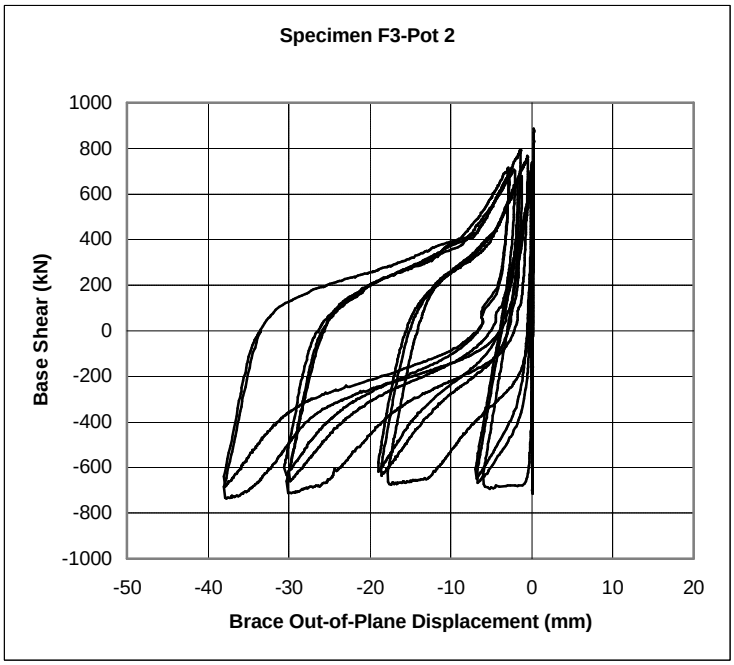

(b)

FIGURE 5-17 Base Shear-Out of Plane Displacement Hystereses for Specimen F3: (a) Pot 1W (West Side Brace Middle Pot-Cycles 1-13); (b) Pot 2E (East Side Brace Intermediate Pot-All Cycles)

5.4.4 Performance of CFSS Members

CFSS members provided ductile, fuller and less pinched (with comparison to the hystereses of Specimen F4) hysteretic behavior for the braces in Specimen F3. CFSS members and U brackets prevented out-of-plane and in-plane brace buckling especially at early stages of cyclic loading. After several cycles at displacement levels greater than the buckling displacement, bearing failure of the intermediate studs led to loss of contact between the buckling restrainers and the brace, resulting in reduced base shear strength and system stiffness.

Figures 5-18 and 5-19 show the west and east sides stud midheight maximum axial strains at various drift levels. All gauges recorded outer flange axial strains below the yield strains. Up to 2.0% drift, the studs performed with no overall inelastic behavior except some local damage in the intermediate studs, around the connection to braces. This behavior could be attributable to the fact that each stud was laterally loaded at two points in Specimen F3 (since two braces are present in the X configuration), resulting in a substantial reduction in demand as compared to Specimen F1.

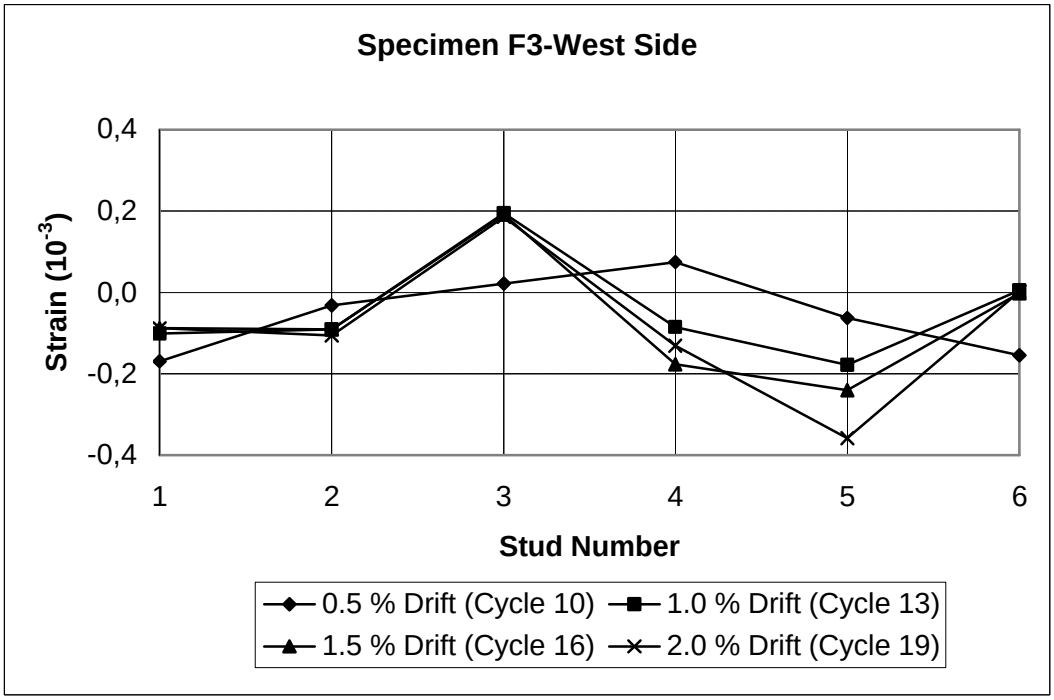

FIGURE 5-18 West Side Stud Strains at Various Drift Levels

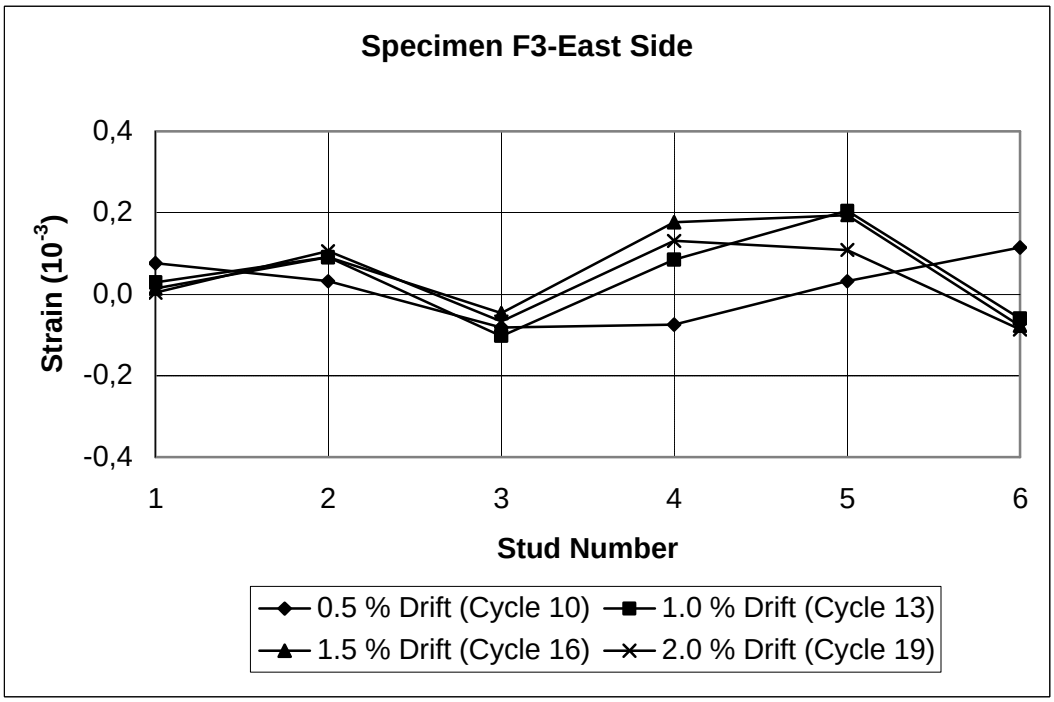

FIGURE 5-19 East Side Stud Strains at Various Drift Levels

5.5 Specimen F4

5.5.1 Base Shear-Drift Hystereses

Figure 5-20 shows experimental base shear force versus drift hysteresis curves for Specimen F4 and Bare Frame 2 (modeled). The hysteresis for Specimen F4 is fairly symmetrical in the elastic and inelastic cycles. The loops after subtracting the contribution of the bare frame are illustrated in Figure 5-21. The overall behavior of Specimen F4 was ductile and stable up to 2.16% drift, although significant pinching is visible in the hystereses. These hysteretic curves are in good agreement with the curves given in previous work on concentrically braced steel frames.

These slender braces behaved like tension-only braces during the testing due to their negligible buckling strength. Therefore, although they resisted some degree of compression force up to the onset of buckling, this strength did not contribute significantly to the overall shape of the hysteresis curves. During the subsequent cycles, an increase in the base shear strength is apparent from the hyteresis, as illustrated in Figure 5-20. This is actually due to the boundary frame contribution as seen from Figure 5-21. In fact, the infill hysteresis exhibits reasonably elastic-plastic behavior (during each excursion) up to the application of the last cycle (2.16% drift). The ratio of the maximum tension strength to the strength at the displacement level of Specimen F3 buckling is 1.28.

During the first excursions of each imposed cycle, the ratio of the maximum positive and negative base shear at that cycle to the strength at buckling at 0.54%, 1.08%, 1.62%, and 2.16% drifts reached 1.00, 1.10, 1.20, and 1.36. For infill-only case, these ratios are 1.00, 0.98, 1.01, and 1.14. Same ratios for the negative side of the hystereses are 1.00, 1.07, 1.20, and 1.34 for the total frame, and are 1.00, 0.94, 1.03, and 1.12 for the infill only case. Also apparent from Appendix F, up to 1.7% strain was reached in the bar braces at 2.16% drift. Hysteretic loops show that energy was dissipated by tension yielding rather than brace buckling. Specimen F4 exhibited a displacement ductility ratio (μ) of 4.

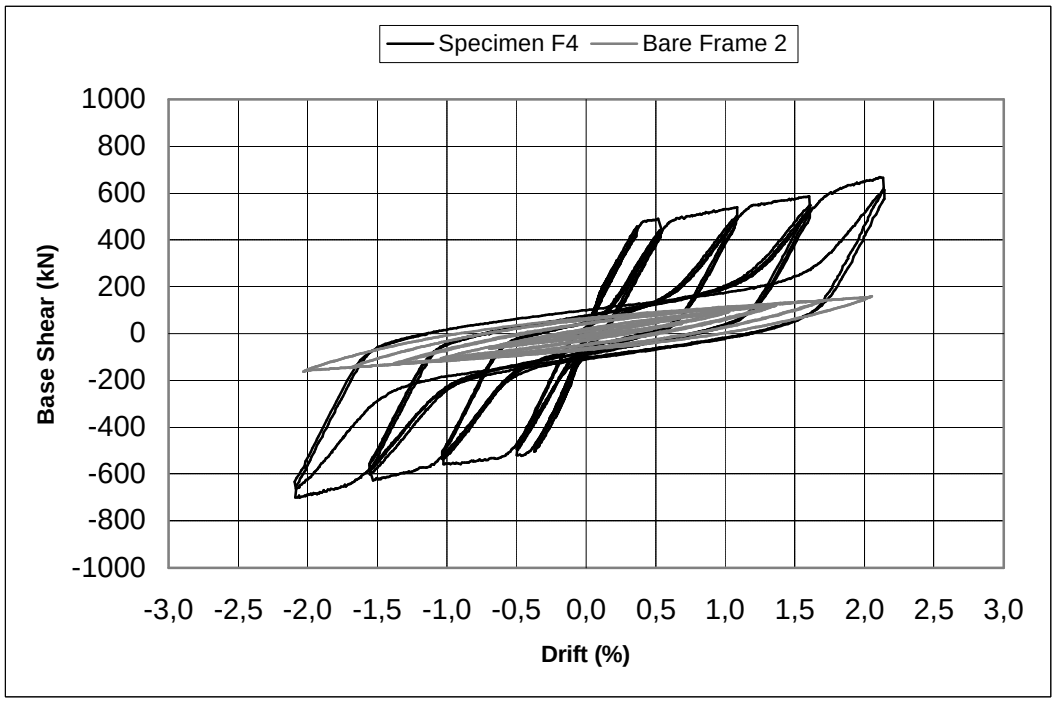

FIGURE 5-20 Specimen F4 and Modeled Bare Frame 2 Hystereses

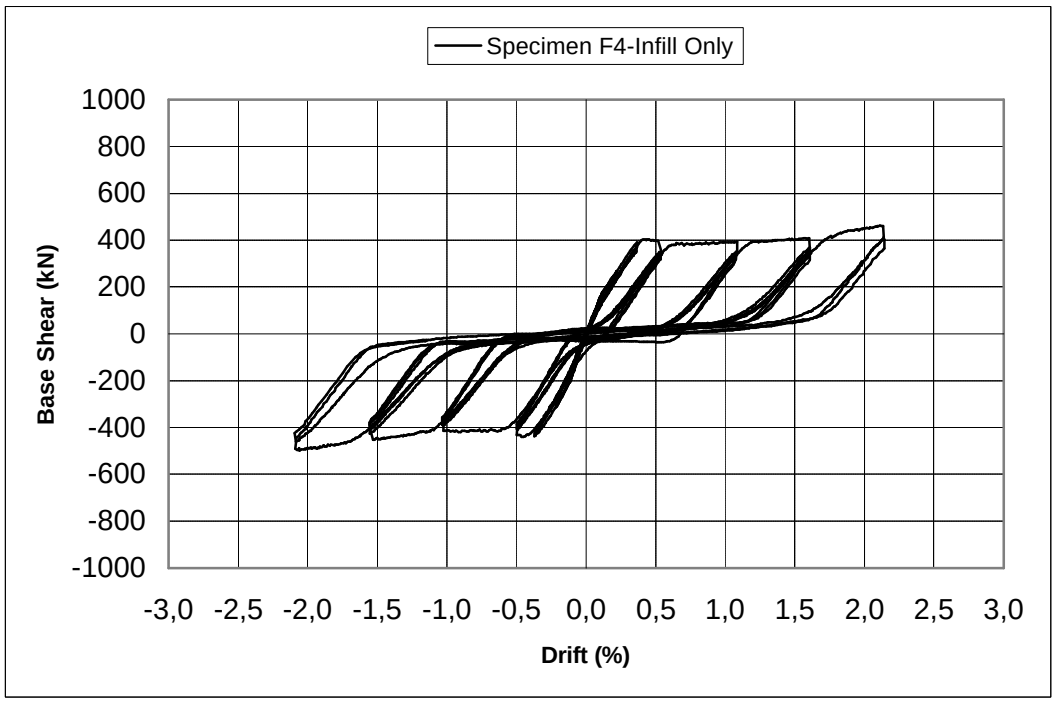

FIGURE 5-21 Specimen F4 Hysteresis (Infill Only)

Table 5.1 (presented earlier) shows that the contribution of the bar braces to initial stiffness is about 90%. An experimental elastic K factor of 0.63 was found for a L value taken as the clear brace length between the gussets. This K factor has been obtained using the measured strain gauge data for Specimen F4 given in Appendix F, in Figure F-1, following the same procedure to obtain the moment diagram as was done for other specimens before.

Shown in Figure 5.22 are the theoretical pushover curves envelope (as per the FEMA 368 procedure described in Appendix A) superimposed on the hysteretic curves of Specimen F4. The initial stiffness and the negative base shear at brace buckling are approximately 29% and 7% over-estimated respectively. Although theoretical results on the negative base shear side match reasonably with the experimental results, relatively larger differences were obtained on the positive side. Again, this could be attributed to the modeling issues in FEMA 368, and, partly, behavioral differences of the boundary frame under cyclic loading as seen from the experimental hysteresis curves given in Section 4.5.

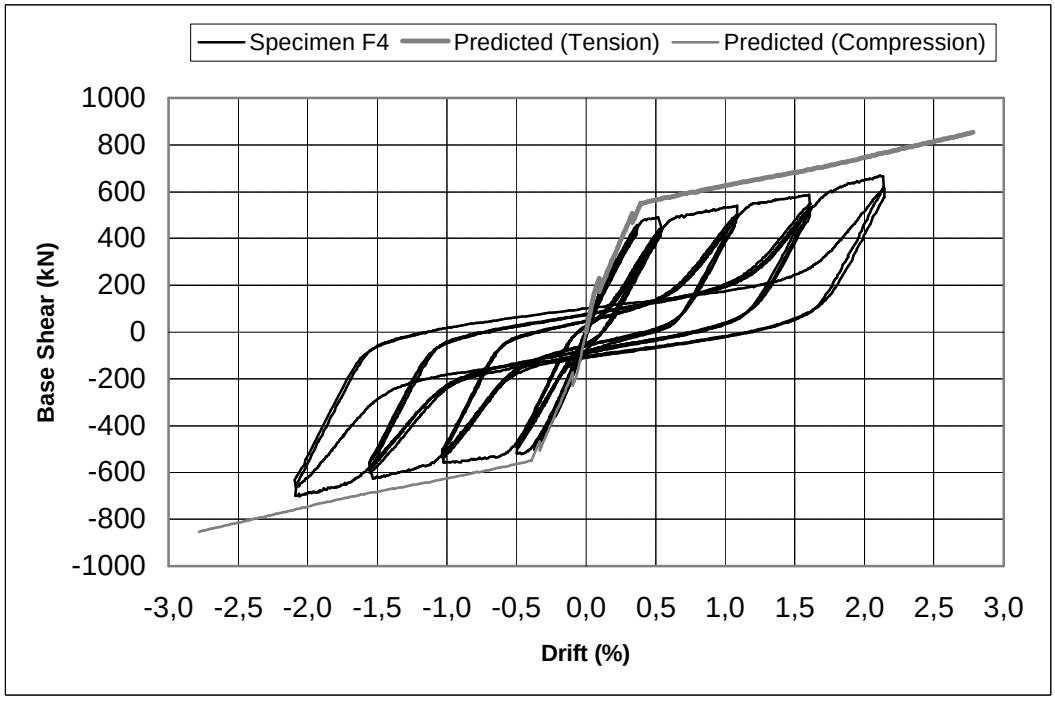

FIGURE 5-22 Experimental Hysteresis and Predicted Pushover Curves for Specimen F4

5.5.2 Hysteretic Energy Dissipation

Figure 5-23 illustrates the variation of cumulative energy dissipation with cumulative number of cycles for the total frame, infill-only, and the boundary frame contributions. No significant energy was dissipated during the elastic cycles, and starting from the brace yielding cycle, the cumulative energy increases. Figure 5-23 and Table 5.1 (presented earlier) reveal that only 39% of the total energy was dissipated by the infill versus 61% for the boundary frame. Also apparent on that figure, the contribution of the boundary frame to cumulative energy dissipation is dominant over the infill at larger drifts, due to the inelastic behavior of the beam-to-column double angle connections. However, strain gauges mounted the boundary frame beams and columns remained within the elastic limits, as per the design intent.

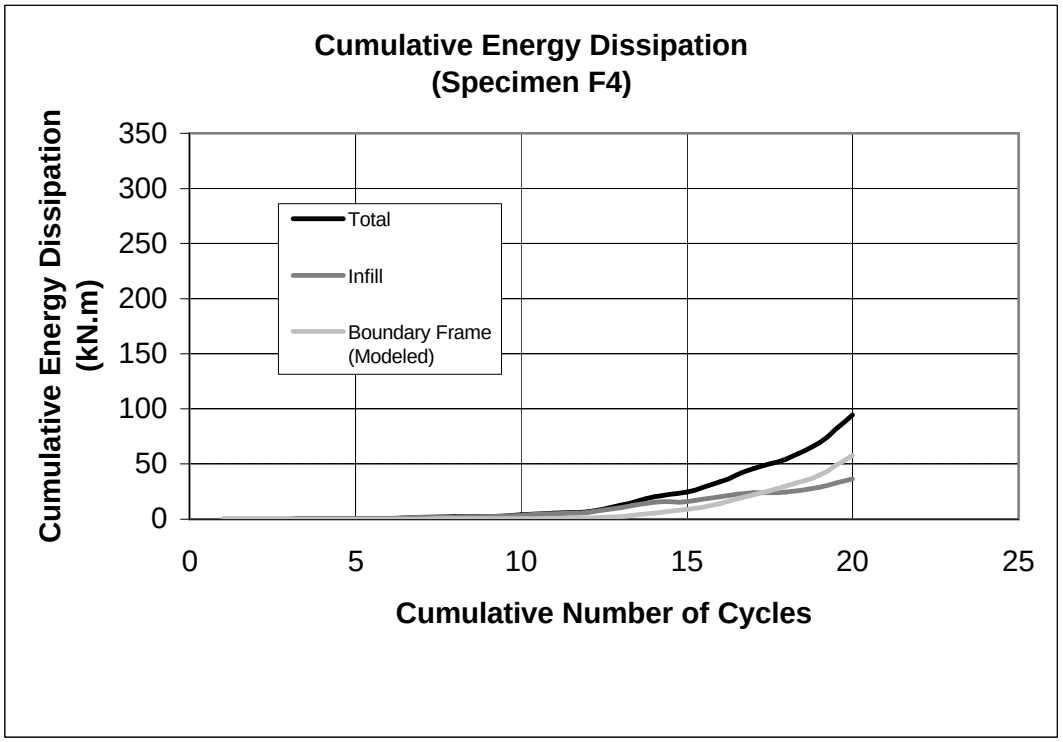

FIGURE 5-23 Cumulative Energy Dissipation by Component for Specimen F4

5.5.3 Base Shear versus Out-of-Plane Displacement Hystereses

Given in Figure 5-24 are the base shear versus out-of-plane displacement hystereses to evaluate the effectiveness of CFSS members used in Specimen F3 as well as the brace slenderness. The location and the labels of the displacement potentiometers are given in Section 3, in Figure 3-29b. Note that the data for Pot 1E illustrated in Figure 5-24a were truncated during the early stages of testing as the potentiometer capacity was exceeded. Figures 5-24b and 5-24c give the out-of-plane displacements captured by Pot 2E and Pot 3W for more cycles. These curves are highly different from the ones obtained in other specimens.

Out-of-plane displacements were substantial due to the absence of CFSS members, as shown in Section 4.4. However, since the braces are very slender, and resulted in elastic buckling, an important percentage of the residual out-of-plane deformations were recoverable during the early inelastic cycles. On the other hand, these displacements became significant by the end of testing.

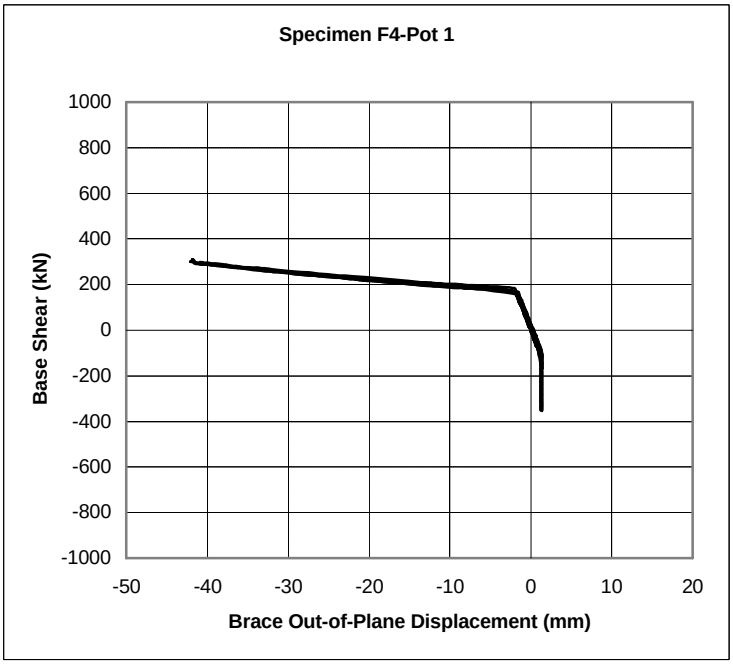

(a)

FIGURE 5-24 Base Shear-Out of Plane Displacement Hystereses for Specimen F4: (a) Pot 1E (East Side Brace Middle Pot-Cycles 1-6);

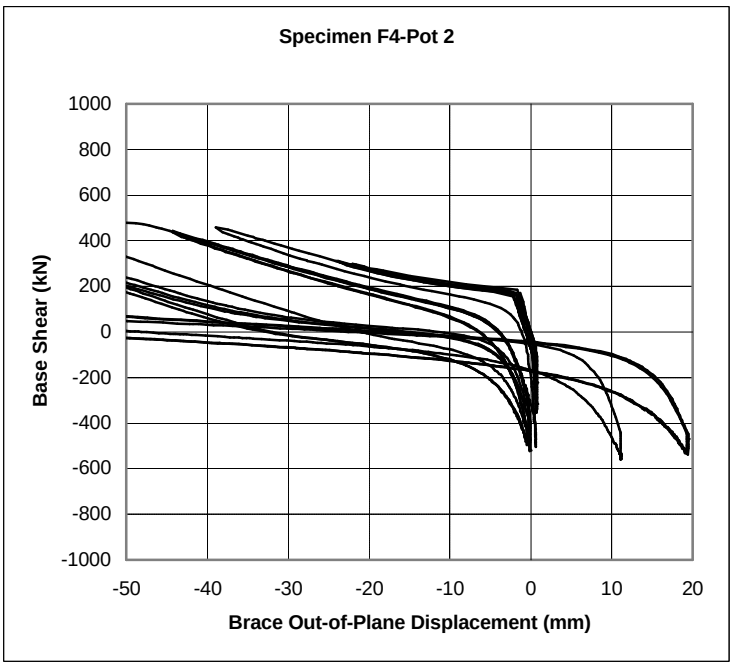

(b)

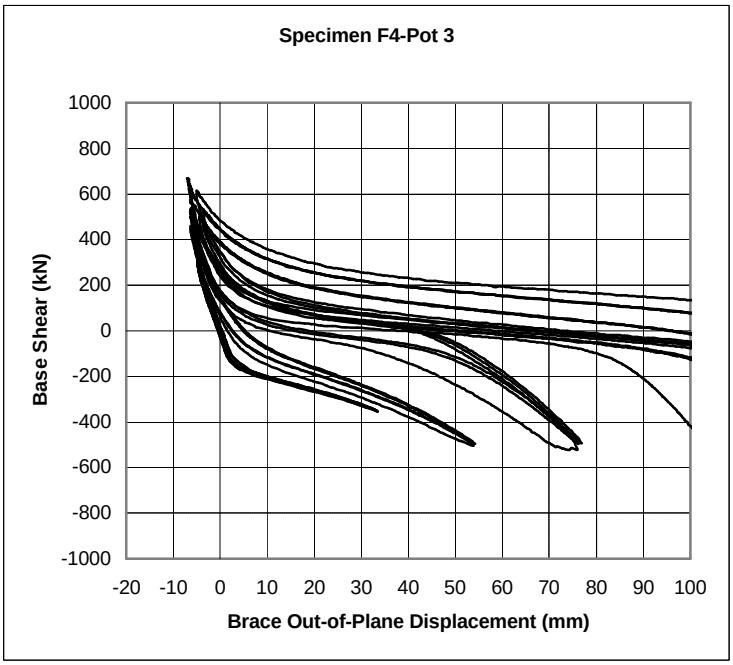

(c)

FIGURE 5-24 Base Shear-Out of Plane Displacement Hystereses for Specimen F4 (continued): (b) Pot 2E (East Side Brace Intermediate Pot-Cycles 1-15); (c) Pot 3W (West Side Brace Intermediate Pot-All Cycles)

5.6 Summary and Comparison

Using experimental hystereses, some behavioral characteristics of Specimens F1, F2, F3, and F4 are summarized and compared in this section. Total initial stiffness, initial stiffness of infill, yield or buckling base shear, yield or buckling displacement, maximum attained percent drift, achieved displacement ductility, and cumulative energy dissipations by component (total and infill-only) are quantified in Table 5-1 presented earlier. To better compare the effectiveness of each specimen, normalized values of base shear and energy dissipation (infill-only) were calculated and given in Table 5-2. Since the yield (or buckling) displacement increments are very close to each other (11.4mm for Specimens F1 and F2, and 11.9 mm for Specimens F3 and F4), these values were not normalized. Cumulative hysteretic energy dissipation can then be normalized as follows:

$$E_{HN} = \frac{E_H}{V_y \delta_y} \tag{5-4}$$

where

E_{HN}= normalized cumulative hysteretic energy dissipation

E_H = cumulative hysteretic energy dissipation

V_y = yield (or buckling) base shear

δ_y = experimentally obtained yield or buckling displacement

Note that, for the purpose of normalization, the average of the base shear reached in tension at each of the large plastic deformation cycles was used for the value of V_y, and the experimental yield displacement was used for Specimens F1 and F2. For Specimens F3 and F4, because the maximum base shear strength drops after first buckling, the average of the base shears reached in the subsequent cycles only was used to define V_y, and the experimental buckling displacement was used for δ_y (i.e. δ_b).

TABLE 5-2 Normalized Characteristics of Tested Specimens (Infill-Only)

Specimen	V_y (kN)	δ_y (mm)	$E_{H,\ infill}$ (kN.mm)	$V_y / (V_{y,F1})$	E_{HN}
F1	661.3	11.4	227,000	1.00	30.1
F2	673.0	11.4	192,000	1.02	25.0
F3	592.3	11.9	169,000	0.90	24.0
F4	442.0	11.9	37,000	0.67	7.0

Table 5-2 shows that braces having CFSS members had better hysteretic energy dissipation. Cumulative hysteretic energy was the greatest in Specimen F1, although this specimen had less maximum displacement ductility due to its lower fracture life as compared to Specimen F2. Experimental fracture lives ($\Delta_{f,exp}$) versus experimental K factors (K_{exp}) were 32.9 versus 19.7 for Specimen F1 and were 77.3 versus 64.7 for Specimen F2.

Variation of cumulative energy dissipation with cumulative number of cycles for all specimens is shown in Figures 5-25 and 5-26 for comparison purposes. A comparison of the hysteretic behavior of all specimens is made easier by Figure 5-27. Note that on that figure, experimental KL/r values are also shown for each specimen.

Specimen F1 exhibited stable behavior and dissipated significant cumulative energy. The hysteretic curves were stable up to a displacement ductility of 4 and fuller than those for any other specimen. CFSS members and U brackets as buckling restrainers prevented the tube brace from early buckling, prior to their inelastic behavior at large drifts due to bearing failure and torsional response. The tube brace ultimately developed local buckling under reversed cyclic displacements, and fractured by development of cracking at the local buckling location. Specimen F1 achieved the maximum hysteretic energy dissipation for the infill alone. Percent energy dissipation amounts for other specimens are 85%, 74%, and 16% of Specimen F1 for Specimens F2, F3, and F4 respectively.

Specimen F2 dissipated the largest amount of total hysteretic energy, essentially due to its higher fracture life. A displacement ductility of 6 was reached prior to fracture, the largest value for all specimens tested (but Specimens F3 and F4 were not tested up to failure for reasons described in Section 4.4.3). Infill (tube brace) failure occurred at the brace to gusset connection in the net section area (as illustrated in Section 4, in Figures 4-16 and 4-17). The out-of-plane buckling displacements of the brace were significant, in excess of 10% of the brace clear length. Although residual out-of-plane displacements caused significant strength degradation in compression, the behavior was ductile and stable.

Solid bar braces in Specimen F3 dissipated a relatively moderate amount of energy with ductile but pinched hysteretic curves. Up to displacement ductility of 4, the braces dissipated energy by yielding and buckling under reversed displacement cycles.

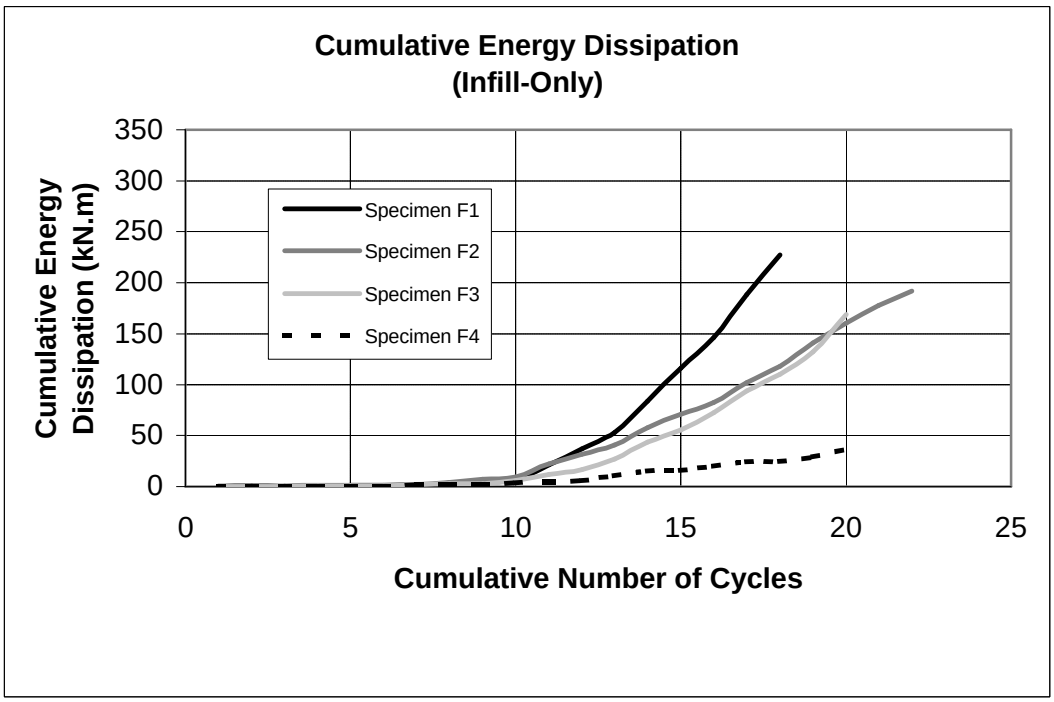

FIGURE 5-25 Comparison of Cumulative Energy Dissipation (Infill-Only)

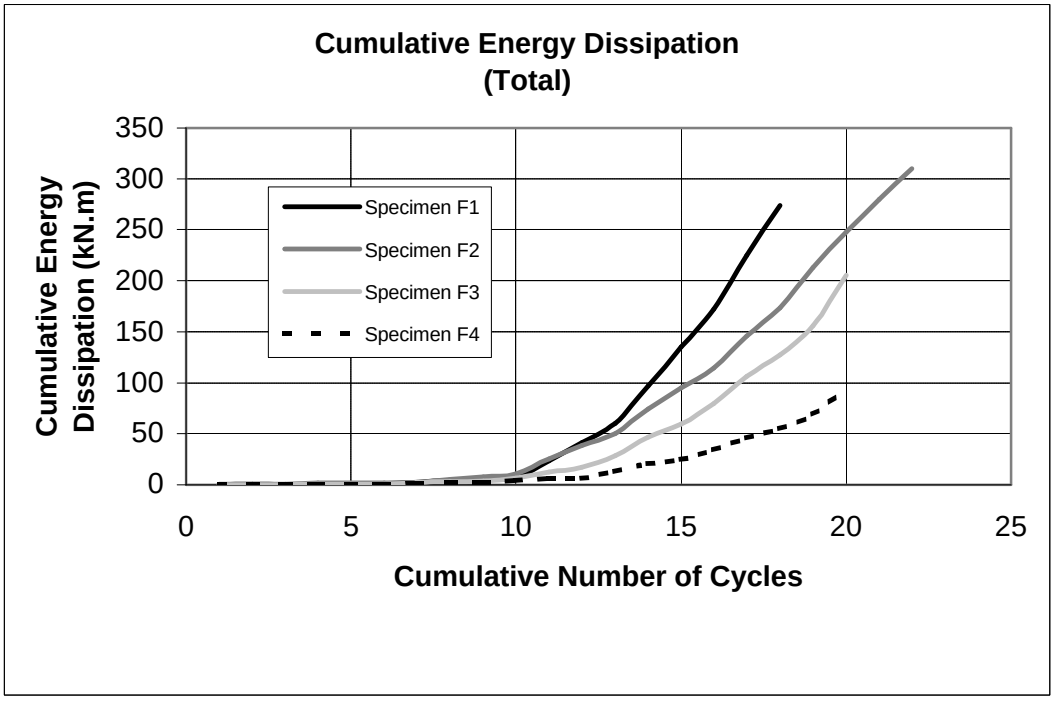

FIGURE 5-26 Comparison of Cumulative Energy Dissipation (Total)

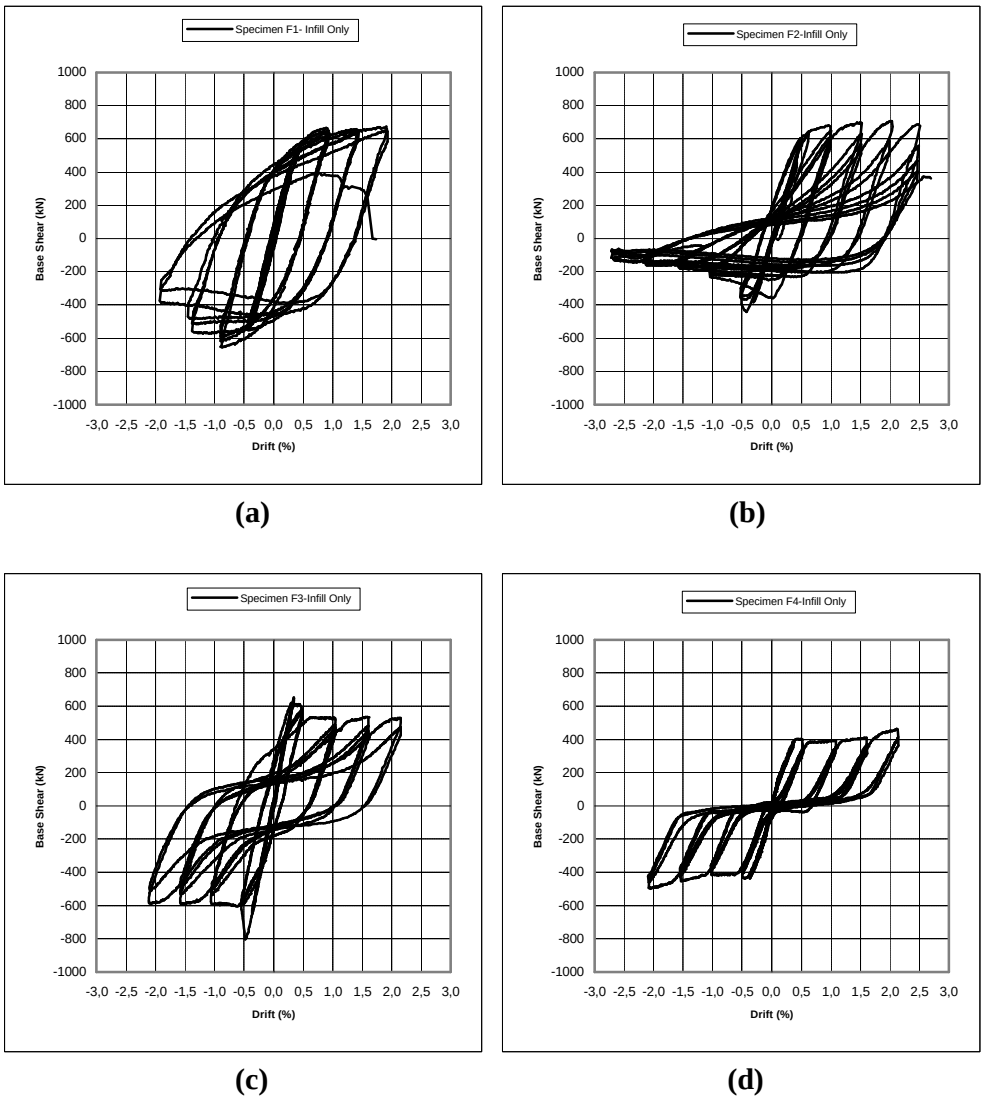

FIGURE 5-27 Comparison of Base Shear versus Drift Hysteresis Curves for Infills: (a) Specimen F1 (KL/r=19.7); (b) Specimen F2 (KL/r=77.3); (c) Specimen F3 (KL/r=65.5); (d) Specimen F4 (KL/r=195.7)

CFSS members and U brackets reduced the buckling length of the braces effectively. After initial buckling of the east side brace when the peak base shear was obtained, strength degradation stabilized under subsequent cycles.

The least amount of cumulative energy was dissipated by Specimen F4. The hysteresis curves were stable yet significantly pinched, as expected. Energy was essentially dissipated through the yielding of the braces in tension only. A displacement ductility of 4 was reached without any visible damage. Note that the largest out-of-plane displacements were obtained for this specimen, in excess of 14% of the brace clear length.

All specimens survived reversed cyclic displacement histories prior to initiation of fracture up to large drift values. The maximum drift was reached by Specimen F2, at 2.88%. Specimens F1, F3, and F4 exhibited maximum drifts of 1.92%, 2.16%, and 2.16% respectively.

Although the above comparison refer to absolute cumulative hysteretic energies, the trends remain the same for normalized cumulative hysteretic energies, since, as shown in Table 5-2, normalized energies for Specimens F3 and F4 are less than those for Specimens F1 and F2. This is illustrated in Figures 5-28.

Hysteretic energy dissipation per brace volume used can be another measure to compare the relative effectiveness of these specimens. Shown in Figure 5-29 is the variation of volumetric energy dissipation versus cumulative number of cycles. Peak energy per volume values of 0.049, 0.041, 0.028, and 0.006 kNmm/mm^3 are found for Specimens F1, F2, F3, and F4 respectively (although the last two specimens were not tested to failure). Additionally, at a common ductility of 4, these values become 0.049, 0.025, 0.028, and 0.006 kNmm/mm^3, which show that braces having CFSS had better hysteretic energy dissipation capacity in this research.

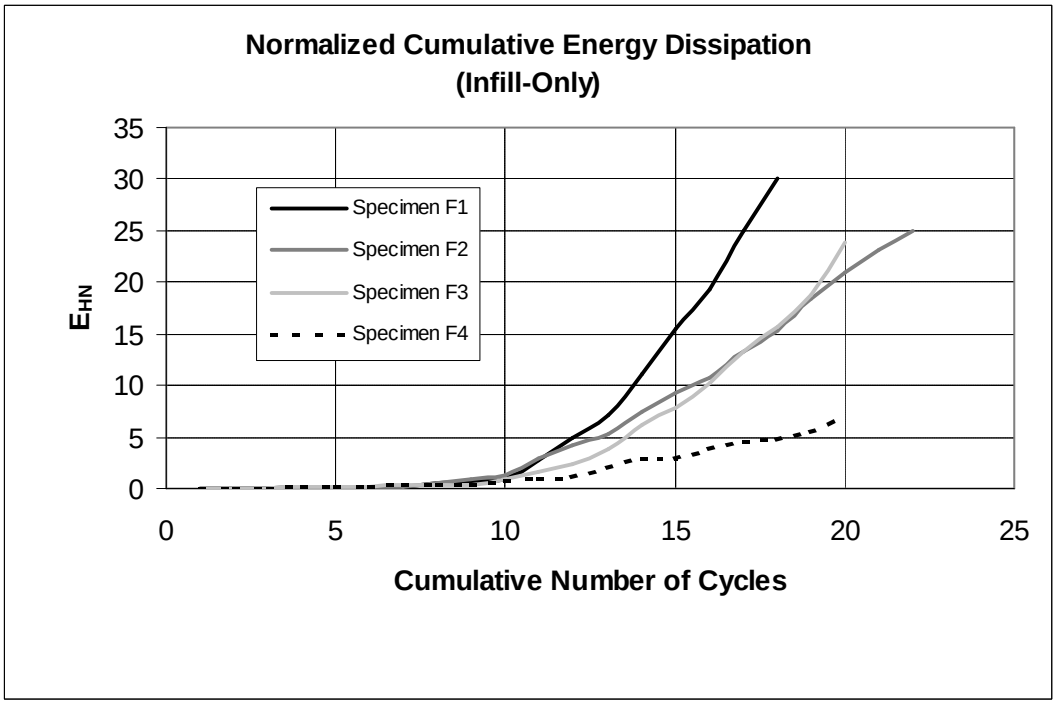

FIGURE 5-28 Comparison of Normalized Cumulative Energy Dissipation (Infill-Only)

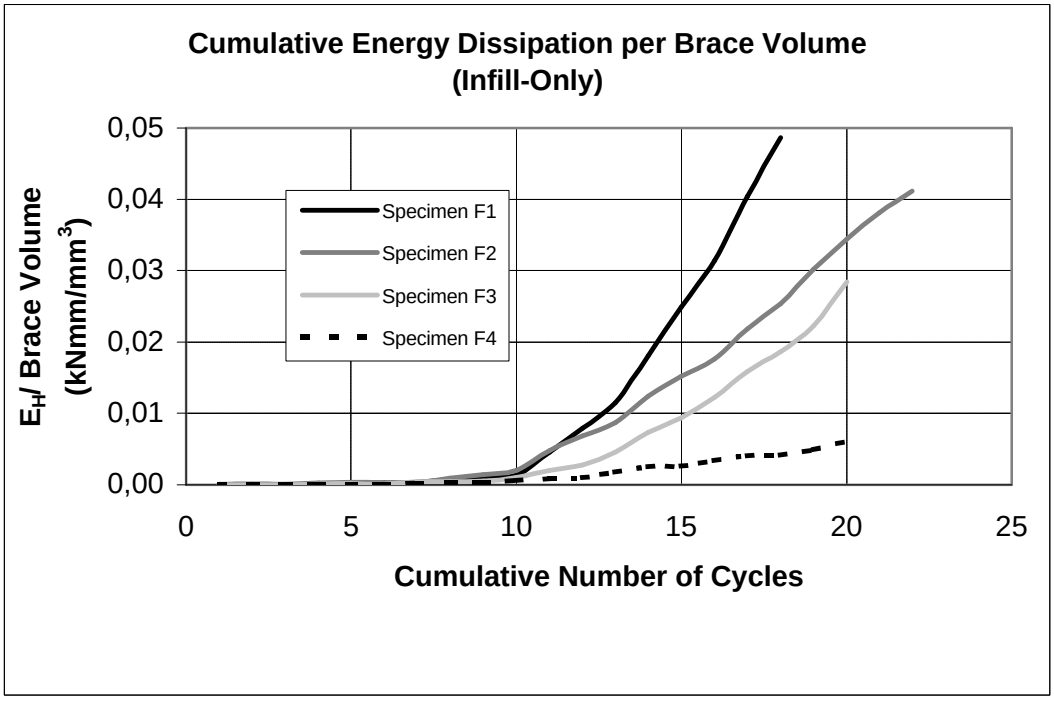

FIGURE 5-29 Comparison of Cumulative Energy Dissipation per Brace Volume Used (Infill-Only)

SECTION 6
CONCLUSIONS

6.1 General

An experimental study of the hysteretic behavior of concentrically braced steel frames with and without vertical cold-formed steel members (CFSS) has been presented in this report. Previous experimental and analytical studies were also reviewed to explore the hysteretic characteristics of steel braces. To investigate the hysteretic energy dissipation capacity of infills made of braces restrained by CFSS for ductile seismic retrofit or new design purposes, four specimens were designed and tested. The same displacement history was followed on frames with and without CFSS members to compare seismic performance.

The challenge in using CFSS members and U brackets as out-of-plane and in-plane buckling restrainers was to investigate whether it could be possible and effective to reduce the buckling length of braces by taking advantage of metallic wall units often constructed as non-structural dividing partitions, with slight modifications in their design. The expectation was more ductile, stable, and fuller hysteretic curves, leading to enhanced hysteretic energy dissipation capacities.

In addition to the use of CFSS members, braces having tubular or rectangular solid bar sections, in single diagonal or X-bracing configurations were selected as other specimen parameters, to investigate the impact of these parameters on the hysteretic behavior of such concentrically braced steel frames.

The major conclusions reached from this experimental study are as follows:

1. Specimen F1 (concentrically braced frame with single tube brace and vertical CFSS members) achieved superior behavior over the other specimens in terms of infill cumulative hysteretic energy dissipation at given drift values. Cumulative energy dissipation of infill for this specimen is 18% more than that of Specimen F2 (without studs). However, maximum drifts attained for Specimens F1 and F2 are 1.92% and 2.88%, and maximum displacement ductilities (μ) of 4 and 6, respectively. This is because experimental fracture life of the tube in Specimen F2 was 97% higher than

that of the tube in Specimen F1, as reducing the buckling length for tubular cross section braces also accelerated their local buckling. If hysteretic energy is instead calculated and compared at a given ductility level, for example at the ductility level at which the tube brace fractured in Specimen F1, then 92% more hysteretic energy is dissipated for Specimen F1, compared to Specimen F2. Initial stiffness and base shear at yield for Specimen F2 are about 65% and 80% of those of Specimen F1 respectively. Experimental buckling length for Specimen F1 was found to be about 1.08 times the brace length between studs (K=1.08), which reasonably agrees with the predicted value of 1.00. For specimen F2, experimentally obtained K factors are 0.90 (assuming clear length without gussets) and 0.78 (observed clear length including the lower gusset and hinge at gusset bottom). Both values are 8% and 12% above the theoretical values.

2. At maximum displacement ductility of 4, infill cumulative energy dissipation for Specimen F3 reached 4.57 times the energy dissipated in Specimen F4, a 357% gain in infill energy dissipation. From this perspective, the use of CFSS and U brackets as buckling restrainers seemed more effective in tension only braced frames rather than tension-compression braced frames. Moreover, provided that all brace connections are ductile, solid braces may be able to sustain larger amounts of reversed axial cyclic displacements, since local stability problems do not exist. While the ratio of maximum total base shears reached by Specimens F3 and F4 is 1.28, this value is 4.93 at initial brace buckling. In other words, the maximum base shear strength is developed in Specimen F3 at initial brace buckling, but maximum strength of Specimen F4 is developed at maximum ductility instead. Similarly, experimentally obtained buckling length for Specimen F3 is about 0.97 times the brace length between studs (K=0.97), and reasonably agrees with the predicted value of 1.00. For specimen F4, an experimental K factor of 0.63 is found to be 25% underestimated (predicted K=0.50).

3. Dissipated hysteretic energy per brace volume can be another measure to compare the relative effectiveness of these specimens, taking into account the total material used. Peak energy per volume values of 0.049, 0.041, 0.028, and 0.006 kNmm/mm^3 are found for Specimens F1, F2, F3, and F4 respectively (although the last two specimens

were not tested to failure). Additionally, at a common ductility of 4, these values become 0.049, 0.025, 0.028, and 0.006 kNmm/mm^3, which show that braces having CFSS had better hysteretic energy dissipation capacity in this research.

4. Structural use of CFSS members as out-of-plane buckling restrainers also helped reduce the out-of-plane displacements of braces. This would minimize the wall cladding damages that may occur as a result of large lateral displacements during buckling of braces under severe earthquake excitations. Performance of CFSS members in Specimen F3 was better than the ones in Specimen F1, which could be attributed to the effect of bracing configurations. CFSS members in Specimen F3 had large amount of connections to the braces, due to the X-brace configuration instead of the single diagonal, leading a more distributed load pattern on the studs.

5. As a side observation, it is also noted that the FEMA 356 (2000) and FEMA 368 (2001) predicted pushover analysis envelopes for concentrically braced frames do not represent well the behavior of braced frames, and therefore may need to be improved.

6. Although the objective of this study was to restraint braces from buckling to maximize the dissipated hysteretic energy, the results obtained also re-emphasize the known lesser potential fracture life of tubular braces compared to other sections.

6.2 Recommendations for Further Research

The proposed retrofitting systems using ductile concentric braces with CFSS members are promising to increase the hysteretic energy dissipation through brace yielding and inelastic buckling in seismically vulnerable steel frames. Other types of bracing configurations with CFSS members can be tested in a similar way to evaluate their hysteretic performances and establish improved configurations. For example, Chevron braced systems could be of interest, because the seismic demands in story beams using those CFSS members would be reduced due to the better balance between the tension and compression capacity of each brace.

Furthermore, theoretical and experimental studies are also required to better understand the inelastic cyclic response of braced frames under earthquake loading. In particular, the

modeling of local buckling and fracture in hysteretic brace models still needs to improved and integrated into the commonly available models. For static pushover analysis, more refined brace axial hinge models should be developed and incorporated into documents such as FEMA 356 (2000) and FEMA 368 (2001) for performance-based design of concentrically braced steel frames.

SECTION 7
REFERENCES

AISC (1999) “Load and Resistance Factor Design (LRFD) Specification for Structural Steel Buildings”, American Institute of Steel Construction, Chicago, IL.

AISC (2001) “Manual of Steel Construction, Load and Resistance Factor Design”, Third Edition, American Institute of Steel Construction, Chicago, IL.

AISC (2002) “Seismic Provisions for Structural Steel Buildings”, American Institute of Steel Construction, Chicago, IL.

AISI (1996) “Cold-Formed Steel Design Manual”, American Iron and Steel Institute, Washington, DC.

Astaneh-Asl, A., Goel, S.C. and Hanson, R.D. (1985) “Cyclic Out-of-Plane Buckling of Double-Angle Bracing”, Journal of Structural Engineering, ASCE, 111(5), pp.1135-1153.

Astaneh-Asl, A. (1998) “Seismic Behavior and Design of Gusset Plates”, Steel Tips, American Institute of Steel Construction, Chicago, IL.

ASTM (2002), “Standard Test Methods and Definitions for Mechanical Testing of Steel Products”, A 370-97a, American Society for Testing and Materials, Philadelphia, PA.

ATC-24 (1992) “Guidelines for Cyclic Seismic Testing of Components of Steel Structures”, Applied Technology Council, California.

Berman, J. (2002) “Experimental Investigation of Light-Gauge Steel Plate Shear Walls for the Seismic Retrofit of Buildings”, M.Sc. Thesis, Submitted to the Graduate School of the State University of New York at Buffalo.

Black, R.G., Wenger W.A.B. and Popov E.P. (1980) “Inelastic Buckling of Steel Struts under Cyclic Load Reversals”, Report No. UCB/EERC-80/40, Berkeley, California.

Black, C., Makris, N. and Aiken, I. (2002) “Component Testing, Stability Analysis and Characterization of Buckling-Restrained Unbonded Braces”, PEER Report 2002/08, Pacific Earthquake Engineering Research Center, University of California, Berkeley.

Bruneau, M., Uang, C.M. and Whittaker, A. (1998) “Ductile Design of Steel Structures”, McGraw-Hill, NY.

CAN/CSA-S16-2001 (2001) “ Limit States Design of Steel Structures”, Canadian Standards Association, Willowdale, Ontario, Canada.

Chen, C.C., Chen, S.Y. and Liaw, J.J. (2001) “Application of Low Yield Strength Steel on Controlled Plastification Ductile Concentrically Braced Frames”, Canadian Journal of Civil Engineering, Vol. 28, pp.823-836.

Chen, W.F., Goto, Y. and Liew, J.Y.R. (1996) “Stability Design of Semi-Rigid Frames”, John Wiley&Sons, Inc., NY.

Clark, P.W., Kasai, K., Aiken, I.D., and Kimura, I. (2000) ”Evaluation of Design Methodologies for Structures Incorporating Steel Unbonded Braces for Energy Dissipation”, Proceedings of 12th World Conference on Earthquake Engineering, Paper No. 2240, New Zealand.

CSI (1998) “SAP2000 Integrated Finite Element Analysis and Design of Structures- Detailed Tutorial Including Pushover Analysis”, Computers and Structures, Inc., Berkeley, California.

Dafalias, Y.F. and Popov, E.P. (1976) “Plastic Internal Variables Formalism of Cyclic Plasticity”, Journal of Applied Mechanics, ASCE, Vol. 43, pp.645-651.

Dietrich Industries, Inc. (2001) “Curtain Wall/Light Gage Structural Framing Products”, ICBO No. 4784P, LA RR No. 25132.

El-Tayem, A.A. and Goel, S.C. (1986) “Effective Length Factor the Design of X-Bracing Systems”, Engineering Journal, AISC, Vol.24, pp.41-45.

FEMA 356 (2000) “Prestandard and Commentary for the Seismic Rehabilitation of Buildings”, Federal Emergency Management Agency, Washington, D.C.

FEMA 368 (2001) “NEHRP Recommended Provisions for Seismic Regulations for New Buildings and Other Structures: Part 1- Provisions”, Federal Emergency Management Agency, Washington, D.C.

Huang, Y.H., Wada, A., Sugihara, H., Narikawa, M., Takeuchi, T., and Iwata, M. (2000) “Seismic Performance of Moment Resistant Steel Frame with Hysteretic Damper”, Proceedings of 3rd International Conference on Behavior of Steel Structures in Seismic Areas (STESSA 2000), Montreal, Canada, pp.403-409.

Ikeda, K., Mahin, S.A. and Dermitzakis, S.N. (1984) “Phenomenological Modeling of Steel Braces under Cyclic Loading” Report No. UCB/EERC-84/09, Berkeley, California.

Ikeda, K. and Mahin, S.A. (1984) “A Refined Physical Theory Model for Predicting the Seismic Behavior of Braced Steel Frames”, Report No. UCB/EERC-84/12, Berkeley, California.

Iwata, M., Kato, T. and Wada, A. (2000) “Buckling-Restrained Braces as Hysteretic Dampers”, Proceedings of 3rd International Conference on Behavior of Steel Structures in Seismic Areas (STESSA 2000), Montreal, Canada, pp.33-38.

Jain, A.K., Goel, S.C. and Hanson, R.D. (1980) “Hysteretic Cycles of Axially Loaded Steel Members”, Journal of the Structural Division, ASCE, Vol.106, No. ST8, pp.1777-1795.

Jain, A.K., Redwood, R.G. and Lu, F. (1993) “Seismic Response of Concentrically Braced Dual Steel Frames”, Canadian Journal of Civil Engineering, Vol.20, pp.672-687.

Khatib, I.F., Mahin, S.A. and Pister, K.S. (1988) “Seismic Behavior of Concentrically Braced Steel Frames”, Report No. UCB/EERC-88/01, Berkeley, California.

Ko et al. (2002) “Application of the Unbonded Brace in Medical Facilities”, Seventh U.S. National Conference on Earthquake Engineering (7NCEE), Paper No.16, July 21-25, Boston, on CD-ROM.

Lee, K. and Bruneau, M. (2002) “Review of Energy Dissipation of Compression Members in Concentrically Braced Frames”, Technical Report MCEER-02-0005, October, Buffalo, NY.

Lee, S. and Goel, S.C. (1987) “Seismic Behavior of Hollow and Concrete-Filled Square Tubular Bracing Members”, Report No. UMEE 87-11, December, Department of Civil Engineering, University of Michigan, Ann Arbor, Michigan.

Nakashima, M. and Wakabayashi, M. (1992) “Analysis and Design of Steel Braces and Braced Frames in Building Structures”, The US-Japan Joint Seminar on Stability and Ductility of Steel Structures under Cyclic Loading, CRC Press, Ann Arbor, pp. 309-321.

Remennikov, A.M. and Walpole, W.R. (1997) “Analytical Prediction of Seismic Behavior for Concentrically-Braced Steel Systems”, Earthquake Engineering and Structural Dynamics, Vol.26, pp.859-874.

Salmon, C.G. and Johnson, J.E. (1996) “Steel Structures: Design and Behavior”, Fourth Edition, Prentice Hall, NJ.

SEAOC (1995) “Vision 2000 Report-Performance-Based Seismic Engineering of Buildings”, The Structural Engineers Association of California, Vol.1-2, April, California.

Tremblay, R. (2000) “Influence of Brace Slenderness on the Seismic Response of Concentrically Braced Steel Frames” Proceedings of 3rd International Conference on Behavior of Steel Structures in Seismic Areas (STESSA 2000), Montreal, Canada, pp.527-534.

Tremblay, R. (2001) “Seismic behavior and design of concentrically braced steel frames.” Engineering Journal, AISC, Third Quarter, pp.148-166.

Tremblay, R. (2002) “Inelastic Seismic Response of Steel Bracing Members”, Journal of Constructional Steel Research, Vol.58, pp.665-701.

Tremblay, R., Bruneau, M., Nakashima, M., Prion, H.G.L., Filiatrault, A., DeVall, R. (1996) “Seismic Design of Steel Buildings: Lessons from the 1995 Hyogo-ken Nanbu Earthquake”, Canadian Journal of Civil Engineering, Vol.23, pp.727-756.

Tremblay, R. and Filiatrault, A. (1996) “Seismic Impact Loading in Inelastic Tension-Only Concentrically Braced Steel Frames: Myth or Reality?” Earthquake Engineering and Structural Dynamics, Vol.25, pp.1373-1389.

Tremblay, R., Archambault, M.-H., Filiatrault, A. (2003) “Seismic Response of Concentrically Braced Steel Frames Made with Rectangular Hollow Bracing Members”, Journal of Structural Engineering, ASCE, Vol.129, Issue 12, pp.1626-1636.

Yang, T.Y., and Whittaker, A. (2002) “MCEER Demonstration Hospitals-Mathematical Models and Preliminary Results”, Technical Report, Multidisciplinary Center for Earthquake Engineering Research, University at Buffalo, Buffalo, NY.

Zayas, V.A., Popov, E.P. and Mahin, S.A. (1980a) “Cyclic Inelastic Buckling of Tubular Steel Braces” Report No. UCB/EERC-80/16, Berkeley, California.

Zayas, V.A., Mahin, S.A. and Popov, E.P. (1980b) “Cyclic Inelastic Behavior of Steel Offshore Structures” Report No. UCB/EERC-80/27, Berkeley, California.

APPENDIX A
ESTIMATION OF SPECIMEN PUSHOVER CURVES

A.1 General

Coupon test results were used as material data in static push-over analysis. Hand calculations were also carried out to check out the computer analysis results. This was done to determine the tension yield force and buckling load of the brace elements as precisely as possible.

AISC (1999) LRFD formulas with resistance factors of ϕ_t =1.00 and ϕ_c = 1.00, were used for the computation of tension and compression capacities of the brace members. Given below are the steps followed in the analysis of specimens.

A.2 Tension Braces

The controlling tension strength of a properly connected brace member is given either by yielding of the gross cross section of the brace away from the connection or by fracture at the effective net area (i.e. through the slots for welding in tube braces) at the connection. In Specimens F1 and F2, gusset-to-square tube connections were designed and constructed in such a way that the failure mode should be the yielding of the gross cross-section. This would provide significant ductility and hysteretic energy dissipation in the system prior to collapse. Higher safety factors were used in the design of gussets and fillet welds to achieve this desired ductile behavior. The anticipated failure mode of the specimens was the fracture somewhere along the brace (most probably at the brace mid-length) due to low-cycle fatigue upon repeated cyclic loading.

Assuming the governing limit state is general yielding of the brace gross cross section rather than net section failure, the nominal tensile strength of the brace (T_n) was set equal to:

$$T_n=A_gF_y \qquad \text{(A-1)}$$

where

A_g= gross area of member

F_y= specified minimum yield stress.

A.3 Compression Braces

Since no premature failure was expected at the connections due to compression strength, only brace buckling strength was considered. A compact section was selected as per AISC (2002) Seismic Provisions to delay local buckling of the steel tube braces. The strength for flexural buckling (P_n) of the braces was set equal to:

$$P_n=A_gF_{cr} \tag{A-2}$$

For $\lambda_c \leq 1.5$ $$F_{cr} = (0.658^{\lambda_c^2})F_y \tag{A-3}$$

For $\lambda_c > 1.5$ $$F_{cr} = \left[\frac{0.877}{\lambda_c^2}\right]F_y \tag{A-4}$$

where

F_{cr}= critical buckling stress in compression

E = modulus of elasticity.

Since the material properties could be obtained from coupon tests within reasonable tolerances, predictions of the braces buckling strength depend only on the accuracy of the estimated effective length factor (K). During the preliminary analysis of the specimens, a literature review was carried out to estimate the appropriate K values (Table A-1).

TABLE A-1 Review of K-Factors in Compression Braces in Steel Frames

Reference	End Restraint	$K_{in\text{-}plane}$	$K_{out\text{-}of\text{-}plane}$
Tremblay (2001)	pinned-pinned	0.50	0.50
FEMA 356 (2000)	pinned-pinned	0.80	1.00
AISC LRFD (1999)	pinned-pinned	1.00	1.00
Bruneau,Uang & Whittaker (1998)	pinned-pinned	0.50	1.00
Remennikov& Walpole (1997)	pinned-pinned	0.70	0.70
Astaneh-Asl (1998)	pinned-pinned	0.65	1.00
El-Tayem&Goel (1986)	pinned-pinned	0.40~0.45	0.425
Astaneh-Asl, Goel &Hanson (1985)	pinned-pinned	1.00	1.00

Note that the K values listed in Table A-1 highly depend on the connections' details provided at the end and at cross over points of X braced frames. A conservative K-factor of 0.50 for in-plane and out-of-plane buckling was assumed in calculations of the compression strength of the braces for Specimens F2 and F4, because the end gusset connections used in this research were assumed to represent a fixed-fixed end condition rather than pinned connections, thus preventing rotation at those connection points. Laterally unbraced lengths (l) for the specimens F2 and F4 were taken as the clear distance between the junction of the brace and gusset members at each end.

For the specimens with CFSS (F1 and F3), maximum diagonal brace length between the centerlines of the vertical studs was taken as the laterally unbraced length. Because the degree of fixity of brace-to-stud connections might vary as the specimens are subjected to progressively increasing displacement cycles during testing, a K-factor of 1.00 was assumed. Additionally, as described in Section 2.3, since the points of inflection in the buckled brace remain almost unchanged in the elastic and inelastic range, the same K factor was used for the nonlinear structural analysis. Based on these assumptions and the available material properties, tube and bar braces of the specimens were designed. A summary is given in Table A-2.

TABLE A-2 Summary of Brace Member Design

Specimen	Section (mm/mm/mm)	Area (mm^2)	r_{min} (mm)	$K_{in\text{-}plane}$	$K_{out\text{-}of\text{-}plane}$	Unbraced Length (mm)	KL/r	P_n (kN)	T_n (kN)
F1	Tube 76.2x76.2x7.9	2006.4	27.2	1.00	1.00	495.3	18.21	751.3	771.9
F2	Tube 76.2x76.2x7.9	2006.4	27.2	0.50	0.50	2324.1	42.72	665.0	771.9
F3	Bar 25.4x25.4	1290.3	7.34	1.00	1.00	495.3	67.48	337.8	486.5
F4	Bar 25.4x25.4	1290.3	7.34	0.50	0.50	2298.7	156.59	91.1	486.5

All specimens were then modeled using SAP 2000 to estimate their monotonic load-displacement behavior. Beam-to-column connections were treated as simple hinged connections, despite the expectations that some degree of semi-rigid behavior would develop. However, as described later, the contribution of the bare frame on the overall behavior is taken into account by combining cyclic test data. Eccentricities within the connections, produced by the difference

between the working points of braces and boundary frame members, were taken into account in the model. As given in Section 3, a special gusset-to-boundary frame connection detail, having no Gusset-to-Column Web Connection as described in the AISC Manual (2001), was used in the specimens.

Since vertical cold-formed steel studs have pinned end connections to the boundary frame beams, their contribution to lateral load and stiffness was assumed to be negligible. Therefore, they were treated only as in-plane and out-of-plane buckling restrainers, and were not included in the model. However, at the junction of braces and studs, additional in-plane and out-of-plane restrainers were used in the model to simulate the restraint provided by the vertical studs. Steel axial plastic hinges were used for the braces as energy dissipating elements. All parameters defining the axial plastic hinge (tension, buckling, and post-buckling range) were assumed as per FEMA 368 (2001). The resulting brace axial hinge properties are illustrated in Figures A-1a to A1d. The boundary frame was modeled using linear elastic members.

The resulting lateral force versus top lateral displacement FEMA 368 pushover curve envelopes obtained for each specimen for tension and compression are shown in Figures A-2a to A-2d. The models of the specimens were laterally pushed to 50.8mm both in tension and compression. Note that these curves include the contribution of the bare frames test data.

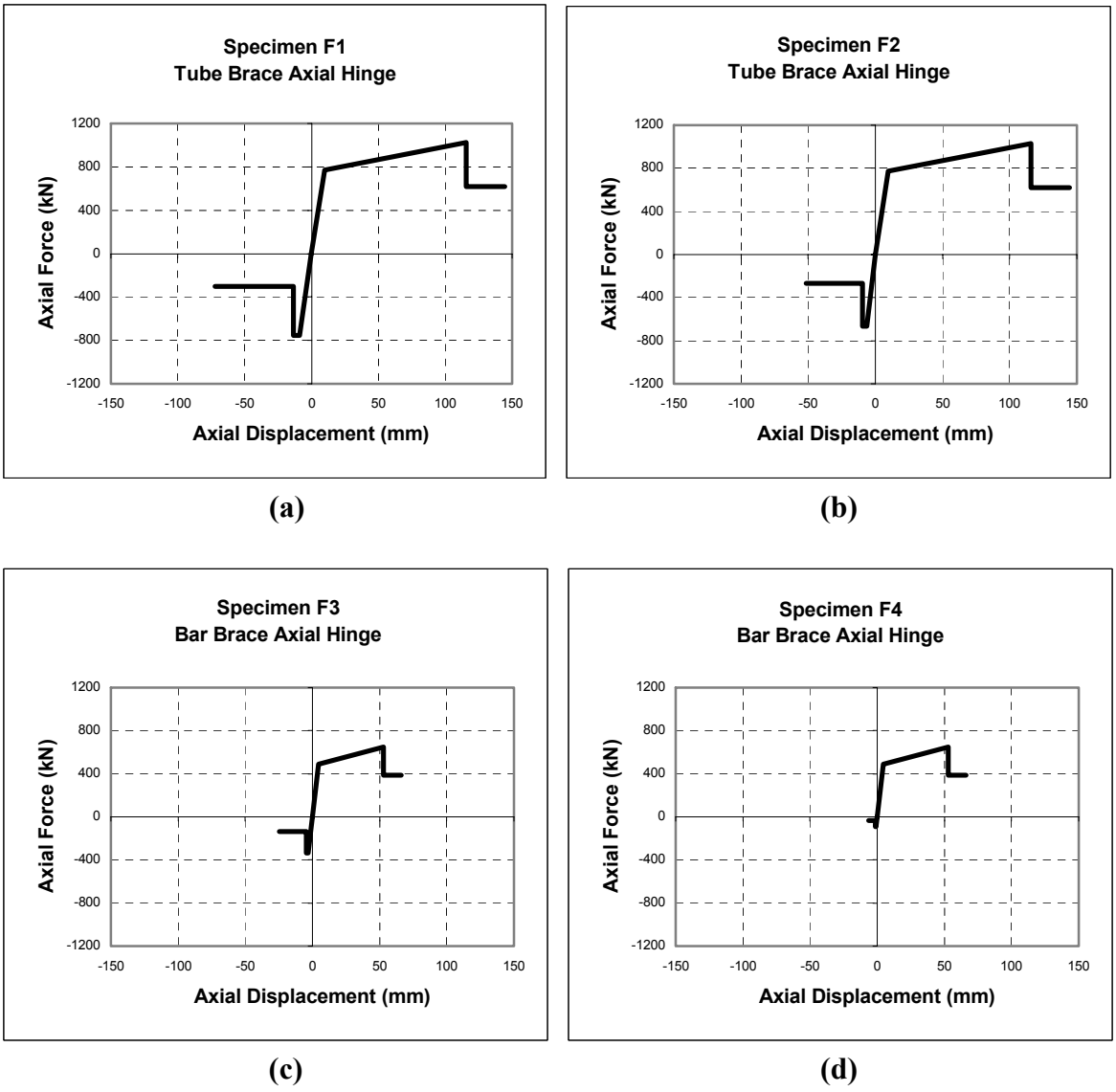

FIGURE A-1 Brace Axial Hinge Properties Used in Static Pushover Analyses of Specimens: (a) Tube Brace Axial Hinge for Specimen F1; (b) Tube Brace Axial Hinge for Specimen F2; (c) Bar Brace Axial Hinge for Specimen F3; (d) Bar Brace Axial Hinge for Specimen F4

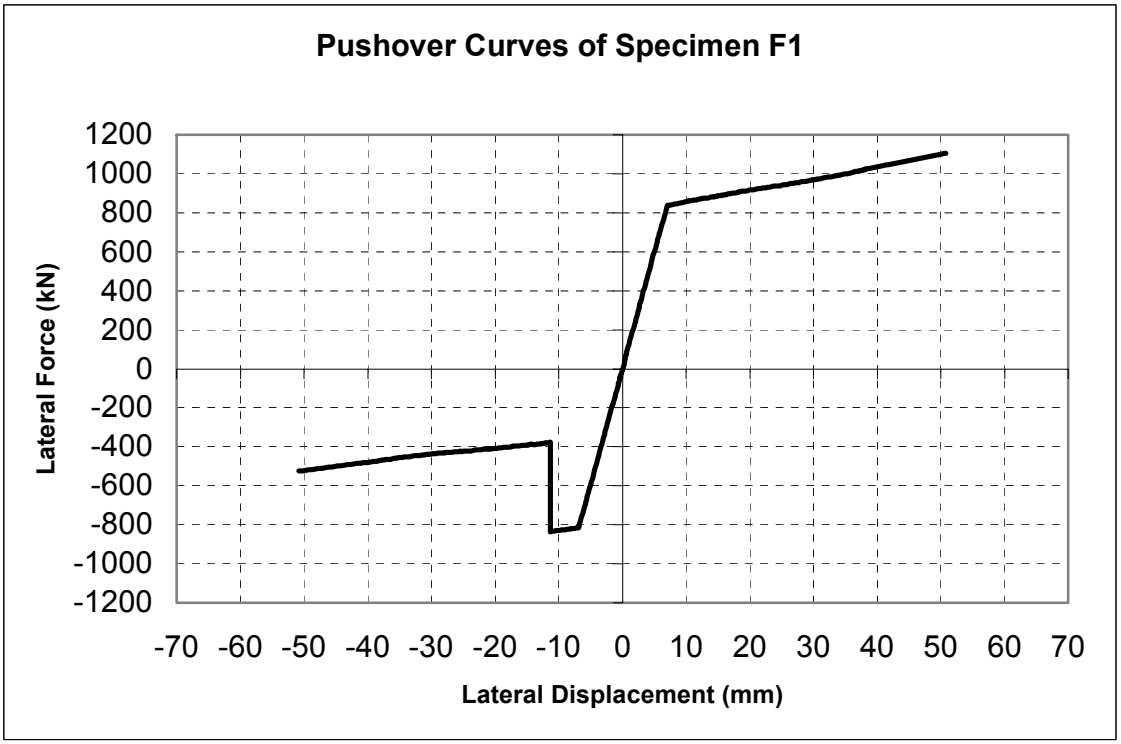

(a)

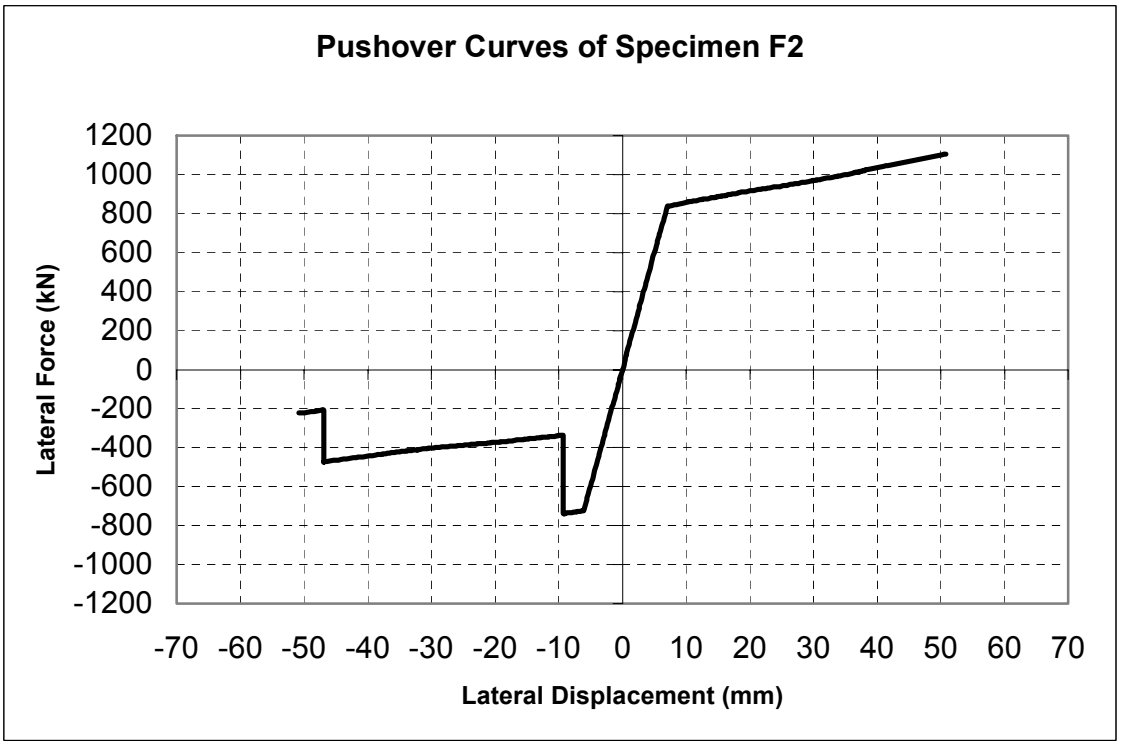

(b)

FIGURE A-2 Static Pushover Curves of Specimens: (a) Specimen F1; (b) Specimen F2

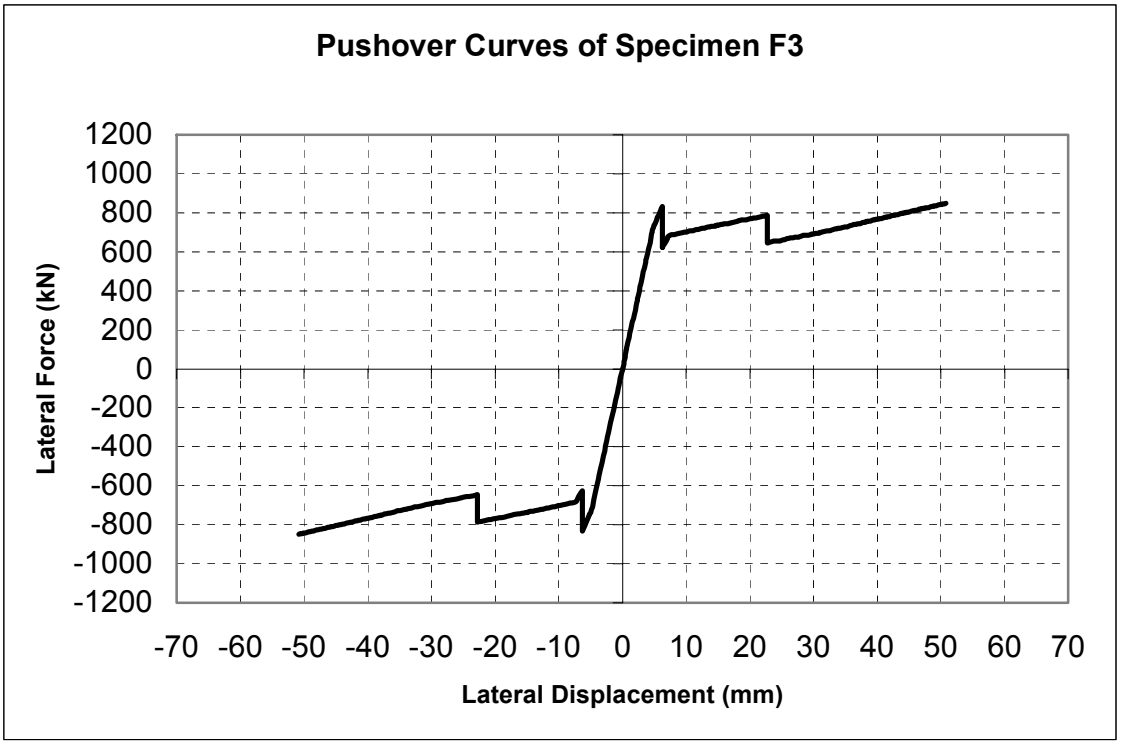

(c)

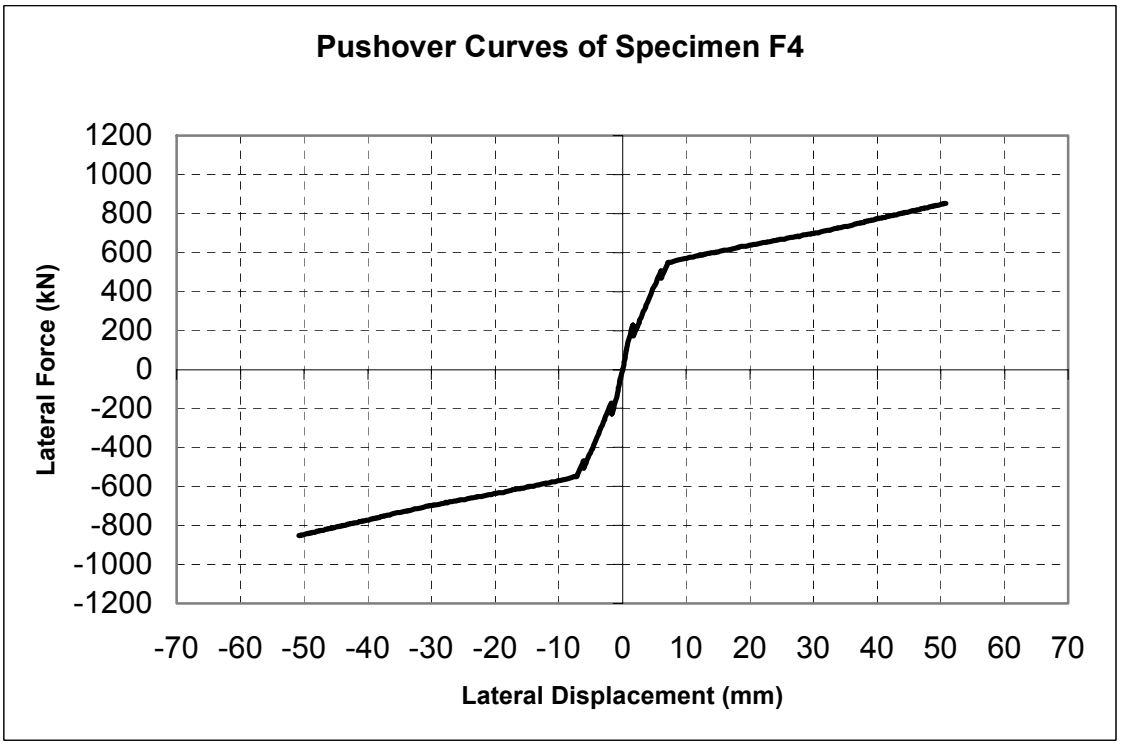

(d)

FIGURE A-2 Static Pushover Curves of Specimens (continued): (c) Specimen F3; (d) Specimen F4

APPENDIX B
HYSTERETIC MODELING OF BARE FRAMES

B.1 General

Double web angle beam-to-column connections were used in the boundary frames of the specimens. Those angles are welded to the beam webs and bolted to the column flanges. Since the bolted connections were designed and constructed as slip critical, some degree of rigidity would be expected in these connections. To quantify this fact, cyclic tests of the bare frames were performed. The obtained boundary frame test results were then used to calibrate an hysteretic model as described in this appendix. Among several empirical and semi-empirical connection models considered, the bounding surface model was chosen to simulate the semi-rigidly connected bare frame cyclic behavior.

B.2 Bounding Surface Model with Internal Variables

The bounding surface model recommended by Dafalias and Popov (1976) enables the force to be predicted at given displacements. Either a moment-rotation or a force-displacement relationship can be modeled. A typical representation of the model is schematically shown in Figure B-1.

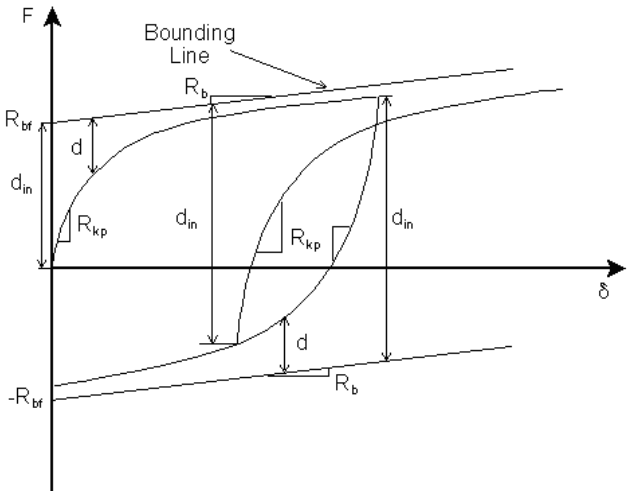

FIGURE B-1 Bounding Surface Model (Adapted from Chen et al., 1996)

Given below are the modeling parameters. Force-displacement relationship in the incremental form is defined as

$$\Delta F = R_{kt} \Delta\delta \tag{B-1}$$

where

ΔF = incremental base shear

R_{kt} = tangent stiffness at the current displacement

$\Delta\delta$ = incremental displacement

The tangent stiffness at the current displacement is expressed in terms of the initial stiffness R_{ki}:

$$R_{kt} = \frac{R_{ki} R_{kp}}{R_{ki} + R_{kp}} \tag{B-2}$$

The plastic tangent stiffness (R_{kp}) of the system can be calculated depending on the plastic internal variables:

$$R_{kp} = R_b + h\left[\frac{d}{d_{in} - d}\right] \tag{B-3}$$

where

R_b = slope of the bounding lines

h = hardening shape parameter

d = distance from the current force to the corresponding bound in the direction of current loading

d_{in} = the value of d at the initiation of each load reversal

This model needed to be modified slightly to capture the changes in initial stiffness at each cycle in which the peak displacement was larger than initial yield displacement. To achieve this, a

linear change in initial stiffness with respect to the maximum displacement of a cycle was defined as follows:

$$R_{ki} = R_{kii} a \left[\frac{\delta_{max}}{\delta_y} + b \right] \tag{B-4}$$

where

R_{kii} = initial stiffness prior to any displacement reaching the yield displacement

a,b = parameters used to fit the experimental data

δ_y = initial yield displacement of the boundary frame

δ_{max} = maximum displacement reached during the next cycle of loading

Furthermore, a limit of 2.5 times the initial stiffness was placed on R_{ki}. All parameters used in this study are summarized in Table B-1.

TABLE B-1 Bounding Surface Model Parameters for Bare Frames 1 and 2

Bare Frame	R_{bf} (kN)	R_b (kN/mm)	h	R_{ki} (kN/mm)	δ_y (mm)	a	b	Error in Energy Dissipated
BF1	90	3	100	10.64	13.5	0.67	0.42	9.71
BF2	80	2.6	25	12.42	7	0.47	0.59	-6.83

APPENDIX C
STRAIN GAUGE DATA FOR SPECIMEN F1

This appendix includes plots of the infill strain gauge data for the gauges attached on the tube brace and CFSS members. Strain gauge locations and labels are shown in Section 3, in Figure 3-26a. Both base shear versus axial strain and axial strain versus drift curves are provided for all cycles.

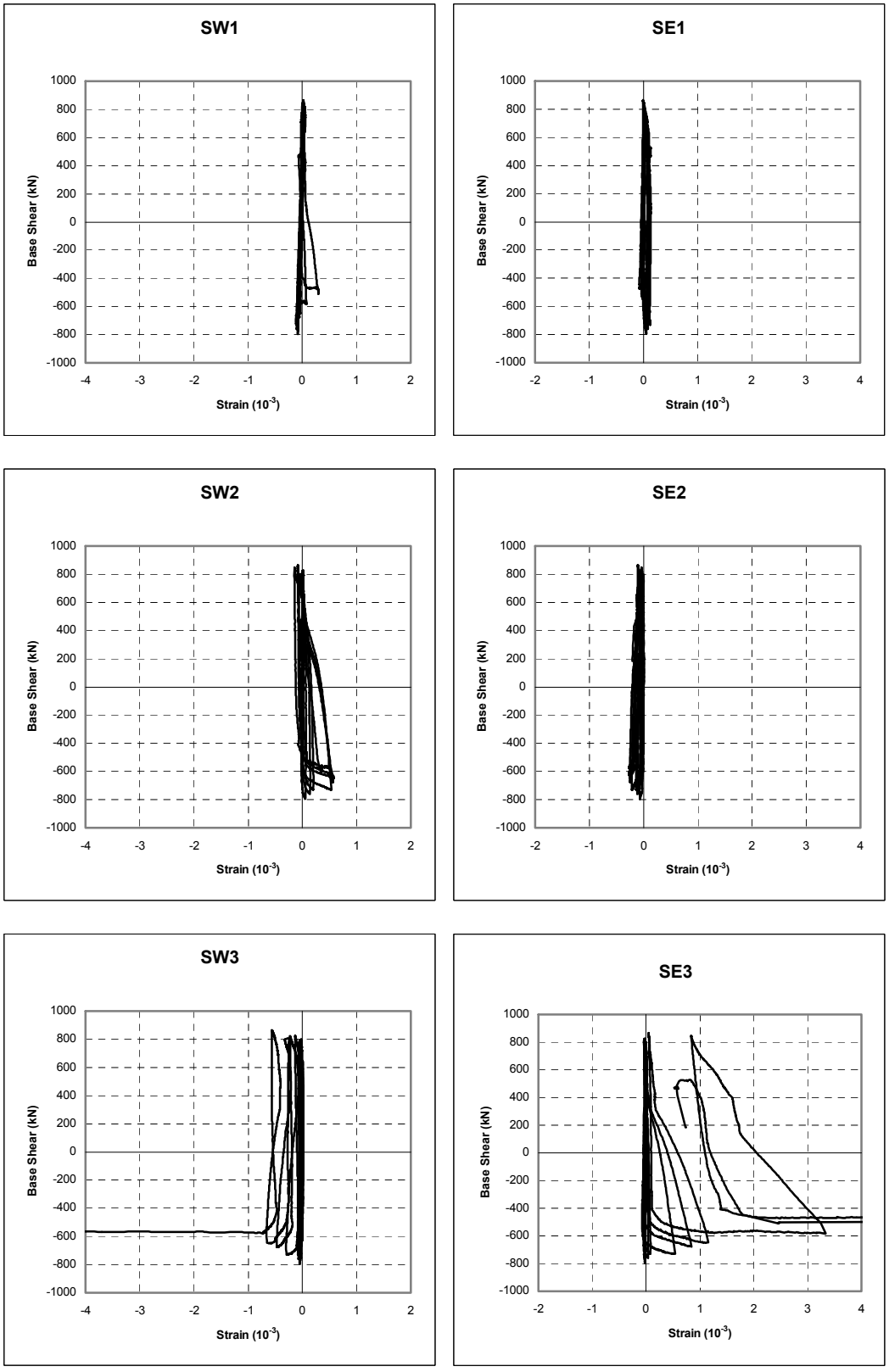

FIGURE C-1 Base Shear versus Outer Flange Strain Hystereses for CFSS Members

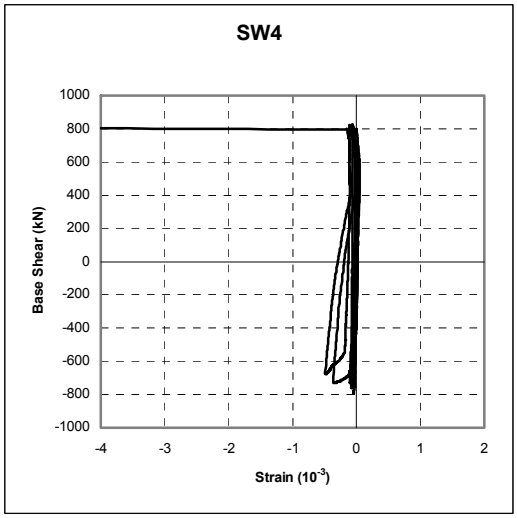

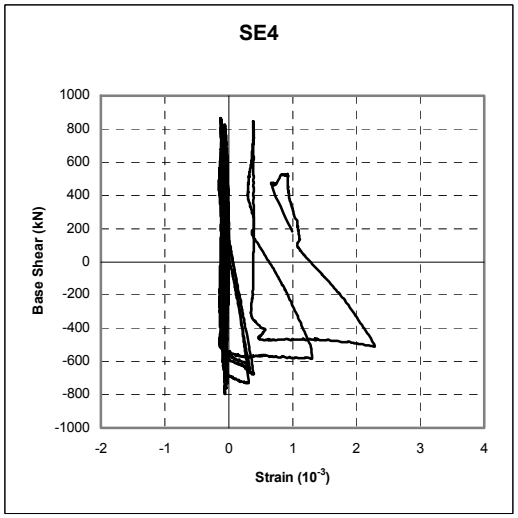

DATA NOT AVAILABLE
FOR SW5

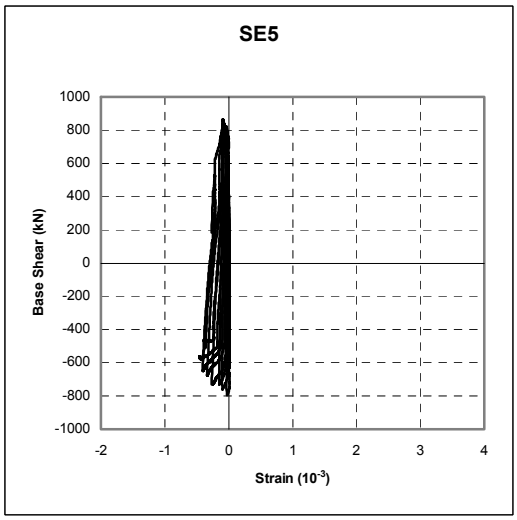

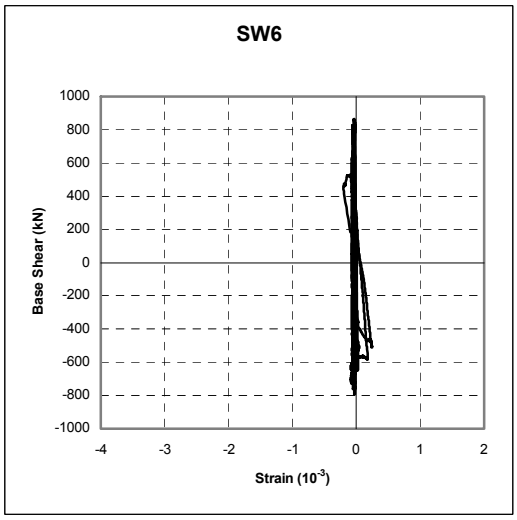

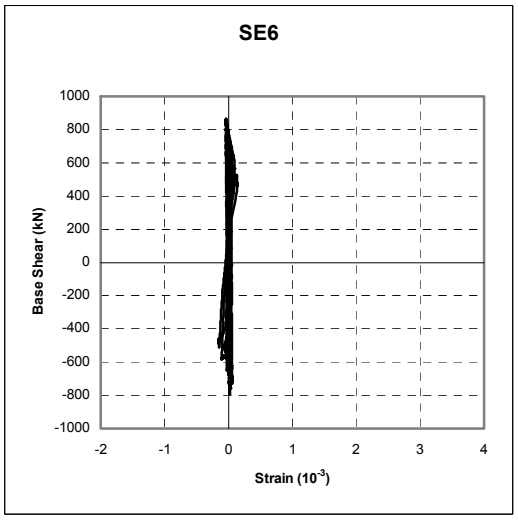

FIGURE C-1 Base Shear versus Outer Flange Strain Hystereses for CFSS Members (continued)

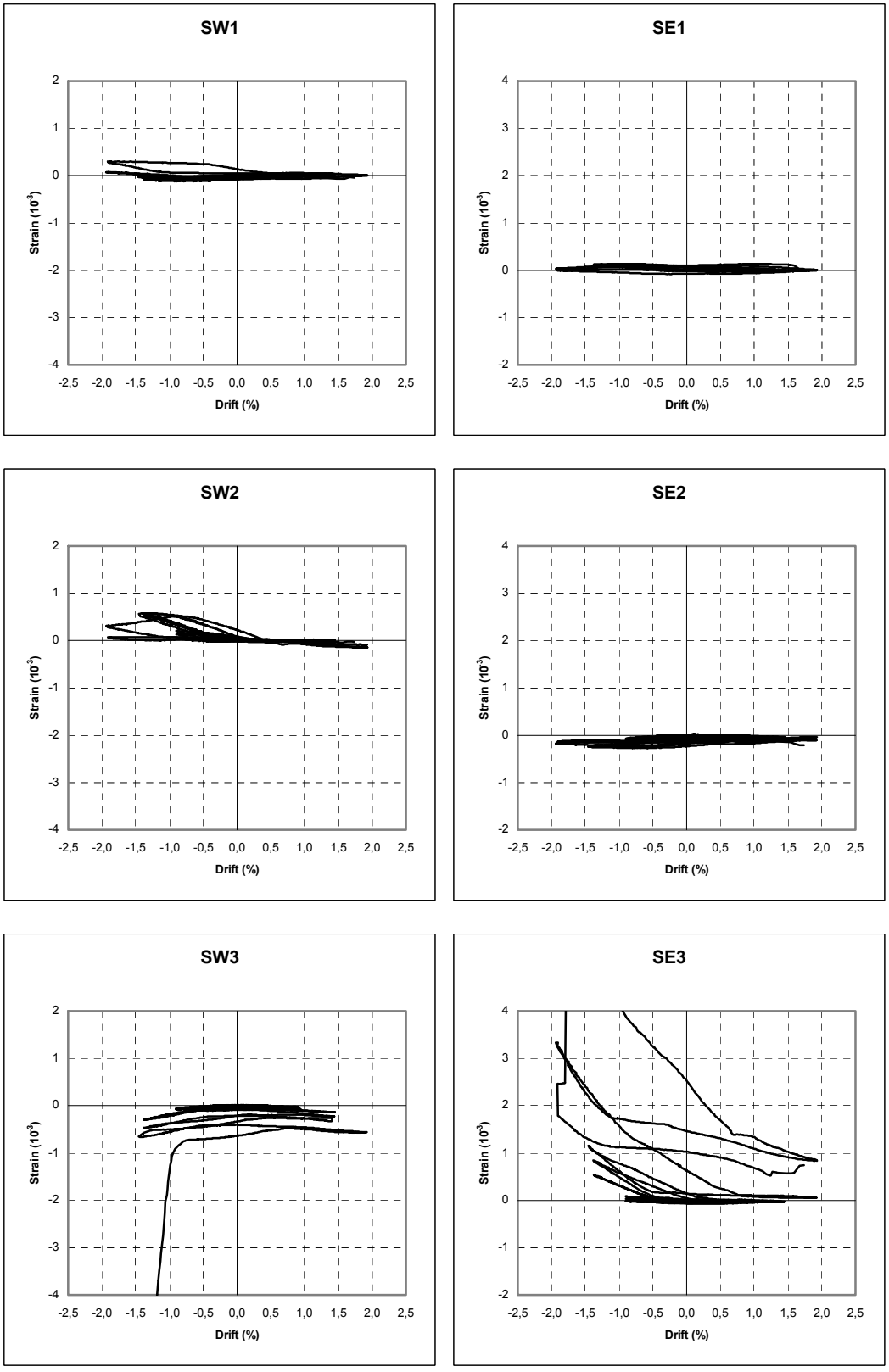

FIGURE C-2 Outer Flange Strain versus Drift Hystereses for CFSS Members

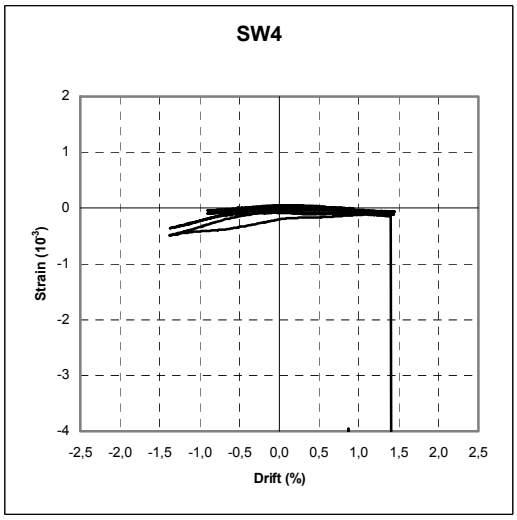

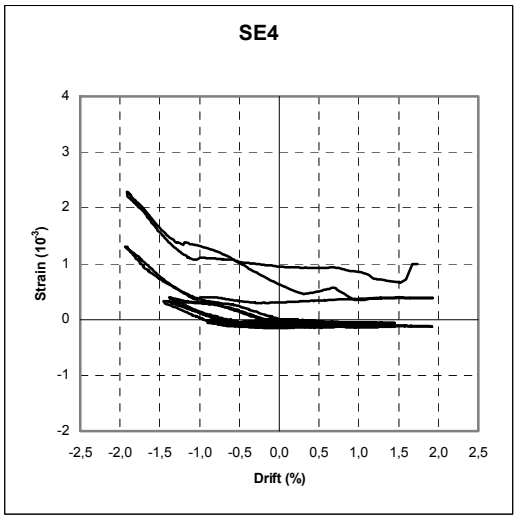

DATA NOT AVAILABLE
FOR SW5

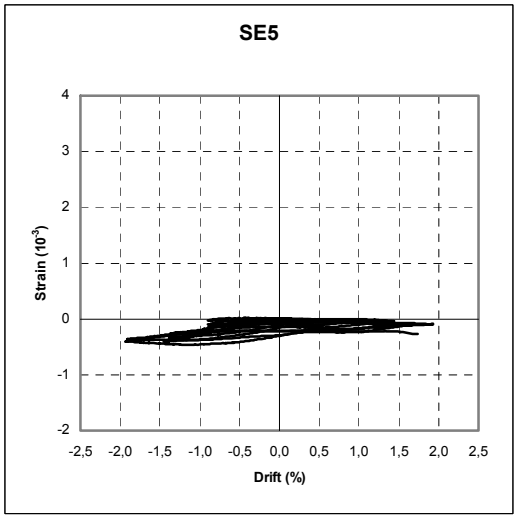

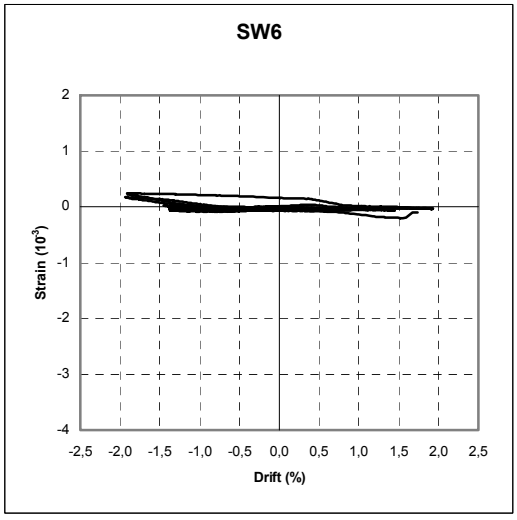

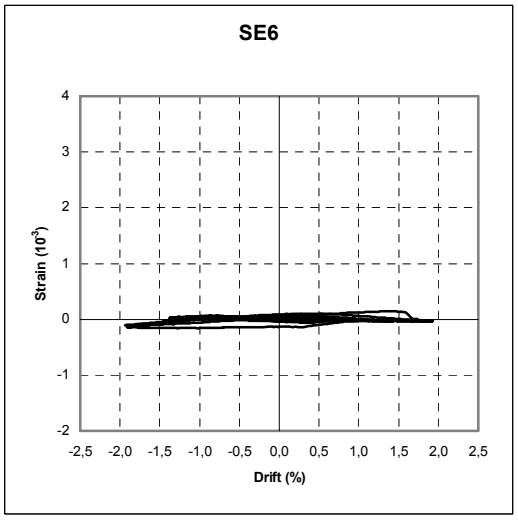

FIGURE C-2 Outer Flange Strain versus Drift Hystereses for CFSS Members (continued)

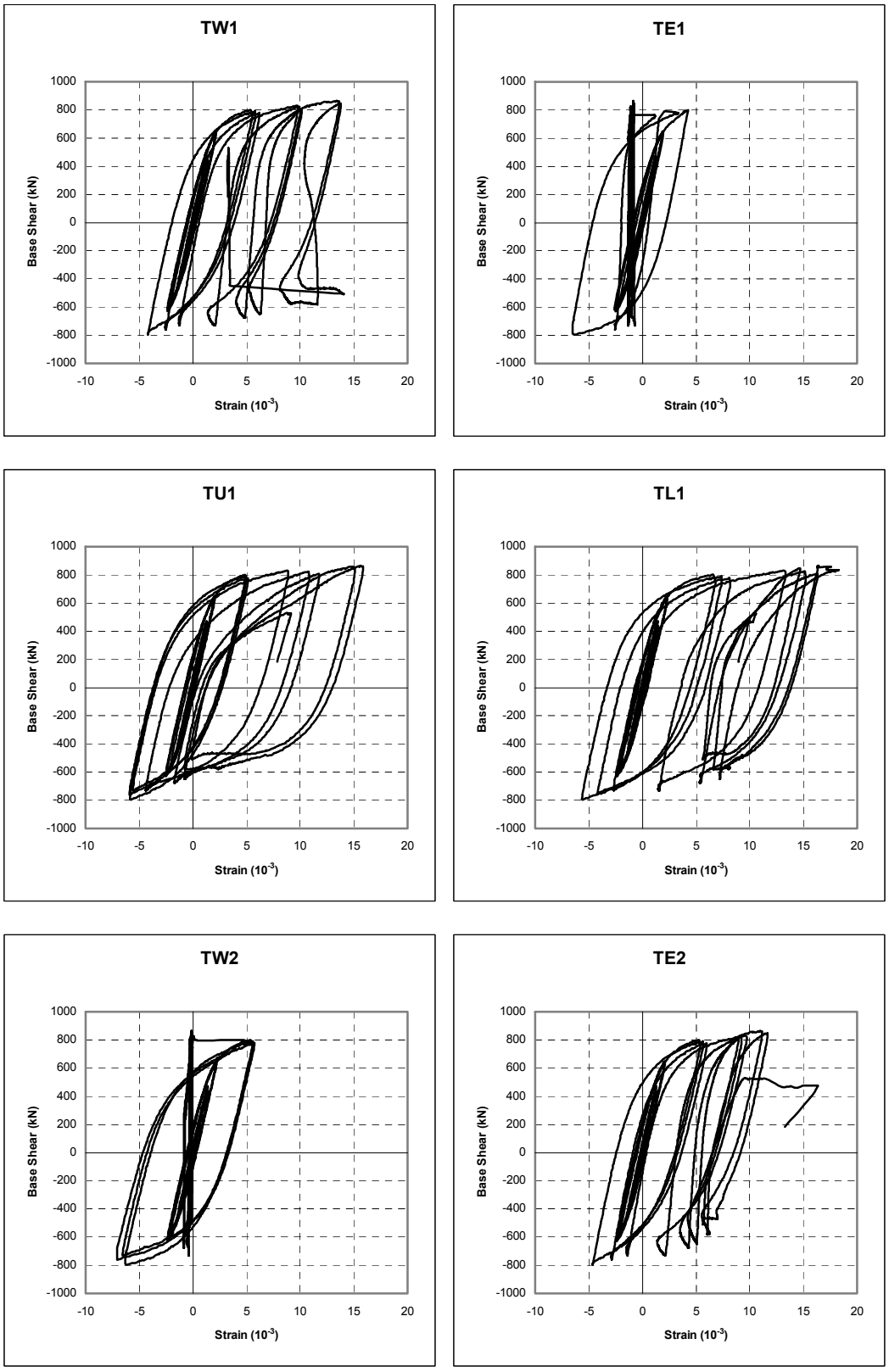

FIGURE C-3 Base Shear versus Tube Brace Axial Strain Hystereses

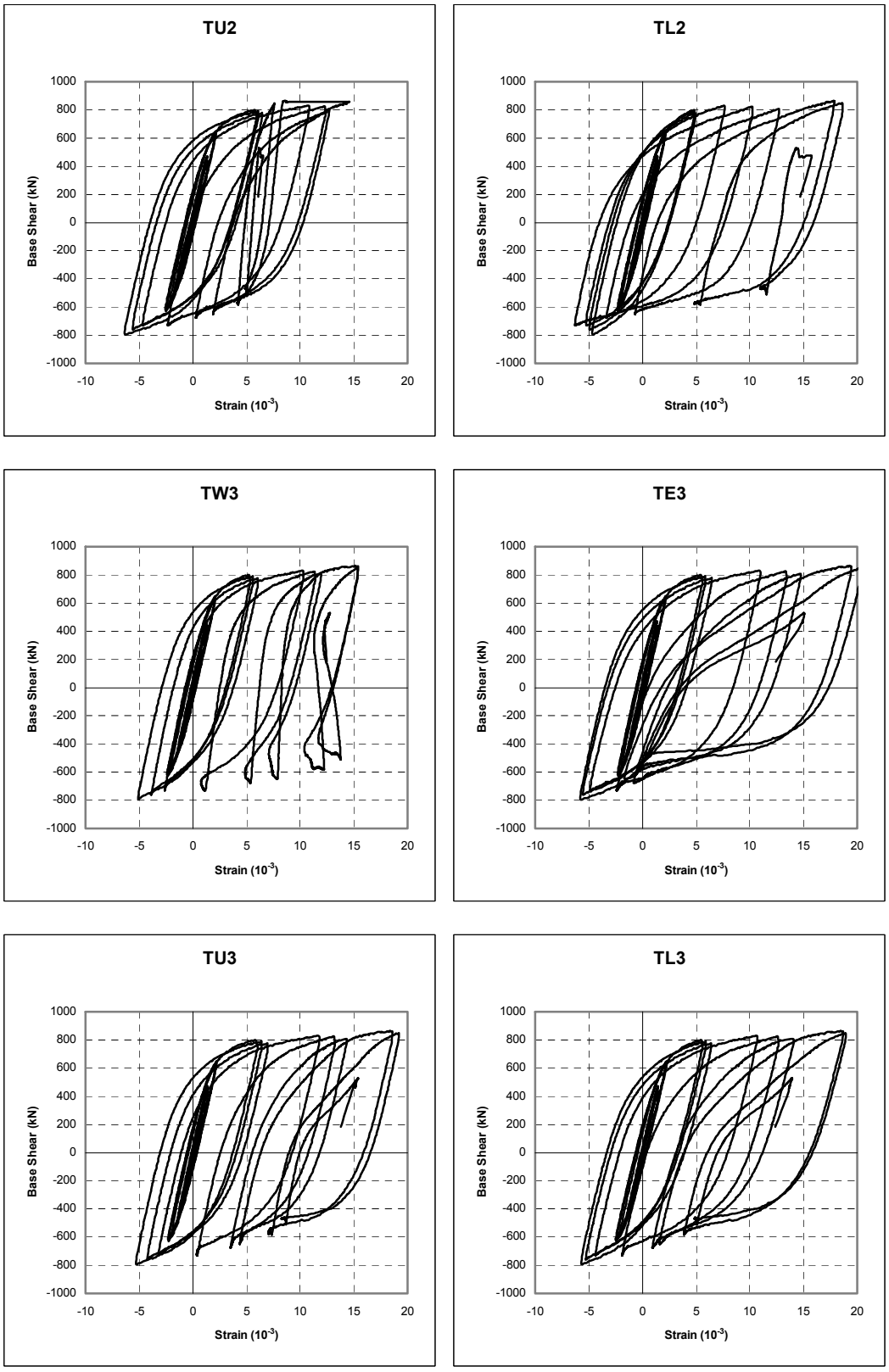

FIGURE C-3 Base Shear versus Tube Brace Axial Strain Hystereses (continued)

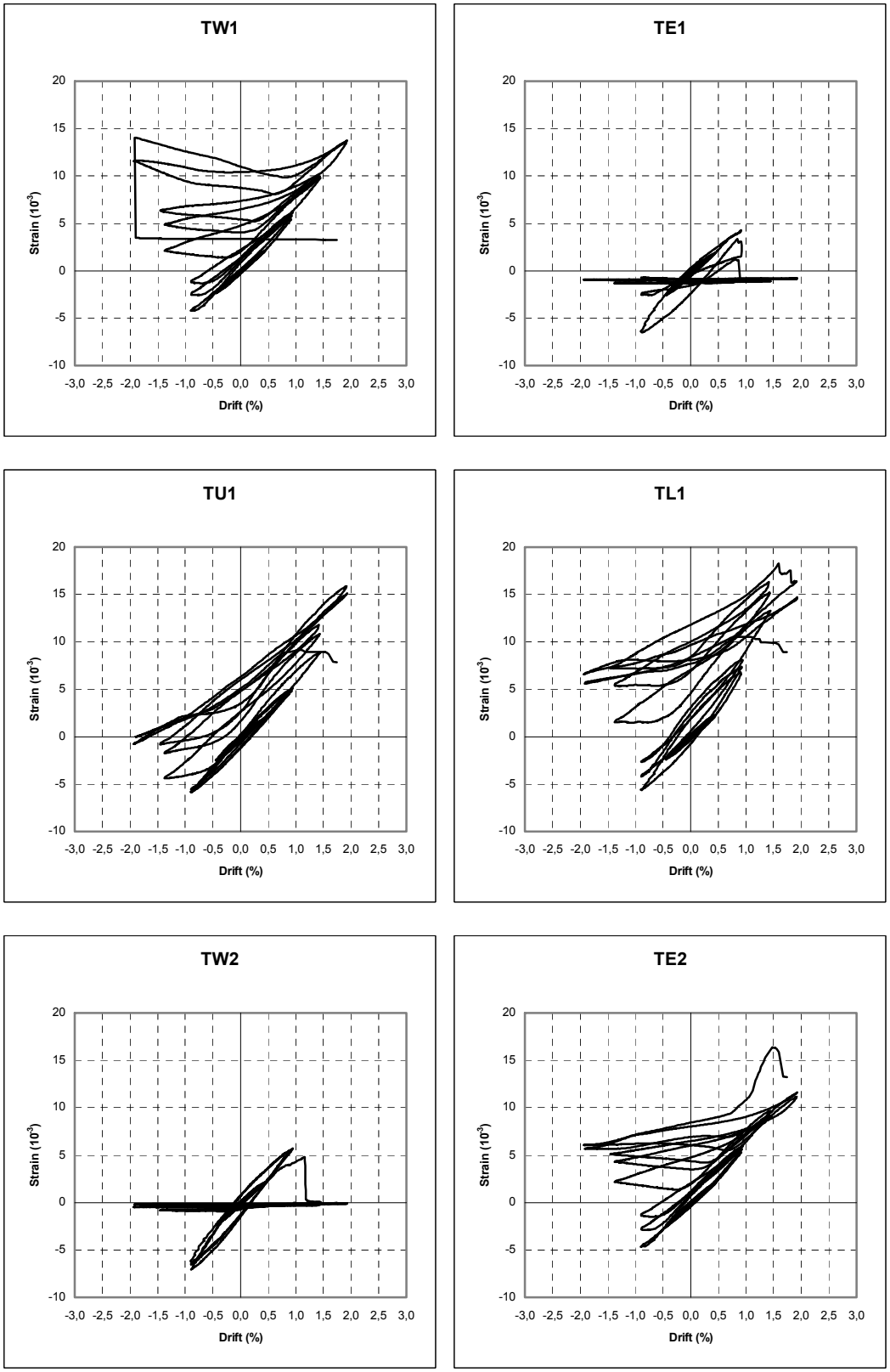

FIGURE C-4 Tube Brace Axial Strain versus Drift Hystereses

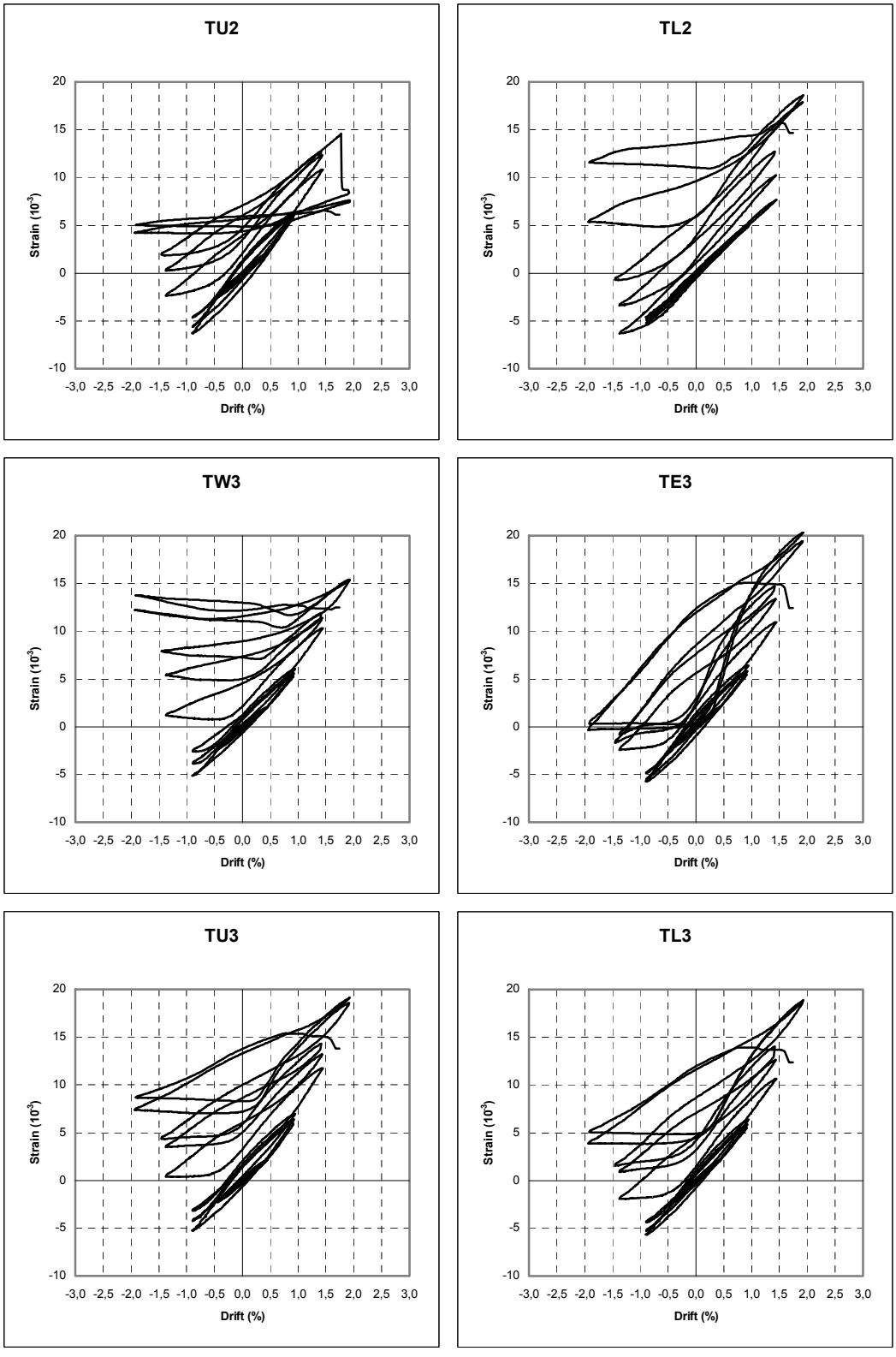

FIGURE C-4 Tube Brace Axial Strain versus Drift Hystereses (continued)

APPENDIX D
STRAIN GAUGE DATA FOR SPECIMEN F2

This appendix includes plots of the infill strain gauge data for the gauges attached on the tube brace. Strain gauge locations and labels are shown in Section 3, in Figure 3-27a. Both base shear versus axial strain and axial strain versus drift curves are provided for all cycles.

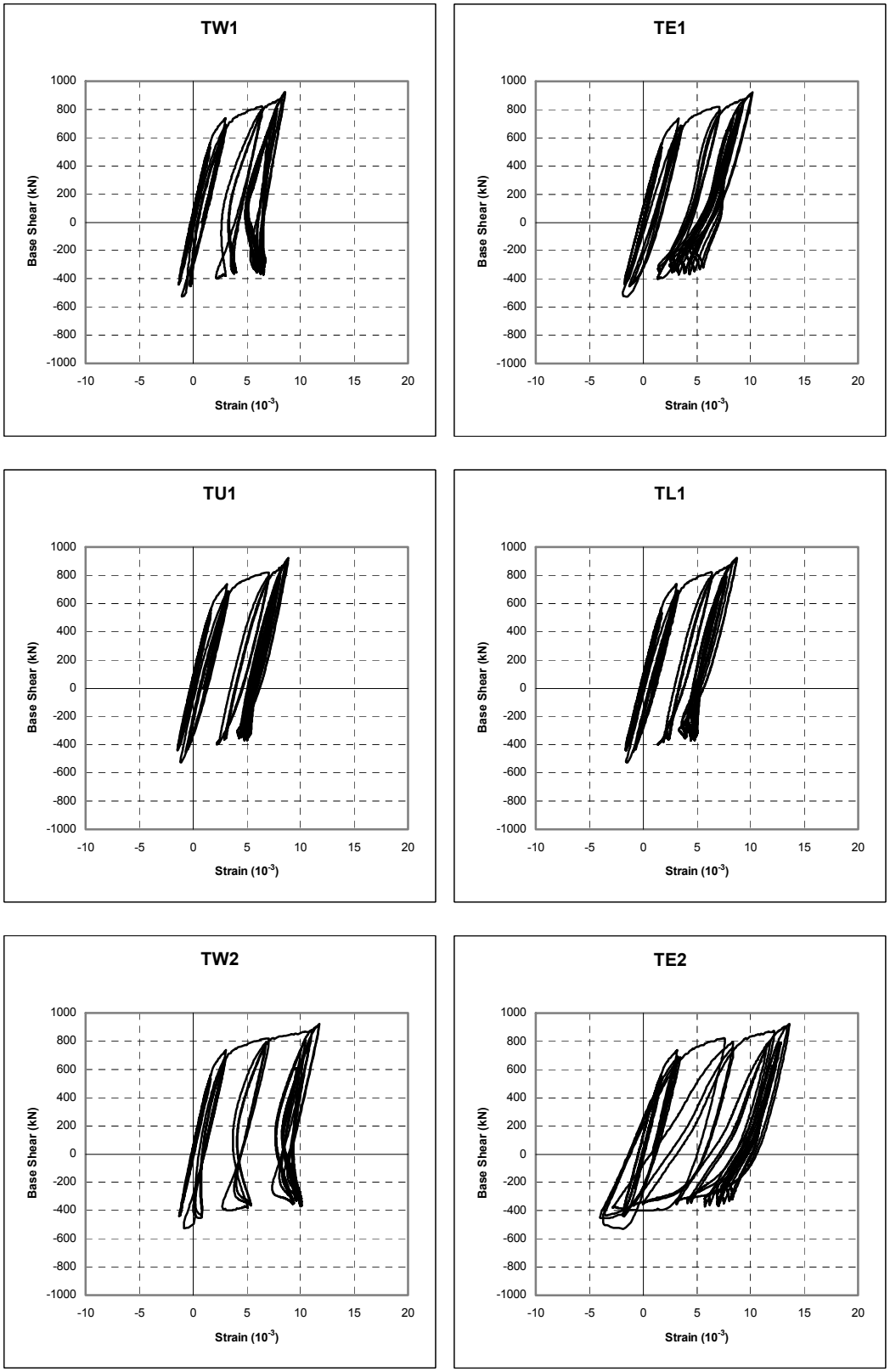

FIGURE D-1 Base Shear versus Tube Brace Axial Strain Hystereses

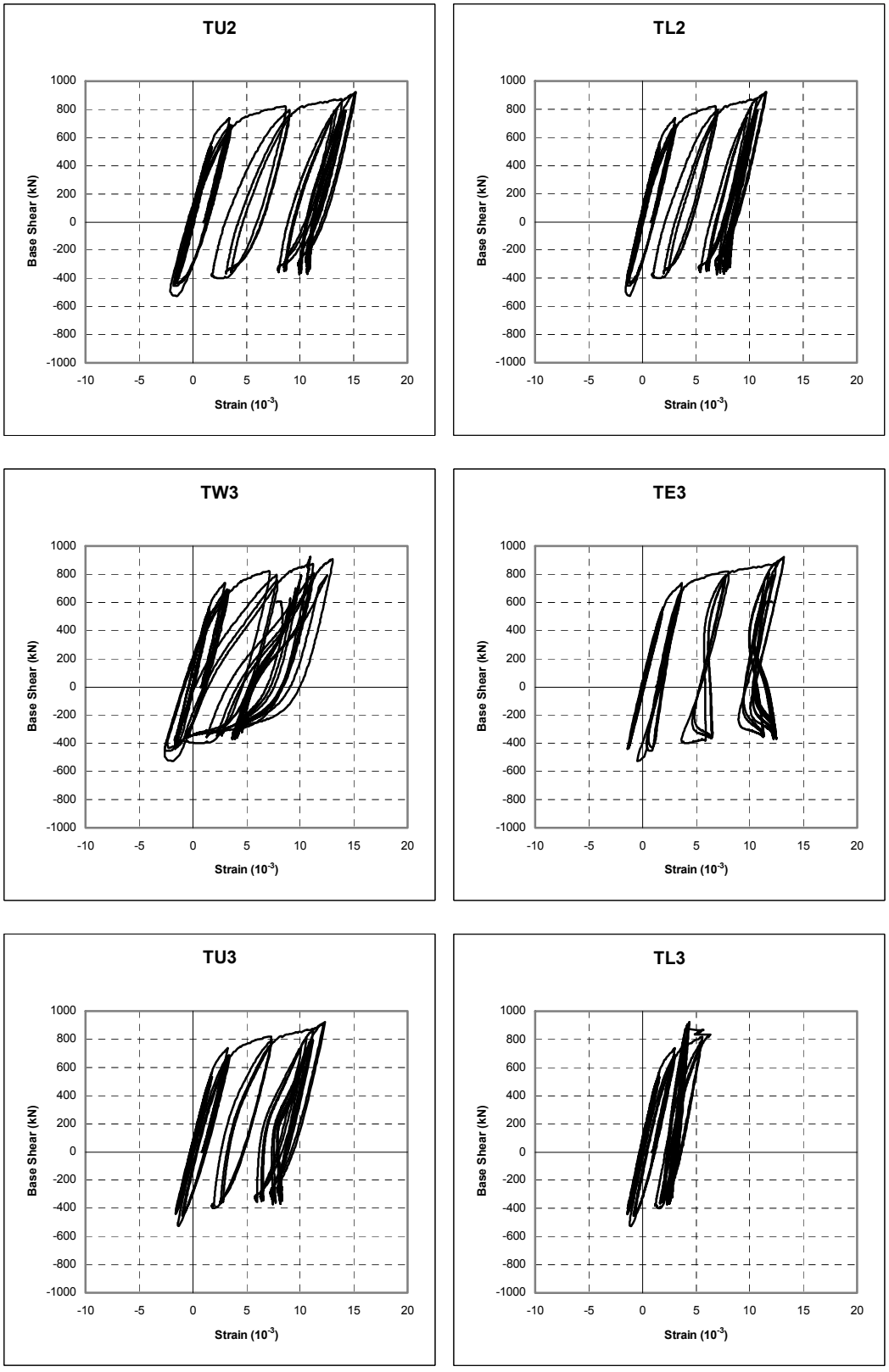

FIGURE D-1 Base Shear versus Tube Brace Axial Strain Hystereses (continued)

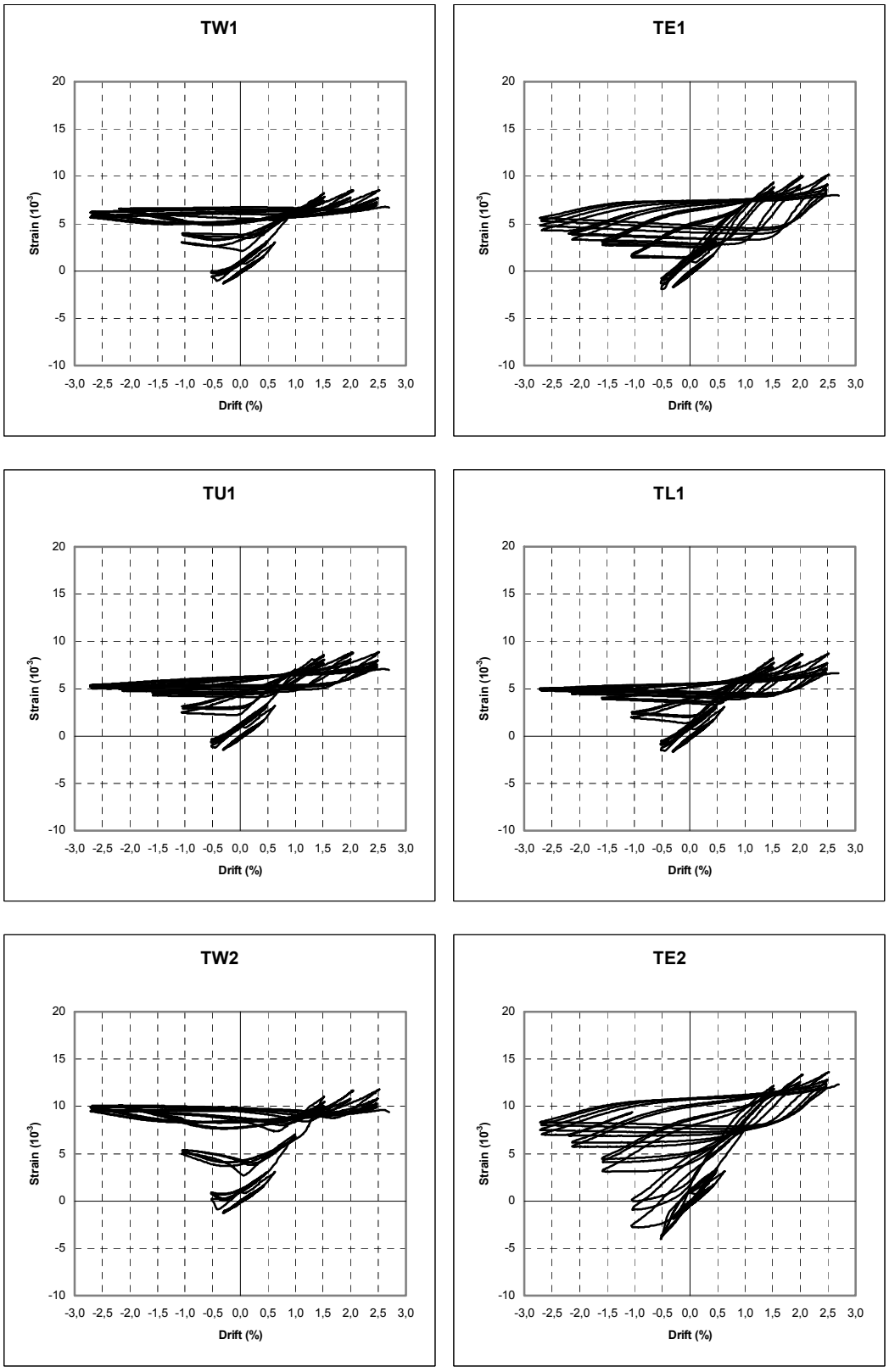

FIGURE D-2 Tube Brace Axial Strain versus Drift Hystereses

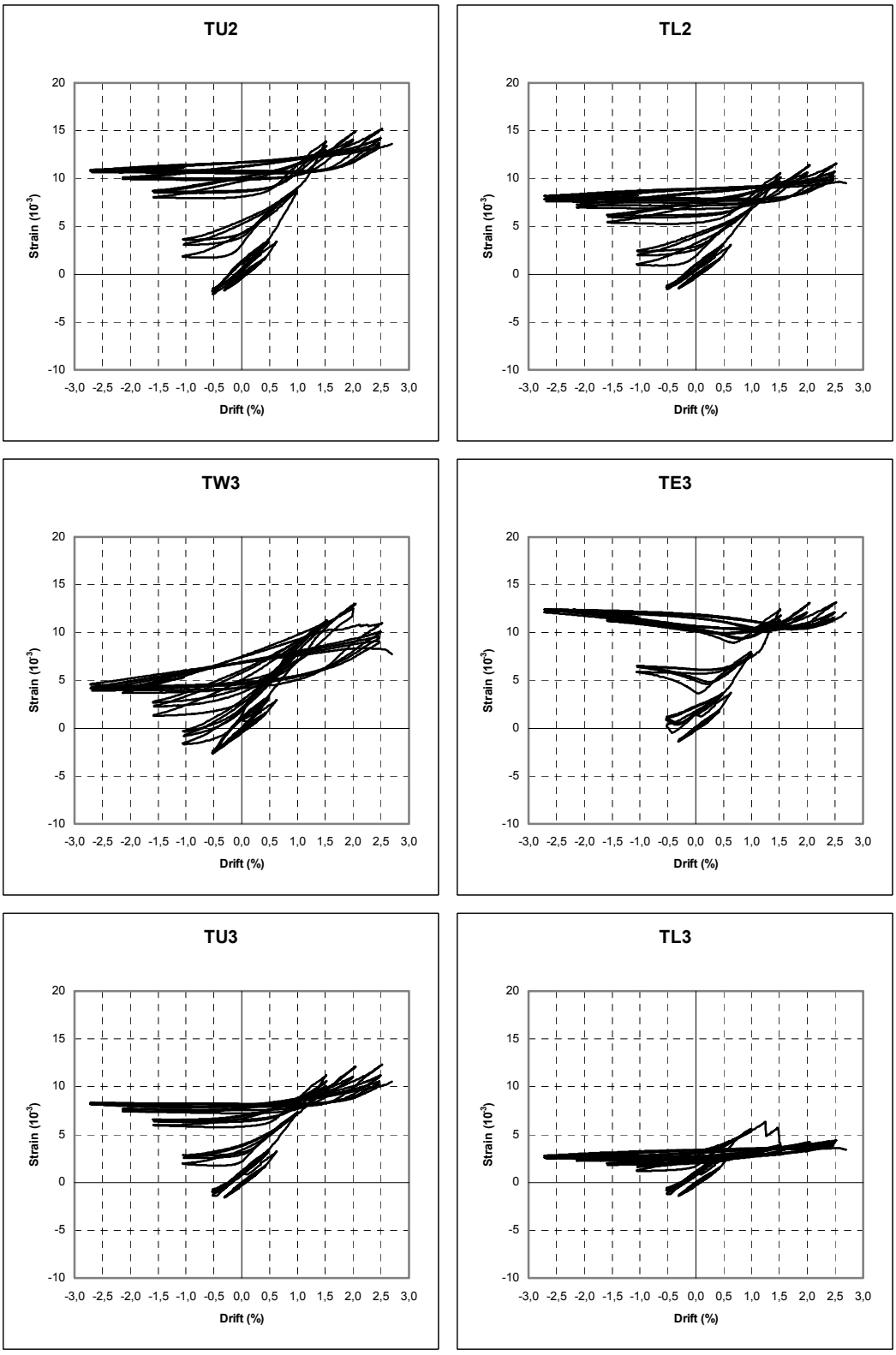

FIGURE D-2 Tube Brace Axial Strain versus Drift Hystereses (continued)

APPENDIX E
STRAIN GAUGE DATA FOR SPECIMEN F3

This appendix includes plots of the infill strain gauge data for the gauges attached on the bar braces and CFSS members. Strain gauge locations and labels are shown in Section 3, in Figure 3-28a. Both base shear versus axial strain and axial strain versus drift curves are provided for all cycles.

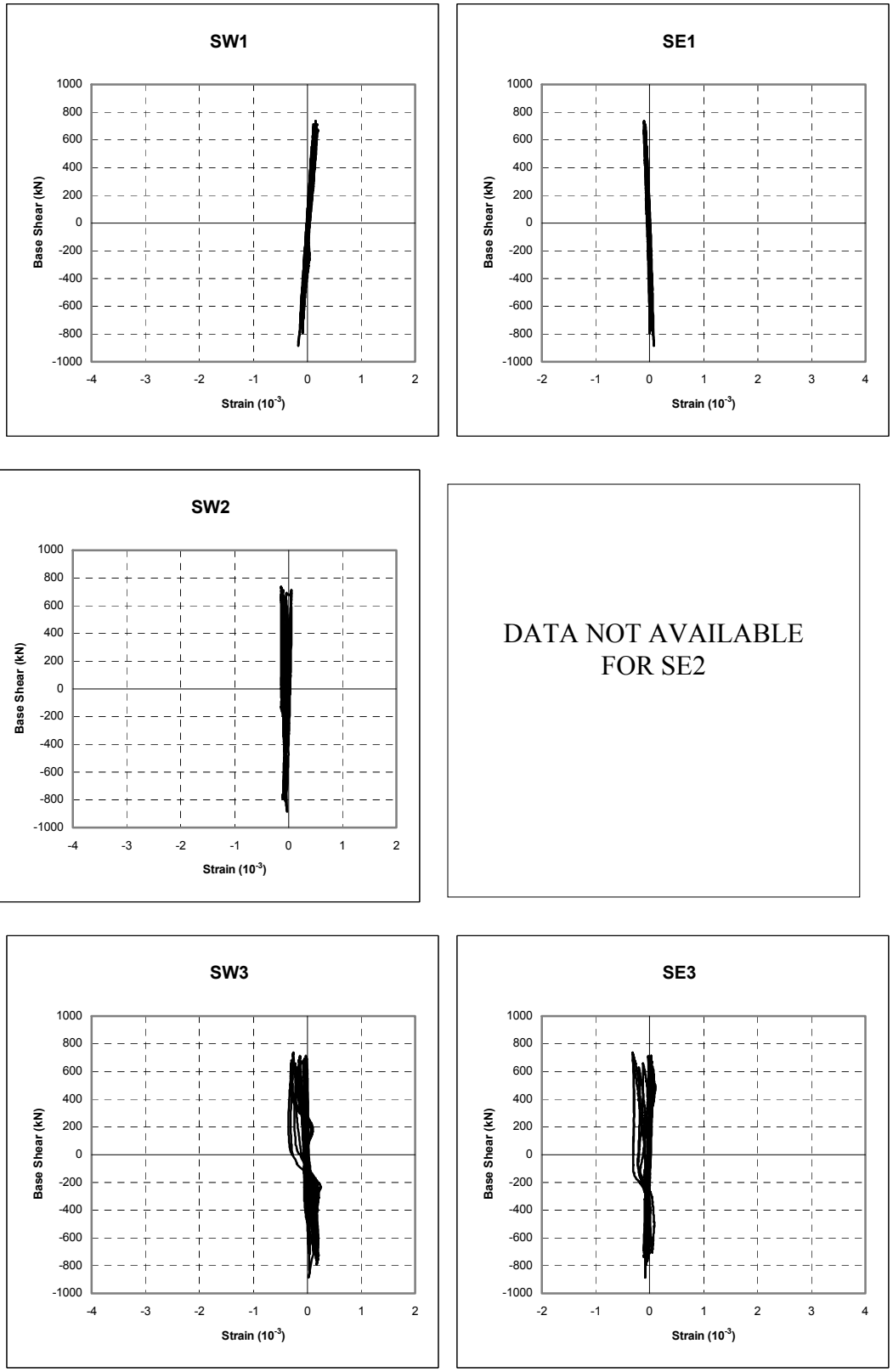

FIGURE E-1 Base Shear versus Outer Flange Strain Hystereses for CFSS Members

DATA NOT AVAILABLE
FOR SW4

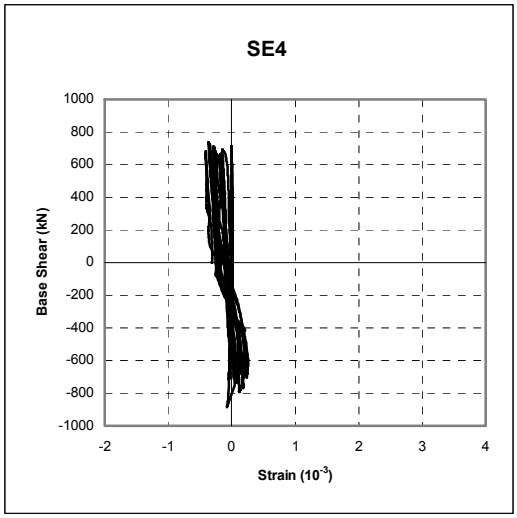

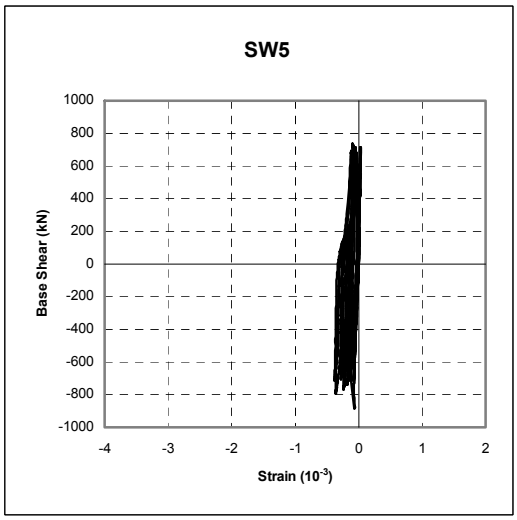

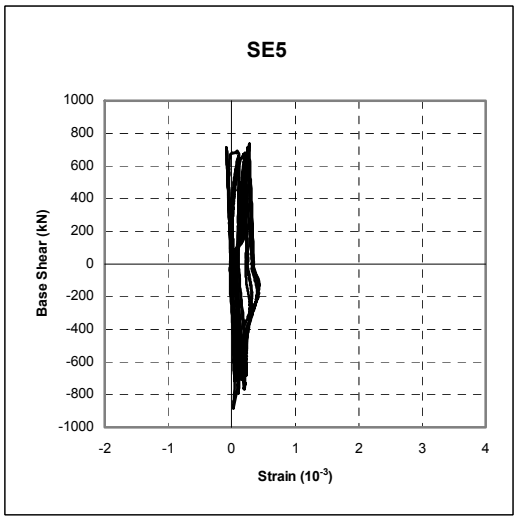

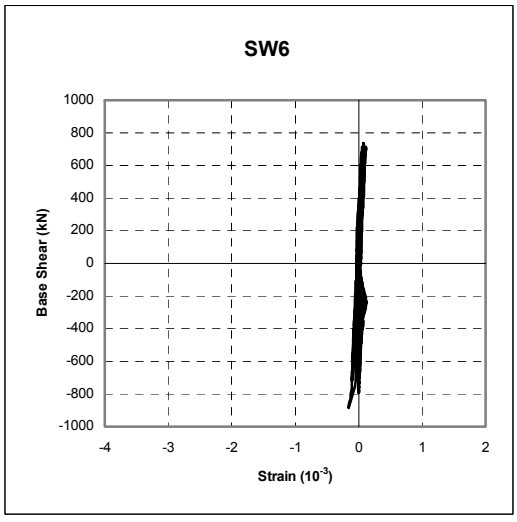

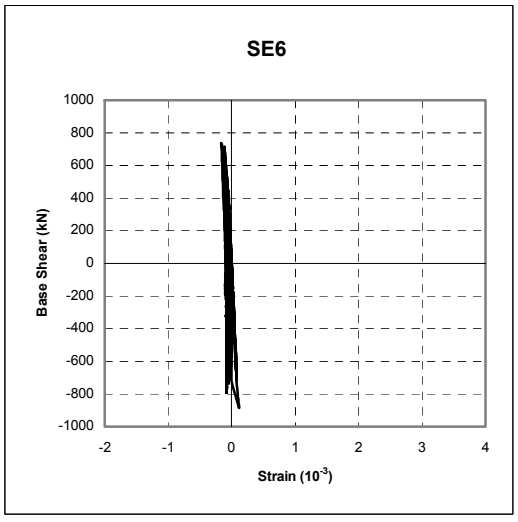

FIGURE E-1 Base Shear versus Outer Flange Strain Hystereses for CFSS Members (continued)

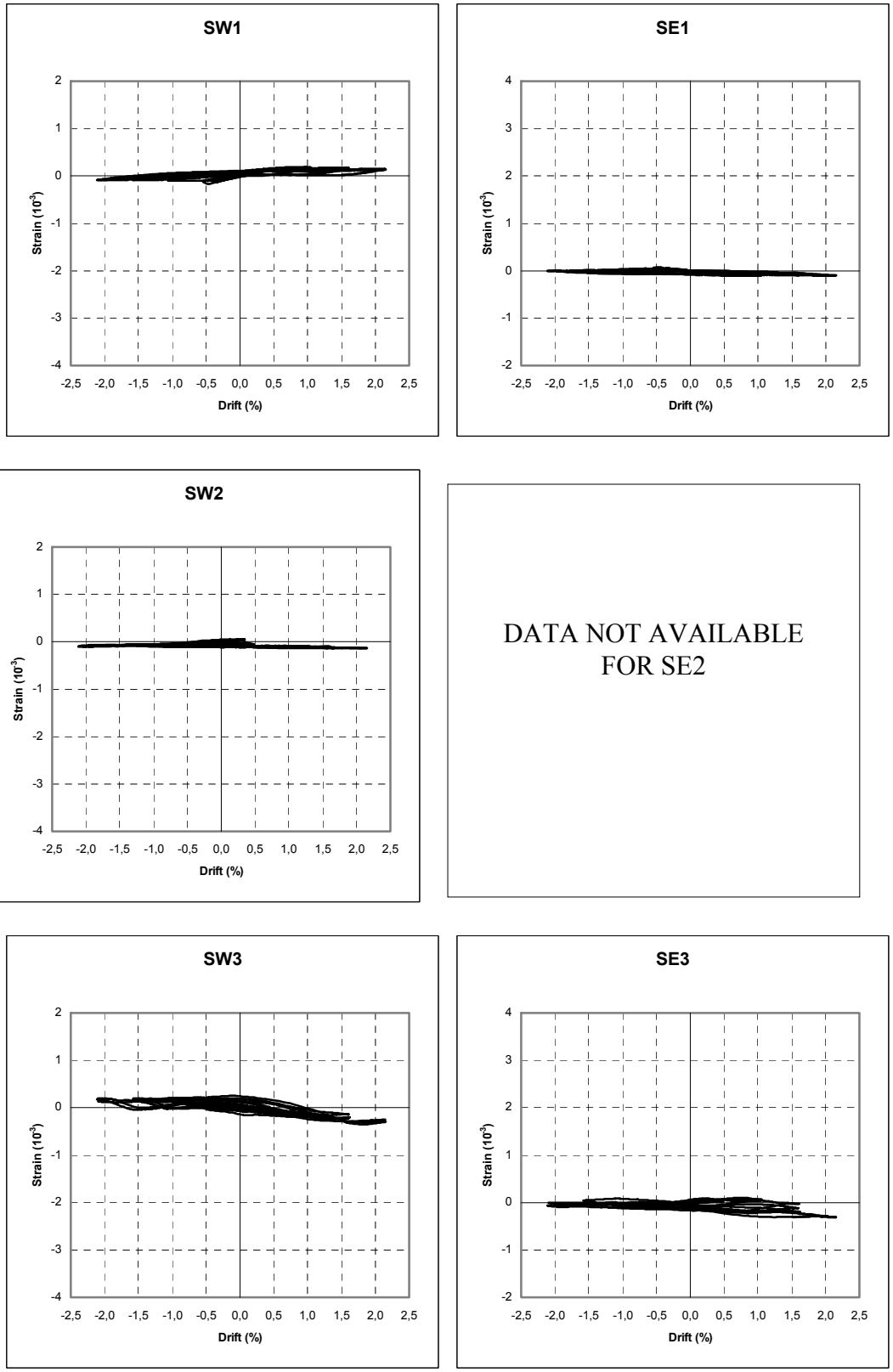

FIGURE E-2 Outer Flange Strain versus Drift Hystereses for CFSS Members

DATA NOT AVAILABLE
FOR SW4

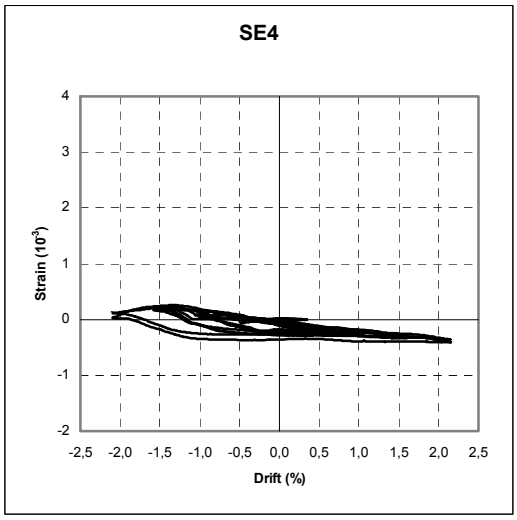

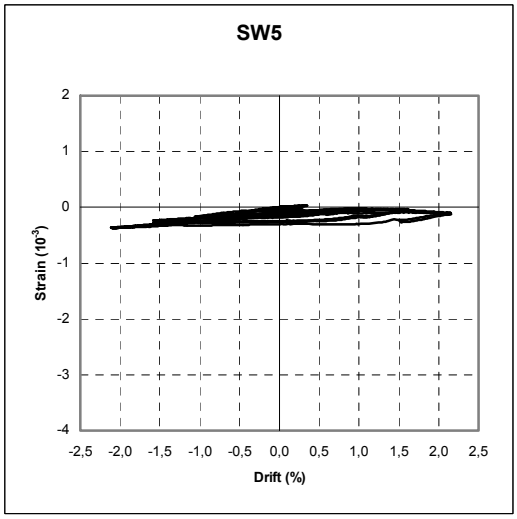

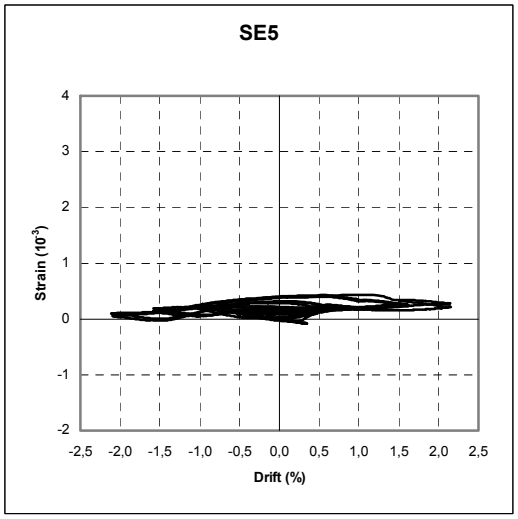

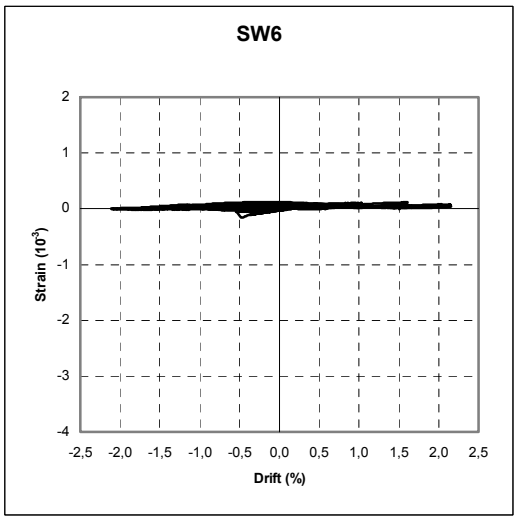

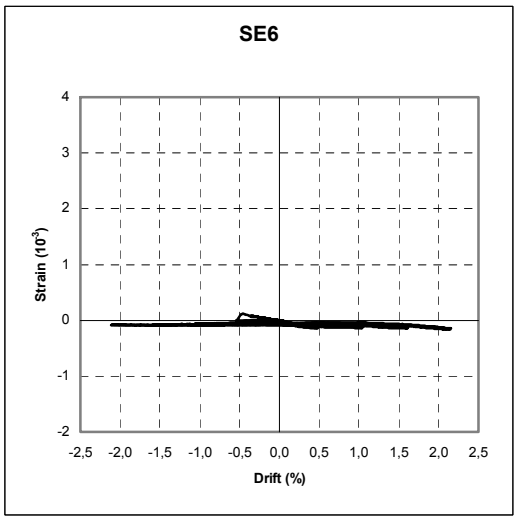

FIGURE E-2 Outer Flange Strain versus Drift Hystereses for CFSS Members (continued)

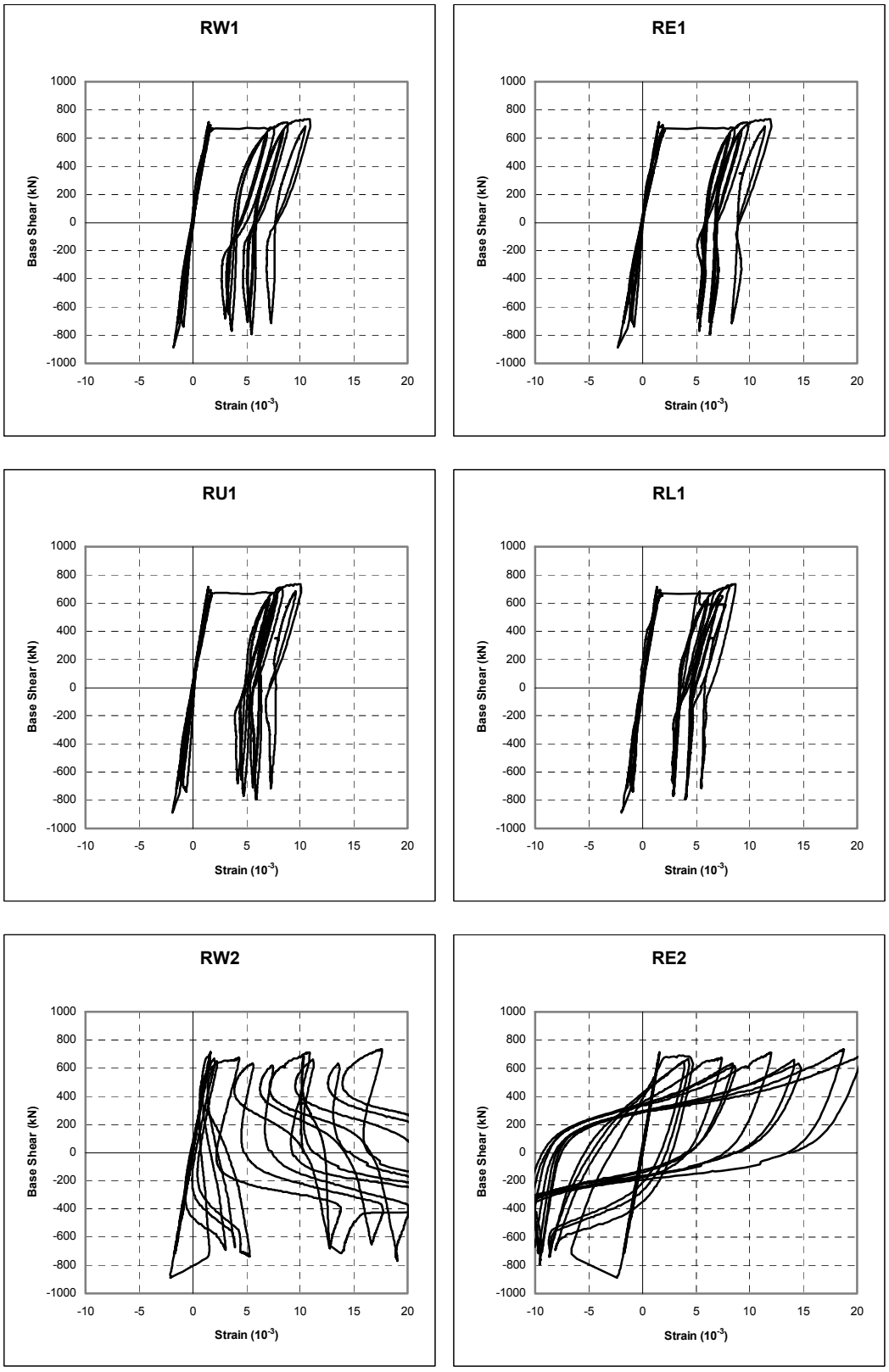

FIGURE E-3 Base Shear versus Bar Brace Axial Strain Hystereses

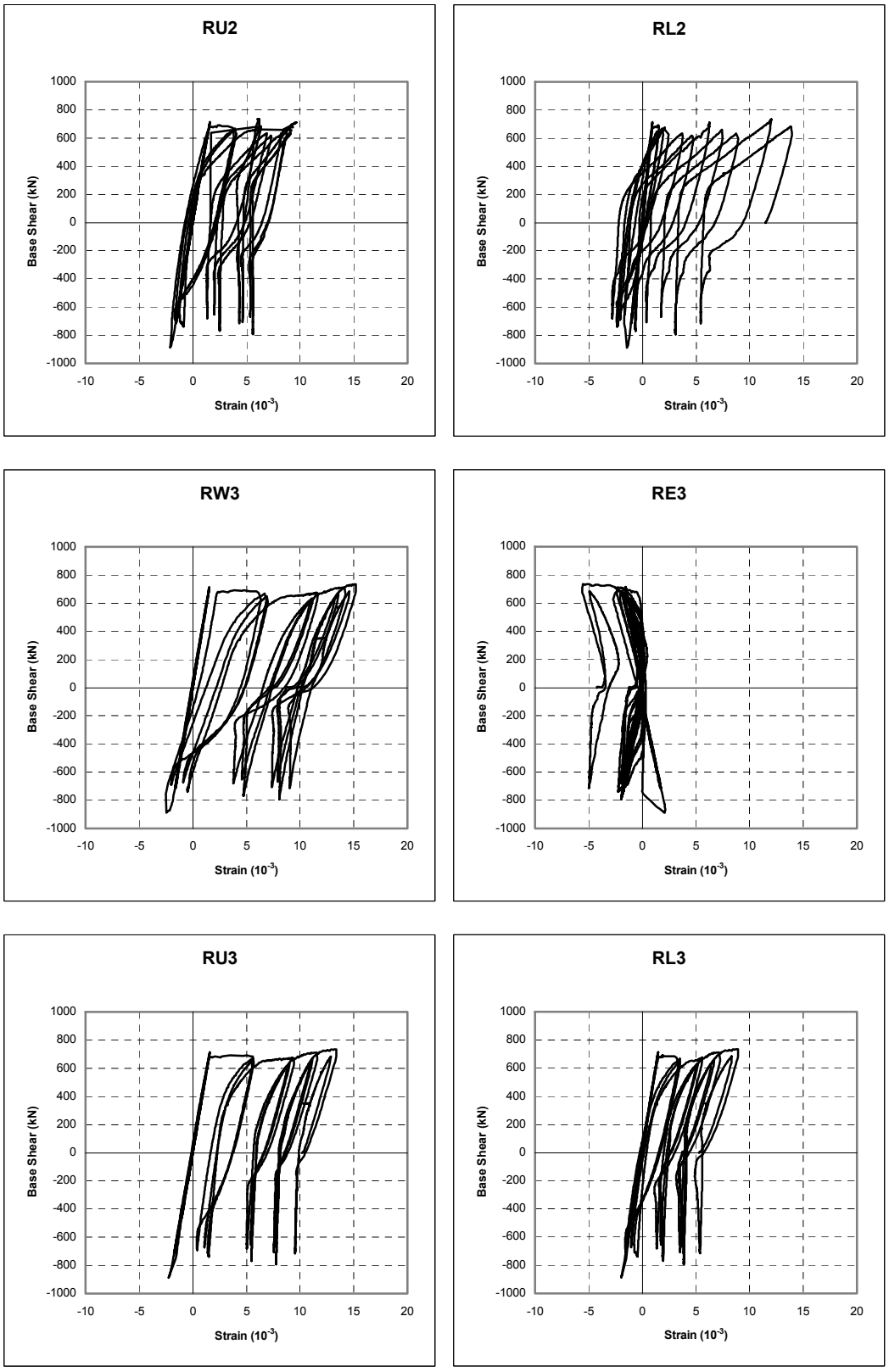

FIGURE E-3 Base Shear versus Bar Brace Axial Strain Hystereses (continued)

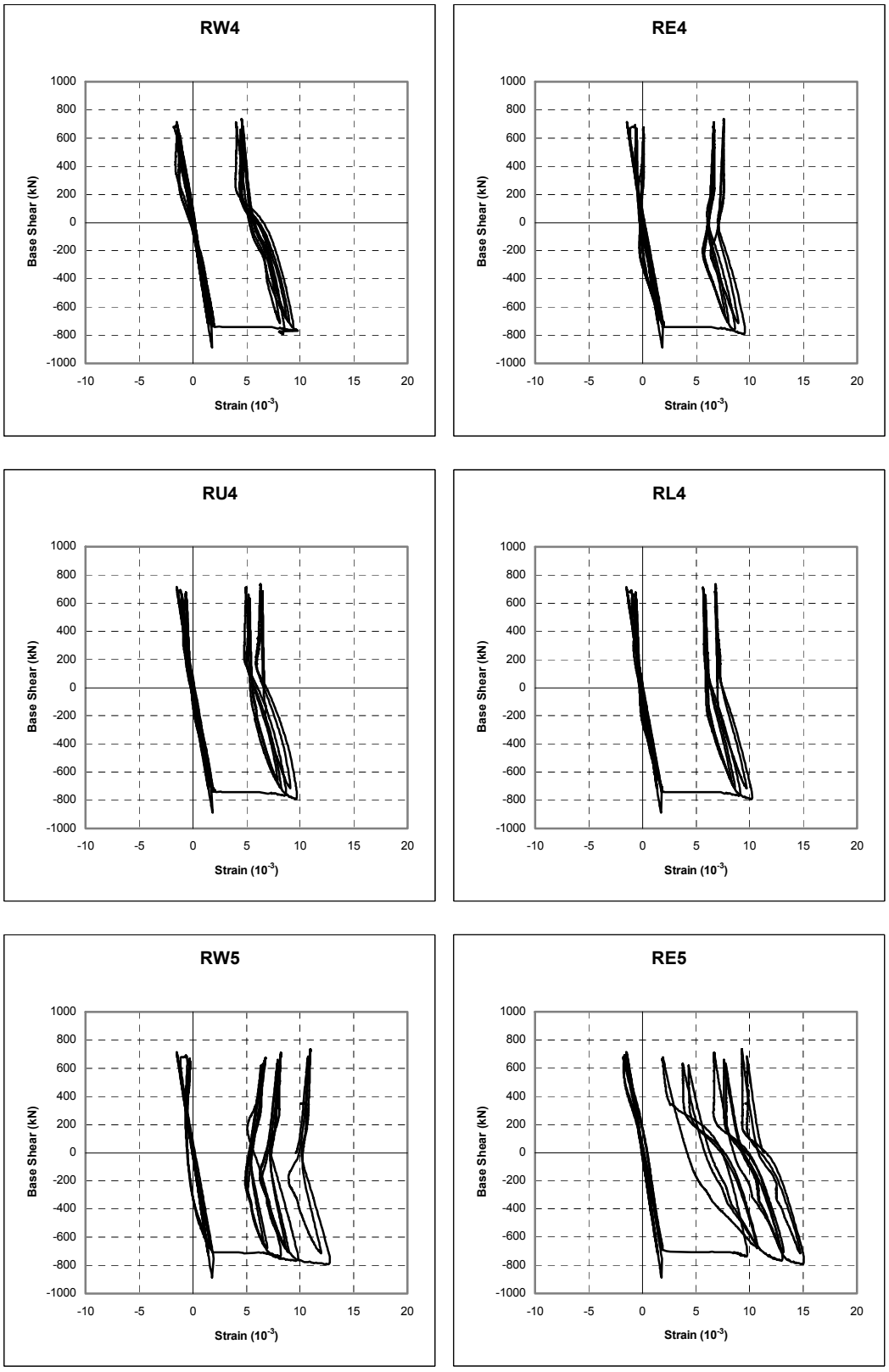

FIGURE E-3 Base Shear versus Bar Brace Axial Strain Hystereses (continued)

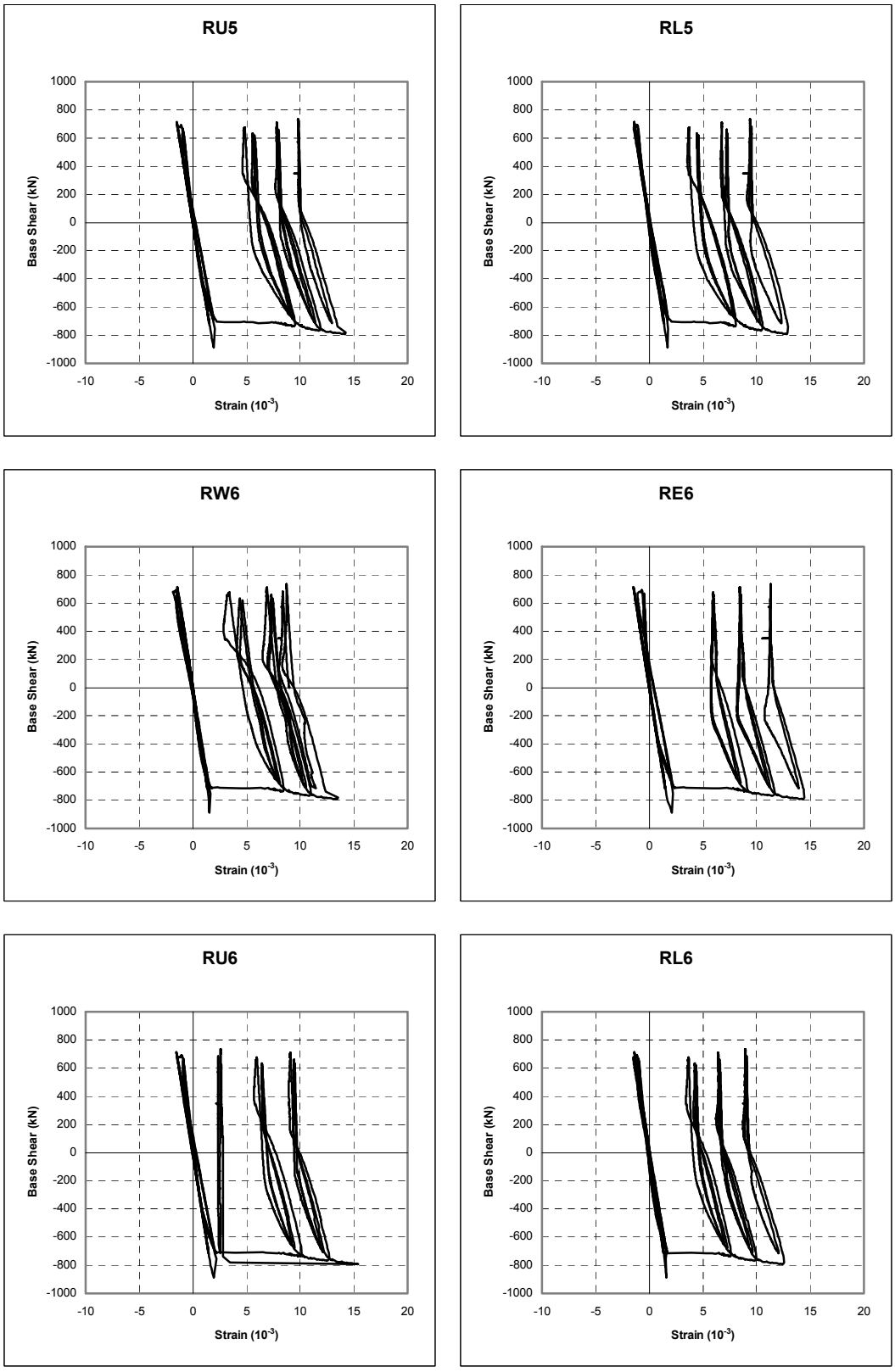

FIGURE E-3 Base Shear versus Bar Brace Axial Strain Hystereses (continued)

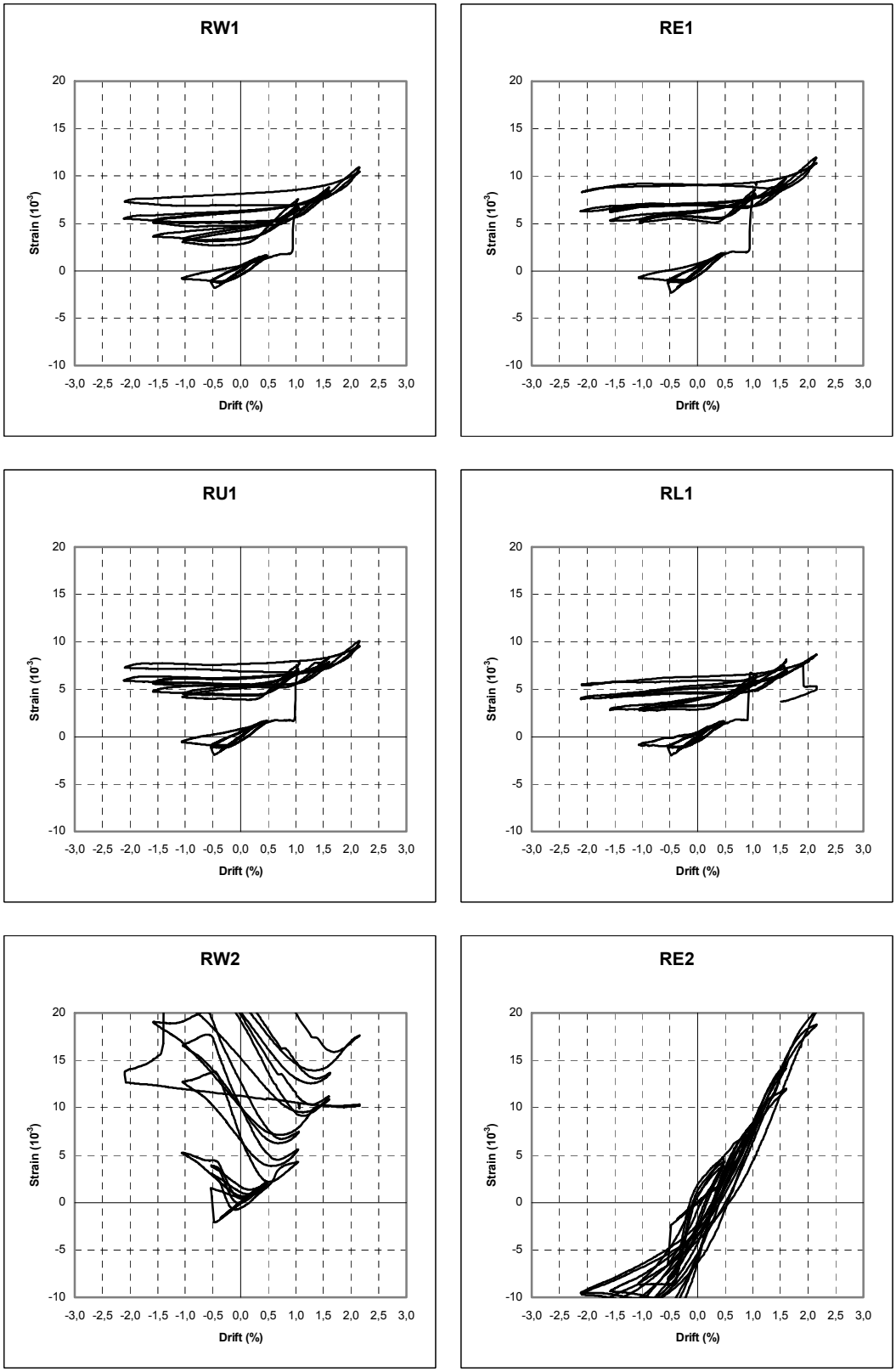

FIGURE E-4 Bar Brace Axial Strain versus Drift Hystereses

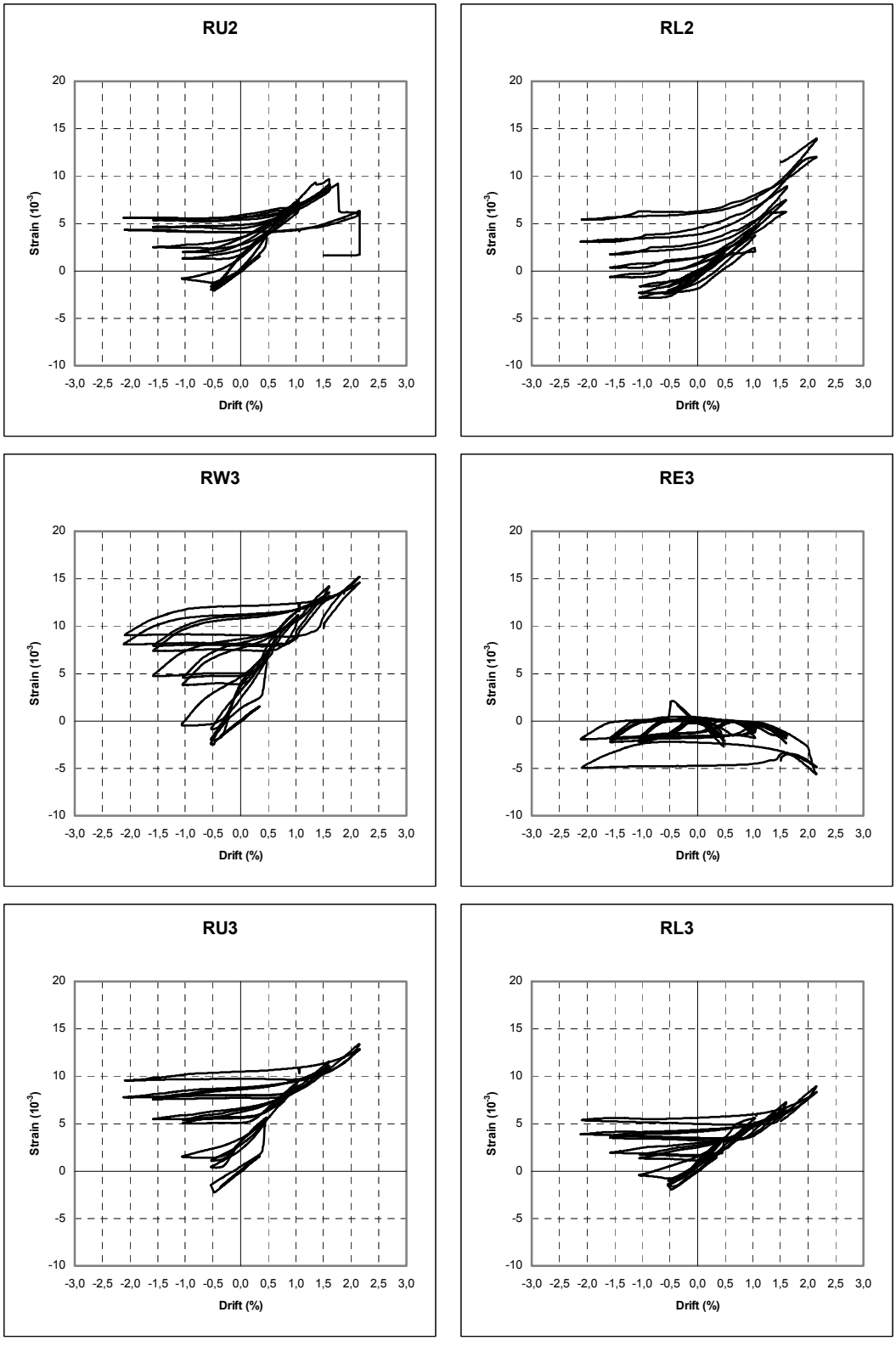

FIGURE E-4 Bar Brace Axial Strain versus Drift Hystereses (continued)

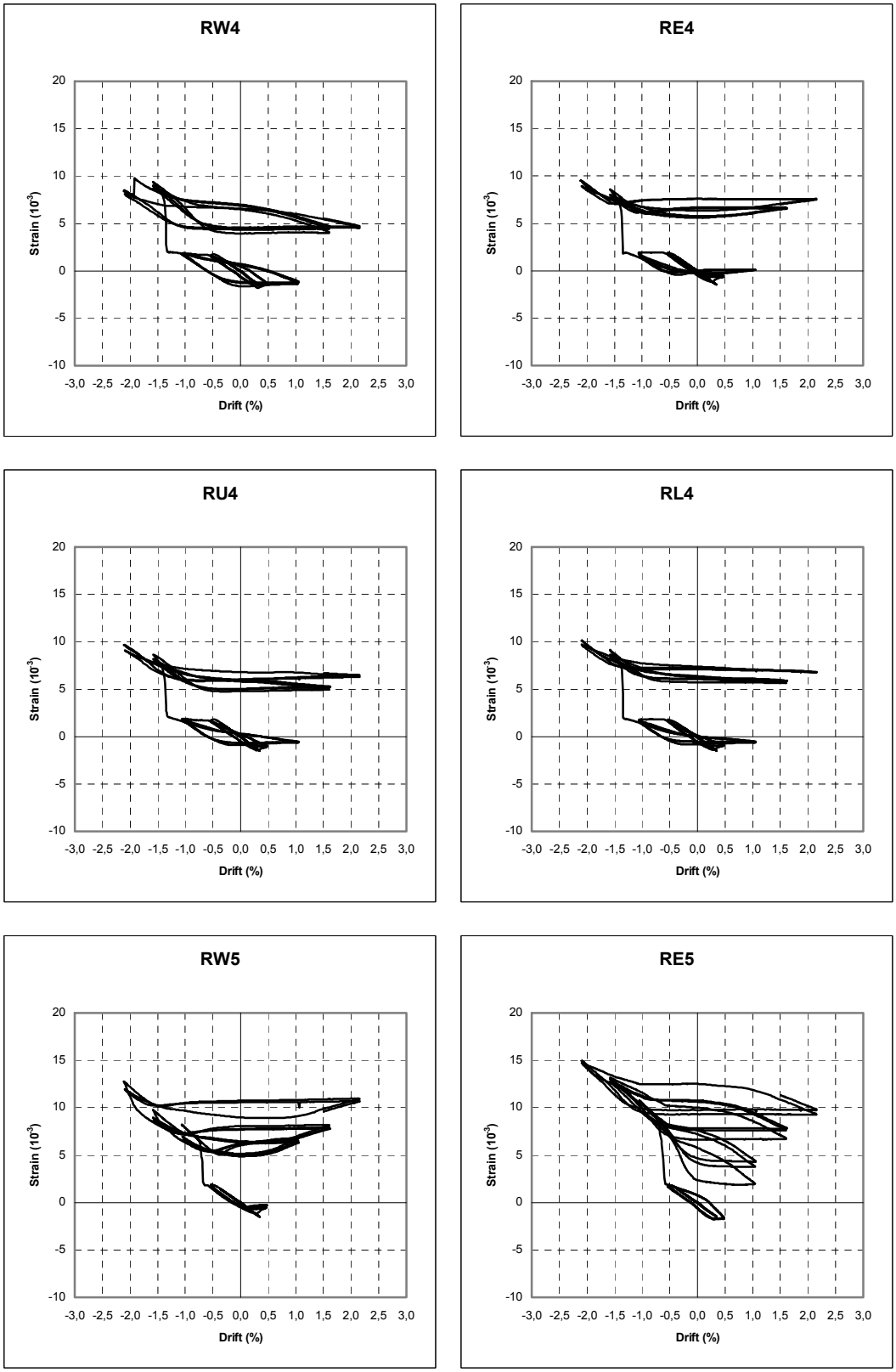

FIGURE E-4 Bar Brace Axial Strain versus Drift Hystereses (continued)

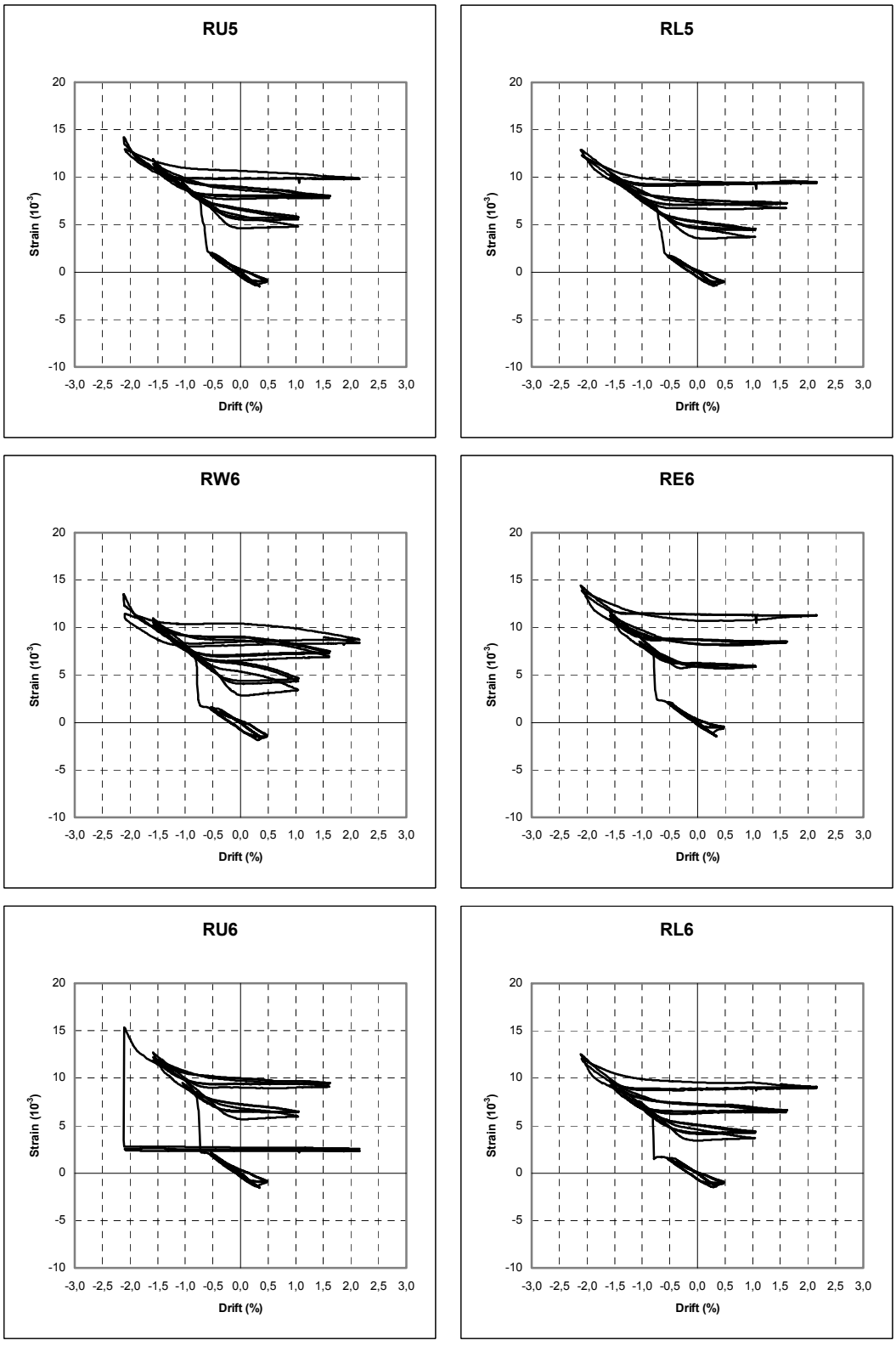

FIGURE E-4 Bar Brace Axial Strain versus Drift Hystereses (continued)

APPENDIX F
STRAIN GAUGE DATA FOR SPECIMEN F4

This appendix includes plots of the infill strain gauge data for the gauges attached on the bar braces. Strain gauge locations and labels are shown in Section 3, in Figure 3-29a. Both base shear versus axial strain and axial strain versus drift curves are provided for all cycles.

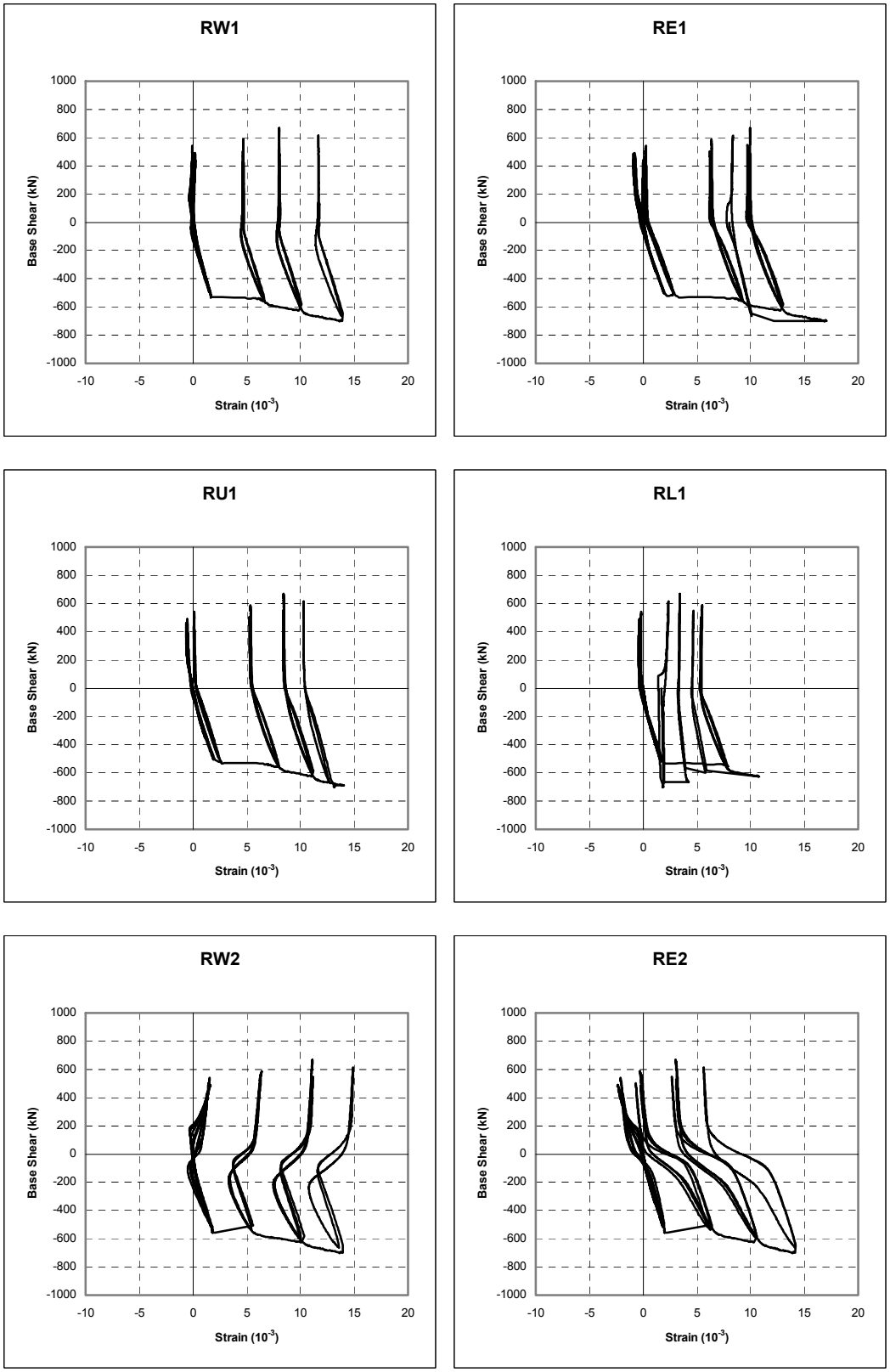

FIGURE F-1 Base Shear versus Bar Brace Axial Strain Hystereses

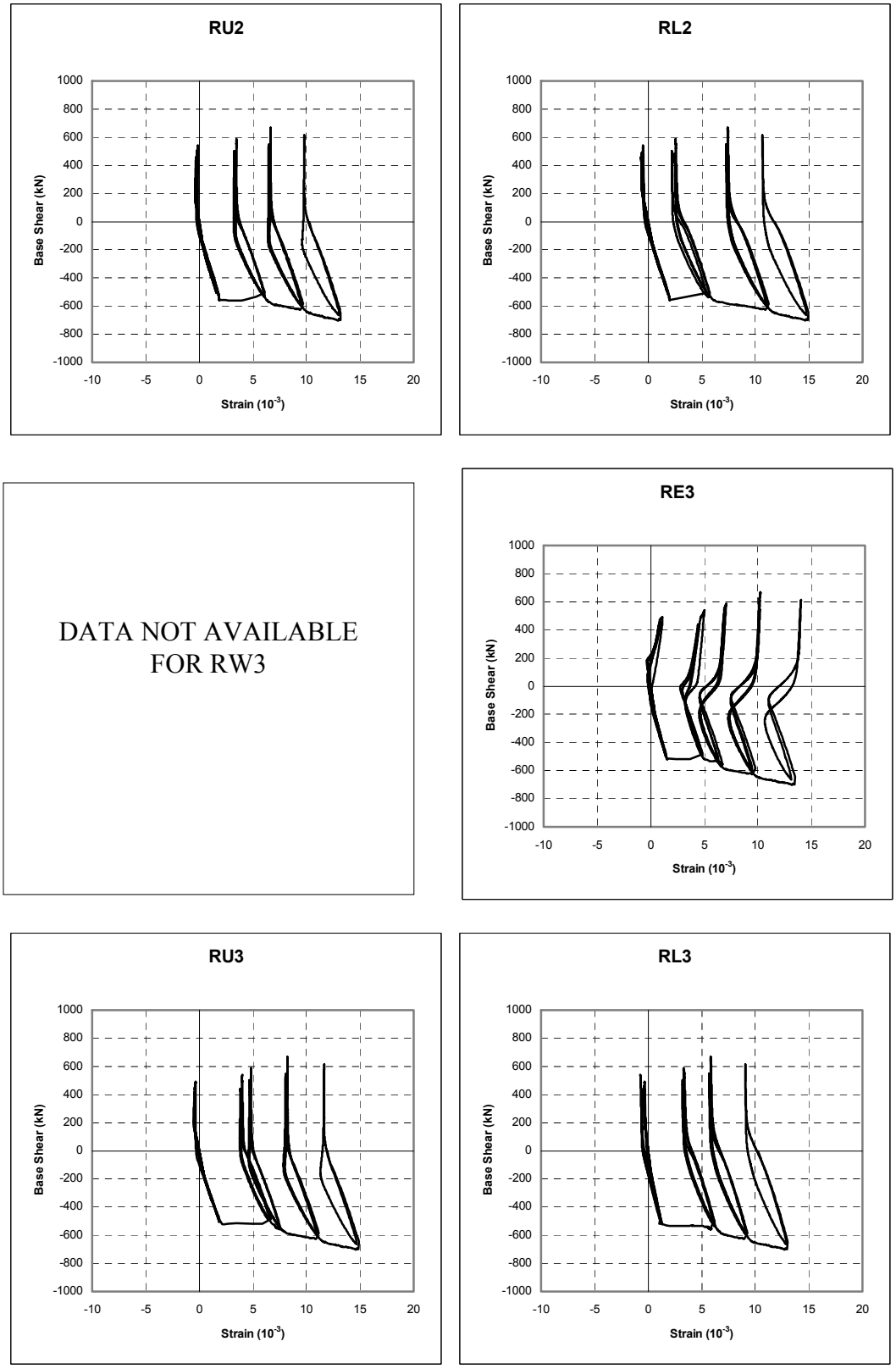

FIGURE F-1 Base Shear versus Bar Brace Axial Strain Hystereses (continued)

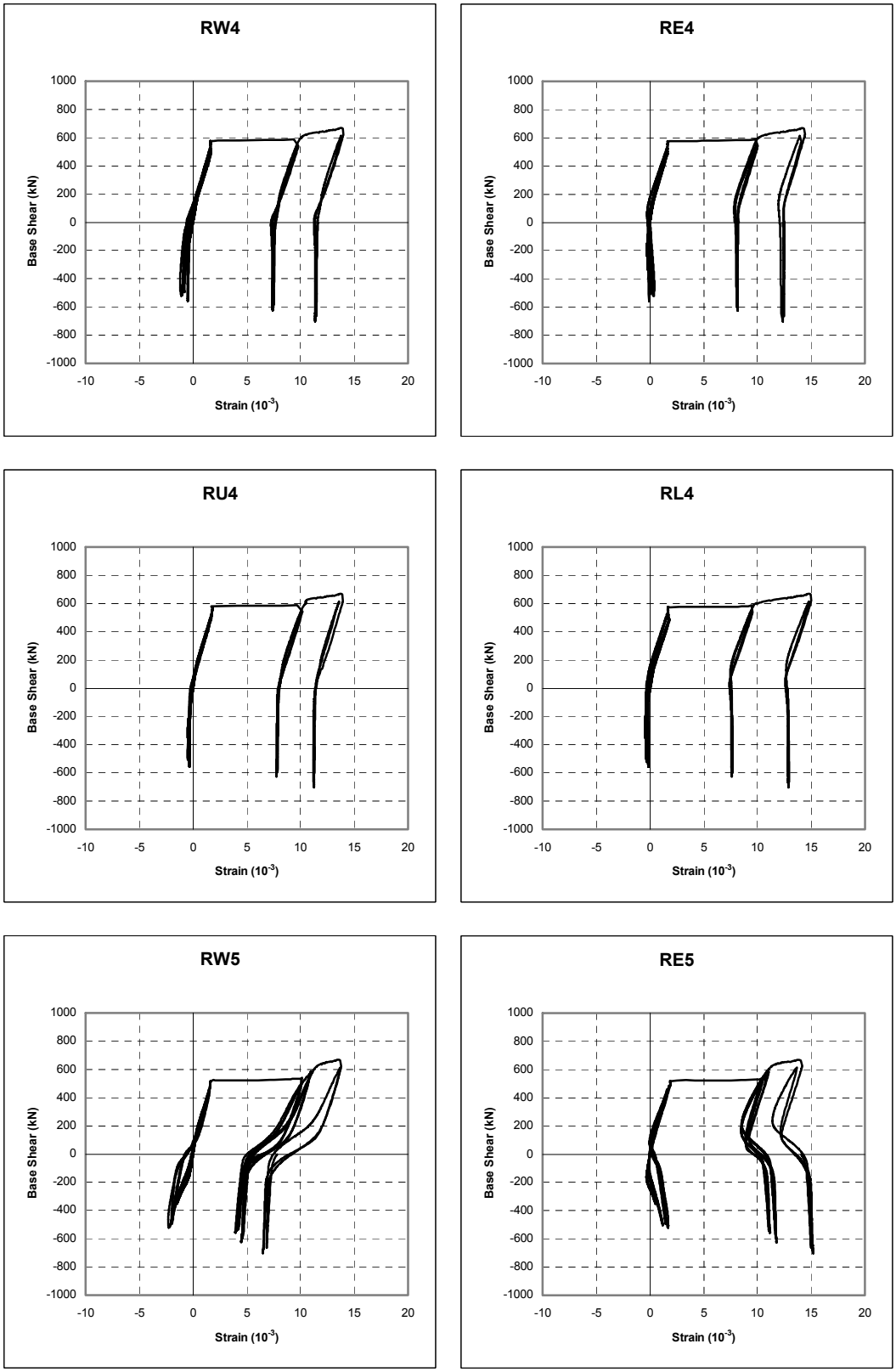

FIGURE F-1 Base Shear versus Bar Brace Axial Strain Hystereses (continued)

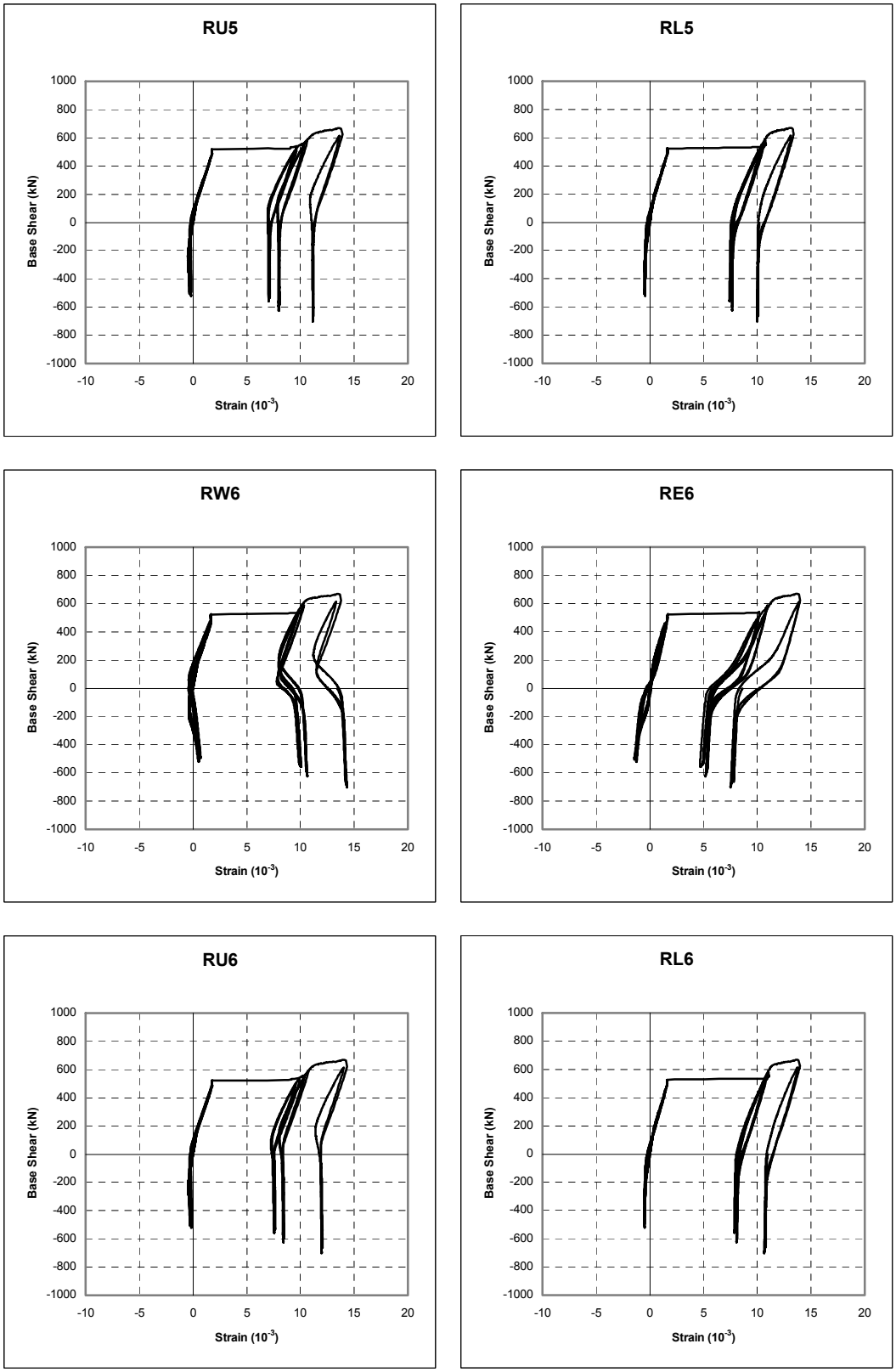

FIGURE F-1 Base Shear versus Bar Brace Axial Strain Hystereses (continued)

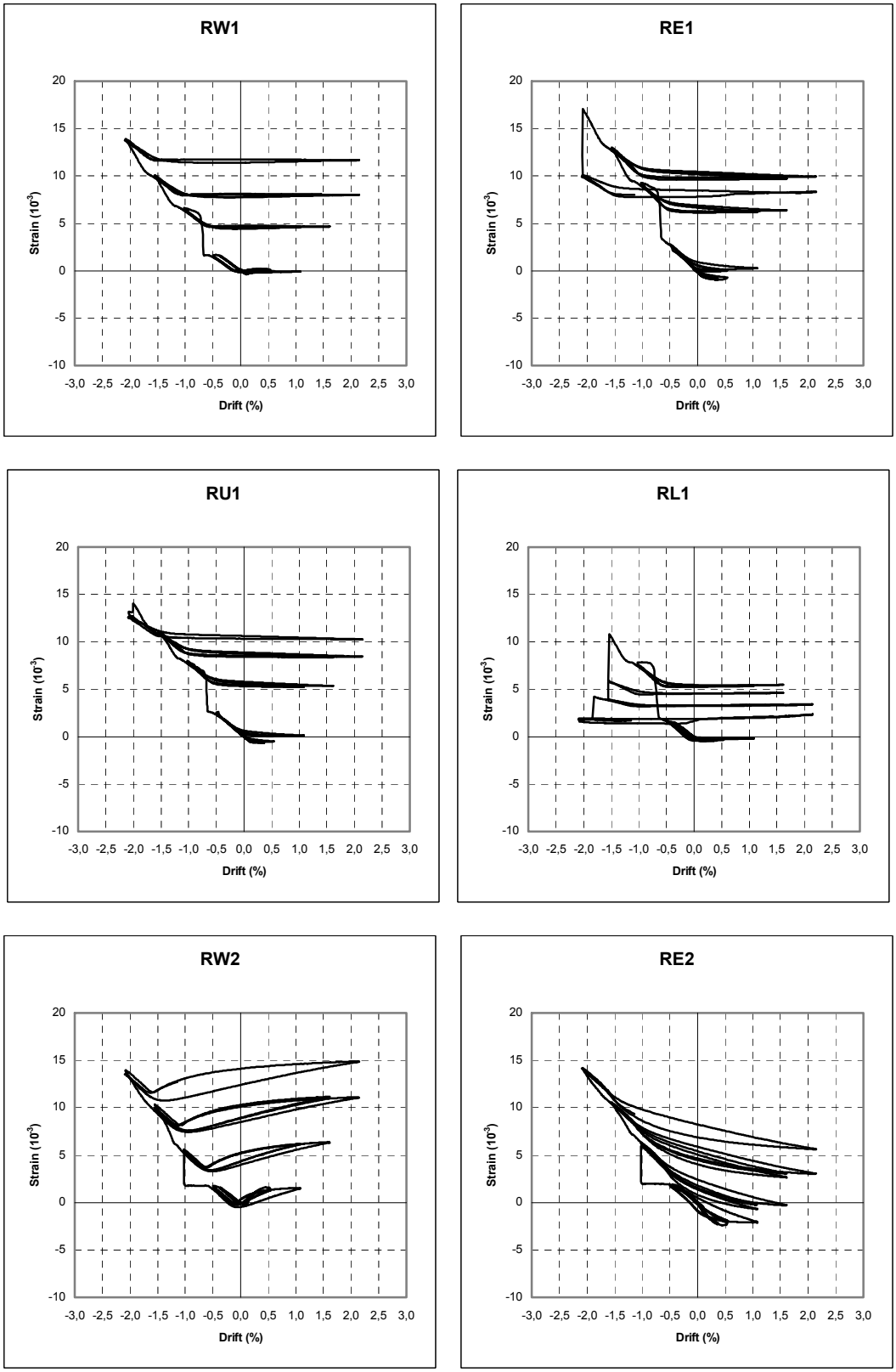

FIGURE F-2 Bar Brace Axial Strain versus Drift Hystereses

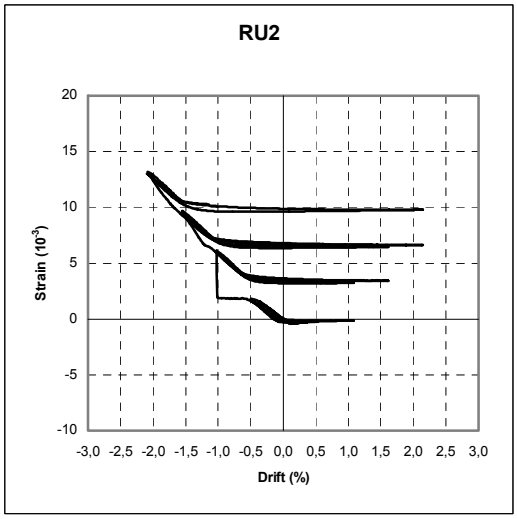

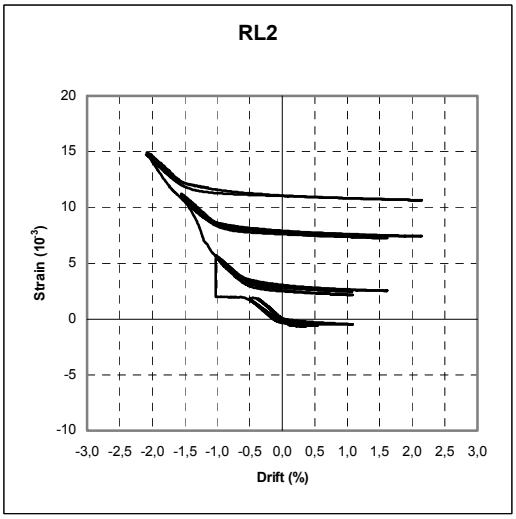

DATA NOT AVAILABLE
FOR RW3

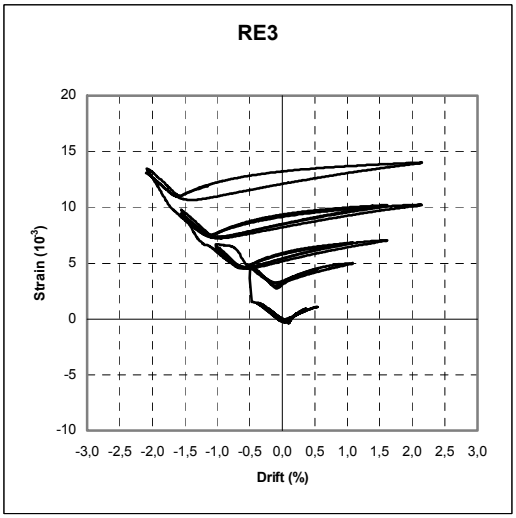

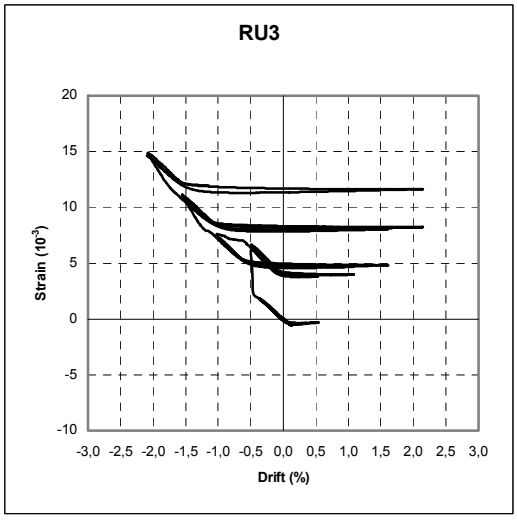

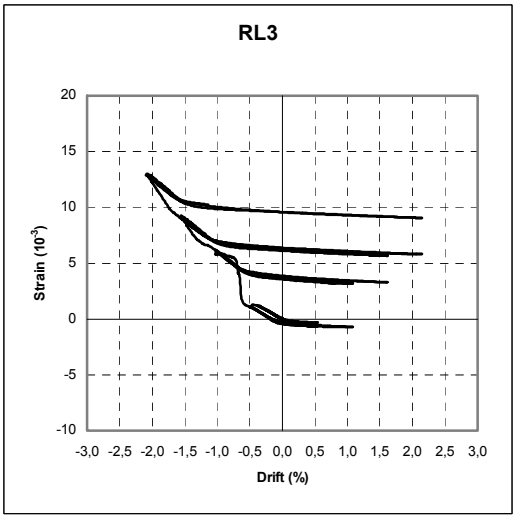

FIGURE F-2 Bar Brace Axial Strain versus Drift Hystereses (continued)

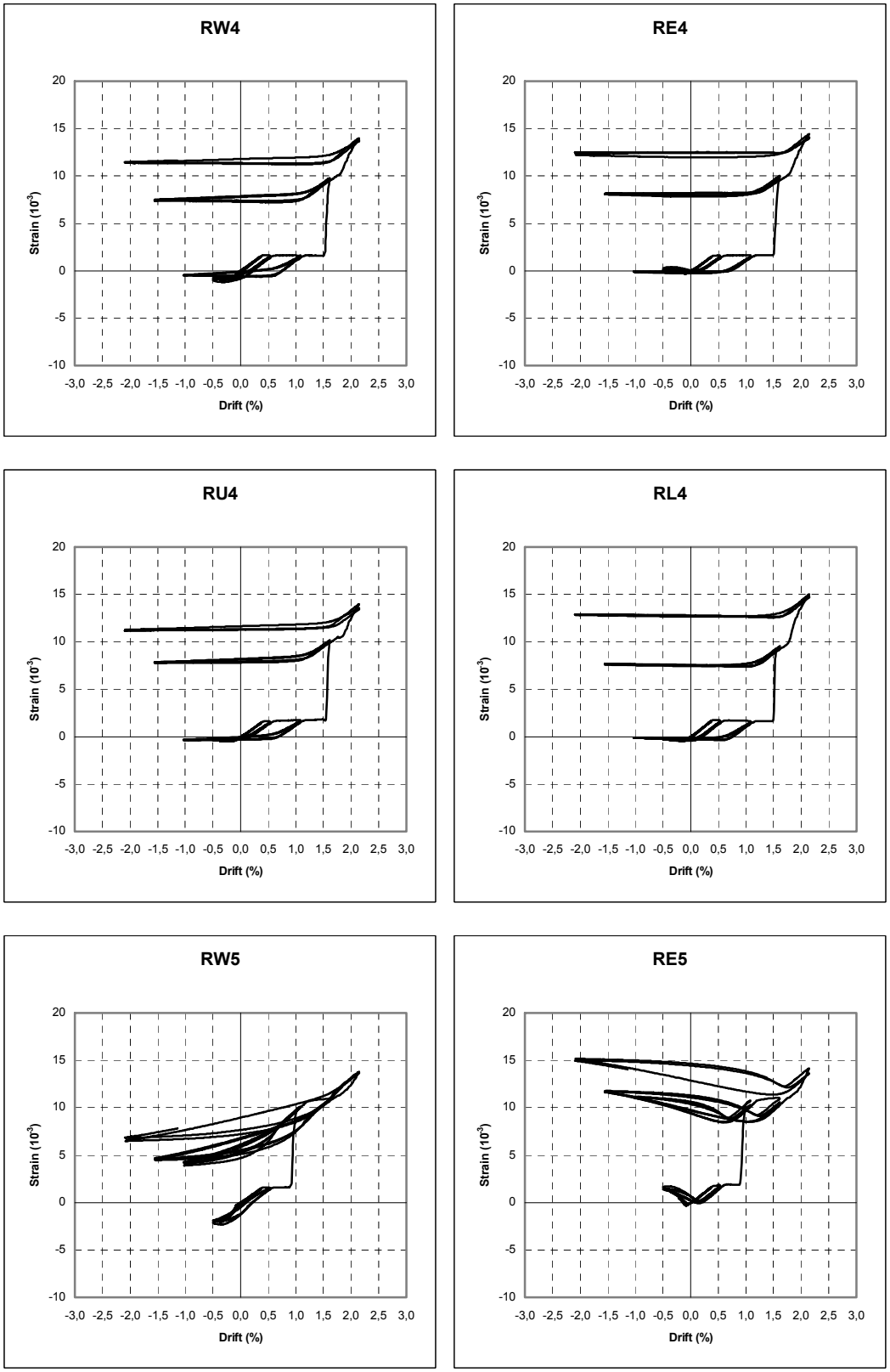

FIGURE F-2 Bar Brace Axial Strain versus Drift Hystereses (continued)

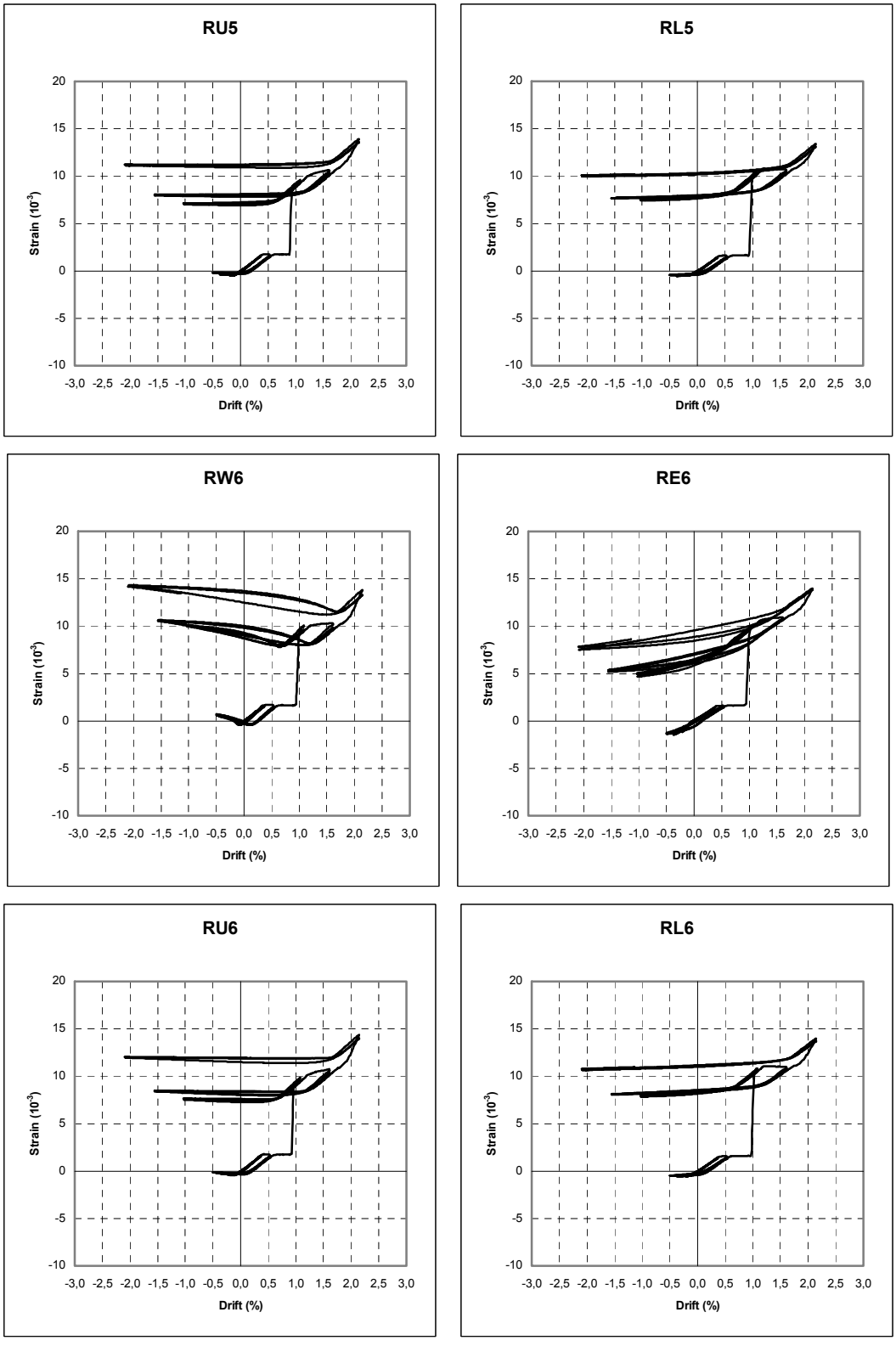

FIGURE F-2 Bar Brace Axial Strain versus Drift Hystereses (continued)

Multidisciplinary Center for Earthquake Engineering Research
List of Technical Reports

The Multidisciplinary Center for Earthquake Engineering Research (MCEER) publishes technical reports on a variety of subjects related to earthquake engineering written by authors funded through MCEER. These reports are available from both MCEER Publications and the National Technical Information Service (NTIS). Requests for reports should be directed to MCEER Publications, Multidisciplinary Center for Earthquake Engineering Research, State University of New York at Buffalo, Red Jacket Quadrangle, Buffalo, New York 14261. Reports can also be requested through NTIS, 5285 Port Royal Road, Springfield, Virginia 22161. NTIS accession numbers are shown in parenthesis, if available.

NCEER-87-0001 "First-Year Program in Research, Education and Technology Transfer," 3/5/87, (PB88-134275, A04, MF-A01).

NCEER-87-0002 "Experimental Evaluation of Instantaneous Optimal Algorithms for Structural Control," by R.C. Lin, T.T. Soong and A.M. Reinhorn, 4/20/87, (PB88-134341, A04, MF-A01).

NCEER-87-0003 "Experimentation Using the Earthquake Simulation Facilities at University at Buffalo," by A.M. Reinhorn and R.L. Ketter, to be published.

NCEER-87-0004 "The System Characteristics and Performance of a Shaking Table," by J.S. Hwang, K.C. Chang and G.C. Lee, 6/1/87, (PB88-134259, A03, MF-A01). This report is available only through NTIS (see address given above).

NCEER-87-0005 "A Finite Element Formulation for Nonlinear Viscoplastic Material Using a Q Model," by O. Gyebi and G. Dasgupta, 11/2/87, (PB88-213764, A08, MF-A01).

NCEER-87-0006 "Symbolic Manipulation Program (SMP) - Algebraic Codes for Two and Three Dimensional Finite Element Formulations," by X. Lee and G. Dasgupta, 11/9/87, (PB88-218522, A05, MF-A01).

NCEER-87-0007 "Instantaneous Optimal Control Laws for Tall Buildings Under Seismic Excitations," by J.N. Yang, A. Akbarpour and P. Ghaemmaghami, 6/10/87, (PB88-134333, A06, MF-A01). This report is only available through NTIS (see address given above).

NCEER-87-0008 "IDARC: Inelastic Damage Analysis of Reinforced Concrete Frame - Shear-Wall Structures," by Y.J. Park, A.M. Reinhorn and S.K. Kunnath, 7/20/87, (PB88-134325, A09, MF-A01). This report is only available through NTIS (see address given above).

NCEER-87-0009 "Liquefaction Potential for New York State: A Preliminary Report on Sites in Manhattan and Buffalo," by M. Budhu, V. Vijayakumar, R.F. Giese and L. Baumgras, 8/31/87, (PB88-163704, A03, MF-A01). This report is available only through NTIS (see address given above).

NCEER-87-0010 "Vertical and Torsional Vibration of Foundations in Inhomogeneous Media," by A.S. Veletsos and K.W. Dotson, 6/1/87, (PB88-134291, A03, MF-A01). This report is only available through NTIS (see address given above).

NCEER-87-0011 "Seismic Probabilistic Risk Assessment and Seismic Margins Studies for Nuclear Power Plants," by Howard H.M. Hwang, 6/15/87, (PB88-134267, A03, MF-A01). This report is only available through NTIS (see address given above).

NCEER-87-0012 "Parametric Studies of Frequency Response of Secondary Systems Under Ground-Acceleration Excitations," by Y. Yong and Y.K. Lin, 6/10/87, (PB88-134309, A03, MF-A01). This report is only available through NTIS (see address given above).

NCEER-87-0013 "Frequency Response of Secondary Systems Under Seismic Excitation," by J.A. HoLung, J. Cai and Y.K. Lin, 7/31/87, (PB88-134317, A05, MF-A01). This report is only available through NTIS (see address given above).

NCEER-87-0014 "Modelling Earthquake Ground Motions in Seismically Active Regions Using Parametric Time Series Methods," by G.W. Ellis and A.S. Cakmak, 8/25/87, (PB88-134283, A08, MF-A01). This report is only available through NTIS (see address given above).

NCEER-87-0015 "Detection and Assessment of Seismic Structural Damage," by E. DiPasquale and A.S. Cakmak, 8/25/87, (PB88-163712, A05, MF-A01). This report is only available through NTIS (see address given above).

NCEER-87-0016 "Pipeline Experiment at Parkfield, California," by J. Isenberg and E. Richardson, 9/15/87, (PB88-163720, A03, MF-A01). This report is available only through NTIS (see address given above).

NCEER-87-0017 "Digital Simulation of Seismic Ground Motion," by M. Shinozuka, G. Deodatis and T. Harada, 8/31/87, (PB88-155197, A04, MF-A01). This report is available only through NTIS (see address given above).

NCEER-87-0018 "Practical Considerations for Structural Control: System Uncertainty, System Time Delay and Truncation of Small Control Forces," J.N. Yang and A. Akbarpour, 8/10/87, (PB88-163738, A08, MF-A01). This report is only available through NTIS (see address given above).

NCEER-87-0019 "Modal Analysis of Nonclassically Damped Structural Systems Using Canonical Transformation," by J.N. Yang, S. Sarkani and F.X. Long, 9/27/87, (PB88-187851, A04, MF-A01).

NCEER-87-0020 "A Nonstationary Solution in Random Vibration Theory," by J.R. Red-Horse and P.D. Spanos, 11/3/87, (PB88-163746, A03, MF-A01).

NCEER-87-0021 "Horizontal Impedances for Radially Inhomogeneous Viscoelastic Soil Layers," by A.S. Veletsos and K.W. Dotson, 10/15/87, (PB88-150859, A04, MF-A01).

NCEER-87-0022 "Seismic Damage Assessment of Reinforced Concrete Members," by Y.S. Chung, C. Meyer and M. Shinozuka, 10/9/87, (PB88-150867, A05, MF-A01). This report is available only through NTIS (see address given above).

NCEER-87-0023 "Active Structural Control in Civil Engineering," by T.T. Soong, 11/11/87, (PB88-187778, A03, MF-A01).

NCEER-87-0024 "Vertical and Torsional Impedances for Radially Inhomogeneous Viscoelastic Soil Layers," by K.W. Dotson and A.S. Veletsos, 12/87, (PB88-187786, A03, MF-A01).

NCEER-87-0025 "Proceedings from the Symposium on Seismic Hazards, Ground Motions, Soil-Liquefaction and Engineering Practice in Eastern North America," October 20-22, 1987, edited by K.H. Jacob, 12/87, (PB88-188115, A23, MF-A01). This report is available only through NTIS (see address given above).

NCEER-87-0026 "Report on the Whittier-Narrows, California, Earthquake of October 1, 1987," by J. Pantelic and A. Reinhorn, 11/87, (PB88-187752, A03, MF-A01). This report is available only through NTIS (see address given above).

NCEER-87-0027 "Design of a Modular Program for Transient Nonlinear Analysis of Large 3-D Building Structures," by S. Srivastav and J.F. Abel, 12/30/87, (PB88-187950, A05, MF-A01). This report is only available through NTIS (see address given above).

NCEER-87-0028 "Second-Year Program in Research, Education and Technology Transfer," 3/8/88, (PB88-219480, A04, MF-A01).

NCEER-88-0001 "Workshop on Seismic Computer Analysis and Design of Buildings With Interactive Graphics," by W. McGuire, J.F. Abel and C.H. Conley, 1/18/88, (PB88-187760, A03, MF-A01). This report is only available through NTIS (see address given above).

NCEER-88-0002 "Optimal Control of Nonlinear Flexible Structures," by J.N. Yang, F.X. Long and D. Wong, 1/22/88, (PB88-213772, A06, MF-A01).

NCEER-88-0003 "Substructuring Techniques in the Time Domain for Primary-Secondary Structural Systems," by G.D. Manolis and G. Juhn, 2/10/88, (PB88-213780, A04, MF-A01).

NCEER-88-0004 "Iterative Seismic Analysis of Primary-Secondary Systems," by A. Singhal, L.D. Lutes and P.D. Spanos, 2/23/88, (PB88-213798, A04, MF-A01).

NCEER-88-0005 "Stochastic Finite Element Expansion for Random Media," by P.D. Spanos and R. Ghanem, 3/14/88, (PB88-213806, A03, MF-A01).

NCEER-88-0006 "Combining Structural Optimization and Structural Control," by F.Y. Cheng and C.P. Pantelides, 1/10/88, (PB88-213814, A05, MF-A01).

NCEER-88-0007 "Seismic Performance Assessment of Code-Designed Structures," by H.H-M. Hwang, J-W. Jaw and H-J. Shau, 3/20/88, (PB88-219423, A04, MF-A01). This report is only available through NTIS (see address given above).

NCEER-88-0008 "Reliability Analysis of Code-Designed Structures Under Natural Hazards," by H.H-M. Hwang, H. Ushiba and M. Shinozuka, 2/29/88, (PB88-229471, A07, MF-A01). This report is only available through NTIS (see address given above).

NCEER-88-0009 "Seismic Fragility Analysis of Shear Wall Structures," by J-W Jaw and H.H-M. Hwang, 4/30/88, (PB89-102867, A04, MF-A01).

NCEER-88-0010 "Base Isolation of a Multi-Story Building Under a Harmonic Ground Motion - A Comparison of Performances of Various Systems," by F-G Fan, G. Ahmadi and I.G. Tadjbakhsh, 5/18/88, (PB89-122238, A06, MF-A01). This report is only available through NTIS (see address given above).

NCEER-88-0011 "Seismic Floor Response Spectra for a Combined System by Green's Functions," by F.M. Lavelle, L.A. Bergman and P.D. Spanos, 5/1/88, (PB89-102875, A03, MF-A01).

NCEER-88-0012 "A New Solution Technique for Randomly Excited Hysteretic Structures," by G.Q. Cai and Y.K. Lin, 5/16/88, (PB89-102883, A03, MF-A01).

NCEER-88-0013 "A Study of Radiation Damping and Soil-Structure Interaction Effects in the Centrifuge," by K. Weissman, supervised by J.H. Prevost, 5/24/88, (PB89-144703, A06, MF-A01).

NCEER-88-0014 "Parameter Identification and Implementation of a Kinematic Plasticity Model for Frictional Soils," by J.H. Prevost and D.V. Griffiths, to be published.

NCEER-88-0015 "Two- and Three- Dimensional Dynamic Finite Element Analyses of the Long Valley Dam," by D.V. Griffiths and J.H. Prevost, 6/17/88, (PB89-144711, A04, MF-A01).

NCEER-88-0016 "Damage Assessment of Reinforced Concrete Structures in Eastern United States," by A.M. Reinhorn, M.J. Seidel, S.K. Kunnath and Y.J. Park, 6/15/88, (PB89-122220, A04, MF-A01). This report is only available through NTIS (see address given above).

NCEER-88-0017 "Dynamic Compliance of Vertically Loaded Strip Foundations in Multilayered Viscoelastic Soils," by S. Ahmad and A.S.M. Israil, 6/17/88, (PB89-102891, A04, MF-A01).

NCEER-88-0018 "An Experimental Study of Seismic Structural Response With Added Viscoelastic Dampers," by R.C. Lin, Z. Liang, T.T. Soong and R.H. Zhang, 6/30/88, (PB89-122212, A05, MF-A01). This report is available only through NTIS (see address given above).

NCEER-88-0019 "Experimental Investigation of Primary - Secondary System Interaction," by G.D. Manolis, G. Juhn and A.M. Reinhorn, 5/27/88, (PB89-122204, A04, MF-A01).

NCEER-88-0020 "A Response Spectrum Approach For Analysis of Nonclassically Damped Structures," by J.N. Yang, S. Sarkani and F.X. Long, 4/22/88, (PB89-102909, A04, MF-A01).

NCEER-88-0021 "Seismic Interaction of Structures and Soils: Stochastic Approach," by A.S. Veletsos and A.M. Prasad, 7/21/88, (PB89-122196, A04, MF-A01). This report is only available through NTIS (see address given above).

NCEER-88-0022 "Identification of the Serviceability Limit State and Detection of Seismic Structural Damage," by E. DiPasquale and A.S. Cakmak, 6/15/88, (PB89-122188, A05, MF-A01). This report is available only through NTIS (see address given above).

NCEER-88-0023 "Multi-Hazard Risk Analysis: Case of a Simple Offshore Structure," by B.K. Bhartia and E.H. Vanmarcke, 7/21/88, (PB89-145213, A05, MF-A01).

NCEER-88-0024 "Automated Seismic Design of Reinforced Concrete Buildings," by Y.S. Chung, C. Meyer and M. Shinozuka, 7/5/88, (PB89-122170, A06, MF-A01). This report is available only through NTIS (see address given above).

NCEER-88-0025 "Experimental Study of Active Control of MDOF Structures Under Seismic Excitations," by L.L. Chung, R.C. Lin, T.T. Soong and A.M. Reinhorn, 7/10/88, (PB89-122600, A04, MF-A01).

NCEER-88-0026 "Earthquake Simulation Tests of a Low-Rise Metal Structure," by J.S. Hwang, K.C. Chang, G.C. Lee and R.L. Ketter, 8/1/88, (PB89-102917, A04, MF-A01).

NCEER-88-0027 "Systems Study of Urban Response and Reconstruction Due to Catastrophic Earthquakes," by F. Kozin and H.K. Zhou, 9/22/88, (PB90-162348, A04, MF-A01).

NCEER-88-0028 "Seismic Fragility Analysis of Plane Frame Structures," by H.H-M. Hwang and Y.K. Low, 7/31/88, (PB89-131445, A06, MF-A01).

NCEER-88-0029 "Response Analysis of Stochastic Structures," by A. Kardara, C. Bucher and M. Shinozuka, 9/22/88, (PB89-174429, A04, MF-A01).

NCEER-88-0030 "Nonnormal Accelerations Due to Yielding in a Primary Structure," by D.C.K. Chen and L.D. Lutes, 9/19/88, (PB89-131437, A04, MF-A01).

NCEER-88-0031 "Design Approaches for Soil-Structure Interaction," by A.S. Veletsos, A.M. Prasad and Y. Tang, 12/30/88, (PB89-174437, A03, MF-A01). This report is available only through NTIS (see address given above).

NCEER-88-0032 "A Re-evaluation of Design Spectra for Seismic Damage Control," by C.J. Turkstra and A.G. Tallin, 11/7/88, (PB89-145221, A05, MF-A01).

NCEER-88-0033 "The Behavior and Design of Noncontact Lap Splices Subjected to Repeated Inelastic Tensile Loading," by V.E. Sagan, P. Gergely and R.N. White, 12/8/88, (PB89-163737, A08, MF-A01).

NCEER-88-0034 "Seismic Response of Pile Foundations," by S.M. Mamoon, P.K. Banerjee and S. Ahmad, 11/1/88, (PB89-145239, A04, MF-A01).

NCEER-88-0035 "Modeling of R/C Building Structures With Flexible Floor Diaphragms (IDARC2)," by A.M. Reinhorn, S.K. Kunnath and N. Panahshahi, 9/7/88, (PB89-207153, A07, MF-A01).

NCEER-88-0036 "Solution of the Dam-Reservoir Interaction Problem Using a Combination of FEM, BEM with Particular Integrals, Modal Analysis, and Substructuring," by C-S. Tsai, G.C. Lee and R.L. Ketter, 12/31/88, (PB89-207146, A04, MF-A01).

NCEER-88-0037 "Optimal Placement of Actuators for Structural Control," by F.Y. Cheng and C.P. Pantelides, 8/15/88, (PB89-162846, A05, MF-A01).

NCEER-88-0038 "Teflon Bearings in Aseismic Base Isolation: Experimental Studies and Mathematical Modeling," by A. Mokha, M.C. Constantinou and A.M. Reinhorn, 12/5/88, (PB89-218457, A10, MF-A01). This report is available only through NTIS (see address given above).

NCEER-88-0039 "Seismic Behavior of Flat Slab High-Rise Buildings in the New York City Area," by P. Weidlinger and M. Ettouney, 10/15/88, (PB90-145681, A04, MF-A01).

NCEER-88-0040 "Evaluation of the Earthquake Resistance of Existing Buildings in New York City," by P. Weidlinger and M. Ettouney, 10/15/88, to be published.

NCEER-88-0041 "Small-Scale Modeling Techniques for Reinforced Concrete Structures Subjected to Seismic Loads," by W. Kim, A. El-Attar and R.N. White, 11/22/88, (PB89-189625, A05, MF-A01).

NCEER-88-0042 "Modeling Strong Ground Motion from Multiple Event Earthquakes," by G.W. Ellis and A.S. Cakmak, 10/15/88, (PB89-174445, A03, MF-A01).

NCEER-88-0043 "Nonstationary Models of Seismic Ground Acceleration," by M. Grigoriu, S.E. Ruiz and E. Rosenblueth, 7/15/88, (PB89-189617, A04, MF-A01).

NCEER-88-0044 "SARCF User's Guide: Seismic Analysis of Reinforced Concrete Frames," by Y.S. Chung, C. Meyer and M. Shinozuka, 11/9/88, (PB89-174452, A08, MF-A01).

NCEER-88-0045 "First Expert Panel Meeting on Disaster Research and Planning," edited by J. Pantelic and J. Stoyle, 9/15/88, (PB89-174460, A05, MF-A01).

NCEER-88-0046 "Preliminary Studies of the Effect of Degrading Infill Walls on the Nonlinear Seismic Response of Steel Frames," by C.Z. Chrysostomou, P. Gergely and J.F. Abel, 12/19/88, (PB89-208383, A05, MF-A01).

NCEER-88-0047 "Reinforced Concrete Frame Component Testing Facility - Design, Construction, Instrumentation and Operation," by S.P. Pessiki, C. Conley, T. Bond, P. Gergely and R.N. White, 12/16/88, (PB89-174478, A04, MF-A01).

NCEER-89-0001 "Effects of Protective Cushion and Soil Compliancy on the Response of Equipment Within a Seismically Excited Building," by J.A. HoLung, 2/16/89, (PB89-207179, A04, MF-A01).

NCEER-89-0002 "Statistical Evaluation of Response Modification Factors for Reinforced Concrete Structures," by H.H-M. Hwang and J-W. Jaw, 2/17/89, (PB89-207187, A05, MF-A01).

NCEER-89-0003 "Hysteretic Columns Under Random Excitation," by G-Q. Cai and Y.K. Lin, 1/9/89, (PB89-196513, A03, MF-A01).

NCEER-89-0004 "Experimental Study of `Elephant Foot Bulge' Instability of Thin-Walled Metal Tanks," by Z-H. Jia and R.L. Ketter, 2/22/89, (PB89-207195, A03, MF-A01).

NCEER-89-0005 "Experiment on Performance of Buried Pipelines Across San Andreas Fault," by J. Isenberg, E. Richardson and T.D. O'Rourke, 3/10/89, (PB89-218440, A04, MF-A01). This report is available only through NTIS (see address given above).

NCEER-89-0006 "A Knowledge-Based Approach to Structural Design of Earthquake-Resistant Buildings," by M. Subramani, P. Gergely, C.H. Conley, J.F. Abel and A.H. Zaghw, 1/15/89, (PB89-218465, A06, MF-A01).

NCEER-89-0007 "Liquefaction Hazards and Their Effects on Buried Pipelines," by T.D. O'Rourke and P.A. Lane, 2/1/89, (PB89-218481, A09, MF-A01).

NCEER-89-0008 "Fundamentals of System Identification in Structural Dynamics," by H. Imai, C-B. Yun, O. Maruyama and M. Shinozuka, 1/26/89, (PB89-207211, A04, MF-A01).

NCEER-89-0009 "Effects of the 1985 Michoacan Earthquake on Water Systems and Other Buried Lifelines in Mexico," by A.G. Ayala and M.J. O'Rourke, 3/8/89, (PB89-207229, A06, MF-A01).

NCEER-89-R010 "NCEER Bibliography of Earthquake Education Materials," by K.E.K. Ross, Second Revision, 9/1/89, (PB90-125352, A05, MF-A01). This report is replaced by NCEER-92-0018.

NCEER-89-0011 "Inelastic Three-Dimensional Response Analysis of Reinforced Concrete Building Structures (IDARC-3D), Part I - Modeling," by S.K. Kunnath and A.M. Reinhorn, 4/17/89, (PB90-114612, A07, MF-A01). This report is available only through NTIS (see address given above).

NCEER-89-0012 "Recommended Modifications to ATC-14," by C.D. Poland and J.O. Malley, 4/12/89, (PB90-108648, A15, MF-A01).

NCEER-89-0013 "Repair and Strengthening of Beam-to-Column Connections Subjected to Earthquake Loading," by M. Corazao and A.J. Durrani, 2/28/89, (PB90-109885, A06, MF-A01).

NCEER-89-0014 "Program EXKAL2 for Identification of Structural Dynamic Systems," by O. Maruyama, C-B. Yun, M. Hoshiya and M. Shinozuka, 5/19/89, (PB90-109877, A09, MF-A01).

NCEER-89-0015 "Response of Frames With Bolted Semi-Rigid Connections, Part I - Experimental Study and Analytical Predictions," by P.J. DiCorso, A.M. Reinhorn, J.R. Dickerson, J.B. Radziminski and W.L. Harper, 6/1/89, to be published.

NCEER-89-0016 "ARMA Monte Carlo Simulation in Probabilistic Structural Analysis," by P.D. Spanos and M.P. Mignolet, 7/10/89, (PB90-109893, A03, MF-A01).

NCEER-89-P017 "Preliminary Proceedings from the Conference on Disaster Preparedness - The Place of Earthquake Education in Our Schools," Edited by K.E.K. Ross, 6/23/89, (PB90-108606, A03, MF-A01).

NCEER-89-0017 "Proceedings from the Conference on Disaster Preparedness - The Place of Earthquake Education in Our Schools," Edited by K.E.K. Ross, 12/31/89, (PB90-207895, A012, MF-A02). This report is available only through NTIS (see address given above).

NCEER-89-0018 "Multidimensional Models of Hysteretic Material Behavior for Vibration Analysis of Shape Memory Energy Absorbing Devices, by E.J. Graesser and F.A. Cozzarelli, 6/7/89, (PB90-164146, A04, MF-A01).

NCEER-89-0019 "Nonlinear Dynamic Analysis of Three-Dimensional Base Isolated Structures (3D-BASIS)," by S. Nagarajaiah, A.M. Reinhorn and M.C. Constantinou, 8/3/89, (PB90-161936, A06, MF-A01). This report has been replaced by NCEER-93-0011.

NCEER-89-0020 "Structural Control Considering Time-Rate of Control Forces and Control Rate Constraints," by F.Y. Cheng and C.P. Pantelides, 8/3/89, (PB90-120445, A04, MF-A01).

NCEER-89-0021 "Subsurface Conditions of Memphis and Shelby County," by K.W. Ng, T-S. Chang and H-H.M. Hwang, 7/26/89, (PB90-120437, A03, MF-A01).

NCEER-89-0022 "Seismic Wave Propagation Effects on Straight Jointed Buried Pipelines," by K. Elhmadi and M.J. O'Rourke, 8/24/89, (PB90-162322, A10, MF-A02).

NCEER-89-0023 "Workshop on Serviceability Analysis of Water Delivery Systems," edited by M. Grigoriu, 3/6/89, (PB90-127424, A03, MF-A01).

NCEER-89-0024 "Shaking Table Study of a 1/5 Scale Steel Frame Composed of Tapered Members," by K.C. Chang, J.S. Hwang and G.C. Lee, 9/18/89, (PB90-160169, A04, MF-A01).

NCEER-89-0025 "DYNA1D: A Computer Program for Nonlinear Seismic Site Response Analysis - Technical Documentation," by Jean H. Prevost, 9/14/89, (PB90-161944, A07, MF-A01). This report is available only through NTIS (see address given above).

NCEER-89-0026 "1:4 Scale Model Studies of Active Tendon Systems and Active Mass Dampers for Aseismic Protection," by A.M. Reinhorn, T.T. Soong, R.C. Lin, Y.P. Yang, Y. Fukao, H. Abe and M. Nakai, 9/15/89, (PB90-173246, A10, MF-A02). This report is available only through NTIS (see address given above).

NCEER-89-0027 "Scattering of Waves by Inclusions in a Nonhomogeneous Elastic Half Space Solved by Boundary Element Methods," by P.K. Hadley, A. Askar and A.S. Cakmak, 6/15/89, (PB90-145699, A07, MF-A01).

NCEER-89-0028 "Statistical Evaluation of Deflection Amplification Factors for Reinforced Concrete Structures," by H.H.M. Hwang, J-W. Jaw and A.L. Ch'ng, 8/31/89, (PB90-164633, A05, MF-A01).

NCEER-89-0029 "Bedrock Accelerations in Memphis Area Due to Large New Madrid Earthquakes," by H.H.M. Hwang, C.H.S. Chen and G. Yu, 11/7/89, (PB90-162330, A04, MF-A01).

NCEER-89-0030 "Seismic Behavior and Response Sensitivity of Secondary Structural Systems," by Y.Q. Chen and T.T. Soong, 10/23/89, (PB90-164658, A08, MF-A01).

NCEER-89-0031 "Random Vibration and Reliability Analysis of Primary-Secondary Structural Systems," by Y. Ibrahim, M. Grigoriu and T.T. Soong, 11/10/89, (PB90-161951, A04, MF-A01).

NCEER-89-0032 "Proceedings from the Second U.S. - Japan Workshop on Liquefaction, Large Ground Deformation and Their Effects on Lifelines, September 26-29, 1989," Edited by T.D. O'Rourke and M. Hamada, 12/1/89, (PB90-209388, A22, MF-A03).

NCEER-89-0033 "Deterministic Model for Seismic Damage Evaluation of Reinforced Concrete Structures," by J.M. Bracci, A.M. Reinhorn, J.B. Mander and S.K. Kunnath, 9/27/89, (PB91-108803, A06, MF-A01).

NCEER-89-0034 "On the Relation Between Local and Global Damage Indices," by E. DiPasquale and A.S. Cakmak, 8/15/89, (PB90-173865, A05, MF-A01).

NCEER-89-0035 "Cyclic Undrained Behavior of Nonplastic and Low Plasticity Silts," by A.J. Walker and H.E. Stewart, 7/26/89, (PB90-183518, A10, MF-A01).

NCEER-89-0036 "Liquefaction Potential of Surficial Deposits in the City of Buffalo, New York," by M. Budhu, R. Giese and L. Baumgrass, 1/17/89, (PB90-208455, A04, MF-A01).

NCEER-89-0037 "A Deterministic Assessment of Effects of Ground Motion Incoherence," by A.S. Veletsos and Y. Tang, 7/15/89, (PB90-164294, A03, MF-A01).

NCEER-89-0038 "Workshop on Ground Motion Parameters for Seismic Hazard Mapping," July 17-18, 1989, edited by R.V. Whitman, 12/1/89, (PB90-173923, A04, MF-A01).

NCEER-89-0039 "Seismic Effects on Elevated Transit Lines of the New York City Transit Authority," by C.J. Costantino, C.A. Miller and E. Heymsfield, 12/26/89, (PB90-207887, A06, MF-A01).

NCEER-89-0040 "Centrifugal Modeling of Dynamic Soil-Structure Interaction," by K. Weissman, Supervised by J.H. Prevost, 5/10/89, (PB90-207879, A07, MF-A01).

NCEER-89-0041 "Linearized Identification of Buildings With Cores for Seismic Vulnerability Assessment," by I-K. Ho and A.E. Aktan, 11/1/89, (PB90-251943, A07, MF-A01).

NCEER-90-0001 "Geotechnical and Lifeline Aspects of the October 17, 1989 Loma Prieta Earthquake in San Francisco," by T.D. O'Rourke, H.E. Stewart, F.T. Blackburn and T.S. Dickerman, 1/90, (PB90-208596, A05, MF-A01).

NCEER-90-0002 "Nonnormal Secondary Response Due to Yielding in a Primary Structure," by D.C.K. Chen and L.D. Lutes, 2/28/90, (PB90-251976, A07, MF-A01).

NCEER-90-0003 "Earthquake Education Materials for Grades K-12," by K.E.K. Ross, 4/16/90, (PB91-251984, A05, MF-A05). This report has been replaced by NCEER-92-0018.

NCEER-90-0004 "Catalog of Strong Motion Stations in Eastern North America," by R.W. Busby, 4/3/90, (PB90-251984, A05, MF-A01).

NCEER-90-0005 "NCEER Strong-Motion Data Base: A User Manual for the GeoBase Release (Version 1.0 for the Sun3)," by P. Friberg and K. Jacob, 3/31/90 (PB90-258062, A04, MF-A01).

NCEER-90-0006 "Seismic Hazard Along a Crude Oil Pipeline in the Event of an 1811-1812 Type New Madrid Earthquake," by H.H.M. Hwang and C-H.S. Chen, 4/16/90, (PB90-258054, A04, MF-A01).

NCEER-90-0007 "Site-Specific Response Spectra for Memphis Sheahan Pumping Station," by H.H.M. Hwang and C.S. Lee, 5/15/90, (PB91-108811, A05, MF-A01).

NCEER-90-0008 "Pilot Study on Seismic Vulnerability of Crude Oil Transmission Systems," by T. Ariman, R. Dobry, M. Grigoriu, F. Kozin, M. O'Rourke, T. O'Rourke and M. Shinozuka, 5/25/90, (PB91-108837, A06, MF-A01).

NCEER-90-0009 "A Program to Generate Site Dependent Time Histories: EQGEN," by G.W. Ellis, M. Srinivasan and A.S. Cakmak, 1/30/90, (PB91-108829, A04, MF-A01).

NCEER-90-0010 "Active Isolation for Seismic Protection of Operating Rooms," by M.E. Talbott, Supervised by M. Shinozuka, 6/8/9, (PB91-110205, A05, MF-A01).

NCEER-90-0011 "Program LINEARID for Identification of Linear Structural Dynamic Systems," by C-B. Yun and M. Shinozuka, 6/25/90, (PB91-110312, A08, MF-A01).

NCEER-90-0012 "Two-Dimensional Two-Phase Elasto-Plastic Seismic Response of Earth Dams," by A.N. Yiagos, Supervised by J.H. Prevost, 6/20/90, (PB91-110197, A13, MF-A02).

NCEER-90-0013 "Secondary Systems in Base-Isolated Structures: Experimental Investigation, Stochastic Response and Stochastic Sensitivity," by G.D. Manolis, G. Juhn, M.C. Constantinou and A.M. Reinhorn, 7/1/90, (PB91-110320, A08, MF-A01).

NCEER-90-0014 "Seismic Behavior of Lightly-Reinforced Concrete Column and Beam-Column Joint Details," by S.P. Pessiki, C.H. Conley, P. Gergely and R.N. White, 8/22/90, (PB91-108795, A11, MF-A02).

NCEER-90-0015 "Two Hybrid Control Systems for Building Structures Under Strong Earthquakes," by J.N. Yang and A. Danielians, 6/29/90, (PB91-125393, A04, MF-A01).

NCEER-90-0016 "Instantaneous Optimal Control with Acceleration and Velocity Feedback," by J.N. Yang and Z. Li, 6/29/90, (PB91-125401, A03, MF-A01).

NCEER-90-0017 "Reconnaissance Report on the Northern Iran Earthquake of June 21, 1990," by M. Mehrain, 10/4/90, (PB91-125377, A03, MF-A01).

NCEER-90-0018 "Evaluation of Liquefaction Potential in Memphis and Shelby County," by T.S. Chang, P.S. Tang, C.S. Lee and H. Hwang, 8/10/90, (PB91-125427, A09, MF-A01).

NCEER-90-0019 "Experimental and Analytical Study of a Combined Sliding Disc Bearing and Helical Steel Spring Isolation System," by M.C. Constantinou, A.S. Mokha and A.M. Reinhorn, 10/4/90, (PB91-125385, A06, MF-A01). This report is available only through NTIS (see address given above).

NCEER-90-0020 "Experimental Study and Analytical Prediction of Earthquake Response of a Sliding Isolation System with a Spherical Surface," by A.S. Mokha, M.C. Constantinou and A.M. Reinhorn, 10/11/90, (PB91-125419, A05, MF-A01).

NCEER-90-0021 "Dynamic Interaction Factors for Floating Pile Groups," by G. Gazetas, K. Fan, A. Kaynia and E. Kausel, 9/10/90, (PB91-170381, A05, MF-A01).

NCEER-90-0022 "Evaluation of Seismic Damage Indices for Reinforced Concrete Structures," by S. Rodriguez-Gomez and A.S. Cakmak, 9/30/90, PB91-171322, A06, MF-A01).

NCEER-90-0023 "Study of Site Response at a Selected Memphis Site," by H. Desai, S. Ahmad, E.S. Gazetas and M.R. Oh, 10/11/90, (PB91-196857, A03, MF-A01).

NCEER-90-0024 "A User's Guide to Strongmo: Version 1.0 of NCEER's Strong-Motion Data Access Tool for PCs and Terminals," by P.A. Friberg and C.A.T. Susch, 11/15/90, (PB91-171272, A03, MF-A01).

NCEER-90-0025 "A Three-Dimensional Analytical Study of Spatial Variability of Seismic Ground Motions," by L-L. Hong and A.H.-S. Ang, 10/30/90, (PB91-170399, A09, MF-A01).

NCEER-90-0026 "MUMOID User's Guide - A Program for the Identification of Modal Parameters," by S. Rodriguez-Gomez and E. DiPasquale, 9/30/90, (PB91-171298, A04, MF-A01).

NCEER-90-0027 "SARCF-II User's Guide - Seismic Analysis of Reinforced Concrete Frames," by S. Rodriguez-Gomez, Y.S. Chung and C. Meyer, 9/30/90, (PB91-171280, A05, MF-A01).

NCEER-90-0028 "Viscous Dampers: Testing, Modeling and Application in Vibration and Seismic Isolation," by N. Makris and M.C. Constantinou, 12/20/90 (PB91-190561, A06, MF-A01).

NCEER-90-0029 "Soil Effects on Earthquake Ground Motions in the Memphis Area," by H. Hwang, C.S. Lee, K.W. Ng and T.S. Chang, 8/2/90, (PB91-190751, A05, MF-A01).

NCEER-91-0001 "Proceedings from the Third Japan-U.S. Workshop on Earthquake Resistant Design of Lifeline Facilities and Countermeasures for Soil Liquefaction, December 17-19, 1990," edited by T.D. O'Rourke and M. Hamada, 2/1/91, (PB91-179259, A99, MF-A04).

NCEER-91-0002 "Physical Space Solutions of Non-Proportionally Damped Systems," by M. Tong, Z. Liang and G.C. Lee, 1/15/91, (PB91-179242, A04, MF-A01).

NCEER-91-0003 "Seismic Response of Single Piles and Pile Groups," by K. Fan and G. Gazetas, 1/10/91, (PB92-174994, A04, MF-A01).

NCEER-91-0004 "Damping of Structures: Part 1 - Theory of Complex Damping," by Z. Liang and G. Lee, 10/10/91, (PB92-197235, A12, MF-A03).

NCEER-91-0005 "3D-BASIS - Nonlinear Dynamic Analysis of Three Dimensional Base Isolated Structures: Part II," by S. Nagarajaiah, A.M. Reinhorn and M.C. Constantinou, 2/28/91, (PB91-190553, A07, MF-A01). This report has been replaced by NCEER-93-0011.

NCEER-91-0006 "A Multidimensional Hysteretic Model for Plasticity Deforming Metals in Energy Absorbing Devices," by E.J. Graesser and F.A. Cozzarelli, 4/9/91, (PB92-108364, A04, MF-A01).

NCEER-91-0007 "A Framework for Customizable Knowledge-Based Expert Systems with an Application to a KBES for Evaluating the Seismic Resistance of Existing Buildings," by E.G. Ibarra-Anaya and S.J. Fenves, 4/9/91, (PB91-210930, A08, MF-A01).

NCEER-91-0008 "Nonlinear Analysis of Steel Frames with Semi-Rigid Connections Using the Capacity Spectrum Method," by G.G. Deierlein, S-H. Hsieh, Y-J. Shen and J.F. Abel, 7/2/91, (PB92-113828, A05, MF-A01).

NCEER-91-0009 "Earthquake Education Materials for Grades K-12," by K.E.K. Ross, 4/30/91, (PB91-212142, A06, MF-A01). This report has been replaced by NCEER-92-0018.

NCEER-91-0010 "Phase Wave Velocities and Displacement Phase Differences in a Harmonically Oscillating Pile," by N. Makris and G. Gazetas, 7/8/91, (PB92-108356, A04, MF-A01).

NCEER-91-0011 "Dynamic Characteristics of a Full-Size Five-Story Steel Structure and a 2/5 Scale Model," by K.C. Chang, G.C. Yao, G.C. Lee, D.S. Hao and Y.C. Yeh," 7/2/91, (PB93-116648, A06, MF-A02).

NCEER-91-0012 "Seismic Response of a 2/5 Scale Steel Structure with Added Viscoelastic Dampers," by K.C. Chang, T.T. Soong, S-T. Oh and M.L. Lai, 5/17/91, (PB92-110816, A05, MF-A01).

NCEER-91-0013 "Earthquake Response of Retaining Walls; Full-Scale Testing and Computational Modeling," by S. Alampalli and A-W.M. Elgamal, 6/20/91, to be published.

NCEER-91-0014 "3D-BASIS-M: Nonlinear Dynamic Analysis of Multiple Building Base Isolated Structures," by P.C. Tsopelas, S. Nagarajaiah, M.C. Constantinou and A.M. Reinhorn, 5/28/91, (PB92-113885, A09, MF-A02).

NCEER-91-0015 "Evaluation of SEAOC Design Requirements for Sliding Isolated Structures," by D. Theodossiou and M.C. Constantinou, 6/10/91, (PB92-114602, A11, MF-A03).

NCEER-91-0016 "Closed-Loop Modal Testing of a 27-Story Reinforced Concrete Flat Plate-Core Building," by H.R. Somaprasad, T. Toksoy, H. Yoshiyuki and A.E. Aktan, 7/15/91, (PB92-129980, A07, MF-A02).

NCEER-91-0017 "Shake Table Test of a 1/6 Scale Two-Story Lightly Reinforced Concrete Building," by A.G. El-Attar, R.N. White and P. Gergely, 2/28/91, (PB92-222447, A06, MF-A02).

NCEER-91-0018 "Shake Table Test of a 1/8 Scale Three-Story Lightly Reinforced Concrete Building," by A.G. El-Attar, R.N. White and P. Gergely, 2/28/91, (PB93-116630, A08, MF-A02).

NCEER-91-0019 "Transfer Functions for Rigid Rectangular Foundations," by A.S. Veletsos, A.M. Prasad and W.H. Wu, 7/31/91, to be published.

NCEER-91-0020 "Hybrid Control of Seismic-Excited Nonlinear and Inelastic Structural Systems," by J.N. Yang, Z. Li and A. Danielians, 8/1/91, (PB92-143171, A06, MF-A02).

NCEER-91-0021 "The NCEER-91 Earthquake Catalog: Improved Intensity-Based Magnitudes and Recurrence Relations for U.S. Earthquakes East of New Madrid," by L. Seeber and J.G. Armbruster, 8/28/91, (PB92-176742, A06, MF-A02).

NCEER-91-0022 "Proceedings from the Implementation of Earthquake Planning and Education in Schools: The Need for Change - The Roles of the Changemakers," by K.E.K. Ross and F. Winslow, 7/23/91, (PB92-129998, A12, MF-A03).

NCEER-91-0023 "A Study of Reliability-Based Criteria for Seismic Design of Reinforced Concrete Frame Buildings," by H.H.M. Hwang and H-M. Hsu, 8/10/91, (PB92-140235, A09, MF-A02).

NCEER-91-0024 "Experimental Verification of a Number of Structural System Identification Algorithms," by R.G. Ghanem, H. Gavin and M. Shinozuka, 9/18/91, (PB92-176577, A18, MF-A04).

NCEER-91-0025 "Probabilistic Evaluation of Liquefaction Potential," by H.H.M. Hwang and C.S. Lee," 11/25/91, (PB92-143429, A05, MF-A01).

NCEER-91-0026 "Instantaneous Optimal Control for Linear, Nonlinear and Hysteretic Structures - Stable Controllers," by J.N. Yang and Z. Li, 11/15/91, (PB92-163807, A04, MF-A01).

NCEER-91-0027 "Experimental and Theoretical Study of a Sliding Isolation System for Bridges," by M.C. Constantinou, A. Kartoum, A.M. Reinhorn and P. Bradford, 11/15/91, (PB92-176973, A10, MF-A03).

NCEER-92-0001 "Case Studies of Liquefaction and Lifeline Performance During Past Earthquakes, Volume 1: Japanese Case Studies," Edited by M. Hamada and T. O'Rourke, 2/17/92, (PB92-197243, A18, MF-A04).

NCEER-92-0002 "Case Studies of Liquefaction and Lifeline Performance During Past Earthquakes, Volume 2: United States Case Studies," Edited by T. O'Rourke and M. Hamada, 2/17/92, (PB92-197250, A20, MF-A04).

NCEER-92-0003 "Issues in Earthquake Education," Edited by K. Ross, 2/3/92, (PB92-222389, A07, MF-A02).

NCEER-92-0004 "Proceedings from the First U.S. - Japan Workshop on Earthquake Protective Systems for Bridges," Edited by I.G. Buckle, 2/4/92, (PB94-142239, A99, MF-A06).

NCEER-92-0005 "Seismic Ground Motion from a Haskell-Type Source in a Multiple-Layered Half-Space," A.P. Theoharis, G. Deodatis and M. Shinozuka, 1/2/92, to be published.

NCEER-92-0006 "Proceedings from the Site Effects Workshop," Edited by R. Whitman, 2/29/92, (PB92-197201, A04, MF-A01).

NCEER-92-0007 "Engineering Evaluation of Permanent Ground Deformations Due to Seismically-Induced Liquefaction," by M.H. Baziar, R. Dobry and A-W.M. Elgamal, 3/24/92, (PB92-222421, A13, MF-A03).

NCEER-92-0008 "A Procedure for the Seismic Evaluation of Buildings in the Central and Eastern United States," by C.D. Poland and J.O. Malley, 4/2/92, (PB92-222439, A20, MF-A04).

NCEER-92-0009 "Experimental and Analytical Study of a Hybrid Isolation System Using Friction Controllable Sliding Bearings," by M.Q. Feng, S. Fujii and M. Shinozuka, 5/15/92, (PB93-150282, A06, MF-A02).

NCEER-92-0010 "Seismic Resistance of Slab-Column Connections in Existing Non-Ductile Flat-Plate Buildings," by A.J. Durrani and Y. Du, 5/18/92, (PB93-116812, A06, MF-A02).

NCEER-92-0011 "The Hysteretic and Dynamic Behavior of Brick Masonry Walls Upgraded by Ferrocement Coatings Under Cyclic Loading and Strong Simulated Ground Motion," by H. Lee and S.P. Prawel, 5/11/92, to be published.

NCEER-92-0012 "Study of Wire Rope Systems for Seismic Protection of Equipment in Buildings," by G.F. Demetriades, M.C. Constantinou and A.M. Reinhorn, 5/20/92, (PB93-116655, A08, MF-A02).

NCEER-92-0013 "Shape Memory Structural Dampers: Material Properties, Design and Seismic Testing," by P.R. Witting and F.A. Cozzarelli, 5/26/92, (PB93-116663, A05, MF-A01).

NCEER-92-0014 "Longitudinal Permanent Ground Deformation Effects on Buried Continuous Pipelines," by M.J. O'Rourke, and C. Nordberg, 6/15/92, (PB93-116671, A08, MF-A02).

NCEER-92-0015 "A Simulation Method for Stationary Gaussian Random Functions Based on the Sampling Theorem," by M. Grigoriu and S. Balopoulou, 6/11/92, (PB93-127496, A05, MF-A01).

NCEER-92-0016 "Gravity-Load-Designed Reinforced Concrete Buildings: Seismic Evaluation of Existing Construction and Detailing Strategies for Improved Seismic Resistance," by G.W. Hoffmann, S.K. Kunnath, A.M. Reinhorn and J.B. Mander, 7/15/92, (PB94-142007, A08, MF-A02).

NCEER-92-0017 "Observations on Water System and Pipeline Performance in the Limón Area of Costa Rica Due to the April 22, 1991 Earthquake," by M. O'Rourke and D. Ballantyne, 6/30/92, (PB93-126811, A06, MF-A02).

NCEER-92-0018 "Fourth Edition of Earthquake Education Materials for Grades K-12," Edited by K.E.K. Ross, 8/10/92, (PB93-114023, A07, MF-A02).

NCEER-92-0019 "Proceedings from the Fourth Japan-U.S. Workshop on Earthquake Resistant Design of Lifeline Facilities and Countermeasures for Soil Liquefaction," Edited by M. Hamada and T.D. O'Rourke, 8/12/92, (PB93-163939, A99, MF-E11).

NCEER-92-0020 "Active Bracing System: A Full Scale Implementation of Active Control," by A.M. Reinhorn, T.T. Soong, R.C. Lin, M.A. Riley, Y.P. Wang, S. Aizawa and M. Higashino, 8/14/92, (PB93-127512, A06, MF-A02).

NCEER-92-0021 "Empirical Analysis of Horizontal Ground Displacement Generated by Liquefaction-Induced Lateral Spreads," by S.F. Bartlett and T.L. Youd, 8/17/92, (PB93-188241, A06, MF-A02).

NCEER-92-0022 "IDARC Version 3.0: Inelastic Damage Analysis of Reinforced Concrete Structures," by S.K. Kunnath, A.M. Reinhorn and R.F. Lobo, 8/31/92, (PB93-227502, A07, MF-A02).

NCEER-92-0023 "A Semi-Empirical Analysis of Strong-Motion Peaks in Terms of Seismic Source, Propagation Path and Local Site Conditions, by M. Kamiyama, M.J. O'Rourke and R. Flores-Berrones, 9/9/92, (PB93-150266, A08, MF-A02).

NCEER-92-0024 "Seismic Behavior of Reinforced Concrete Frame Structures with Nonductile Details, Part I: Summary of Experimental Findings of Full Scale Beam-Column Joint Tests," by A. Beres, R.N. White and P. Gergely, 9/30/92, (PB93-227783, A05, MF-A01).

NCEER-92-0025 "Experimental Results of Repaired and Retrofitted Beam-Column Joint Tests in Lightly Reinforced Concrete Frame Buildings," by A. Beres, S. El-Borgi, R.N. White and P. Gergely, 10/29/92, (PB93-227791, A05, MF-A01).

NCEER-92-0026 "A Generalization of Optimal Control Theory: Linear and Nonlinear Structures," by J.N. Yang, Z. Li and S. Vongchavalitkul, 11/2/92, (PB93-188621, A05, MF-A01).

NCEER-92-0027 "Seismic Resistance of Reinforced Concrete Frame Structures Designed Only for Gravity Loads: Part I - Design and Properties of a One-Third Scale Model Structure," by J.M. Bracci, A.M. Reinhorn and J.B. Mander, 12/1/92, (PB94-104502, A08, MF-A02).

NCEER-92-0028 "Seismic Resistance of Reinforced Concrete Frame Structures Designed Only for Gravity Loads: Part II - Experimental Performance of Subassemblages," by L.E. Aycardi, J.B. Mander and A.M. Reinhorn, 12/1/92, (PB94-104510, A08, MF-A02).

NCEER-92-0029 "Seismic Resistance of Reinforced Concrete Frame Structures Designed Only for Gravity Loads: Part III - Experimental Performance and Analytical Study of a Structural Model," by J.M. Bracci, A.M. Reinhorn and J.B. Mander, 12/1/92, (PB93-227528, A09, MF-A01).

NCEER-92-0030 "Evaluation of Seismic Retrofit of Reinforced Concrete Frame Structures: Part I - Experimental Performance of Retrofitted Subassemblages," by D. Choudhuri, J.B. Mander and A.M. Reinhorn, 12/8/92, (PB93-198307, A07, MF-A02).

NCEER-92-0031 "Evaluation of Seismic Retrofit of Reinforced Concrete Frame Structures: Part II - Experimental Performance and Analytical Study of a Retrofitted Structural Model," by J.M. Bracci, A.M. Reinhorn and J.B. Mander, 12/8/92, (PB93-198315, A09, MF-A03).

NCEER-92-0032 "Experimental and Analytical Investigation of Seismic Response of Structures with Supplemental Fluid Viscous Dampers," by M.C. Constantinou and M.D. Symans, 12/21/92, (PB93-191435, A10, MF-A03). This report is available only through NTIS (see address given above).

NCEER-92-0033 "Reconnaissance Report on the Cairo, Egypt Earthquake of October 12, 1992," by M. Khater, 12/23/92, (PB93-188621, A03, MF-A01).

NCEER-92-0034 "Low-Level Dynamic Characteristics of Four Tall Flat-Plate Buildings in New York City," by H. Gavin, S. Yuan, J. Grossman, E. Pekelis and K. Jacob, 12/28/92, (PB93-188217, A07, MF-A02).

NCEER-93-0001 "An Experimental Study on the Seismic Performance of Brick-Infilled Steel Frames With and Without Retrofit," by J.B. Mander, B. Nair, K. Wojtkowski and J. Ma, 1/29/93, (PB93-227510, A07, MF-A02).

NCEER-93-0002 "Social Accounting for Disaster Preparedness and Recovery Planning," by S. Cole, E. Pantoja and V. Razak, 2/22/93, (PB94-142114, A12, MF-A03).

NCEER-93-0003 "Assessment of 1991 NEHRP Provisions for Nonstructural Components and Recommended Revisions," by T.T. Soong, G. Chen, Z. Wu, R-H. Zhang and M. Grigoriu, 3/1/93, (PB93-188639, A06, MF-A02).

NCEER-93-0004 "Evaluation of Static and Response Spectrum Analysis Procedures of SEAOC/UBC for Seismic Isolated Structures," by C.W. Winters and M.C. Constantinou, 3/23/93, (PB93-198299, A10, MF-A03).

NCEER-93-0005 "Earthquakes in the Northeast - Are We Ignoring the Hazard? A Workshop on Earthquake Science and Safety for Educators," edited by K.E.K. Ross, 4/2/93, (PB94-103066, A09, MF-A02).

NCEER-93-0006 "Inelastic Response of Reinforced Concrete Structures with Viscoelastic Braces," by R.F. Lobo, J.M. Bracci, K.L. Shen, A.M. Reinhorn and T.T. Soong, 4/5/93, (PB93-227486, A05, MF-A02).

NCEER-93-0007 "Seismic Testing of Installation Methods for Computers and Data Processing Equipment," by K. Kosar, T.T. Soong, K.L. Shen, J.A. HoLung and Y.K. Lin, 4/12/93, (PB93-198299, A07, MF-A02).

NCEER-93-0008 "Retrofit of Reinforced Concrete Frames Using Added Dampers," by A. Reinhorn, M. Constantinou and C. Li, to be published.

NCEER-93-0009 "Seismic Behavior and Design Guidelines for Steel Frame Structures with Added Viscoelastic Dampers," by K.C. Chang, M.L. Lai, T.T. Soong, D.S. Hao and Y.C. Yeh, 5/1/93, (PB94-141959, A07, MF-A02).

NCEER-93-0010 "Seismic Performance of Shear-Critical Reinforced Concrete Bridge Piers," by J.B. Mander, S.M. Waheed, M.T.A. Chaudhary and S.S. Chen, 5/12/93, (PB93-227494, A08, MF-A02).

NCEER-93-0011 "3D-BASIS-TABS: Computer Program for Nonlinear Dynamic Analysis of Three Dimensional Base Isolated Structures," by S. Nagarajaiah, C. Li, A.M. Reinhorn and M.C. Constantinou, 8/2/93, (PB94-141819, A09, MF-A02).

NCEER-93-0012 "Effects of Hydrocarbon Spills from an Oil Pipeline Break on Ground Water," by O.J. Helweg and H.H.M. Hwang, 8/3/93, (PB94-141942, A06, MF-A02).

NCEER-93-0013 "Simplified Procedures for Seismic Design of Nonstructural Components and Assessment of Current Code Provisions," by M.P. Singh, L.E. Suarez, E.E. Matheu and G.O. Maldonado, 8/4/93, (PB94-141827, A09, MF-A02).

NCEER-93-0014 "An Energy Approach to Seismic Analysis and Design of Secondary Systems," by G. Chen and T.T. Soong, 8/6/93, (PB94-142767, A11, MF-A03).

NCEER-93-0015 "Proceedings from School Sites: Becoming Prepared for Earthquakes - Commemorating the Third Anniversary of the Loma Prieta Earthquake," Edited by F.E. Winslow and K.E.K. Ross, 8/16/93, (PB94-154275, A16, MF-A02).

NCEER-93-0016 "Reconnaissance Report of Damage to Historic Monuments in Cairo, Egypt Following the October 12, 1992 Dahshur Earthquake," by D. Sykora, D. Look, G. Croci, E. Karaesmen and E. Karaesmen, 8/19/93, (PB94-142221, A08, MF-A02).

NCEER-93-0017 "The Island of Guam Earthquake of August 8, 1993," by S.W. Swan and S.K. Harris, 9/30/93, (PB94-141843, A04, MF-A01).

NCEER-93-0018 "Engineering Aspects of the October 12, 1992 Egyptian Earthquake," by A.W. Elgamal, M. Amer, K. Adalier and A. Abul-Fadl, 10/7/93, (PB94-141983, A05, MF-A01).

NCEER-93-0019 "Development of an Earthquake Motion Simulator and its Application in Dynamic Centrifuge Testing," by I. Krstelj, Supervised by J.H. Prevost, 10/23/93, (PB94-181773, A-10, MF-A03).

NCEER-93-0020 "NCEER-Taisei Corporation Research Program on Sliding Seismic Isolation Systems for Bridges: Experimental and Analytical Study of a Friction Pendulum System (FPS)," by M.C. Constantinou, P. Tsopelas, Y-S. Kim and S. Okamoto, 11/1/93, (PB94-142775, A08, MF-A02).

NCEER-93-0021 "Finite Element Modeling of Elastomeric Seismic Isolation Bearings," by L.J. Billings, Supervised by R. Shepherd, 11/8/93, to be published.

NCEER-93-0022 "Seismic Vulnerability of Equipment in Critical Facilities: Life-Safety and Operational Consequences," by K. Porter, G.S. Johnson, M.M. Zadeh, C. Scawthorn and S. Eder, 11/24/93, (PB94-181765, A16, MF-A03).

NCEER-93-0023 "Hokkaido Nansei-oki, Japan Earthquake of July 12, 1993, by P.I. Yanev and C.R. Scawthorn, 12/23/93, (PB94-181500, A07, MF-A01).

NCEER-94-0001 "An Evaluation of Seismic Serviceability of Water Supply Networks with Application to the San Francisco Auxiliary Water Supply System," by I. Markov, Supervised by M. Grigoriu and T. O'Rourke, 1/21/94, (PB94-204013, A07, MF-A02).

NCEER-94-0002 "NCEER-Taisei Corporation Research Program on Sliding Seismic Isolation Systems for Bridges: Experimental and Analytical Study of Systems Consisting of Sliding Bearings, Rubber Restoring Force Devices and Fluid Dampers," Volumes I and II, by P. Tsopelas, S. Okamoto, M.C. Constantinou, D. Ozaki and S. Fujii, 2/4/94, (PB94-181740, A09, MF-A02 and PB94-181757, A12, MF-A03).

NCEER-94-0003 "A Markov Model for Local and Global Damage Indices in Seismic Analysis," by S. Rahman and M. Grigoriu, 2/18/94, (PB94-206000, A12, MF-A03).

NCEER-94-0004 "Proceedings from the NCEER Workshop on Seismic Response of Masonry Infills," edited by D.P. Abrams, 3/1/94, (PB94-180783, A07, MF-A02).

NCEER-94-0005 "The Northridge, California Earthquake of January 17, 1994: General Reconnaissance Report," edited by J.D. Goltz, 3/11/94, (PB193943, A10, MF-A03).

NCEER-94-0006 "Seismic Energy Based Fatigue Damage Analysis of Bridge Columns: Part I - Evaluation of Seismic Capacity," by G.A. Chang and J.B. Mander, 3/14/94, (PB94-219185, A11, MF-A03).

NCEER-94-0007 "Seismic Isolation of Multi-Story Frame Structures Using Spherical Sliding Isolation Systems," by T.M. Al-Hussaini, V.A. Zayas and M.C. Constantinou, 3/17/94, (PB193745, A09, MF-A02).

NCEER-94-0008 "The Northridge, California Earthquake of January 17, 1994: Performance of Highway Bridges," edited by I.G. Buckle, 3/24/94, (PB94-193851, A06, MF-A02).

NCEER-94-0009 "Proceedings of the Third U.S.-Japan Workshop on Earthquake Protective Systems for Bridges," edited by I.G. Buckle and I. Friedland, 3/31/94, (PB94-195815, A99, MF-A06).

NCEER-94-0010 "3D-BASIS-ME: Computer Program for Nonlinear Dynamic Analysis of Seismically Isolated Single and Multiple Structures and Liquid Storage Tanks," by P.C. Tsopelas, M.C. Constantinou and A.M. Reinhorn, 4/12/94, (PB94-204922, A09, MF-A02).

NCEER-94-0011 "The Northridge, California Earthquake of January 17, 1994: Performance of Gas Transmission Pipelines," by T.D. O'Rourke and M.C. Palmer, 5/16/94, (PB94-204989, A05, MF-A01).

NCEER-94-0012 "Feasibility Study of Replacement Procedures and Earthquake Performance Related to Gas Transmission Pipelines," by T.D. O'Rourke and M.C. Palmer, 5/25/94, (PB94-206638, A09, MF-A02).

NCEER-94-0013 "Seismic Energy Based Fatigue Damage Analysis of Bridge Columns: Part II - Evaluation of Seismic Demand," by G.A. Chang and J.B. Mander, 6/1/94, (PB95-18106, A08, MF-A02).

NCEER-94-0014 "NCEER-Taisei Corporation Research Program on Sliding Seismic Isolation Systems for Bridges: Experimental and Analytical Study of a System Consisting of Sliding Bearings and Fluid Restoring Force/Damping Devices," by P. Tsopelas and M.C. Constantinou, 6/13/94, (PB94-219144, A10, MF-A03).

NCEER-94-0015 "Generation of Hazard-Consistent Fragility Curves for Seismic Loss Estimation Studies," by H. Hwang and J-R. Huo, 6/14/94, (PB95-181996, A09, MF-A02).

NCEER-94-0016 "Seismic Study of Building Frames with Added Energy-Absorbing Devices," by W.S. Pong, C.S. Tsai and G.C. Lee, 6/20/94, (PB94-219136, A10, A03).

NCEER-94-0017 "Sliding Mode Control for Seismic-Excited Linear and Nonlinear Civil Engineering Structures," by J. Yang, J. Wu, A. Agrawal and Z. Li, 6/21/94, (PB95-138483, A06, MF-A02).

NCEER-94-0018 "3D-BASIS-TABS Version 2.0: Computer Program for Nonlinear Dynamic Analysis of Three Dimensional Base Isolated Structures," by A.M. Reinhorn, S. Nagarajaiah, M.C. Constantinou, P. Tsopelas and R. Li, 6/22/94, (PB95-182176, A08, MF-A02).

NCEER-94-0019 "Proceedings of the International Workshop on Civil Infrastructure Systems: Application of Intelligent Systems and Advanced Materials on Bridge Systems," Edited by G.C. Lee and K.C. Chang, 7/18/94, (PB95-252474, A20, MF-A04).

NCEER-94-0020 "Study of Seismic Isolation Systems for Computer Floors," by V. Lambrou and M.C. Constantinou, 7/19/94, (PB95-138533, A10, MF-A03).

NCEER-94-0021 "Proceedings of the U.S.-Italian Workshop on Guidelines for Seismic Evaluation and Rehabilitation of Unreinforced Masonry Buildings," Edited by D.P. Abrams and G.M. Calvi, 7/20/94, (PB95-138749, A13, MF-A03).

NCEER-94-0022 "NCEER-Taisei Corporation Research Program on Sliding Seismic Isolation Systems for Bridges: Experimental and Analytical Study of a System Consisting of Lubricated PTFE Sliding Bearings and Mild Steel Dampers," by P. Tsopelas and M.C. Constantinou, 7/22/94, (PB95-182184, A08, MF-A02).

NCEER-94-0023 “Development of Reliability-Based Design Criteria for Buildings Under Seismic Load,” by Y.K. Wen, H. Hwang and M. Shinozuka, 8/1/94, (PB95-211934, A08, MF-A02).

NCEER-94-0024 “Experimental Verification of Acceleration Feedback Control Strategies for an Active Tendon System,” by S.J. Dyke, B.F. Spencer, Jr., P. Quast, M.K. Sain, D.C. Kaspari, Jr. and T.T. Soong, 8/29/94, (PB95-212320, A05, MF-A01).

NCEER-94-0025 “Seismic Retrofitting Manual for Highway Bridges,” Edited by I.G. Buckle and I.F. Friedland, published by the Federal Highway Administration (PB95-212676, A15, MF-A03).

NCEER-94-0026 “Proceedings from the Fifth U.S.-Japan Workshop on Earthquake Resistant Design of Lifeline Facilities and Countermeasures Against Soil Liquefaction,” Edited by T.D. O’Rourke and M. Hamada, 11/7/94, (PB95-220802, A99, MF-E08).

NCEER-95-0001 "Experimental and Analytical Investigation of Seismic Retrofit of Structures with Supplemental Damping: Part 1 - Fluid Viscous Damping Devices," by A.M. Reinhorn, C. Li and M.C. Constantinou, 1/3/95, (PB95-266599, A09, MF-A02).

NCEER-95-0002 "Experimental and Analytical Study of Low-Cycle Fatigue Behavior of Semi-Rigid Top-And-Seat Angle Connections," by G. Pekcan, J.B. Mander and S.S. Chen, 1/5/95, (PB95-220042, A07, MF-A02).

NCEER-95-0003 "NCEER-ATC Joint Study on Fragility of Buildings," by T. Anagnos, C. Rojahn and A.S. Kiremidjian, 1/20/95, (PB95-220026, A06, MF-A02).

NCEER-95-0004 "Nonlinear Control Algorithms for Peak Response Reduction," by Z. Wu, T.T. Soong, V. Gattulli and R.C. Lin, 2/16/95, (PB95-220349, A05, MF-A01).

NCEER-95-0005 "Pipeline Replacement Feasibility Study: A Methodology for Minimizing Seismic and Corrosion Risks to Underground Natural Gas Pipelines," by R.T. Eguchi, H.A. Seligson and D.G. Honegger, 3/2/95, (PB95-252326, A06, MF-A02).

NCEER-95-0006 "Evaluation of Seismic Performance of an 11-Story Frame Building During the 1994 Northridge Earthquake," by F. Naeim, R. DiSulio, K. Benuska, A. Reinhorn and C. Li, to be published.

NCEER-95-0007 "Prioritization of Bridges for Seismic Retrofitting," by N. Basöz and A.S. Kiremidjian, 4/24/95, (PB95-252300, A08, MF-A02).

NCEER-95-0008 "Method for Developing Motion Damage Relationships for Reinforced Concrete Frames," by A. Singhal and A.S. Kiremidjian, 5/11/95, (PB95-266607, A06, MF-A02).

NCEER-95-0009 "Experimental and Analytical Investigation of Seismic Retrofit of Structures with Supplemental Damping: Part II - Friction Devices," by C. Li and A.M. Reinhorn, 7/6/95, (PB96-128087, A11, MF-A03).

NCEER-95-0010 "Experimental Performance and Analytical Study of a Non-Ductile Reinforced Concrete Frame Structure Retrofitted with Elastomeric Spring Dampers," by G. Pekcan, J.B. Mander and S.S. Chen, 7/14/95, (PB96-137161, A08, MF-A02).

NCEER-95-0011 "Development and Experimental Study of Semi-Active Fluid Damping Devices for Seismic Protection of Structures," by M.D. Symans and M.C. Constantinou, 8/3/95, (PB96-136940, A23, MF-A04).

NCEER-95-0012 "Real-Time Structural Parameter Modification (RSPM): Development of Innervated Structures," by Z. Liang, M. Tong and G.C. Lee, 4/11/95, (PB96-137153, A06, MF-A01).

NCEER-95-0013 "Experimental and Analytical Investigation of Seismic Retrofit of Structures with Supplemental Damping: Part III - Viscous Damping Walls," by A.M. Reinhorn and C. Li, 10/1/95, (PB96-176409, A11, MF-A03).

NCEER-95-0014 "Seismic Fragility Analysis of Equipment and Structures in a Memphis Electric Substation," by J-R. Huo and H.H.M. Hwang, 8/10/95, (PB96-128087, A09, MF-A02).

NCEER-95-0015 "The Hanshin-Awaji Earthquake of January 17, 1995: Performance of Lifelines," Edited by M. Shinozuka, 11/3/95, (PB96-176383, A15, MF-A03).

NCEER-95-0016 "Highway Culvert Performance During Earthquakes," by T.L. Youd and C.J. Beckman, available as NCEER-96-0015.

NCEER-95-0017 "The Hanshin-Awaji Earthquake of January 17, 1995: Performance of Highway Bridges," Edited by I.G. Buckle, 12/1/95, to be published.

NCEER-95-0018 "Modeling of Masonry Infill Panels for Structural Analysis," by A.M. Reinhorn, A. Madan, R.E. Valles, Y. Reichmann and J.B. Mander, 12/8/95, (PB97-110886, MF-A01, A06).

NCEER-95-0019 "Optimal Polynomial Control for Linear and Nonlinear Structures," by A.K. Agrawal and J.N. Yang, 12/11/95, (PB96-168737, A07, MF-A02).

NCEER-95-0020 "Retrofit of Non-Ductile Reinforced Concrete Frames Using Friction Dampers," by R.S. Rao, P. Gergely and R.N. White, 12/22/95, (PB97-133508, A10, MF-A02).

NCEER-95-0021 "Parametric Results for Seismic Response of Pile-Supported Bridge Bents," by G. Mylonakis, A. Nikolaou and G. Gazetas, 12/22/95, (PB97-100242, A12, MF-A03).

NCEER-95-0022 "Kinematic Bending Moments in Seismically Stressed Piles," by A. Nikolaou, G. Mylonakis and G. Gazetas, 12/23/95, (PB97-113914, MF-A03, A13).

NCEER-96-0001 "Dynamic Response of Unreinforced Masonry Buildings with Flexible Diaphragms," by A.C. Costley and D.P. Abrams," 10/10/96, (PB97-133573, MF-A03, A15).

NCEER-96-0002 "State of the Art Review: Foundations and Retaining Structures," by I. Po Lam, to be published.

NCEER-96-0003 "Ductility of Rectangular Reinforced Concrete Bridge Columns with Moderate Confinement," by N. Wehbe, M. Saiidi, D. Sanders and B. Douglas, 11/7/96, (PB97-133557, A06, MF-A02).

NCEER-96-0004 "Proceedings of the Long-Span Bridge Seismic Research Workshop," edited by I.G. Buckle and I.M. Friedland, to be published.

NCEER-96-0005 "Establish Representative Pier Types for Comprehensive Study: Eastern United States," by J. Kulicki and Z. Prucz, 5/28/96, (PB98-119217, A07, MF-A02).

NCEER-96-0006 "Establish Representative Pier Types for Comprehensive Study: Western United States," by R. Imbsen, R.A. Schamber and T.A. Osterkamp, 5/28/96, (PB98-118607, A07, MF-A02).

NCEER-96-0007 "Nonlinear Control Techniques for Dynamical Systems with Uncertain Parameters," by R.G. Ghanem and M.I. Bujakov, 5/27/96, (PB97-100259, A17, MF-A03).

NCEER-96-0008 "Seismic Evaluation of a 30-Year Old Non-Ductile Highway Bridge Pier and Its Retrofit," by J.B. Mander, B. Mahmoodzadegan, S. Bhadra and S.S. Chen, 5/31/96, (PB97-110902, MF-A03, A10).

NCEER-96-0009 "Seismic Performance of a Model Reinforced Concrete Bridge Pier Before and After Retrofit," by J.B. Mander, J.H. Kim and C.A. Ligozio, 5/31/96, (PB97-110910, MF-A02, A10).

NCEER-96-0010 "IDARC2D Version 4.0: A Computer Program for the Inelastic Damage Analysis of Buildings," by R.E. Valles, A.M. Reinhorn, S.K. Kunnath, C. Li and A. Madan, 6/3/96, (PB97-100234, A17, MF-A03).

NCEER-96-0011 "Estimation of the Economic Impact of Multiple Lifeline Disruption: Memphis Light, Gas and Water Division Case Study," by S.E. Chang, H.A. Seligson and R.T. Eguchi, 8/16/96, (PB97-133490, A11, MF-A03).

NCEER-96-0012 "Proceedings from the Sixth Japan-U.S. Workshop on Earthquake Resistant Design of Lifeline Facilities and Countermeasures Against Soil Liquefaction, Edited by M. Hamada and T. O'Rourke, 9/11/96, (PB97-133581, A99, MF-A06).

NCEER-96-0013 "Chemical Hazards, Mitigation and Preparedness in Areas of High Seismic Risk: A Methodology for Estimating the Risk of Post-Earthquake Hazardous Materials Release," by H.A. Seligson, R.T. Eguchi, K.J. Tierney and K. Richmond, 11/7/96, (PB97-133565, MF-A02, A08).

NCEER-96-0014 "Response of Steel Bridge Bearings to Reversed Cyclic Loading," by J.B. Mander, D-K. Kim, S.S. Chen and G.J. Premus, 11/13/96, (PB97-140735, A12, MF-A03).

NCEER-96-0015 "Highway Culvert Performance During Past Earthquakes," by T.L. Youd and C.J. Beckman, 11/25/96, (PB97-133532, A06, MF-A01).

NCEER-97-0001 "Evaluation, Prevention and Mitigation of Pounding Effects in Building Structures," by R.E. Valles and A.M. Reinhorn, 2/20/97, (PB97-159552, A14, MF-A03).

NCEER-97-0002 "Seismic Design Criteria for Bridges and Other Highway Structures," by C. Rojahn, R. Mayes, D.G. Anderson, J. Clark, J.H. Hom, R.V. Nutt and M.J. O'Rourke, 4/30/97, (PB97-194658, A06, MF-A03).

NCEER-97-0003 “Proceedings of the U.S.-Italian Workshop on Seismic Evaluation and Retrofit,” Edited by D.P. Abrams and G.M. Calvi, 3/19/97, (PB97-194666, A13, MF-A03).

NCEER-97-0004 "Investigation of Seismic Response of Buildings with Linear and Nonlinear Fluid Viscous Dampers," by A.A. Seleemah and M.C. Constantinou, 5/21/97, (PB98-109002, A15, MF-A03).

NCEER-97-0005 "Proceedings of the Workshop on Earthquake Engineering Frontiers in Transportation Facilities," edited by G.C. Lee and I.M. Friedland, 8/29/97, (PB98-128911, A25, MR-A04).

NCEER-97-0006 "Cumulative Seismic Damage of Reinforced Concrete Bridge Piers," by S.K. Kunnath, A. El-Bahy, A. Taylor and W. Stone, 9/2/97, (PB98-108814, A11, MF-A03).

NCEER-97-0007 "Structural Details to Accommodate Seismic Movements of Highway Bridges and Retaining Walls," by R.A. Imbsen, R.A. Schamber, E. Thorkildsen, A. Kartoum, B.T. Martin, T.N. Rosser and J.M. Kulicki, 9/3/97, (PB98-108996, A09, MF-A02).

NCEER-97-0008 "A Method for Earthquake Motion-Damage Relationships with Application to Reinforced Concrete Frames," by A. Singhal and A.S. Kiremidjian, 9/10/97, (PB98-108988, A13, MF-A03).

NCEER-97-0009 "Seismic Analysis and Design of Bridge Abutments Considering Sliding and Rotation," by K. Fishman and R. Richards, Jr., 9/15/97, (PB98-108897, A06, MF-A02).

NCEER-97-0010 "Proceedings of the FHWA/NCEER Workshop on the National Representation of Seismic Ground Motion for New and Existing Highway Facilities," edited by I.M. Friedland, M.S. Power and R.L. Mayes, 9/22/97, (PB98-128903, A21, MF-A04).

NCEER-97-0011 "Seismic Analysis for Design or Retrofit of Gravity Bridge Abutments," by K.L. Fishman, R. Richards, Jr. and R.C. Divito, 10/2/97, (PB98-128937, A08, MF-A02).

NCEER-97-0012 "Evaluation of Simplified Methods of Analysis for Yielding Structures," by P. Tsopelas, M.C. Constantinou, C.A. Kircher and A.S. Whittaker, 10/31/97, (PB98-128929, A10, MF-A03).

NCEER-97-0013 "Seismic Design of Bridge Columns Based on Control and Repairability of Damage," by C-T. Cheng and J.B. Mander, 12/8/97, (PB98-144249, A11, MF-A03).

NCEER-97-0014 "Seismic Resistance of Bridge Piers Based on Damage Avoidance Design," by J.B. Mander and C-T. Cheng, 12/10/97, (PB98-144223, A09, MF-A02).

NCEER-97-0015 “Seismic Response of Nominally Symmetric Systems with Strength Uncertainty,” by S. Balopoulou and M. Grigoriu, 12/23/97, (PB98-153422, A11, MF-A03).

NCEER-97-0016 “Evaluation of Seismic Retrofit Methods for Reinforced Concrete Bridge Columns,” by T.J. Wipf, F.W. Klaiber and F.M. Russo, 12/28/97, (PB98-144215, A12, MF-A03).

NCEER-97-0017 “Seismic Fragility of Existing Conventional Reinforced Concrete Highway Bridges,” by C.L. Mullen and A.S. Cakmak, 12/30/97, (PB98-153406, A08, MF-A02).

NCEER-97-0018 “Loss Asssessment of Memphis Buildings,” edited by D.P. Abrams and M. Shinozuka, 12/31/97, (PB98-144231, A13, MF-A03).

NCEER-97-0019 “Seismic Evaluation of Frames with Infill Walls Using Quasi-static Experiments,” by K.M. Mosalam, R.N. White and P. Gergely, 12/31/97, (PB98-153455, A07, MF-A02).

NCEER-97-0020 “Seismic Evaluation of Frames with Infill Walls Using Pseudo-dynamic Experiments,” by K.M. Mosalam, R.N. White and P. Gergely, 12/31/97, (PB98-153430, A07, MF-A02).

NCEER-97-0021 “Computational Strategies for Frames with Infill Walls: Discrete and Smeared Crack Analyses and Seismic Fragility,” by K.M. Mosalam, R.N. White and P. Gergely, 12/31/97, (PB98-153414, A10, MF-A02).

NCEER-97-0022 "Proceedings of the NCEER Workshop on Evaluation of Liquefaction Resistance of Soils," edited by T.L. Youd and I.M. Idriss, 12/31/97, (PB98-155617, A15, MF-A03).

MCEER-98-0001 "Extraction of Nonlinear Hysteretic Properties of Seismically Isolated Bridges from Quick-Release Field Tests," by Q. Chen, B.M. Douglas, E.M. Maragakis and I.G. Buckle, 5/26/98, (PB99-118838, A06, MF-A01).

MCEER-98-0002 "Methodologies for Evaluating the Importance of Highway Bridges," by A. Thomas, S. Eshenaur and J. Kulicki, 5/29/98, (PB99-118846, A10, MF-A02).

MCEER-98-0003 "Capacity Design of Bridge Piers and the Analysis of Overstrength," by J.B. Mander, A. Dutta and P. Goel, 6/1/98, (PB99-118853, A09, MF-A02).

MCEER-98-0004 "Evaluation of Bridge Damage Data from the Loma Prieta and Northridge, California Earthquakes," by N. Basoz and A. Kiremidjian, 6/2/98, (PB99-118861, A15, MF-A03).

MCEER-98-0005 "Screening Guide for Rapid Assessment of Liquefaction Hazard at Highway Bridge Sites," by T. L. Youd, 6/16/98, (PB99-118879, A06, not available on microfiche).

MCEER-98-0006 "Structural Steel and Steel/Concrete Interface Details for Bridges," by P. Ritchie, N. Kauhl and J. Kulicki, 7/13/98, (PB99-118945, A06, MF-A01).

MCEER-98-0007 "Capacity Design and Fatigue Analysis of Confined Concrete Columns," by A. Dutta and J.B. Mander, 7/14/98, (PB99-118960, A14, MF-A03).

MCEER-98-0008 "Proceedings of the Workshop on Performance Criteria for Telecommunication Services Under Earthquake Conditions," edited by A.J. Schiff, 7/15/98, (PB99-118952, A08, MF-A02).

MCEER-98-0009 "Fatigue Analysis of Unconfined Concrete Columns," by J.B. Mander, A. Dutta and J.H. Kim, 9/12/98, (PB99-123655, A10, MF-A02).

MCEER-98-0010 "Centrifuge Modeling of Cyclic Lateral Response of Pile-Cap Systems and Seat-Type Abutments in Dry Sands," by A.D. Gadre and R. Dobry, 10/2/98, (PB99-123606, A13, MF-A03).

MCEER-98-0011 "IDARC-BRIDGE: A Computational Platform for Seismic Damage Assessment of Bridge Structures," by A.M. Reinhorn, V. Simeonov, G. Mylonakis and Y. Reichman, 10/2/98, (PB99-162919, A15, MF-A03).

MCEER-98-0012 "Experimental Investigation of the Dynamic Response of Two Bridges Before and After Retrofitting with Elastomeric Bearings," by D.A. Wendichansky, S.S. Chen and J.B. Mander, 10/2/98, (PB99-162927, A15, MF-A03).

MCEER-98-0013 "Design Procedures for Hinge Restrainers and Hinge Sear Width for Multiple-Frame Bridges," by R. Des Roches and G.L. Fenves, 11/3/98, (PB99-140477, A13, MF-A03).

MCEER-98-0014 "Response Modification Factors for Seismically Isolated Bridges," by M.C. Constantinou and J.K. Quarshie, 11/3/98, (PB99-140485, A14, MF-A03).

MCEER-98-0015 "Proceedings of the U.S.-Italy Workshop on Seismic Protective Systems for Bridges," edited by I.M. Friedland and M.C. Constantinou, 11/3/98, (PB2000-101711, A22, MF-A04).

MCEER-98-0016 "Appropriate Seismic Reliability for Critical Equipment Systems: Recommendations Based on Regional Analysis of Financial and Life Loss," by K. Porter, C. Scawthorn, C. Taylor and N. Blais, 11/10/98, (PB99-157265, A08, MF-A02).

MCEER-98-0017 "Proceedings of the U.S. Japan Joint Seminar on Civil Infrastructure Systems Research," edited by M. Shinozuka and A. Rose, 11/12/98, (PB99-156713, A16, MF-A03).

MCEER-98-0018 "Modeling of Pile Footings and Drilled Shafts for Seismic Design," by I. PoLam, M. Kapuskar and D. Chaudhuri, 12/21/98, (PB99-157257, A09, MF-A02).

MCEER-99-0001 "Seismic Evaluation of a Masonry Infilled Reinforced Concrete Frame by Pseudodynamic Testing," by S.G. Buonopane and R.N. White, 2/16/99, (PB99-162851, A09, MF-A02).

MCEER-99-0002 "Response History Analysis of Structures with Seismic Isolation and Energy Dissipation Systems: Verification Examples for Program SAP2000," by J. Scheller and M.C. Constantinou, 2/22/99, (PB99-162869, A08, MF-A02).

MCEER-99-0003 "Experimental Study on the Seismic Design and Retrofit of Bridge Columns Including Axial Load Effects," by A. Dutta, T. Kokorina and J.B. Mander, 2/22/99, (PB99-162877, A09, MF-A02).

MCEER-99-0004 "Experimental Study of Bridge Elastomeric and Other Isolation and Energy Dissipation Systems with Emphasis on Uplift Prevention and High Velocity Near-source Seismic Excitation," by A. Kasalanati and M. C. Constantinou, 2/26/99, (PB99-162885, A12, MF-A03).

MCEER-99-0005 "Truss Modeling of Reinforced Concrete Shear-flexure Behavior," by J.H. Kim and J.B. Mander, 3/8/99, (PB99-163693, A12, MF-A03).

MCEER-99-0006 "Experimental Investigation and Computational Modeling of Seismic Response of a 1:4 Scale Model Steel Structure with a Load Balancing Supplemental Damping System," by G. Pekcan, J.B. Mander and S.S. Chen, 4/2/99, (PB99-162893, A11, MF-A03).

MCEER-99-0007 "Effect of Vertical Ground Motions on the Structural Response of Highway Bridges," by M.R. Button, C.J. Cronin and R.L. Mayes, 4/10/99, (PB2000-101411, A10, MF-A03).

MCEER-99-0008 "Seismic Reliability Assessment of Critical Facilities: A Handbook, Supporting Documentation, and Model Code Provisions," by G.S. Johnson, R.E. Sheppard, M.D. Quilici, S.J. Eder and C.R. Scawthorn, 4/12/99, (PB2000-101701, A18, MF-A04).

MCEER-99-0009 "Impact Assessment of Selected MCEER Highway Project Research on the Seismic Design of Highway Structures," by C. Rojahn, R. Mayes, D.G. Anderson, J.H. Clark, D'Appolonia Engineering, S. Gloyd and R.V. Nutt, 4/14/99, (PB99-162901, A10, MF-A02).

MCEER-99-0010 "Site Factors and Site Categories in Seismic Codes," by R. Dobry, R. Ramos and M.S. Power, 7/19/99, (PB2000-101705, A08, MF-A02).

MCEER-99-0011 "Restrainer Design Procedures for Multi-Span Simply-Supported Bridges," by M.J. Randall, M. Saiidi, E. Maragakis and T. Isakovic, 7/20/99, (PB2000-101702, A10, MF-A02).

MCEER-99-0012 "Property Modification Factors for Seismic Isolation Bearings," by M.C. Constantinou, P. Tsopelas, A. Kasalanati and E. Wolff, 7/20/99, (PB2000-103387, A11, MF-A03).

MCEER-99-0013 "Critical Seismic Issues for Existing Steel Bridges," by P. Ritchie, N. Kauhl and J. Kulicki, 7/20/99, (PB2000-101697, A09, MF-A02).

MCEER-99-0014 "Nonstructural Damage Database," by A. Kao, T.T. Soong and A. Vender, 7/24/99, (PB2000-101407, A06, MF-A01).

MCEER-99-0015 "Guide to Remedial Measures for Liquefaction Mitigation at Existing Highway Bridge Sites," by H.G. Cooke and J. K. Mitchell, 7/26/99, (PB2000-101703, A11, MF-A03).

MCEER-99-0016 "Proceedings of the MCEER Workshop on Ground Motion Methodologies for the Eastern United States," edited by N. Abrahamson and A. Becker, 8/11/99, (PB2000-103385, A07, MF-A02).

MCEER-99-0017 "Quindío, Colombia Earthquake of January 25, 1999: Reconnaissance Report," by A.P. Asfura and P.J. Flores, 10/4/99, (PB2000-106893, A06, MF-A01).

MCEER-99-0018 "Hysteretic Models for Cyclic Behavior of Deteriorating Inelastic Structures," by M.V. Sivaselvan and A.M. Reinhorn, 11/5/99, (PB2000-103386, A08, MF-A02).

MCEER-99-0019 "Proceedings of the 7th U.S.- Japan Workshop on Earthquake Resistant Design of Lifeline Facilities and Countermeasures Against Soil Liquefaction," edited by T.D. O'Rourke, J.P. Bardet and M. Hamada, 11/19/99, (PB2000-103354, A99, MF-A06).

MCEER-99-0020 "Development of Measurement Capability for Micro-Vibration Evaluations with Application to Chip Fabrication Facilities," by G.C. Lee, Z. Liang, J.W. Song, J.D. Shen and W.C. Liu, 12/1/99, (PB2000-105993, A08, MF-A02).

MCEER-99-0021 "Design and Retrofit Methodology for Building Structures with Supplemental Energy Dissipating Systems," by G. Pekcan, J.B. Mander and S.S. Chen, 12/31/99, (PB2000-105994, A11, MF-A03).

MCEER-00-0001 "The Marmara, Turkey Earthquake of August 17, 1999: Reconnaissance Report," edited by C. Scawthorn; with major contributions by M. Bruneau, R. Eguchi, T. Holzer, G. Johnson, J. Mander, J. Mitchell, W. Mitchell, A. Papageorgiou, C. Scaethorn, and G. Webb, 3/23/00, (PB2000-106200, A11, MF-A03).

MCEER-00-0002 "Proceedings of the MCEER Workshop for Seismic Hazard Mitigation of Health Care Facilities," edited by G.C. Lee, M. Ettouney, M. Grigoriu, J. Hauer and J. Nigg, 3/29/00, (PB2000-106892, A08, MF-A02).

MCEER-00-0003 "The Chi-Chi, Taiwan Earthquake of September 21, 1999: Reconnaissance Report," edited by G.C. Lee and C.H. Loh, with major contributions by G.C. Lee, M. Bruneau, I.G. Buckle, S.E. Chang, P.J. Flores, T.D. O'Rourke, M. Shinozuka, T.T. Soong, C-H. Loh, K-C. Chang, Z-J. Chen, J-S. Hwang, M-L. Lin, G-Y. Liu, K-C. Tsai, G.C. Yao and C-L. Yen, 4/30/00, (PB2001-100980, A10, MF-A02).

MCEER-00-0004 "Seismic Retrofit of End-Sway Frames of Steel Deck-Truss Bridges with a Supplemental Tendon System: Experimental and Analytical Investigation," by G. Pekcan, J.B. Mander and S.S. Chen, 7/1/00, (PB2001-100982, A10, MF-A02).

MCEER-00-0005 "Sliding Fragility of Unrestrained Equipment in Critical Facilities," by W.H. Chong and T.T. Soong, 7/5/00, (PB2001-100983, A08, MF-A02).

MCEER-00-0006 "Seismic Response of Reinforced Concrete Bridge Pier Walls in the Weak Direction," by N. Abo-Shadi, M. Saiidi and D. Sanders, 7/17/00, (PB2001-100981, A17, MF-A03).

MCEER-00-0007 "Low-Cycle Fatigue Behavior of Longitudinal Reinforcement in Reinforced Concrete Bridge Columns," by J. Brown and S.K. Kunnath, 7/23/00, (PB2001-104392, A08, MF-A02).

MCEER-00-0008 "Soil Structure Interaction of Bridges for Seismic Analysis," I. PoLam and H. Law, 9/25/00, (PB2001-105397, A08, MF-A02).

MCEER-00-0009 "Proceedings of the First MCEER Workshop on Mitigation of Earthquake Disaster by Advanced Technologies (MEDAT-1), edited by M. Shinozuka, D.J. Inman and T.D. O'Rourke, 11/10/00, (PB2001-105399, A14, MF-A03).

MCEER-00-0010 "Development and Evaluation of Simplified Procedures for Analysis and Design of Buildings with Passive Energy Dissipation Systems," by O.M. Ramirez, M.C. Constantinou, C.A. Kircher, A.S. Whittaker, M.W. Johnson, J.D. Gomez and C. Chrysostomou, 11/16/01, (PB2001-105523, A23, MF-A04).

MCEER-00-0011 "Dynamic Soil-Foundation-Structure Interaction Analyses of Large Caissons," by C-Y. Chang, C-M. Mok, Z-L. Wang, R. Settgast, F. Waggoner, M.A. Ketchum, H.M. Gonnermann and C-C. Chin, 12/30/00, (PB2001-104373, A07, MF-A02).

MCEER-00-0012 "Experimental Evaluation of Seismic Performance of Bridge Restrainers," by A.G. Vlassis, E.M. Maragakis and M. Saiid Saiidi, 12/30/00, (PB2001-104354, A09, MF-A02).

MCEER-00-0013 "Effect of Spatial Variation of Ground Motion on Highway Structures," by M. Shinozuka, V. Saxena and G. Deodatis, 12/31/00, (PB2001-108755, A13, MF-A03).

MCEER-00-0014 "A Risk-Based Methodology for Assessing the Seismic Performance of Highway Systems," by S.D. Werner, C.E. Taylor, J.E. Moore, II, J.S. Walton and S. Cho, 12/31/00, (PB2001-108756, A14, MF-A03).

MCEER-01-0001 "Experimental Investigation of P-Delta Effects to Collapse During Earthquakes," by D. Vian and M. Bruneau, 6/25/01, (PB2002-100534, A17, MF-A03).

MCEER-01-0002 "Proceedings of the Second MCEER Workshop on Mitigation of Earthquake Disaster by Advanced Technologies (MEDAT-2)," edited by M. Bruneau and D.J. Inman, 7/23/01, (PB2002-100434, A16, MF-A03).

MCEER-01-0003 "Sensitivity Analysis of Dynamic Systems Subjected to Seismic Loads," by C. Roth and M. Grigoriu, 9/18/01, (PB2003-100884, A12, MF-A03).

MCEER-01-0004 "Overcoming Obstacles to Implementing Earthquake Hazard Mitigation Policies: Stage 1 Report," by D.J. Alesch and W.J. Petak, 12/17/01, (PB2002-107949, A07, MF-A02).

MCEER-01-0005 "Updating Real-Time Earthquake Loss Estimates: Methods, Problems and Insights," by C.E. Taylor, S.E. Chang and R.T. Eguchi, 12/17/01, (PB2002-107948, A05, MF-A01).

MCEER-01-0006 "Experimental Investigation and Retrofit of Steel Pile Foundations and Pile Bents Under Cyclic Lateral Loadings," by A. Shama, J. Mander, B. Blabac and S. Chen, 12/31/01, (PB2002-107950, A13, MF-A03).

MCEER-02-0001 "Assessment of Performance of Bolu Viaduct in the 1999 Duzce Earthquake in Turkey" by P.C. Roussis, M.C. Constantinou, M. Erdik, E. Durukal and M. Dicleli, 5/8/02, (PB2003-100883, A08, MF-A02).

MCEER-02-0002 "Seismic Behavior of Rail Counterweight Systems of Elevators in Buildings," by M.P. Singh, Rildova and L.E. Suarez, 5/27/02. (PB2003-100882, A11, MF-A03).

MCEER-02-0003 "Development of Analysis and Design Procedures for Spread Footings," by G. Mylonakis, G. Gazetas, S. Nikolaou and A. Chauncey, 10/02/02, (PB2004-101636, A13, MF-A03, CD-A13).

MCEER-02-0004 "Bare-Earth Algorithms for Use with SAR and LIDAR Digital Elevation Models," by C.K. Huyck, R.T. Eguchi and B. Houshmand, 10/16/02, (PB2004-101637, A07, CD-A07).

MCEER-02-0005 "Review of Energy Dissipation of Compression Members in Concentrically Braced Frames," by K.Lee and M. Bruneau, 10/18/02, (PB2004-101638, A10, CD-A10).

MCEER-03-0001 "Experimental Investigation of Light-Gauge Steel Plate Shear Walls for the Seismic Retrofit of Buildings" by J. Berman and M. Bruneau, 5/2/03, (PB2004-101622, A10, MF-A03, CD-A10).

MCEER-03-0002 "Statistical Analysis of Fragility Curves," by M. Shinozuka, M.Q. Feng, H. Kim, T. Uzawa and T. Ueda, 6/16/03, (PB2004-101849, A09, CD-A09).

MCEER-03-0003 "Proceedings of the Eighth U.S.-Japan Workshop on Earthquake Resistant Design f Lifeline Facilities and Countermeasures Against Liquefaction," edited by M. Hamada, J.P. Bardet and T.D. O'Rourke, 6/30/03.

MCEER-03-0004 "Proceedings of the PRC-US Workshop on Seismic Analysis and Design of Special Bridges," edited by L.C. Fan and G.C. Lee, 7/15/03.

MCEER-03-0005 "Urban Disaster Recovery: A Framework and Simulation Model," by S.B. Miles and S.E. Chang, 7/25/03.

MCEER-03-0006 "Behavior of Underground Piping Joints Due to Static and Dynamic Loading," by R.D. Meis, M. Maragakis and R. Siddharthan, 11/17/03.

MCEER-03-0007 "Seismic Vulnerability of Timber Bridges and Timber Substructures," by A.A. Shama, J.B. Mander, I.M. Friedland and D.R. Allicock, 12/15/03.

MCEER-04-0001 "Experimental Study of Seismic Isolation Systems with Emphasis on Secondary System Response and Verification of Accuracy of Dynamic Response History Analysis Methods," by E. Wolff and M. Constantinou, 1/16/04.

MCEER-04-0002 "Tension, Compression and Cyclic Testing of Engineered Cementitious Composite Materials," by K. Kesner and S.L. Billington, 3/1/04.

MCEER-04-0003 "Cyclic Testing of Braces Laterally Restrained by Steel Studs to Enhance Performance During Earthquakes," by O.C. Celik, J.W. Berman and M. Bruneau, 3/16/04.

MULTIDISCIPLINARY CENTER FOR EARTHQUAKE ENGINEERING RESEARCH

A National Center of Excellence in Advanced Technology Applications

University at Buffalo, State University of New York
Red Jacket Quadrangle ▪ Buffalo, New York 14261
Phone: (716) 645-3391 ▪ Fax: (716) 645-3399
E-mail: *mceer@mceermail.buffalo.edu* ▪ WWW Site *http://mceer.buffalo.edu*

University at Buffalo *The State University of New York*

ISSN 1520-295X